UNIVERSITY OF TECHNOLOGY SYDNEY

Ecohydrological interactions and landscape response to recent hydroclimatic events in Australia

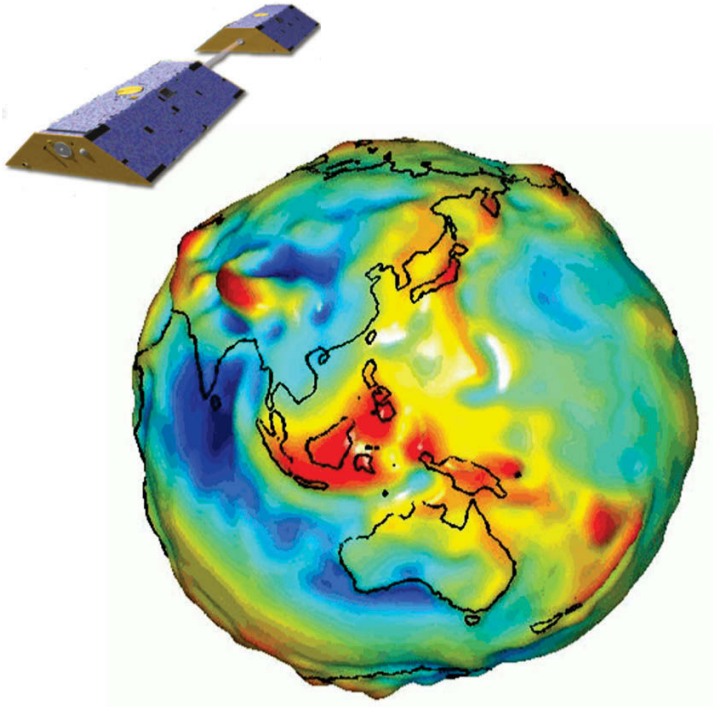

Zunyi Xie

A thesis submitted in fulfilment of the requirements for the degree of

Doctor of Philosophy

Climate Change Cluster

Faculty of Science

University of Technology Sydney

April 2017

Certificate of original authorship

I certify that the work in this thesis has not previously been submitted for a degree nor has it been submitted as part of requirements for a degree except as fully acknowledged within the text.

I also certify that the thesis has been written by me. Any help that I have received in my research work and the preparation of the thesis itself has been acknowledged. In addition, I certify that all information sources and literature used are indicated in the thesis.

Signature of student:

Date: 13-04-2017

Acknowledgements

This project was supported by a joint scholarship of China Scholarship Council and University of Technology Sydney. Foremost, I would like to thank my principal supervisor Professor Alfredo Huete and co-supervisor Professor Graziella Caprarelli for their continuous support during my four years' PhD study. It has been a challenging but rewarding experience, which would not have been possible without their assistance. I thank Professor Huete for holding me to a high research standard by providing insightful comments on my work and constructive criticisms at different stages of my research. I appreciate very much his persistence and encouragement, for believing in me. I am also very grateful for the job opportunity he provided with me over the last two years, which substantially improved my technical skills and helped me financially. I would like to extend a special thanks to Professor Caprarelli for bringing me to UTS to pursue my PhD. She has been always there ready to help throughout my candidature, which I really appreciate.

My heartfelt gratitude also goes to many people who contributed to my PhD project in ways both small and large, including;

- My current team colleagues Rakhesh Devadas, Xuanlong Ma (Richard), Chris Watson, Leandro Giovannini, Nguyen Ngoc Tran, Paras Sidiqui, Ekena Rangel Pinage; my previous team colleagues Natalia Restrepo-Coupe, Kevin Davies, Qunying Luo, Wouter Maes; Professor Derek Eamus, Professor Qiang Yu and his visiting scholars, James Cleverly, Chao Chen, Mirela Tulbure, Mark Broich, Professor Deborah Edwards etc for their invaluable academic support.
- UTS friends Xunhe Zhang, Sicong Gao, Mingming Cheng, Jianxiu Shen, Xueling Li, Jie He, Qinggaozi Zhu, Hao Shi, Wenbo Wang, Maoying Qiao, Wenjie Zhang, Jiaqi Dong, Nikki Bramwell, Buddhi Dayananda, Stephen Fujiwara, Sofie Voerman etc for being wonderful friends and companions of me throughout my PhD.

- Faculty staff Marea Martlew, John Moore etc for assisting with the administration. UTS staff Richard Lum, Belinda Lee and Professor Tony Moon for their consistent assistance, encouragement and considered advice, which ensured I had a very pleasant study experience in UTS.
- Local friends Eric Pawsey, Eric's family and friends, Geoffrey Pearce, Dung Tran, Peter Mylan etc. In particular, I extend my special thanks to Geoffrey Pearce and Dung Tran for looking after me during my first two years in Sydney, assisting me in settling down here and helped me edit English of my thesis and publications. I would also like to thank Eric Pawsey, who treated me as his family, and more importantly, provided a home for me in Australia.

Last but not least, I would like to thank my family and friends in China for their support and understanding throughout my candidature, particularly my parents, who have been working so hard to raise me and support my education. They are great parents for me.

I have been going through cycles of sadness, anger, and 'despair', followed by 'fight back' feelings during my PhD, and I am lucky to have all of the people mentioned above in my life to support me all the time. The completion of my PhD has brought me a deep sense of satisfaction and achievement, which greatly inspired a village boy like me to believe where there is a will, there is a way.

Publications

Peer reviewed journal articles arising directly from this thesis

Journal publications

1. **Xie, Z.**, Huete, A., Restrepo-Coupe, N., Ma, X., Devadas, R., & Caprarelli, G. (2016). Spatial partitioning and temporal evolution of Australia's total water storage under extreme hydroclimatic impacts. *Remote Sensing of Environment, 183*, 43-52.

2. **Xie, Z.**, Huete, A., Ma, X., Restrepo-Coupe, N., Devadas, R., Clarke, K., & Lewis, M. (2016). Landsat and GRACE observations of arid wetland dynamics in central Australia under multi-decadal hydroclimatic extremes. *Journal of Hydrology, 543*,818-831.

Conference Proceedings

Xie, Z., Huete, A., Restrepo-Coupe, N., Devadas, R., Davies, K., & Waston C. (2015). Terrestrial total water storage dynamics of Australia's recent dry and wet events. *Proceeding of 2015 IEEE International Geoscience and Remote Sensing Symposium (IGARSS)*, 992-995, Milan, Italy; 07/2015

Table of Contents

List of Figures

List of Tables

Abbreviations

AOES	Advanced Orbital Ephemeris System
AVHRR	Advanced Very High Resolution Radiometer
AWAP	Australian Water Availability Project
BOM	Bureau of Meteorology
CAMS	Climate Anomaly Monitoring System
CDR	Climate Data Record
CI	Confidence Interval
CLM	Community Land Model
CSIRO	Commonwealth Scientific and Industrial Research Organisation
CSR	University of Texas Centre for Space Research
DEM	Digital Elevation Model
DLCD	Dynamic Land Cover Dataset
DSWE	Dynamic Surface Water Extent
ENSO	El Niño-Southern Oscillation
EROS	Earth Resources Observation and Science Centre
ESA	European Space Agency
ET	Evapotranspiration
ETM+	Enhanced Thematic Mapper Plus
EVI	Enhanced Vegetation Index

fPAR	Fraction of Photosynthetically Active Radiation
GDEs	Groundwater Dependent Ecosystems
GFZ	GeoForschungsZentrum
GLDAS	Global Land Data Assimilation System
GRACE	Gravity Recovery and Climate Experiment
HadISST	Hadley Centre Sea Ice and Sea Surface Temperature
IOD	Indian Ocean Dipole
IPCC	Intergovernmental Panel on Climate Change
JAXA	Japan's National Space Development Agency
JPL	Jet Propulsion Laboratory
MDB	Murray-Darling Basin
MEI	Multivariate ENSO Index
MNDWI	Modified Normalized Difference Wetness Index
MODIS	Moderate Resolution Imaging Spectroradiometer
NASA	National Aeronautics and Space Administration
NDVI	Normalized Difference Vegetation Index
NIR	Near-infrared
NLWRA	National Land and Water Resources Audit
NOAA	National Oceanic and Atmospheric Administration
OLI	Operational Land Imager
OLS	Ordinary Least Squares
PCCA	Partial Cross-Correlation Analysis
QA	Quality assessment

SAM	Southern Annular Mode
SEACI	South Eastern Australian Climate Initiative
SPCCA	Semi Partial Cross-Correlation Analysis
SRTM	Shuttle Radar Topography Mission
SST	Sea Surface Temperature
STL	Seasonal Decomposition of Time Series by LOESS
TRMM	Tropical Rainfall Measuring Mission
TW	Landsat Thematic Mapper
TWSA	Total Water Storage Anomaly
USCCGRP	United States Climate Change Global Research Program
USGS	United States Geological Survey

Abstract

Amplification of the water cycle as a consequence of climate change is predicted to increase the climate variability as well as the frequency and severity of droughts and wet extremes over continents such as Australia. Australia has recently experienced three large-scale hydroclimatic extremes, including a decadal millennium drought from 2001 to 2009 (termed the 'big dry'), followed by a short wet pulse during 2010 and 2011 (termed the 'big wet'), and another continent-wide dry condition in 2015. These dry and wet events exerted pronounced negative impacts on water resources, natural ecosystems and agriculture over large areas of Australia. Despite these extreme hydroclimatic impacts, the fate of ecohydrological resources such as the loss and recovery of water storage and vegetation remain largely unknown.

The overall goal of this thesis is to study the ecohydrological interactions and landscape response to Australia's early 21st century hydroclimatic extremes. To achieve thesis objectives, I (1) firstly investigated the spatial partitioning and temporal evolution of water resources across Australia under extreme hydroclimatic impacts, (2) then assessed the associations between the climate variability and dynamics in water resources and vegetation productivity, (3) furthermore examined the resilience of regional arid ecosystems to the highly variable water regimes and large-scale hydrological fluctuations, and (4) conducted a synthesized assessment of ecohydrological variations and interactions under these dry and wet events at continental, regional and biome scales, respectively.

Results show that highly variable continental patterns were observed in water resources and vegetation, involving differences in the direction, magnitude, and duration of total water storage and surface greenness responses to drought and wet periods. These responses clustered into three distinct geographic zones that correlated well with the influences from three large-scale climate modes: the El Niño-Southern Oscillation (ENSO), the Indian Ocean Dipole (IOD) and the Southern Annular Mode (SAM). At regional scale, ecosystems such as arid wetlands exhibit strong ecological resilience to

hydroclimatic extremes, and are presumably sensitive to future altered water regimes due to climate change. In addition, Total Water Storage Anomaly (TWSA) data derived from Gravity Recovery And Climate Experiment (GRACE) satellites was found to be a valuable indicator for ecohydrological system performances and effectively linking the extreme climate variability with Australia's ecosystems.

This thesis highlights the value of Remote Sensing techniques (e.g. GRACE satellites) as important tools for improved assessments and management of water resources and associated ecosystems in Australia, particularly in the face of future increasing hydroclimatic extremes.

Chapter 1: Introduction

1.1 General research background

1.1.1 Global hydrological cycle and water balance

Water covers around 70 percent of the Earth's surface and is an essential element for life (Gleick 1993). The global hydrological cycle describes the circulation of water, in which water is cycled between land, the oceans and the atmosphere through four main stages: evaporation, condensation, precipitation and runoff (Fig.1.1) (Pagano and Sorooshian 2006). Driven by the sun and gravity, water moves between all these stages and acts as a powerful vehicle for rearranging the Earth's energy budget, but the total amount of water on the Earth remains fairly constant (Takle et al. 2007). The hydrological cycle influences weather patterns, which over time adds up to become the climate of any given location around the world (Chahine 1992).

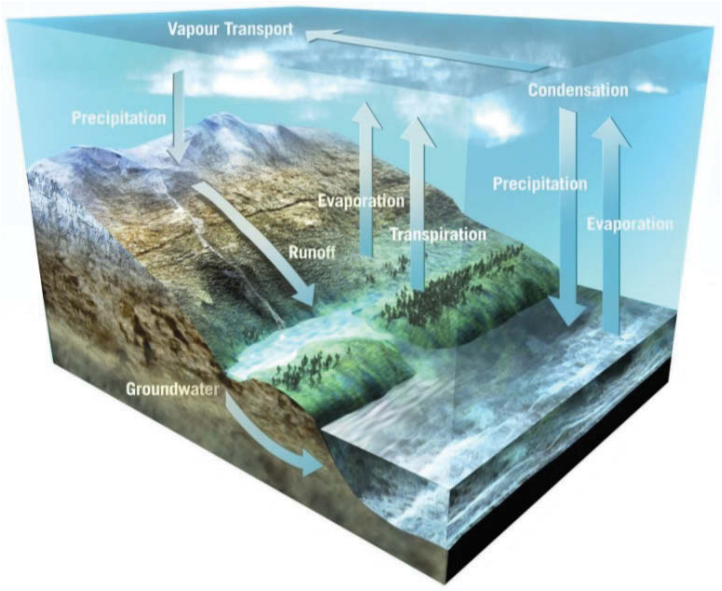

Figure 1.1. The global hydrological cycle (ESA/AOES Medialab)

The water balance, representing a balance in the quantity of water within the hydrological cycle, assesses the current status and trends in water resource availability over a specified area or over the entire Earth (Lozán and Hupfer 2007; Xu and Singh 1998). Precipitation is the input of the water balance and this is later portioned by physical hydrological processes into different water resources on the land such as surface water, soil moisture, groundwater etc, which flow into the oceans and eventually

return to the atmosphere (Oki and Kanae 2006). A general water balance expression of a water tight catchment over a given period is (Verstraeten et al. 2008; Zeng et al. 2012):

$$\Delta S = P - E - R \quad (1.1)$$

where P is precipitation; E is evapotranspiration; R is runoff; ΔS is the change in terrestrial water storage (Fig.1.2).

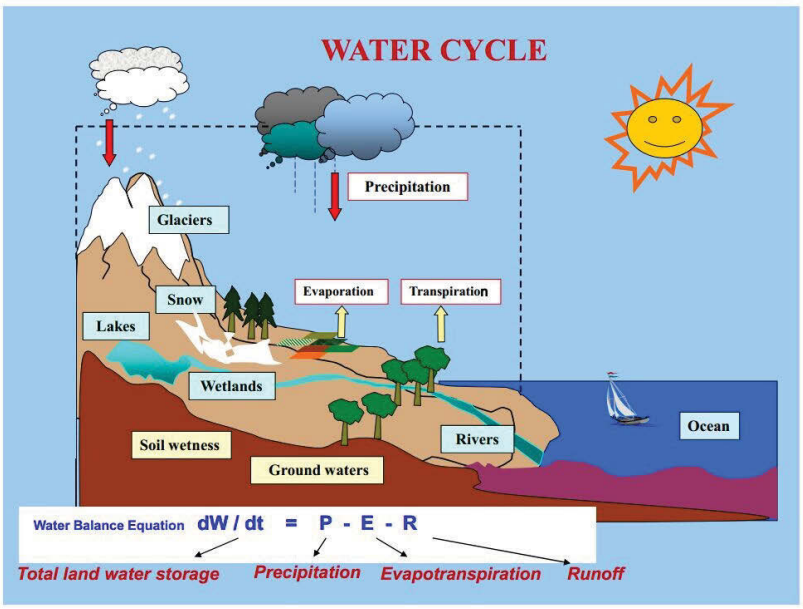

Figure 1.2. Water balance in hydrological cycle (USCCGRP)

1.1.2 Ecosystems and their interactions with water resources

An ecosystem is a community of interacting biologies (e.g. plants, animals and organisms) in a given area in conjunction with the non-living or abiotic environment (e.g. air, water and mineral soil) (Levin 1998). Ecosystems can be of any size and many types such as: wetlands, forests and grasslands or even the entire planet, in which these biotic and abiotic components are linked together through nutrient cycles and energy flows (Lavorel and Garnier 2002). Vegetation plays a key role in ecosystems and are involved in various global biogeochemical cycles (e.g. water, carbon and nitrogen cycles).

On one hand, ecosystems interact with all sorts of water sources (e.g. surface water, soil moisture and groundwater) to maintain their structure, function and biodiversity. Thus, a healthy and active ecosystem ultimately depends on the continued availability

and quality of water. On the other hand, ecosystems lie at the heart of the global water cycle, offering services to mitigate the extremes of drought and flood (Fig.1.3). As a result, recognizing the water cycle as a biophysical process is essential for achieving sustainable ecohydrological management (Cosgrove 2012).

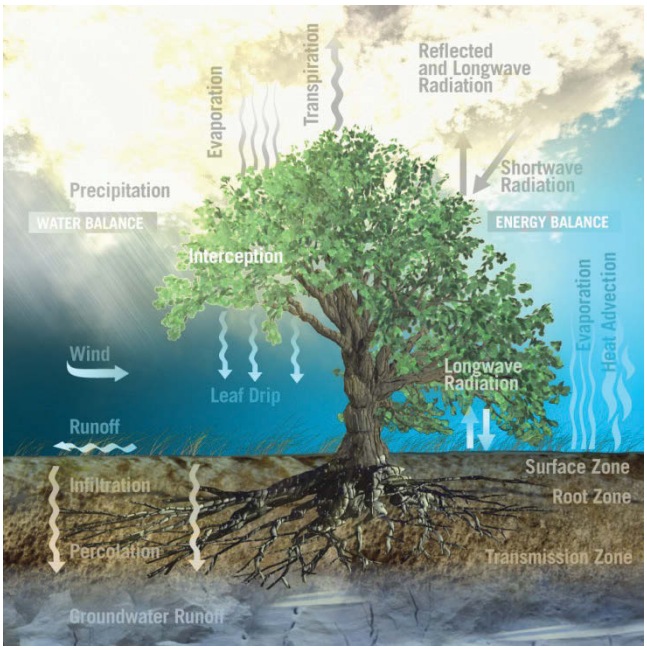

Figure 1.3. Interactions between ecosystems and water resources (ESA/AOES Medialab)

1.1.3 Climate change and intensifying hydrological cycle

"Climate change" refers to changes in the global environment that may alter the capacity of the Earth to sustain life. Global warming is one of the most significant and apparent recent climate changes, which has been identified as being mostly due to anthropogenic activities (Karl and Trenberth 2003; Ramanathan et al. 2001). Since the term "global warming" was first used in 1975 (Broecker 1975), it has become one of the hottest scientific topics among scientists seeking its causes and impacts. Starting from the early 20th century, the global Earth surface temperature has risen about 0.8 °C, with two-thirds of the increase occurring since 1980 (Carnesale and Chameides 2011).

One of the important consequences of global warming is an intensifying global water cycle over the past few decades (Chou et al. 2013). This intensification of the hydrological cycle is mainly shown in terms of increasing atmospheric water vapour content and precipitation, which eventually results in wet regions around the world getting wetter and dry regions drier (Allan et al. 2010; Held and Soden 2006; John et al.

2009; Knutson and Manabe 1995; Li et al. 2011; Wentz et al. 2007). There are good physical reasons for this. In a warmer climate, the moisture content of the troposphere is likely to increase, governed by the Clausius-Clapeyron expansion with a relative humidity that tends to change less strongly (Trenberth and Stepaniak 2003). This results in an increased water vapour concentration in the lower troposphere. Over climatologically wet regions dominated by an ascending motion, the upward motion induces positive anomalies of moisture convergence which finally enhances precipitation. Vice versa, the downward motion flow over climatologically dry regions causes negative anomalies of moisture convergence, which slows the processes for producing precipitation (Chou and Lan 2012). Apart from the physical basis, the tendency for moist regions to become wetter while dry regions become drier in response to global warming has also been captured by both models and observations (Allan and Soden 2008; Lenderink and Van Meijgaard 2008). This effect is often termed as the "rich-get-richer mechanism" (Emori and Brown 2005; Held and Soden 2006) or the "thermodynamic contribution" (Chou and Neelin 2004; Chou et al. 2009).

1.1.4 Increasing hydroclimatic extreme events

Hydroclimatic extreme events, commonly known as floods and droughts (Shelton 2009), often lead to changes in water-resource availability, and cause adverse impacts on health, survival, infrastructure, communities and ecosystems (Meehl et al. 2005; Meehl et al. 2007). To date, hydroclimatic events are still poorly understood, and robustly planning for and preventing them remains a challenge.

Climate changes, such as global warming, have intensified the global hydrological cycle by adding more moisture to the warmer air. This has led to rising rates of global precipitation, evaporation, and freshwater discharge, which resulted in more extreme flooding events occurring over wet areas while increasingly common mega-droughts over dry regions have occurred (Famiglietti and Rodell 2013). Being forced by anthropogenic greenhouse gases, the problem is only going to get worse over time (Stocker et al. 2013).

Based on ocean salinity measurements gathered around the world over the years 1950 – 2000, recent study showed that ocean salinity patterns revealed a strong intensification of global hydrological cycle in response to global warming (Durack et al.

2012). Moreover, this study observed robust evidence of the intensifying global hydrological cycle at a rate of 8 ± 5% per degree of surface warming, which is double the response projected by current climate models (Meehl et al. 2005). This phenomenon was shown to be particularly significant in the waters surrounding Australia, southern Africa and western South America, indicating future increasing hydroclimatic events for places like Australia (Durack et al. 2012), which has already been experiencing increased episodes of droughts and flooding over the last few decades.

1.2 Australian ecohydrology

Australia has a vast land area, encompassing a wide range of ecological and hydroclimatic conditions. Recent studies suggested that Australia is expected to experience an increasing frequency and intensity of hydroclimatic extreme events, during which variations in Australian ecohydrology often play an important role in the inter-annual fluctuations of the global carbon and water cycles (Boening et al. 2012; Bastos et al. 2013; Fasullo et al. 2013; Poulter et al. 2014).

Australia, with a land area of 7.69 million km², accounts for five per cent of the world's land mass and is the planet's sixth largest country after Russia, Canada, China, the USA, and Brazil (Geoscience Australia 2009). It is the smallest of the world's continents and also the lowest, the flattest and the driest inhabited continent (Johnson 2004). Australia consists of six states (Fig.1.4): New South Wales (NSW), Queensland (QLD), South Australia (SA), Tasmania (TAS), Victoria (VIC) and Western Australia (WA), and two major mainland territories (Fig.1.4): the Australian Capital Territory (ACT) and the Northern Territory (NT).

Figure 1.4. Australia states map

1.2.1 Hydrogeology and soil

Australia is one of the oldest continents geologically and has become the flattest land mass on earth through millions of years of erosion (Fig.1.5 A). It is home to rocks dating from more than 3000 million years while others are the result of volcanic activities that continued up to only a few thousand years ago (Geoscience Australia 2010). Australia was shaped by tectonic Earth movements and long-term changes in sea level, and most of its landforms are the result of prolonged erosion by wind and water. Around half of Australia's rivers drain inland and often end in ephemeral salt lakes, with very long historical drainage patterns. Some individual valleys have maintained their position for millions of years (Geoscience Australia 2010).

The soils constitute one of the greatest natural resources for humans and ecosystems in Australia. They are mainly composed of weathered rocks, forming on sorted sediments in sand sheets, dune fields and riverine plains (Fig.1.5 B). Soils spread over the continent under various climatic conditions, mostly lying in the alpine zones of south-eastern Australia and Tasmania, through the Mediterranean zones of south-western and southern Australia and the wet and dry tropics of Queensland, to the very low rainfall areas of the centre (Northcote 1960-1968). Due to the low and unreliable rainfall, soils in most of the arid to semi-arid regions over outback Australia are not suitable for arable agriculture or sown pasture. The surface and underground water resources of the areas are very low or saline, making irrigation impossible (Isbell et al. 1997).

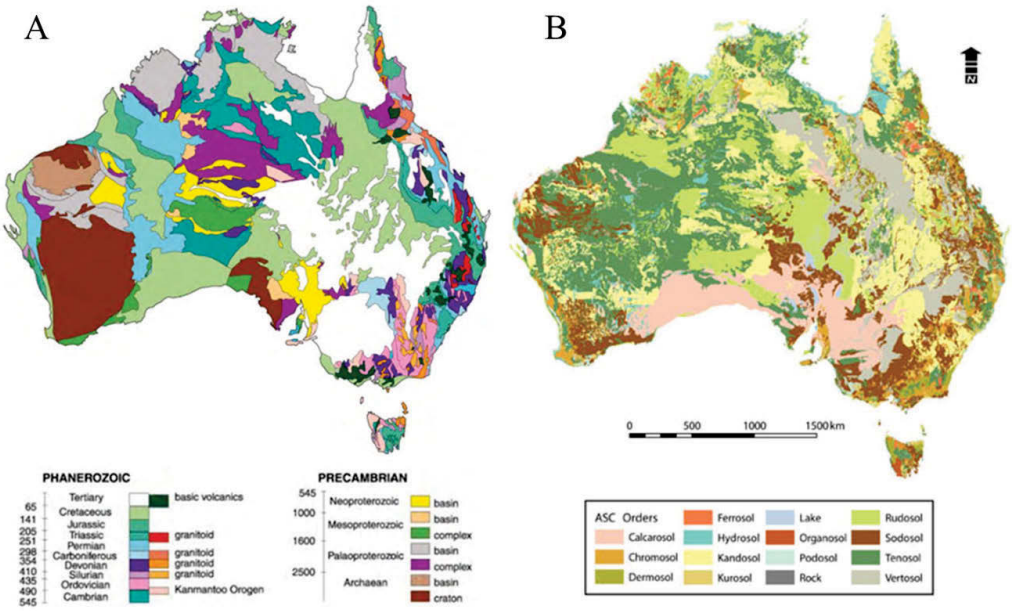

Figure 1.5. (A) Basic geological regions of Australia based on age (Geoscience Australia). (B) Australian Soil Classification map (Northcote 1960-1968).

1.2.2 Climate drivers

Australia is characterized by extreme climate variability driven by multiple large-scale climate modes (Fig. 1.6), among which the three dominant ocean-atmosphere systems are: the El Niño-Southern Oscillation (ENSO), the Indian Ocean Dipole (IOD) and the Southern Annular Mode (SAM) (Cai et al. 2011; Meyers et al. 2007; Risbey et al. 2009). The Intergovernmental Panel on Climate Change (IPCC) concluded that global warming is expected to increase the frequency of extreme climatic events associated with these three climate modes in the 21st century (Rogelj 2013). Moreover, recent study found that when the three climate modes synchronise, the interaction amongst them will bring more than the effect of any single mode, causing extreme drought or flooding across Australia (Cleverly et al. 2016).

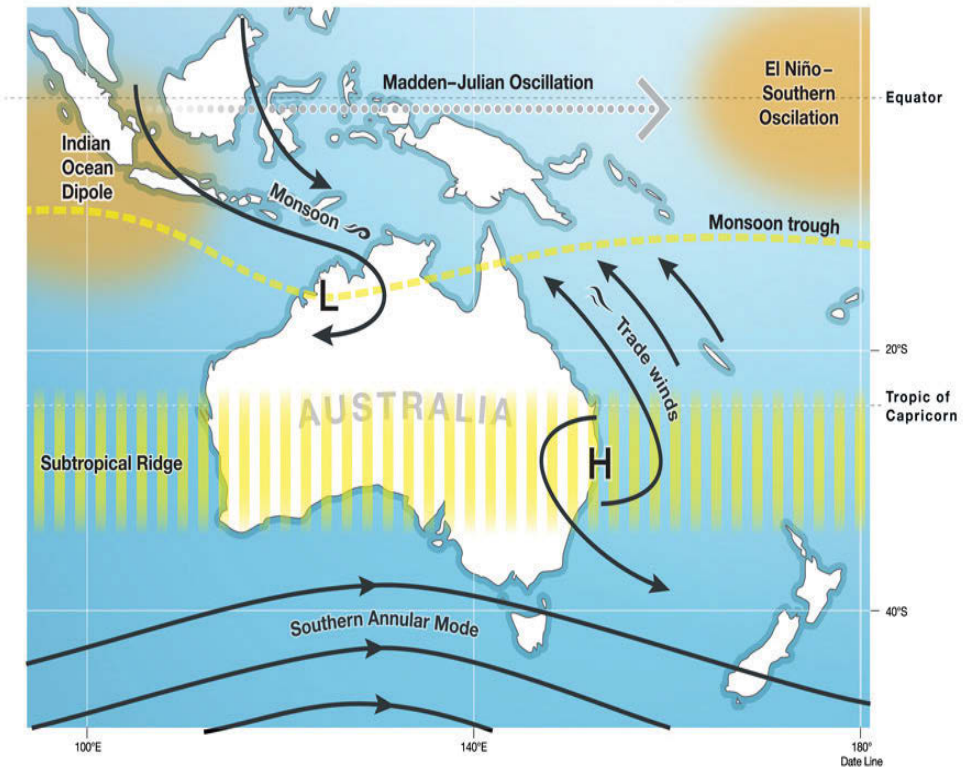

Figure 1.6. The main climate drivers of rainfall variability in the Australian region (BOM).

1.2.3 Climate of Australia

Australia experiences a variety of climates due to its vast size and is under the control of various climate modes, within generally six climatic zones (Fig.1.7 A), including (BOM 2001):

1) Temperate zone: covers the coastal hinterland of New South Wales, much of Victoria, Tasmania and the south-eastern corner of South Australia;

2) Desert zone: arid/semi-arid areas of outback Australia, stretching across the South Australia and Western Australia, far south-western Queensland and north-western corner of New South Wales and part of the Northern Territory.

3) Grasslands (or savanna) zone: is a belt-like area surrounding the desert zone areas in the center with additional small part in the middle of the Northern Territory.

4) Equatorial zone: the far tip of Queensland.

5) Tropical zone: parts of the Western Australia, Northern Territory and Queensland ranging from 10 ~ 15˚S.

6) Mediterranean (or sub-tropical) zone: the coastal and inland fringe along the Queensland coast and the coastal fringe south of Western Australia.

The seasons in the Temperate, Grassslands and Desert zones are (Reid 1995): Spring (September to November), Summer (December to February), Autumn (March to May) and Winter (June to August) while there are only two seasons (dry and wet) in the Equatorial, Tropical and Mediterranean zones: Dry (April to October) and Wet (November to March).

Australia is the driest continent apart from Antarctica, with average annual rainfall below 600 mm over 80% of the continent, and below 300 mm over 50% (Fig.1.7 B). Rainfall is distributed unevenly across Australia; some places in the desert area of Australia receive less than 100 mm rainfall annually while some areas in far North Queensland coast can have rainfall exceeding 4000 mm a year. The dryness of the Australian landmass is mainly attributed to four factors: shape of the landmass, low elevation of landforms, cold ocean currents off the west coast and the dominance of high-pressure systems (Nicholls et al. 1997). Previous studies indicated that average rainfall has slightly increased since 1900 but with strong spatial variation of increases in northern Australia and declines in southern regions (CSIRO and BOM 2014).

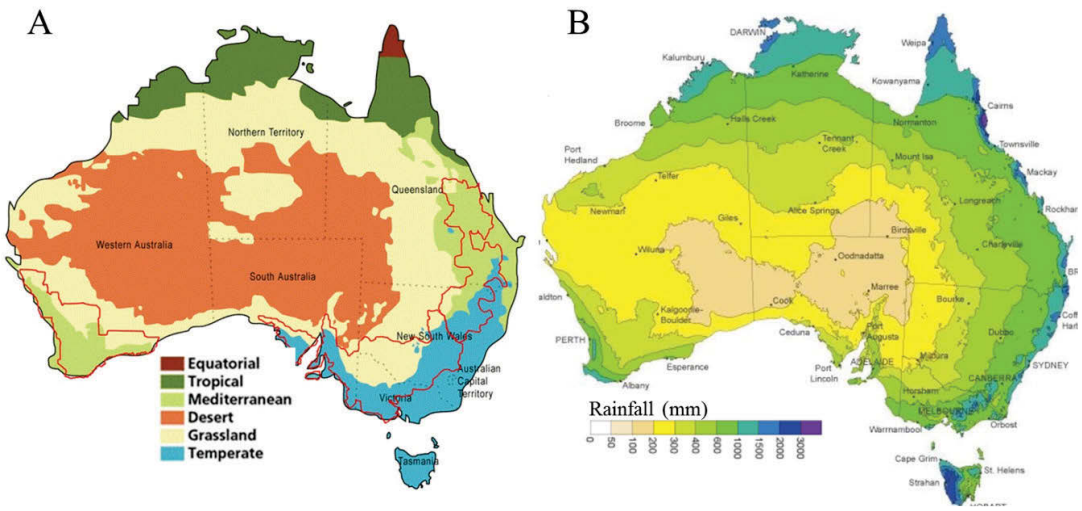

Figure 1.7. (A) Major climatic zones of Australia with red polygon highlighting the Agriculture areas (BOM). (B) Mean annual precipitation over 1961-1990 (BOM).

1.2.4 Land cover type

Australia, well-known for its relatively low vegetation cover globally, has undergone enormous land-use changes since human settlement, resulting in increases in deforestation and forest degradation (Bradshaw 2012). In order to identify the land cover types of Australia and build the associated land use management systems (e.g. land use types, irrigated areas, deforestation and regrowth forest), the Dynamic Land Cover Dataset (DLCD) was developed by Geoscience Australia and the Bureau of Agricultural and Resource Economics and Sciences (Lymburner et al. 2011). This Australian land cover classification system (Fig.1.8) shows that Grasslands are the dominant feature of Australia's landscapes, covering more than one third of the land area. Tree dominated landscapes (e.g. open and sparse tree cover classes) comes second, accounting for slightly less than 30% of Australia's land area. Shrub dominated landscapes take up around one fifth of the continent, with an area of almost 1.6 million square kilometres in total.

Agriculture, including irrigated and rain-fed cropping and pastures, cover less than 10% of Australia's land area and are mainly located in areas with climates ranging from tropical to temperate and Mediterranean-style (e.g. north-eastern, south-eastern and south-western parts of Australia). The remaining areas include: fresh and salt lakes, wetlands, and urban areas occupy approximately 1.5% of Australia's land area. The intensity of human activities in Australia is much lower than those in other countries (Sanderson et al. 2002), with most impact centred in urban and agricultural areas. Even in large croplands, irrigation and river extraction activities are not intensive with rain-fed cropland accounting for more than 95% (NLWRA 2001).

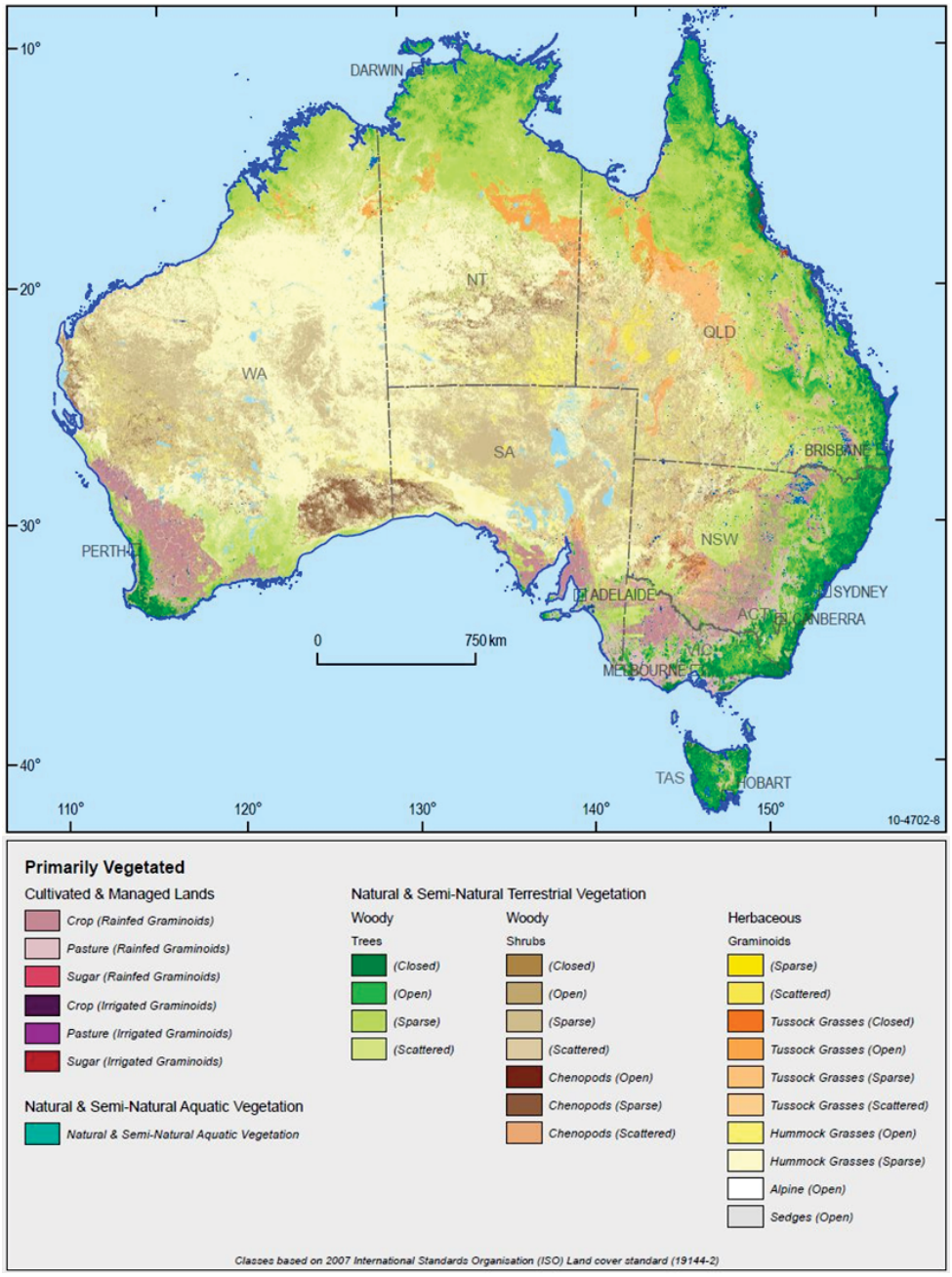

Figure 1.8. Australia Land Cover Map compiled from the National Dynamic Land Cover Dataset from 2000 – 2008 (Lymburner et al. 2011).

1.2.5 Natural hazards

Natural hazards and disasters commonly caused by extreme climatic events across Australia are (Steffen et al. 2013):

1) Bushfires: Bushfires in Australia are common and frequent, particularly during the summer months. They have been active and increasing in southern NSW, Victoria, Tasmania and parts of South Australia, over the last 30 years (Hennessy et al. 2005).

2) Flooding: Rainfall distribution in Australia is extremely uneven. Eastern and north-eastern tropical areas of Australia receive high levels of rainfall each year. During La Niña years, the heavy rain in these areas often creates damaging floods (Heberger 2011).

3) Drought: Studies indicate that mega-drought occurs in some parts of Australia on average once every 18 years (Australian Bureau of Agricultural 2012). Some droughts are long lived while others are short and intense, but both causing significant damage. Droughts can be both continental and localised and are sometimes, but not always, related to El Niño events, making drought forecasting very difficult.

4) Cyclones: Australia is attacked by tropical cyclones primarily between December and April but sometimes from November to May. Cyclones are most likely to occur in northern Australia, in particular, between Broome and Exmouth. Severe cyclones can cause billions of dollars of damage and many deaths (Kuleshov et al. 2008).

The frequency of extreme climatic events has been increasing over the last four decades due to greenhouse warming, and is likely to increase in future, which may exert substantial ecological and hydrological impacts on Australia (Cai et al. 2014a; IPCC 2014).

1.3 Australia's recent hydroclimatic extremes and their impacts

Australia is a land of extremes, and famous for both droughts and floods. This has been truer than ever in the 21st century. Since 2000, Australia has experienced three large-scale hydroclimatic extremes, including a decadal millennium drought from 2001 to 2009 (termed the 'big dry'), followed by a short wet pulse (termed the 'big wet') during 2010 and 2011, and another continent-wide dry condition in 2015. The 'big dry' led to a reduction of more than half of the water storage for mainland capital cities and severe declines in agricultural production (Steffen et al. 2013). It also had adverse impacts on ecosystems, which suffered from reduced water availability and natural disasters such as frequent bushfires (Van Dijk et al. 2013). Overall, since 2001 the Australian Federal Government had provided $4.5 billion AUD in drought assistance.

The following 'big wet' caused widespread flooding over most of eastern Australia, which affected at least 70 towns and more than 200,000 people with a total economic loss estimated to be around $2.38 billion AUD (Heberger 2011). 2015 was ranked as Australia's fifth hottest year on record with a September-October rainfall of just 17 mm - the third lowest total on record. This 2015 El Niño event eventually became the seventeenth of the 26 big El Niño events since 1900 that have brought catastrophic bushfires historically to Victoria, Tasmania and South Australia and severe drought in Queensland (David Jones 2016). Moreover, it may also be related to the devastating Great Barrier Reef coral bleaching (Terry Hughes et al. 2016) and the concurrent dieback of mangroves in Queensland's Gulf Country (Norm Duke and Wild 2016). The world's weather was reported to be on a highly unpredictable path of extremes which may continue to 2016-17 (Hannam 2016). Recent study suggested that the number of El Niño and La Niña years may stay the same with climate change, but the frequency of ENSO-related catastrophic weather events affecting Australia are likely to quadruple this century if greenhouse gas emissions remain on a rising trajectory (Cai et al. 2015).

1.4 Overview of literature

Climate change leads to anomalous behaviour in climate modes, increasing the frequency and severity of hydroclimatic events (Cai et al. 2014a; IPCC 2014). Recent evidence demonstrated that variations in Australia's ecohydrology under hydroclimatic extremes play an increasingly important role in the inter-annual variability of the global carbon and water cycles (Bastos et al. 2013; Boening et al. 2012; Fasullo et al. 2013; Poulter et al. 2014).

1.4.1 Hydrological studies

Numerous studies have focused on the hydrological impacts of the 'big dry', particularly over south-eastern Australia where one of the most important drainage basins – the Murray-Darling Basin (MDB) is located (Kirby et al. 2012; Leblanc et al. 2011; Leblanc et al. 2009; Van Dijk et al. 2013). The MDB is commonly called the “bread basket” because it accounts for about 30% of the gross value of Australia's agricultural production (Liu et al. 2015). Besides the agricultural land in the basin (~67%

for pasture and cropping), 32% of the MDB is covered by native forest that provides home for many important animal species (Koehn 2015).

Leblanc et al. (2009) found the multi-year drought led to an almost complete drying of surface water and significant groundwater depletion over the MDB. The following 2010-11 'big wet' watered the MDB but at some places in the basin only the surface water was replenished instead of groundwater (Leblanc et al. 2011; Tulbure et al. 2016). In addition, there were also studies conducted on the impacts of the prolonged drought and intensive wet period on ecosystems, economy, and society over this region (Kirby et al. 2012; Steffen et al. 2013; Van Dijk et al. 2013). The 'big dry', previously considered as a localized drought over southeast Australia (Leblanc et al. 2009; Ummenhofer et al. 2009), was later proven to be a continent-wide event (Heberger 2011; McGrath et al. 2012). McGrath et al. (2012) showed a pronounced reduction in water storage and rainfall across broad areas of Australia during the drought, particularly over north-western Australia. By contrast, the La Niña induced 'big wet' brought record-breaking rains in 2010-2011 and triggered a global land carbon sink anomaly, of which more than half was attributed to Australia's ecosystems (Ahlström et al. 2015; Poulter et al. 2014). The dramatic increase in rainfall from this La Niña event also resulted in a recorded global sea-level drop (Boening et al. 2012; Fasullo et al. 2013).

1.4.2 Ecological studies

Australia's recent large-scale drought and flooding events provide unique opportunities to understand ecosystem responses to hydroclimatic extremes. Studies have been carried out to investigate the impacts of hydrological variations on intra and inter-annual variability in surface greenness over Australia during the 'big dry' and 'big wet' (Broich et al. 2014; McGrath et al. 2012). Yang et al. (2014) did the first study on direct use of Total Water Storage Anomaly (TWSA) data derived from the Gravity Recovery and Climate Experiment twin satellites (GRACE), to examine hydrological controls on temporal variability in vegetation during the 'big dry'. They found the GRACE-TWSA is a valuable indicator for surface greenness dynamics especially during hydroclimatic periods, which sometimes cannot be captured by conventional hydrological indicators, such as precipitation and soil moisture (Yang et al. 2014). A recent study of Ma et al. (2015) observed abrupt shifts in phenology and vegetation productivity under the climate extremes, with widespread reductions or collapse in the

normal patterns of seasonality over south-eastern Australia. They further found that semi-arid ecosystems exhibit the largest sensitivity to hydroclimatic variations among other ecosystems (Ma et al. 2015). This demonstrates that ecosystems in arid or semi-arid areas, like over most parts of Australia, are particular vulnerable to hydroclimatic extremes (Huete 2016).

1.4.3 Climatological studies

Australia's wild 21st century hydroclimatic events, including a protracted drought period, a dramatic wet pulse and another anomalous El Niño event in 2015, were mostly attributed to the variations in climate systems and their interactions.

The 'big dry' event is of continental scale but the concurrent droughts over different areas of Australia were due to various reasons. For example, the drought in south-eastern Australia was attributed to a significant lack of the "negative" phase of the Indian Ocean Dipole (IOD) in conjunction with increased air temperature (Ummenhofer et al. 2009). In comparison, the dry event over north-western Australia was mainly caused by the decrease in tropical cyclone frequency (McGrath et al. 2012; Nott 2011), which is the major source of the water for this region (Cullen and Grierson 2007). Moreover, the large reduction in rainfall over south-western Australia was a result of the combination of long-term positive IOD and upward Southern Annular Mode (SAM) trend during winter (Cai et al. 2014c). Previous studies based on climate models suggested that the Australian Millennium Drought was generally attributed to natural variability in climate systems (Ummenhofer et al. 2011). However, recent study showed that the late 20th century changes in climate modes were also partly due to anthropogenic greenhouse warming, which significantly influenced many regional rainfalls over Australia, causing droughts like 'big dry' (Cai et al. 2015).

Although the 2010-11 'big wet' was mostly attributed to one of the strongest La Niña events in the past nine decades (BOM 2012; Nicholls 2011), recent studies showed that it was also partly explained by a concurrent extreme positive excursion of SAM particularly over regional areas (Hendon et al. 2014). SAM was estimated to have accounted for around 10% of the 'big wet' rainfall anomaly over eastern Australia and more than 40% along the east-central coastal regions in 2010 (Lim and Hendon 2015).

The annual climate report from the Bureau of Meteorology (BOM) demonstrated the fifth hottest year on record of Australia made 2015 another drought period, which was mostly caused by a strong El Niño event concurrent with a positive phase of IOD and seasonal effects from SAM (Scott Power 2016).

Australian weather and climate have been demonstrated to generally be a result of interactions among various climate systems rather than the effect of any single climate mode (Risbey et al. 2009). The synchronization of the climate modes especially the three major ones influencing Australia – ENSO, IOD and SAM, will often bring more than the effect of any single mode on rainfall/TWS, causing extreme dry or wet hydroclimatic events across Australia (Cleverly et al. 2016).

1.5 Gravity recovery and climate experiment satellites

Despite the recent extreme hydroclimatic impacts, 1) the spatial partitioning and temporal evolution of water resources across Australia, 2) the resilience of ecosystems to the highly variable water regimes and large-scale hydrological fluctuations and 3) the associations between ecohydrological dynamics and the extreme climate variability remain largely unknown. In this thesis, we addressed these issues by applying the Remote Sensing (RS) technique, which with multi-sensor systems of various spatial resolutions and physical properties, can provide an unparalleled way to monitor important land surface dynamics and characteristics over the long-term and at broad scales. In particular, my PhD study highlights the application of GRACE satellites for monitoring ecohydrological dynamics and linking them with climate variability.

1.5.1 Introduction of GRACE

The Gravity Recovery And Climate Experiment (GRACE), launched by NASA and the German Aerospace Centre (DLR), has been making detailed measurements of Earth's gravity field anomalies since March 2002 (Swenson and Wahr 2002). GRACE consists of two identical satellites (nicknamed "Tom" and "Jerry"), one following the other at a distance of about 220 km in a polar orbit around 450 km above the Earth (Fig.1.9). The twin satellites are using a microwave ranging system to accurately measure changes in the speed and separation distance between them which is caused by the gravity variations over different areas over the globe (Tapley et al. 2004a). After

removing the effects of non-gravitational accelerations as detected by on-board accelerometers, the distance measurements can be converted to the gravity anomalies with unprecedented accuracy compared to previous gravitational satellites (Tapley et al. 2004d). Unlike traditional remote sensors that measure electromagnetic emissions in order to infer Earth surface and atmospheric conditions, GRACE is not limited to measurement of atmospheric and near-surface phenomena (Rodell et al. 2009). GRACE has far exceeded its designed five-year lifespan with the spacecraft still working but it has been in a slowly decaying orbit since 2011(NASA 2011). Its successor, GRACE Follow-On mission (GRACE-FO), is scheduled to be launched in August, 2017 by NASA and GeoForschungsZentrum (GFZ) Potsdam (JPL 2014). The orbit and the design of GRACE-FO will be similar to GRACE but the distance between the two spacecraft of GRACE-FO will be measured by lasers instead of the original microwave ranging system (GFZ 2016).

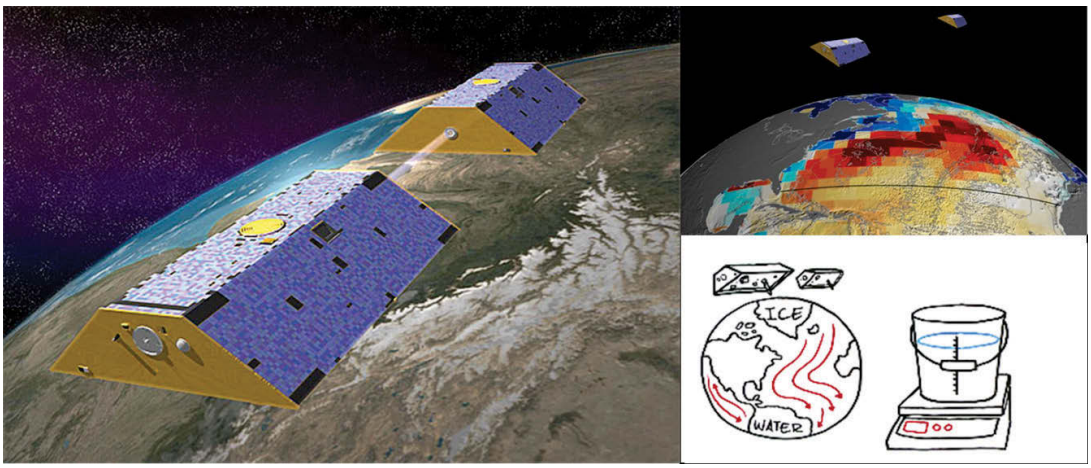

Figure 1.9 The GRACE space gravity mission (JPL, NASA)

1.5.2 Total Water Storage Anomaly (TWSA) data

GRACE is like a giant scale in the sky, measuring the weight (gravity) changes of the Earth periodically (Fig.1.9). Within a given region, the change in mass due to rising or falling water resources (eg. Groundwater, soil moisture and surface water etc) influences the strength of the local gravitational attraction. Therefore, by measuring gravity regionally, GRACE reveals how much a region's water storage changes over time (Famiglietti and Rodell 2013). With the unique relationship between variations in the gravity field and changes in mass at the Earth's surface (Chen et al. 2005; Wahr et al.

2006a), the obtained month-to-month gravity can be inverted for global estimates of vertically integrated terrestrial total water storage anomaly (TWSA), including changes in groundwater, surface water, soil moisture, snow water and biological water (Fig.1.1).

Different gravity-field solutions are produced by various institutions; for this thesis release-5, level-2 TWSA data from three independent GRACE research centres: Jet Propulsion Laboratory (JPL), University of Texas Centre for Space Research (CSR) and the GeoForschungsZentrum (GFZ) Potsdam were averaged to minimize the uncertainties associated with data processing. The ensemble TWSA data has 1° (~110 km) and monthly resolutions, which represents Equivalent Water Height (EWH, in units cm) and includes the following corrections: (1) replacement of C20 (degree 2 order 0) coefficients with the solutions from Satellite Laser Ranging (Cheng and Tapley 2004), (2) removal of noise from the atmosphere and ocean, (3) filtering of north-south striping errors in the global spherical harmonic solutions (Swenson and Wahr 2006a; Tapley et al. 2004a; Zhang et al. 2009), (4) restoration of the energy removed from GRACE data processing using scaling factor (Gent et al. 2011; Long et al. 2015b; Wen-Jian and Hai-Shan 2013).

1.5.3 Scaling factor of TWSA data

The low-pass filtering (i.e., destriping, truncation, and filtering) for removing high-frequency noise in GRACE signal often causes bias and leakage errors in the GRACE-TWSA data. The scaling factor is needed to reduce the errors and crucial for quantifying TWSA before applying the data to resolve any water-related issues (Long et al. 2015b).

The CLM4.0 scaling factor used in this thesis was derived from the NCAR's Community Land Model 4.0 (Gent et al. 2011; Landerer and Swenson 2012; Lawrence et al. 2011). It was the latest updated scaling factor provided by JPL, and was obtained from http://grace.jpl.nasa.gov/data/get-data/monthly-mass-grids-land/(Landerer and Swenson 2012; Swenson and Wahr 2006c) and accounts for the interactions between surface and subsurface water and human activities (e.g., irrigation and river distraction) (Long et al. 2015b).

We concluded and selected CLM4.0 scaling factor as the most appropriate for Australia, considering 1) the relatively uncomplicated hydrological conditions in

Australia (e.g. compared to the Yangtze river basin in Long et al. (2015b)'s paper), where 70% of Australia continent is classified as semi-arid/arid or desert, and more than 95% of Australian agriculture lands are rainfall fed (Jayasuriya 2003) instead of being irrigated, without very intensive human activities; 2) the good performance of the CLM4.0 scaling factor as used in previous GRACE studies for the entire Australian continent (Leblanc et al. 2009; McGrath et al. 2012; Yang et al. 2014). Potential noise and artefacts may be present in CLM 4.0, but this applies to any of the scaling factor products. Other scaling factor products such as LSMs in Global Land Data Assimilation System-1 or PCR-GLOBWB (Global Hydrological Model) also have uncertainties or are not published.

1.5.4 GRACE applications

The periodic measurements of TWS anomalies obtained from GRACE provide hydrologists with the potential to: 1) close the water balance (Famiglietti and Rodell 2013); and 2) to evaluate groundwater variations without costly effort of drilling and instrumenting discrete groundwater bores (Zaitchik et al. 2008). With more than a decade of GRACE observations, long-term trends in terrestrial TWS can now be reliably assessed and compared with hydrological models and standard drought indices.

GRACE observations have revolutionized the ability to monitor mass variability due to a variety of geophysical processes, leading to important discoveries that span the Earth sciences (Tregoning et al. 2012). Originally developed for mass changes in solid Earth (Awange et al. 2011; Tapley et al. 2004a), ice sheets/glaciers (Chen et al. 2006; Velicogna and Wahr 2006) and oceans (Chambers et al. 2004; Tapley et al. 2003), the practical applications of GRACE have been further extended widely into many other fields for 1) detecting groundwater depletion (Castle et al. 2014; Feng et al. 2013; Jiao et al. 2015; Richey et al. 2015a; Richey et al. 2015b; Rodell et al. 2006; Rodell et al. 2009; Scanlon et al. 2012a; Scanlon et al. 2012b; Sun 2013); 2) developing drought indices (Cao et al. 2015; Yirdaw et al. 2008) and monitoring droughts (Borsa et al. 2014; Houborg et al. 2012; Maeda et al. 2015); 3) forewarning pending floods (Reager and Famiglietti 2009; Tangdamrongsub et al. 2016); 4) evaluating water resource changes (Di Long 2013; Jiang et al. 2014; Long et al. 2015a; Swenson et al. 2006); 5) computing large-scale ET (Rodell et al. 2004; Swenson and Wahr 2006a; Zeng et al. 2012); 6)

improving hydrological models and water budget (Lo et al. 2010; Penatti et al. 2015); 7) interpreting surface greenness dynamics (Jones et al. 2014; McGrath et al. 2012; Yang et al. 2014) and so on. GRACE is only accurate enough for quantifying TWS anomalies at a spatial scale of greater than 20 x 10^4 km^2 (footprint), which is limited by the altitude (~450 km) and separated distance (~200 km) of GRACE twin satellites (Wahr et al. 2006b; Zhang et al. 2009). GRACE applications in Australia used to be mainly applied over the Murray-Darling Basin region (Leblanc et al. 2011; Leblanc et al. 2009; Syed et al. 2008) but recently increasing GRACE studies have been conducted for ecohydrological studies over the entire continent (McGrath et al. 2012; Xie et al. 2016a; Xie et al. 2016b; Yang et al. 2014).

1.6 Current issues and corresponding thesis objectives

The overall goal of this thesis was to study the ecohydrological interactions and landscape response to the early 21st century hydroclimatic extremes in Australia. Thesis objectives were addressed using remote sensing and statistical methods, based on a combination of complementary materials, i.e. integrating GRACE-TWSA data with various satellite observations derived from MODIS, TRMM, Landsat, AVHRR; modelling and field datasets, including BOM-rainfall, GLDAS-soil moisture, AWAP-ET and runoff; and other gridded products such as land cover type, soil classification, hydrological maps etc. The current issues and corresponding objectives to address them in this thesis are listed below by chapters;

Chapter 1: This is the introduction to this thesis, in which I firstly described a broad context of hydrological cycles and ecosystems around the world under a changing climate, e.g. global warming. I then provided a comprehensive literature review on the previous ecohydrological and climatological studies of Australia's recent hydroclimatic extremes. Furthermore, I presented current remnant issues Australia is facing and solutions from this thesis. Lastly, I listed the objectives and structure of this PhD thesis.

Chapter 2: Previous studies on Australia's recent hydroclimatic events have mostly focused on the causes of the 'big dry' and the 'big wet', and their impacts on water resources, agriculture and ecosystems separately. Furthermore, these studies treated the 'big dry' and 'big wet' as discrete periods over the entire continent, which is unrealistic considering the diversity of Australia's climate patterns. Less attention has been placed

on the combined spatial and temporal water storage impacts of these hydroclimatic variations. The fate of water resources, such as the loss and recovery of water across different parts of Australia under these drought and wet extremes remains largely unknown. To fill these gaps in current knowledge, I analysed the spatial patterns and temporal dynamics of the total water storage across continental Australia from 2002 to 2014, encompassing large-scale drought and wet extremes. Specifically, I aimed to (1) define the transition date between dry and wet periods on a pixel level; (2) investigate spatially explicit variations in the direction, magnitude, and duration of water drying trends during the 'big dry'; (3) quantify the rate and magnitude of water recovery during the 'big wet'; and (4) spatially partition the combined drying and wetting effects on water storage and relate the resulting patterns to large-scale climate systems.

Chapter 3: Numerous studies have been conducted on the effect of climate modes on precipitation in Australia and globally. However, inconsistencies exist between climate modes and precipitation in historical records. To the best of our knowledge, previous studies have not been conducted directly for assessing the systemic relationships between various climate systems and total water storage (the integrated water, indicating the final water availability). To fill these gaps in current knowledge, I characterised and evaluated the spatial-temporal varying importance of Australia's three major climate modes on water storage and associated ecosystems from 2002 to 2015, encompassing the three recent hydroclimatic extremes. In particular, I aimed to (1) investigate the relative contributions of the three climate modes to the partitioning of the three TWS zones in Australia that were observed in Chapter 2; (2) examine the advantages of using GRACE-TWSA compared to rainfall in assessing the varying extents and fundamental influences from the climate modes on water resources and vegetation; and (3) quantify the ecohydrological implications of the 2015 El Niño event and validate the three-zone-like influences from the climate modes.

Chapter 4: Little attention has been paid to the influences of the large-scale hydroclimatic contexts on local ecological processes such as the vulnerable and important arid wetland ecosystems, which are extensively distributed across Australia. Moreover, the hydrological characteristics and ecological resilience of these arid wetlands to long-term variable hydrological regimes remain largely unknown. To fill these gaps in current knowledge, I examined the hydrological dynamics and ecosystem functioning of the Coongie Lakes arid wetland, the largest Ramsar wetland in Australia.

In particular, I aimed to: (1) investigate spatial-temporal patterns of historical inundation in the Coongie Lakes and their relationship with broad-scale climate modes; (2) quantify vegetation responses to multiple fluctuations between floods and drought conditions; (3) assess the response and resilience of this arid wetland to the early 21st century hydroclimatic extremes; and (4) relate variations in flooding and greening extents to large-scale hydrological drivers (TWS/rainfall).

Chapter 5: I conducted a comprehensive assessment of hydrological dynamics, and the associated changes in ecosystems and their interactions during the consecutive 'big dry' and 'big wet' events. In this chapter, I focussed on a synthesized assessment of the effects that hydroclimatic extremes brought to Australian water resources and ecosystems for improved ecohydrological management and nation-wide protection in Australia. Essentially, I aimed to: (1) investigate the rainfall patterns during the study period and its relationship with TWS; (2) estimate ET, groundwater variations from GRACE-TWSA time series data; (3) monitor the drying and wetting patterns of various water resources; and (4) evaluate the ecological responses to hydrological variations at continental, regional and biome scales respectively.

Chapter 6: This is the final conclusion of this thesis, in which I summarized all the findings from the previous chapters and linked them in an overarching discussion. I also presented the limitations of this thesis and made recommendations for the direction of the future research.

1.7 References

Ahlström, A., Raupach, M.R., Schurgers, G., Smith, B., Arneth, A., Jung, M., Reichstein, M., Canadell, J.G., Friedlingstein, P., & Jain, A.K. (2015). The dominant role of semi-arid ecosystems in the trend and variability of the land CO2 sink. *Science, 348*, 895-899

Allan, R.P., & Soden, B.J. (2008). Atmospheric warming and the amplification of precipitation extremes. *Science, 321*, 1481-1484

Allan, R.P., Soden, B.J., John, V.O., Ingram, W., & Good, P. (2010). Current changes in tropical precipitation. *Environmental Research Letters, 5*, 025205

Australian Bureau of Agricultural (2012). Drought in Australia-Context,policy and management, 28

Awange, J., Fleming, K., Kuhn, M., Featherstone, W., Heck, B., & Anjasmara, I. (2011). On the suitability of the 4× 4 GRACE mascon solutions for remote sensing Australian hydrology. *Remote Sensing of Environment, 115*, 864-875

Bastos, A., Running, S.W., Gouveia, C., & Trigo, R.M. (2013). The global NPP dependence on ENSO: La Niña and the extraordinary year of 2011. *Journal of Geophysical Research: Biogeosciences, 118*, 1247-1255

Boening, C., Willis, J.K., Landerer, F.W., Nerem, R.S., & Fasullo, J. (2012). The 2011 La Niña: So strong, the oceans fell. *Geophysical Research Letters, 39*

BOM (2001). A hundred years of science and service. In. Australia

BOM, A.B.o.M. (2012). Record-breaking La Niña events: An analysis of the La Niña life cycle and the impacts and significance of the 2010–11 and 2011–12 La Niña events in Australia. In

Borsa, A.A., Agnew, D.C., & Cayan, D.R. (2014). Ongoing drought-induced uplift in the western United States. *Science, 345*, 1587-1590

Bradshaw, C.J. (2012). Little left to lose: deforestation and forest degradation in Australia since European colonization. *Journal of Plant Ecology, 5*, 109-120

Broecker, W.S. (1975). Climatic Change: Are We on the Brink of a Pronounced Global Warming? *Science, 189*, 460-463

Broich, M., Huete, A., Tulbure, M., Ma, X., Xin, Q., Paget, M., Restrepo-Coupe, N., Davies, K., Devadas, R., & Held, A. (2014). Land surface phenological response to decadal climate variability across Australia using satellite remote sensing. *Biogeosciences, 11*, 5181-5198

Cai, W., Borlace, S., Lengaigne, M., Van Rensch, P., Collins, M., Vecchi, G., Timmermann, A., Santoso, A., McPhaden, M.J., & Wu, L. (2014a). Increasing frequency of extreme El Niño events due to greenhouse warming. *Nat Clim Change, 4*, 111-116

Cai, W., Purich, A., Cowan, T., van Rensch, P., & Weller, E. (2014c). Did climate change–induced rainfall trends contribute to the Australian Millennium Drought? *Journal of Climate, 27*, 3145-3168

Cai, W., Santoso, A., Wang, G., Yeh, S.-W., An, S.-I., Cobb, K.M., Collins, M., Guilyardi, E., Jin, F.-F., & Kug, J.-S. (2015). ENSO and greenhouse warming. *Nat Clim Change*

Cao, Y., Nan, Z., & Cheng, G. (2015). GRACE Gravity Satellite Observations of Terrestrial Water Storage Changes for Drought Characterization in the Arid Land of North-western China. *Remote Sensing, 7*, 1021-1047

Carnesale, A., & Chameides, W. (2011). America's Climate Choices. *NRC/NAS USA Committee on America's Climate Choices http://download. nap. edu/cart/deliver. cgi*

Castle, S.L., Thomas, B.F., Reager, J.T., Rodell, M., Swenson, S.C., & Famiglietti, J.S. (2014). Groundwater Depletion During Drought Threatens Future Water Security of the Colorado River Basin. *Geophysical Research Letters*

Chahine, M.T. (1992). The hydrological cycle and its influence on climate. *Nature, 359*, 373-380

Chambers, D.P., Wahr, J., & Nerem, R.S. (2004). Preliminary observations of global ocean mass variations with GRACE. *Geophysical Research Letters, 31*

Chen, D., Huang, J., & Jackson, T.J. (2005). Vegetation water content estimation for corn and soybeans using spectral indices derived from MODIS near-and short-wave infrared bands. *Remote Sensing of Environment, 98*, 225-236

Chen, J., Wilson, C., & Tapley, B. (2006). Satellite gravity measurements confirm accelerated melting of Greenland ice sheet. *Science, 313*, 1958-1960

Cheng, M., & Tapley, B.D. (2004). Variations in the Earth's oblateness during the past 28 years. *Journal of Geophysical Research: Solid Earth (1978–2012), 109*

Chou, C., Chiang, J.C., Lan, C.-W., Chung, C.-H., Liao, Y.-C., & Lee, C.-J. (2013). Increase in the range between wet and dry season precipitation. *Nature Geoscience, 6*, 263-267

Chou, C., & Lan, C.-W. (2012). Changes in the annual range of precipitation under global warming. *Journal of climate, 25*, 222-235

Chou, C., & Neelin, J.D. (2004). Mechanisms of global warming impacts on regional tropical precipitation*. *Journal of climate, 17*, 2688-2701

Chou, C., Neelin, J.D., Chen, C.-A., & Tu, J.-Y. (2009). Evaluating the "rich-get-richer" mechanism in tropical precipitation change under global warming. *Journal of climate, 22*, 1982-2005

Cleverly, J., Eamus, D., Luo, Q., Restrepo-Coupe, N., Kljun, N., Ma, X., Ewenz, C., Li, L., & Yu, Q.H., Alfredo (2016). The importance of interacting climate modes on Australia's contribution to global carbon cycle extremes. *Scientific Reports*

Cosgrove, W.J. (2012). *The United Nations World Water Development Report–N° 4–The Dynamics of Global Water Futures: Driving Forces 2011–2050*. UNESCO

CSIRO, & BOM (2014). State of the Climate 2014 *http://www.csiro.au/en/Outcomes/Climate/Understanding/State-of-the-Climate-2014/References.aspx*

Cullen, L.E., & Grierson, P.F. (2007). A stable oxygen, but not carbon, isotope chronology of Callitris columellaris reflects recent climate change in north-western Australia. *Climatic Change, 85*, 213-229

David Jones, A.B.W., Karl Braganza, Scott B. Power (2016). Hasta la vista El Niño – but don't hold out for 'normal' weather just yet. In: The Conversion

Di Long, B.R.S., Laurent Longuevergne,Alexander Y. Sun,D. Nelun Fernando,Himanshu Save (2013). GRACE satellite monitoring of large depletion in water storage in response to the 2011 drought in Texas. *Geophysical Research Letters, 40*, 3395-3401

Durack, P.J., Wijffels, S.E., & Matear, R.J. (2012). Ocean salinities reveal strong global water cycle intensification during 1950 to 2000. *Science, 336*, 455-458

Emori, S., & Brown, S. (2005). Dynamic and thermodynamic changes in mean and extreme precipitation under changed climate. *Geophysical Research Letters, 32*, L17706

Famiglietti, J.S., & Rodell, M. (2013). Water in the Balance. *Science, 340*, 1300-1301

Fasullo, J.T., Boening, C., Landerer, F.W., & Nerem, R.S. (2013). Australia's unique influence on global sea level in 2010–2011. *Geophysical Research Letters*

Feng, W., Zhong, M., Lemoine, J.M., Biancale, R., Hsu, H.T., & Xia, J. (2013). Evaluation of groundwater depletion in North China using the Gravity Recovery and Climate Experiment (GRACE) data and ground-based measurements. *Water Resources Research, 49*, 2110-2118

Gent, P.R., Danabasoglu, G., Donner, L.J., Holland, M.M., Hunke, E.C., Jayne, S.R., Lawrence, D.M., Neale, R.B., Rasch, P.J., & Vertenstein, M. (2011). The community climate system model version 4. *Journal of Climate, 24*, 4973-4991

Geoscience Australia (2009). Australia's size compared. *Retrieved on April, 22*

Geoscience Australia (2010). Australian Landforms and their History. In. Geoscience Australia, http://www.ga.gov.au/scientific-topics/national-location-information/landforms/australian-landforms-and-their-history

GFZ (2016). Development, Operation and Analysis of Gravity Field Satellite Missions. In: Helmholtz Centre Potsdam

Gleick, P.H. (1993). *Water in crisis: a guide to the world's fresh water resources*. Oxford University Press, Inc.

Hannam, P. (2016). Extreme times: world's weather is on a weird track that will continue into 2016. In: The Sydney Morning Herald

Heberger, M. (2011). Australia's Millennium Drought: Impacts and Responses. *The World's Water* (pp. 97-125): Springer

Held, I.M., & Soden, B.J. (2006). Robust responses of the hydrological cycle to global warming. *Journal of climate, 19*, 5686-5699

Hendon, H.H., Lim, E.-P., Arblaster, J.M., & Anderson, D.L. (2014). Causes and predictability of the record wet east Australian spring 2010. *Climate Dynamics, 42*, 1155-1174

Hennessy, K., Lucas, C., Nicholls, N., Bathols, J., Suppiah, R., & Ricketts, J. (2005). Climate change impacts on fire-weather in south-east Australia. *Climate Impacts Group, CSIRO Atmospheric Research and the Australian Government Bureau of Meteorology, Aspendale*

Houborg, R., Rodell, M., Li, B., Reichle, R., & Zaitchik, B.F. (2012). Drought indicators based on model-assimilated Gravity Recovery and Climate Experiment (GRACE) terrestrial water storage observations. *Water Resources Research, 48*

Huete, A. (2016). Ecology: Vegetation's responses to climate variability. *Nature*

IPCC (2014). Climate change 2014: impacts, adaptation, and vulnerability. *Contribution of Working Group II to the Fifth Assessment Report of the Intergovernmental Panel on Climate Change*

Isbell, R.F., McDonald, W.S., & Ashton, L.J. (1997). Concepts and rationale of the Australian soil classification

Jayasuriya, R.T. (2003). Farming systems in Australia. *Australia, NSW Agriculture*

Jiang, D., Wang, J., Huang, Y., Zhou, K., Ding, X., & Fu, J. (2014). The Review of GRACE Data Applications in Terrestrial Hydrology Monitoring. *Advances in Meteorology, 2014*

Jiao, J.J., Zhang, X., & Wang, X. (2015). Satellite-based estimates of groundwater depletion in the Badain Jaran Desert, China. *Scientific Reports, 5*

John, V.O., Allan, R.P., & Soden, B.J. (2009). How robust are observed and simulated precipitation responses to tropical ocean warming? *Geophysical Research Letters, 36*, L14702

Johnson, D. (2004). The geology of Australia. Port Melbourne. In: Victoria: Cambridge University Press

Jones, M.O., Kimball, J.S., & Nemani, R.R. (2014). Asynchronous Amazon forest canopy phenology indicates adaptation to both water and light availability. *Environmental Research Letters, 9*, 124021

JPL (2014). Gravity Recovery and Climate Experiment Follow On - Launch Vehicle. In: NASA

Karl, T.R., & Trenberth, K.E. (2003). Modern global climate change. *Science, 302*, 1719-1723

Kirby, M., Connor, J., Bark, R., Qureshi, E., & Keyworth, S. (2012). The economic impact of water reductions during the Millennium Drought in the Murray-Darling Basin. In, *AARES conference* (pp. 7-10)

Knutson, T.R., & Manabe, S. (1995). Time-mean response over the tropical Pacific to increased C02 in a coupled ocean-atmosphere model. *Journal of climate, 8*, 2181-2199

Koehn, J. (2015). Managing people, water, food and fish in the Murray–Darling Basin, south-eastern Australia. *Fisheries Management and Ecology, 22*, 25-32

Kuleshov, Y., Qi, L., Fawcett, R., & Jones, D. (2008). On tropical cyclone activity in the Southern Hemisphere: trends and the ENSO connection. *Geophysical Research Letters, 35*

Landerer, F., & Swenson, S. (2012). Accuracy of scaled GRACE terrestrial water storage estimates. *Water Resources Research, 48*, W04531

Lavorel, S., & Garnier, E. (2002). Predicting changes in community composition and ecosystem functioning from plant traits: revisiting the Holy Grail. *Functional ecology, 16*, 545-556

Lawrence, D.M., Oleson, K.W., Flanner, M.G., Thornton, P.E., Swenson, S.C., Lawrence, P.J., Zeng, X., Yang, Z.L., Levis, S., & Sakaguchi, K. (2011). Parameterization improvements and functional and structural advances in version 4 of the Community Land Model. *Journal of Advances in Modeling Earth Systems, 3*, 1-27

Leblanc, M., Tweed, S., Ramillien, G., Tregoning, P., Frappart, F., Fakes, A., & Cartwright, I. (2011). Groundwater change in the Murray basin from long-term in situ monitoring and GRACE estimates. *Climate change effects on groundwater resources: A global synthesis of findings and recommendations CRC Press, November, 22*, 169-187

Leblanc, M.J., Tregoning, P., Ramillien, G., Tweed, S.O., & Fakes, A. (2009). Basin-scale, integrated observations of the early 21st century multiyear drought in southeast Australia. *Water Resources Research, 45*, W04408

Lenderink, G., & Van Meijgaard, E. (2008). Increase in hourly precipitation extremes beyond expectations from temperature changes. *Nature Geoscience, 1*, 511-514

Levin, S.A. (1998). Ecosystems and the biosphere as complex adaptive systems. *Ecosystems, 1*, 431-436

Li, L., Jiang, X., Chahine, M.T., Olsen, E.T., Fetzer, E.J., Chen, L., & Yung, Y.L. (2011). The recycling rate of atmospheric moisture over the past two decades (1988–2009). *Environmental Research Letters, 6*, 034018

Lim, E.-P., & Hendon, H.H. (2015). Understanding and predicting the strong Southern Annular Mode and its impact on the record wet east Australian spring 2010. *Climate Dynamics, 44*, 2807-2824

Liu, Y., Langemeier, M., Small, I., Joseph, L., & Fry, W. (2015). Risk management strategies using potato precision farming technology. In, *Agricultural & Applied Economics Association Annual Meeting*

Lo, M.H., Famiglietti, J.S., Yeh, P.F., & Syed, T. (2010). Improving parameter estimation and water table depth simulation in a land surface model using GRACE water storage and estimated base flow data. *Water Resources Research, 46*

Long, D., Longuevergne, L., & Scanlon, B.R. (2015a). Global analysis of approaches for deriving total water storage changes from GRACE satellites. *Water Resources Research, 51*, 2574-2594

Long, D., Yang, Y., Wada, Y., Hong, Y., Liang, W., Chen, Y., Yong, B., Hou, A., Wei, J., & Chen, L. (2015b). Deriving scaling factors using a global hydrological model to restore GRACE total water storage changes for China's Yangtze River Basin. *Remote Sensing of Environment, 168*, 177-193

Lozán, J.L., & Hupfer, P.M. (2007). *Global change: enough water for all?*

Lymburner, L., Tan, P., Mueller, N., Thackway, R., Thankappan, M., Islam, A., Lewis, A., Randall, L., & Senarath, U. (2011). Land Cover Map of Australia, 1st ed., Scale 1:5 000 000. In. Canberra: GeoScience Australia

Ma, X., Huete, A., Moran, S., Ponce-Campos, G., & Eamus, D. (2015). Abrupt shifts in phenology and vegetation productivity under climate extremes. *Journal of Geophysical Research: Biogeosciences, 120*, 2036-2052

Maeda, E.E., Kim, H., Aragão, L.E., Famiglietti, J.S., & Oki, T. (2015). Disruption of hydroecological equilibrium in southwest Amazon mediated by drought. *Geophysical Research Letters, 42*, 7546-7553

McGrath, G.S., Sadler, R., Fleming, K., Tregoning, P., Hinz, C., & Veneklaas, E.J. (2012). Tropical cyclones and the ecohydrology of Australia's recent continental-scale drought. *Geophysical Research Letters, 39*

Meehl, G.A., Arblaster, J.M., & Tebaldi, C. (2005). Understanding future patterns of increased precipitation intensity in climate model simulations. *Geophysical Research Letters, 32*

Meehl, G.A., Stocker, T.F., Collins, W.D., Friedlingstein, P., Gaye, A.T., Gregory, J.M., Kitoh, A., Knutti, R., Murphy, J.M., & Noda, A. (2007). Global climate projections. *Climate change, 2007*, 3-4

NASA (2011). GRACE Orbit Lifetime Prediction. In: NASA

Nicholls, N. (2011). What caused the eastern Australia heavy rains and floods of 2010/11. *Bull Aust Meteorol Oceanogr Soc, 24*, 33-34

Nicholls, N., Drosdowsky, W., & Lavery, B. (1997). Australian rainfall variability and change. *Weather, 52*, 66-72

NLWRA (2001). Australian Agriculture Assessment 2001. National Land and Water Resources Audit – Volumes 1 and 2, Commonwealth of Australia, Canberra, Australia

Norm Duke, & Wild, K. (2016). 'Shocking images' reveal death of 10,000 hectares of mangroves across Northern Australia. In: ABC News

Northcote, K.H., with Beckmann, G. G., Bettenay, E., Churchward, H. M., Van Dijk, D. C., Dimmock, G. M., Hubble, G. D., Isbell, R. F., McArthur, W. M., Murtha, G. G., Nicolls, K. D., Paton, T. R., Thompson, C. H., Webb, A. A. and Wright, M. J (1960-1968). *Atlas of Australian Soils, Sheets 1 to 10*. Melbourne: CSIRO and Melbourne University Press

Nott, J. (2011). A 6000 year tropical cyclone record from Western Australia. *Quaternary Science Reviews, 30*, 713-722

Oki, T., & Kanae, S. (2006). Global hydrological cycles and world water resources. *science, 313*, 1068-1072

Pagano, T.C., & Sorooshian, S. (2006). *Global water cycle (fundamental, theory, mechanisms)*. Wiley Online Library

Penatti, N.C., de Almeida, T.I.R., Ferreira, L.G., Arantes, A.E., & Coe, M.T. (2015). Satellite-based hydrological dynamics of the world's largest continuous wetland. *Remote Sensing of Environment, 170*, 1-13

Poulter, B., Frank, D., Ciais, P., Myneni, R.B., Andela, N., Bi, J., Broquet, G., Canadell, J.G., Chevallier, F., & Liu, Y.Y. (2014). Contribution of semi-arid ecosystems to interannual variability of the global carbon cycle. *Nature, 509*, 600-603

Ramanathan, V., Crutzen, P., Kiehl, J., & Rosenfeld, D. (2001). Aerosols, climate, and the hydrological cycle. *Science, 294*, 2119-2124

Reager, J., & Famiglietti, J. (2009). Global terrestrial water storage capacity and flood potential using GRACE. *Geophysical Research Letters, 36*, L23402

Reid, A.J. (1995). Banksias and Bilbies:Seasons of Australia. In. Moorabin, Victoria

Richey, A.S., Thomas, B.F., Lo, M.H., Famiglietti, J.S., Swenson, S., & Rodell, M. (2015a). Uncertainty in global groundwater storage estimates in a Total Groundwater Stress framework. *Water Resources Research*

Richey, A.S., Thomas, B.F., Lo, M.H., Reager, J.T., Famiglietti, J.S., Voss, K., Swenson, S., & Rodell, M. (2015b). Quantifying renewable groundwater stress with GRACE. *Water Resources Research*

Risbey, J.S., Pook, M.J., McIntosh, P.C., Wheeler, M.C., & Hendon, H.H. (2009). On the remote drivers of rainfall variability in Australia. *Monthly Weather Review, 137*, 3233-3253

Rodell, M., Chen, J., Kato, H., Famiglietti, J.S., Nigro, J., & Wilson, C.R. (2006). Estimating groundwater storage changes in the Mississippi River basin (USA) using GRACE. *Hydrogeology Journal, 15*, 159-166

Rodell, M., Famiglietti, J., Chen, J., Seneviratne, S., Viterbo, P., Holl, S., & Wilson, C. (2004). Basin scale estimates of evapotranspiration using GRACE and other observations. *Geophysical Research Letters, 31*, L20504

Rodell, M., Velicogna, I., & Famiglietti, J.S. (2009). Satellite-based estimates of groundwater depletion in India. *Nature, 460*, 999-1002

Rogelj, J. (2013). Long-term climate change: projections, commitments and irreversibility

Sanderson, E.W., Jaiteh, M., Levy, M.A., Redford, K.H., Wannebo, A.V., & Woolmer, G. (2002). The Human Footprint and the Last of the Wild. *BioScience, 52*, 891-904

Scanlon, B.R., Faunt, C.C., Longuevergne, L., Reedy, R.C., Alley, W.M., McGuire, V.L., & McMahon, P.B. (2012a). Groundwater depletion and sustainability of irrigation in the US High Plains and Central Valley. *Proceedings of the national academy of sciences, 109*, 9320-9325

Scanlon, B.R., Longuevergne, L., & Long, D. (2012b). Ground referencing GRACE satellite estimates of groundwater storage changes in the California Central Valley, USA. *Water Resources Research, 48*

Scott Power, S.L., Kevin Parton (2016). BOM: 2015 Australia's fifth hottest year on record. In: econews

Shelton, M.L. (2009). *Hydroclimatology: perspectives and applications*. Cambridge University Press

Steffen, W.L., Hughes, L., Karoly, D.J., & Commission, C. (2013). *The Critical Decade: Extreme Weather*. Climate Commission Secretariat, Department of Industry, Innovation, Climate Change, Science, Research and Tertiary Education

Stocker, T., Qin, D., Plattner, G., Tignor, M., Allen, S., Boschung, J., Nauels, A., Xia, Y., Bex, V., & Midgley, P. (2013). IPCC, 2013: Climate Change 2013: The Physical Science Basis. Contribution of Working Group I to the Fifth Assessment Report of the Intergovernmental Panel on Climate Change. In: Cambridge Univ Press, Cambridge, United Kingdom and New York, NY, USA

Sun, A.Y. (2013). Predicting groundwater level changes using GRACE data. *Water Resources Research, 49*, 5900-5912

Swenson, S., & Wahr, J. (2002). Methods for inferring regional surface-mass anomalies from Gravity Recovery and Climate Experiment (GRACE) measurements of time-variable gravity. *Journal of Geophysical Research: Solid Earth, 107*

Swenson, S., & Wahr, J. (2006a). Estimating large-scale precipitation minus evapotranspiration from GRACE satellite gravity measurements. *Journal of Hydrometeorology, 7*, 252-270

Swenson, S., & Wahr, J. (2006c). Post-processing removal of correlated errors in GRACE data. *Geophysical Research Letters, 33*, L08402

Swenson, S., Yeh, P.J.F., Wahr, J., & Famiglietti, J. (2006). A comparison of terrestrial water storage variations from GRACE with in situ measurements from Illinois. *Geophysical Research Letters, 33*, L16401

Syed, T.H., Famiglietti, J.S., Rodell, M., Chen, J., & Wilson, C.R. (2008). Analysis of terrestrial water storage changes from GRACE and GLDAS. *Water Resources Research, 44*

Takle, E.S., Roads, J., Rockel, B., & Gutowski Jr, W. (2007). Transferability intercomparison: an opportunity for new insight on the global water cycle and energy budget. *Bulletin of the American Meteorological Society, 88*, 375

Tangdamrongsub, N., Ditmar, P., Steele-Dunne, S., Gunter, B., & Sutanudjaja, E. (2016). Assessing total water storage and identifying flood events over Tonlé Sap basin in Cambodia using GRACE and MODIS satellite observations combined with hydrological models. *Remote Sensing of Environment, 181*, 162-173

Tapley, B., Chambers, D., Bettadpur, S., & Ries, J. (2003). Large scale ocean circulation from the GRACE GGM01 Geoid. *Geophysical Research Letters, 30*

Tapley, B.D., Bettadpur, S., Ries, J.C., Thompson, P.F., & Watkins, M.M. (2004a). GRACE measurements of mass variability in the Earth system. *Science, 305*, 503-505

Tapley, B.D., Bettadpur, S., Watkins, M., & Reigber, C. (2004d). The gravity recovery and climate experiment: Mission overview and early results. *Geophysical Research Letters, 31*

Terry Hughes, Neal Cantin, & McCutcheon, P. (2016). Great Barrier Reef coral bleaching at 95 per cent in northern section, aerial survey reveals. In: ABC News

Tregoning, P., McClusky, S., van Dijk, A., Crosbie, R., & Peña-Arancibia, J. (2012). Assessment of GRACE satellites for groundwater estimation in Australia

Trenberth, K.E., & Stepaniak, D.P. (2003). Seamless poleward atmospheric energy transports and implications for the Hadley circulation. *Journal of climate, 16*

Tulbure, M.G., Broich, M., Stehman, S.V., & Kommareddy, A. (2016). Surface water extent dynamics from three decades of seasonally continuous Landsat time series at subcontinental scale in a semi-arid region. *Remote Sensing of Environment, 178*, 142-157

Ummenhofer, C.C., England, M.H., McIntosh, P.C., Meyers, G.A., Pook, M.J., Risbey, J.S., Gupta, A.S., & Taschetto, A.S. (2009). What causes southeast Australia's worst droughts? *Geophysical Research Letters, 36*, L04706

Ummenhofer, C.C., Sen Gupta, A., Briggs, P.R., England, M.H., McIntosh, P.C., Meyers, G.A., Pook, M.J., Raupach, M.R., & Risbey, J.S. (2011). Indian and Pacific Ocean influences on southeast Australian drought and soil moisture. *Journal of Climate, 24*, 1313-1336

Van Dijk, A.I., Beck, H.E., Crosbie, R.S., Jeu, R.A., Liu, Y.Y., Podger, G.M., Timbal, B., & Viney, N.R. (2013). The Millennium Drought in southeast Australia (2001–2009): Natural and human causes and implications for water resources, ecosystems, economy, and society. *Water Resources Research, 49*, 1040-1057

Velicogna, I., & Wahr, J. (2006). Measurements of time-variable gravity show mass loss in Antarctica. *science, 311*, 1754-1756

Verstraeten, W.W., Veroustraete, F., & Feyen, J. (2008). Assessment of evapotranspiration and soil moisture content across different scales of observation. *Sensors, 8*, 70-117

Wahr, J., Swenson, S., & Velicogna, I. (2006a). Accuracy of GRACE mass estimates. *Geophysical Research Letters, 33*

Wahr, J., Swenson, S., & Velicogna, I. (2006b). Accuracy of GRACE mass estimates. *Geophys. Res. Lett, 33*, L06401

Wen-Jian, H., & Hai-Shan, C. (2013). Impacts of regional-scale land use/land cover change on diurnal temperature range. *Advances in climate change research, 4*, 166-172

Wentz, F.J., Ricciardulli, L., Hilburn, K., & Mears, C. (2007). How much more rain will global warming bring? *Science, 317*, 233-235

Xie, Z., Huete, A., Ma, X., Restrepo-Coupe, N., Devadas, R., Clarke, K., & Lewis, M. (2016a). Landsat and GRACE observations of arid wetland dynamics in a dryland river system under multi-decadal hydroclimatic extremes. *Journal of Hydrology*

Xie, Z., Huete, A., Restrepo-Coupe, N., Ma, X., Devadas, R., & Caprarelli, G. (2016b). Spatial partitioning and temporal evolution of Australia's total water storage under extreme hydroclimatic impacts. *Remote Sensing of Environment*

Xu, C.-Y., & Singh, V.P. (1998). A review on monthly water balance models for water resources investigations. *Water Resources Management, 12*, 20-50

Yang, Y., Long, D., Guan, H., Scanlon, B.R., Simmons, C.T., Jiang, L., & Xu, X. (2014). GRACE satellite observed hydrological controls on interannual and seasonal variability in surface greenness over mainland Australia. *Journal of Geophysical Research: Biogeosciences, 119*, 2245-2260

Yirdaw, S.Z., Snelgrove, K.R., & Agboma, C.O. (2008). GRACE satellite observations of terrestrial moisture changes for drought characterization in the Canadian Prairie. *Journal of Hydrology, 356*, 84-92

Zaitchik, B.F., Rodell, M., & Reichle, R.H. (2008). Assimilation of GRACE terrestrial water storage data into a land surface model: Results for the Mississippi River basin. *Journal of Hydrometeorology, 9*, 535-548

Zeng, Z., Piao, S., Lin, X., Yin, G., Peng, S., Ciais, P., & Myneni, R.B. (2012). Global evapotranspiration over the past three decades: estimation based on the water balance equation combined with empirical models. *Environmental Research Letters, 7*, 014026

Zhang, Z.Z., Chao, B., Lu, Y., & Hsu, H.T. (2009). An effective filtering for GRACE time-variable gravity: Fan filter. *Geophysical Research Letters, 36*, L17311

Chapter 2: Spatial partitioning and temporal evolution of Australia's total water storage under extreme hydroclimatic impacts

Abstract

Australia experienced one of the worst droughts in history during the early 21st-century (termed the 'big dry'), exerting negative impacts on food production and water supply, with increased forest die-back and bushfires across large areas. Following the 'big dry', one of the largest La Niña events in the past century, in conjunction with an extreme positive excursion of the Southern Annular Mode (SAM), resulted in dramatic increased precipitation from 2010 to 2011 (termed the 'big wet'), causing widespread flooding and a recorded sea level drop. Despite these extreme hydroclimatic impacts, the spatial partitioning and temporal evolution of total water storage across Australia remains unknown. In this study we investigated the spatial-temporal impacts of the recent 'big dry' and 'big wet' events on Australia's water storage dynamics using the total water storage anomaly (TWSA) data derived from the Gravity Recovery and Climate Experiment (GRACE) satellites.

Results showed widespread, continental-scale decreases in TWS during the 'big dry', resulting in a net loss of 3.89 ± 0.47 cm (299 km^3) total water, while the 'big wet' induced a sharp increase in TWS, equivalent to 11.68 ± 0.52 cm (898 km^3) of water, or three times the total water loss during the 'big dry'. We found highly variable continental patterns in water resources, involving differences in the direction, magnitude, and duration of TWS responses to drought and wet periods. These responses clustered into three distinct geographic zones that correlated well with the influences from multiple large-scale climate modes. Specifically, a persistent increasing trend in TWS was recorded over northern and northeastern Australia, where the climate is strongly influenced by El Niño-Southern Oscillation (ENSO). By contrast, western Australia, a region predominantly controlled by the Indian Ocean Dipole (IOD), exhibited a continuous decline in TWS during the 'big dry' and only a subtle increase during the 'big wet', indicating a weak recovery of water storage. south-eastern Australia, influenced by combined ENSO, IOD and SAM interactions, exhibited a pronounced TWS drying trend during the 'big dry' followed by rapid TWS increases during the 'big wet', with complete water storage recoveries. A spatial intensification of the water cycle was further identified, with a wetting trend over wetter regions (northern and northeastern Australia) and a drying trend over drier regions (western Australia). Our results highlight the value of GRACE derived TWSA as an important indicator of hydrological

system performance for improved water impact assessments and management of water resources across space and time.

2.1 Introduction

Amplification of the hydrologic cycle as a consequence of climate change is predicted to increase climate variability and the frequency and severity of droughts and wet extremes (AghaKouchak et al. 2014; Cai et al. 2014a; Chou et al. 2013; Easterling et al. 2000; Field and Van Aalst 2014). Recent evidence suggests that Australia's hydroclimatic variations play an important role in the inter-annual variability of the global carbon and water cycles (Boening et al. 2012; Bastos et al. 2013; Fasullo et al. 2013; Poulter et al. 2014). The recent La Niña induced record-breaking rains in 2010-2011 triggered a global land carbon sink anomaly, of which more than half was attributed to Australia's ecosystems (Poulter et al. 2014; Ahlström et al. 2015). The dramatic increase in rainfall from this La Niña event also resulted in a recorded global sea-level drop (Boening et al. 2012; Fasullo et al. 2013).

Australia, on-average, is the driest inhabited continent in the world, and characterized by extreme climate variability due to multiple large-scale climate modes such as the El Niño-Southern Oscillation (ENSO), the Indian Ocean Dipole (IOD) and the Southern Annular Mode (SAM) (Ashok et al. 2003a; Cai et al. 2011; Meyers et al. 2007; Nicholls 1991; Risbey et al. 2009). In the early 21st-century, Australia experienced one of the worst droughts in history, with a prolonged hydroclimatic anomaly period commonly known as the 'Millennium Drought' or 'big dry' that began in 2001 and continued until late 2009 (Ummenhofer et al. 2009; McGrath et al. 2012; Murphy and Timbal 2008; Nicholls 2010). The 'big dry' impacted most Australian mainland capital cities as water storage levels were reduced more than half (Steffen et al. 2013) with severe impacts to the agricultural industry. The Murray-Darling Basin (MDB), which is one of the most productive food and fibre regions in Australia, experienced a 67% decline in water availability and an average 91% reduction in crop production (Kirby et al. 2012; Van Dijk et al. 2013).

The 'big dry' ended abruptly with an abnormal wet period in 2010-2011. Although this 'big wet' was mostly driven by one of the strongest La Niña events in the past nine decades (Nicholls 2011; Trenberth 2012), recent studies have shown that it was also

influenced by an extreme positive excursion of the Southern Annular Mode (SAM) (Hendon et al. 2014; Lim and Hendon 2015). SAM was estimated to have accounted for around 10% of the rainfall anomaly over eastern Australia and more than 40% of the rainfall anomaly along east-central coastal region in 2010 (Hendon et al. 2014; Lim and Hendon 2015). Eastern Australia as a whole (the states of Queensland, New South Wales, and Victoria) received the highest springtime rainfall on record since 1900 (Hendon et al. 2014; Lim and Hendon 2015), resulting in widespread floods (Heberger 2011). Due to the significant social and environmental impacts of these hydroclimatic extremes, a comprehensive characterisation of the spatial and temporal variations of Australia's water storage is urgently needed for managing water resources and making water policies at basin, state, and national levels.

Satellite observations provide an unparalleled method for monitoring water storage dynamics over broad scales, and in the case of the large Australian continent, they complement sparsely located *in-situ* data collection sites. The Gravity Recovery and Climate Experiment (GRACE) twin satellite mission, launched by NASA and the German Aerospace Centre (DLR) in March 2002, was designed to exploit the unique relationship between variations in the gravity field and changes in mass at the Earth's surface (Chen et al. 2005; Tregoning et al. 2012; Wahr et al. 1998; Wahr et al. 2006). GRACE observations have enabled the detection of small changes in the Earth's gravity field, associated with the redistribution of water on and beneath the land surface (Famiglietti and Rodell 2013; Jiang et al. 2014; Rodell et al. 2009). The GRACE derived terrestrial total water storage anomaly (TWSA), thus is an integrative measure of vertical changes in groundwater, surface water, soil moisture, snow water and biological water (Castle et al. 2014; Swenson and Wahr 2006a).

Previous studies on Australia's recent hydroclimatic events have focused on the causes of the 'big dry' and the 'big wet', and their impacts on agriculture and ecosystems (Heberger 2011; Kirby et al. 2012; McGrath et al. 2012; Steffen et al. 2013; Van Dijk et al. 2013; Yang et al. 2014). Further, these studies treated the 'big dry' and 'big wet' as discrete periods over the entire continent, which is unrealistic considering the diversity of Australia's climate patterns. Less attention has been placed on the combined geographic and temporal water storage impacts of these hydroclimatic variations. Thus, GRACE measurements provide unique opportunities to conduct large-scale

hydrological experiments in a natural setting, both to evaluate hydrological patterns and assess their temporal evolution under recent extreme hydroclimatic impacts.

In this study, we analysed the spatial patterns and temporal dynamics of GRACE-derived TWSA across continental Australia from 2002 to 2014, encompassing large-scale drought and wet extremes. Specifically, we aimed to (1) investigate spatially explicit variations in the direction, magnitude, and duration of water drying trends during the 'big dry'; (2) quantify the rate and magnitude of water recovery during the 'big wet'; and (3) spatially partition the combined drying and wetting effects on water storage and analyse the resulting patterns to large-scale climate modes. Results from this study will not only guide the design of Australia's national water-use strategies to a changing climate, but will also generate key knowledge for understanding the water-cycle dynamics over other global regions.

2.2 Data and methods

2.2.1 Terrestrial total water storage

Total water storage anomaly data, derived from release-5, level-2 GRACE data, was obtained from NASA's GRACE Tellus website (JPL 2012) for the Australian continent over the period July 2002 to December 2014. The GRACE TWSA data was pre-processed to remove the signal from atmosphere and ocean and was retrieved at monthly and 1° resolutions, with units of cm (Landerer and Swenson 2012; Swenson and Wahr 2006b). To minimize the uncertainties associated with data processing, an ensemble average TWSA was calculated using GRACE data processed independently by three research centres, NASA Jet Propulsion Laboratory (JPL), University of Texas Center for Space Research (CSR) and the GeoForschungsZentrum (GFZ) Potsdam. As terrestrial gravity variations in space and time are mainly caused by changes in water storage, TWSA was obtained by subtracting the monthly GRACE data by a historical mean (2004-2009). To avoid ambiguities, we use TWSA to refer the GRACE derived total water storage anomaly data and TWS to refer total water storage in the main text.A suitable scaling factor approach is critical for the accurate quantification of GRACE observed TWSA (Long et al. 2015). We chose to use a file of scaling factors obtained from the NCAR's Community Land Model 4.0 (CLM4.0) (Gent et al., 2011; Landerer and Swenson 2012; Lawrence et al., 2011) to correct and restore the GRACE signal loss

during low-pass filtering (i.e., destriping, truncation, and filtering). CLM4.0 accounts for the interactions between surface and subsurface water as well as irrigation and river diversion and provides reliable flux variables and hydrological states even over areas with intensive human activities (Gent et al., 2011; Long et al. 2015; Wen Jian and Hai Shan 2013). With our study area in the Southern Hemisphere, we used the hydrological year to calculate annual values of TWSA, starting from July to end of June. The uncertainty range in TWSA time series was calculated at a 95% Confidence Interval (CI).

2.2.2 Climate index data

Three climate indices were used in this study to represent the coupled ocean-atmosphere systems, previously identified as the major drivers of climate variability over Australia (Risbey et al. 2009; Cai et al. 2011; Cleverly et al. 2016). These included 1) the Multivariate ENSO Index (MEI); 2) the Indian Ocean Dipole Mode Index (DMI) and 3) the Southern Annular Mode Index (SAMI).

The MEI (available from http://www.esrl.noaa.gov/psd/enso/mei/) is based on six observed variables (sea-level pressure, zonal and meridional surface winds, sea surface temperature, surface air temperature, and total cloudiness fraction of the sky) and represents the atmospheric pressure difference between Tahiti and Darwin (Wolter 1987; Wolter and Timlin 1993, 1998, 2011). The DMI, derived from the Hadley Centre Sea Ice and Sea Surface Temperature (HadISST) dataset (Rayner et al. 2003), is a measure of the anomalous zonal SST gradient across the equatorial Indian Ocean and indicates the dynamics of IOD (Saji et al. 1999). Variations in SAM, which is the dominant mode of atmospheric variability in the mid and high latitudes of the Southern Hemisphere (Mo 2000; Thompson and Solomon 2002), are monitored by the SAMI (available from http://www.cpc.ncep.noaa.gov/products/precip/CWlink/daily_ao_index/aao/aao.shtml), and also known as the Antarctic Oscillation index. The climate indices used in this study are monthly time series data extending from July 2002 to December 2014.

2.2.3 Auto-define transition dates between the 'big dry' and the 'big wet'

To better characterize temporal variations of TWS, a per-pixel transition date between dry and wet periods was defined based on the following steps. First, the

TWSA time series data was de-seasonalized and smoothed using 'Seasonal Decomposition of Time Series by LOESS' (STL) scheme (Cleveland et al. 1990). We then calculated the number and the position of turning points (TPs - either peaks or troughs) in the time series (R version 3.1.3, R Core Team, 2015). Next, we determined the transition dates between drought and wet phases (end of the 'big dry' and initiation of the 'big wet') by computing TWSA differences (ΔTWSA) between TWSA values at adjacent turning points. Finally, we defined the 'big dry' end date as the timing when the largest ΔTWSA occurs, which corresponds to the inflection point before the positive TWS gradient related to the start of the 'big wet'. The end of the 'big wet' was defined as the peak of the TWSA time series, from which TWS starts to decline. Using this method the big dry and big wet periods were independently derived for each pixel.

2.2.4. Statistical methods

2.2.4.1 Trend analysis

For each pixel, the temporal extents of the 'big dry' and 'big wet' were determined by the previously derived transition dates, and the TWS rates of drying and wetting and their significance were calculated as the slope and *p-value* of the trends over the stacked monthly grids of TWSA during both events, respectively. A linear regression with the ordinary least squares (OLS) method was applied to estimate the rate of change in TWS.

2.2.4.2 Spatio-temporal variability

For the period from July 2002 to December 2014, mean values of monthly TWSA and de-seasonalized TWSA for Australia were calculated and some monthly images were processed to show the spatio-temporal variability of the continental TWS through time. Multiple linear regressions of distinct temporal segments were assessed to show magnitude and significance of the trends in TWS during drying and wetting phases.

2.2.4.3 Cross correlation analysis

To relate TWS changes during drying and wetting periods to the large-scale climate modes across the Australian continent, spatial cross correlation analysis was applied to quantify the relationships between TWS and the major climate drivers. As the impact

of climate modes on TWS is expected to show finite time lags (0 to 6 months), we only considered positive time lags in which climate modes are leading the changes of TWS. We examined the cross correlations between TWSA and the three climate indices on a per-pixel level for different time lags by shifting the TWSA time series forward one month at a time. The maximum Pearson's correlation coefficient (r) and the corresponding time lag, in months, were obtained to indicate the strength of the relationships between TWS and different climate modes with the optimal lag at any given location across Australia.

2.2.5 Quantifying water loss/gain during the 'big dry' and 'big wet'

The amounts of water storage loss during the 'big dry' and gain during the 'big wet' were expressed in cm on a per-pixel basis by multiplying the rate of change (cm month^{-1}) in TWS during each period by the corresponding duration (in months), respectively. The annual cumulative TWS flux (CTWS) was calculated to represent the total TWS contribution (loss/gain) across Australia from the start of the study period (July 2002) to June of each subsequent year, computed as:

$$\mathrm{CTWS_n} = \sum_{i=1}^{n} (TWSA_{i+1} - TWSA_i) \quad (2.1)$$

where CTWS is cumulative TWS flux (cm) starting from 0 in 2002 ($\mathrm{CTWS_{2002}}$), TWSA is the mean annual value of TWSA (cm), *i* is the year and *n* is the nth year from 2002.

2.2.6 Calculating the rate of recovery in TWS

To assess the rate and magnitude of TWS recovery achieved during the 'big wet' pulse, we calculated the rate of recovery in TWS relative to the total water loss during the 'big dry' for each pixel. The TWS recovery rate was calculated as:

$$\mathrm{TWSreco\%} = \frac{Water\ gain}{Water\ loss} \times 100\% \quad (2.2)$$

where $\mathrm{TWS_{reco}\%}$ is the recovery rate (in percent), *water storage gain* (cm) and *water storage loss* (cm) represent the TWS gain/loss for each pixel during the 'big wet' and 'big dry' periods respectively.

2.3 Results

2.3.1 Spatial and temporal variations in TWS across the continent

The time series of continental-scale averaged total water storage anomalies, from 2002 to 2014, show TWS fluctuations at both seasonal and inter-annual temporal scales with seasonal peak values in March (Austral autumn) and minimum values around November (Austral spring), respectively in each year (Fig.2.1A). The de-seasonalized time series depicts three distinct temporal segments, including an overall drying trend from 2002 to October 2009, followed by a large wet phase from 2010 to 2011, and another drying phase from July 2011 to the end of the period of analyses made here, in December 2014 (Fig.2.1A). The initial drying phase ('big dry') had an average continent-wide drying rate of -0.58 ± 0.06 cm/year (Fig.2.1A), while the wetting phase ('big wet') replenished continent-wide water storage and increased continental-average TWSA values from -1.15 cm in October 2009 to +8.82 cm in July 2011 (Fig.2.1A). The second drying phase commenced from July 2011 until the end of this study, December 2014 with a much higher rate of TWS decline, and by the end of the analyses period, continent-wide TWSA values were nearly equivalent to those at the beginning of the study period in 2002 (Fig.2.1A).

Continent-wide TWSA images for the beginning (Jul 2002), end (Dec 2014), and hydroclimatic drought-wet transition points (Oct 2009 and Jul 2011), are shown in Fig.2.1B-E. These four images highlight the non-uniform drying and wetting patterns across Australia during the 'big dry' and 'big wet' hydroclimatic periods, as well as mixed patterns of simultaneous drying and wetting conditions at the beginning and end of the study period (Fig.2.1B-E). The spatial variability in TWSA on these maps also depicts water loss, water gain and water loss again during the three distinct segment periods.

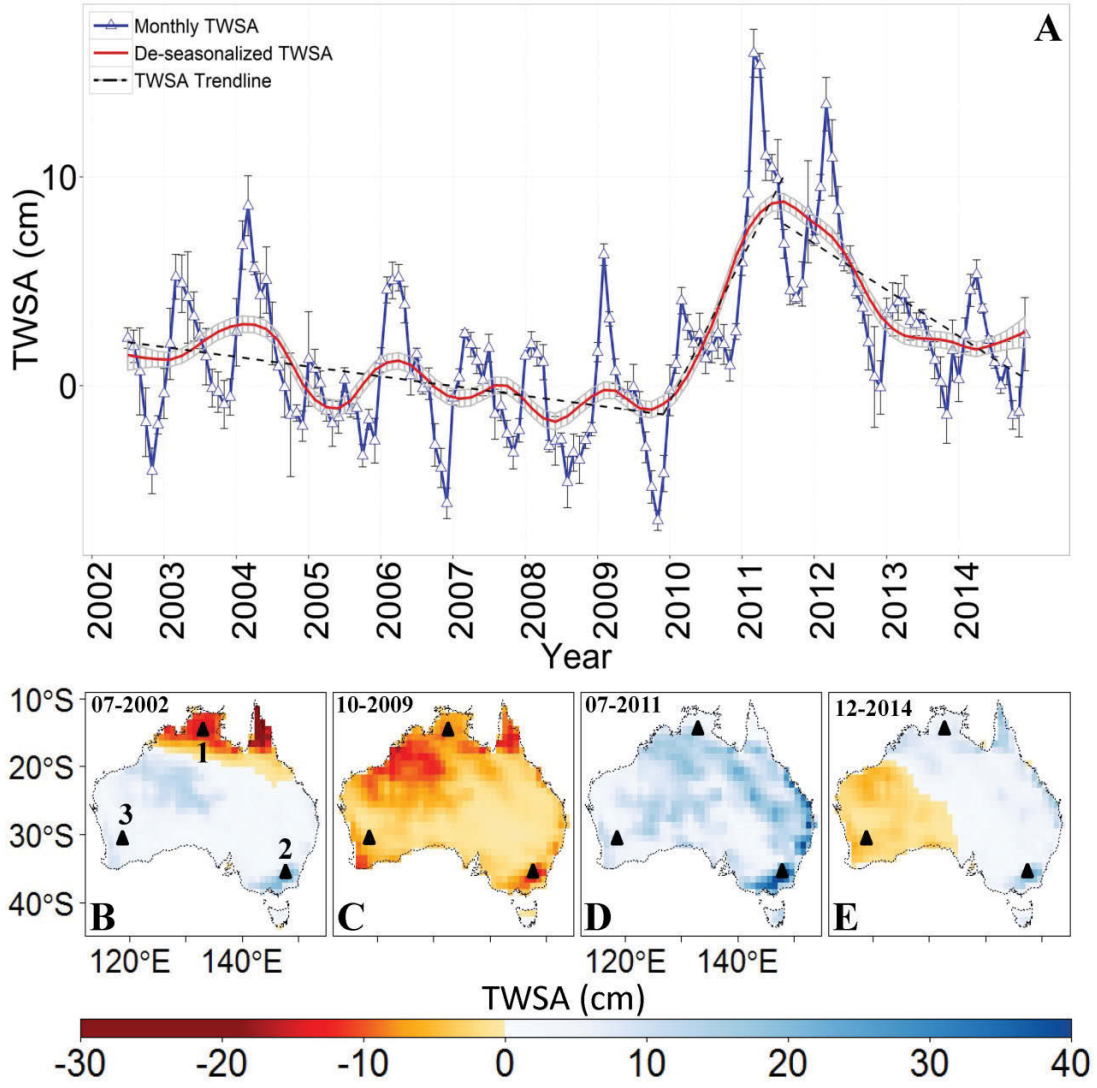

Figure 2.1. (A) Monthly continental average TWSA from July 2002 to December 2014 (solid blue line) with solid red line indicating the smoothed and de-seasonalized TWSA. The black dashed lines are the linear trends of the de-seasonalized TWSA during the drying phase, wetting phase, and second drying phase respectively ($p < 0.05$). The error bars indicate the standard deviations among three GRACE datasets provided by JPL, CSR and GFZ, and the shaded area is 95% CI in the de-seasonalized TWSA; (B-E) show continental TWSA patterns in Jul-2002 (start of the study period), Oct-2009 (end of the 'big dry'), Jul-2011 (end of the 'big wet'), and Dec-2014 (end of the study period) respectively; Triangle symbols (1-3) represent three pixel samples for further analysis of regional TWS variations.

TWS variations of three sample pixels across different regions (the triangle symbols in Fig.2.1B-E) were selected to better reveal the spatial non-uniformity during the 'big dry' and 'big wet' periods (Fig.2.2). The samples include site-1 in northern Australia, site-2 in southeastern Australia (the southern part of MDB), and site-3 in the Wheatbelt

region of the southwestern Australia (Fig.2.2). The de-seasonalized TWSA time series varied in magnitude, timing of dry-wet transition dates, and even the TWS trend direction across the three sites (Fig.2.2). In particular, the northern site (1) experienced increases in TWS during the 'big dry' (Fig.2.2A), while the southwestern (3) and southeastern (2) sites showed similar 'big dry' drying trends, but different wetting trends (Fig.2.2B,C). The southeastern site (2) exhibited the most extreme hydrologic change in TWS (33.2 cm, from -6.1 to 27.1) from the start to the end of the wet phase (indicated by the black circles in Fig.2.2B), while the western site exhibited a change that was less than one-half of site-2, or 13.7 cm (Fig.2.2C).

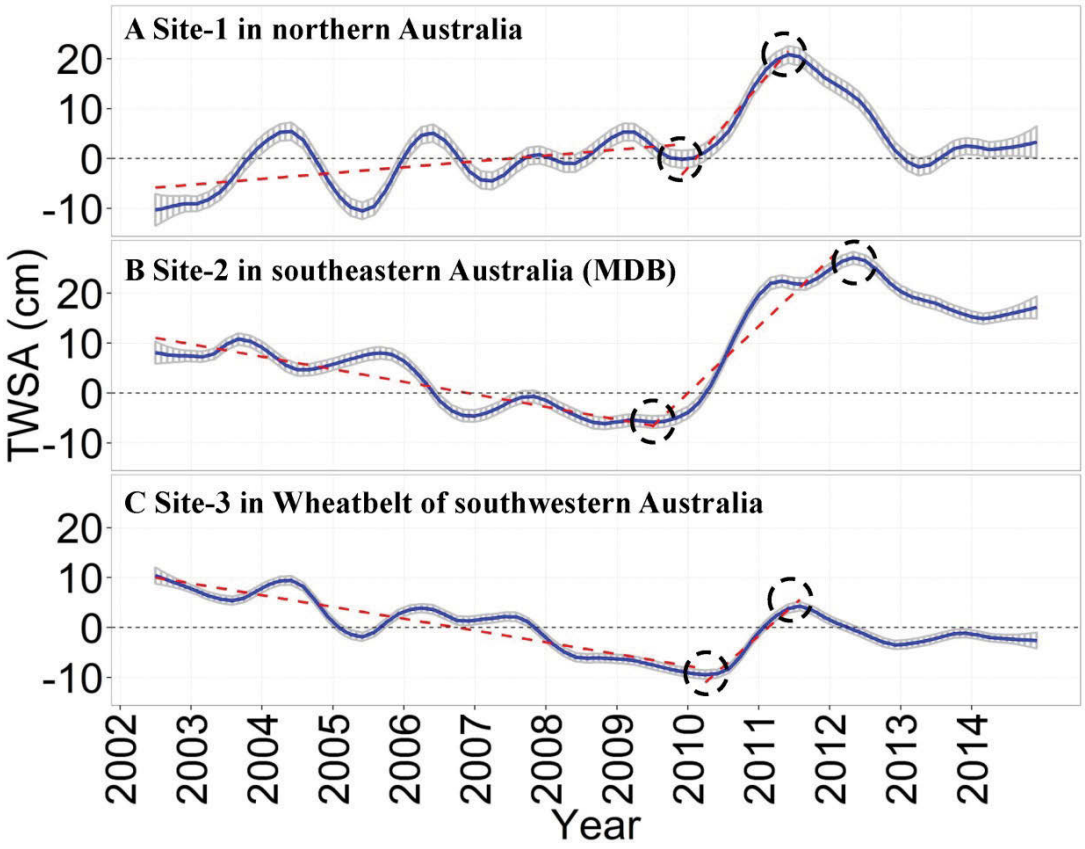

Figure 2.2. Variations in TWSA (de-seasonalized) at three sites in Australia (triangle symbols in Fig.2.1B-E) with the shading representing the 95% CI. The three sites are located in northern Australia (Site-1), southern part of MDB in southeastern Australia (Site-2) and the Wheatbelt region of the southwestern Australia (Site-3). The black circles indicate the end of the 'big dry' and the end of the 'big wet'. The red dashed lines are the linear trends of the de-seasonalized TWSA during the 'big dry' and the 'big wet', respectively.

2.3.2 Transition dates from the end of the 'big dry' to the start of the 'big wet' across the continent

To quantify the non-uniform drying and wetting temporal patterns across the continent, a map of per-pixel transition dates depicting the end of the 'big dry' and onset of the 'big wet' was generated (Fig.2.3A). An east to west chronological wetting pattern associated with the increased rainfall from 'big wet' is observed with water storage conditions initially increasing over east - central Australia (June 2009) followed by an outward wet pulse increase in all directions (central, northern, and southern portions) over Australia (Fig.2.3A). By the end of 2009, over three fourths of Australia had reversed from a drying phase into a wetting phase, with western Australia remaining in drought conditions for another six to eight additional months, until June 2010 (Fig.2.3A). Overall, there was a 12 month lag in the hydroclimatic shift from 'big dry' to 'big wet' conditions between eastern and western parts of Australia (Fig.2.3A).

Continental trends in TWS during the 'big dry', from 2002 until the initiation of the 'big wet', based on the temporally-variable transition date map (Fig.2.3A) are shown in Fig.2.3B. The water storage drying trends show large-scale reductions in TWS over most of Australia with southeastern (~-4 cm/year), northwestern (~-2.5 cm/year) and southwestern (~-2 cm/year) areas experiencing the most severe declines in TWS during the 'big dry' period (the red colour areas in Fig.2.3B). However, over the northern (Latitude < 15˚S) and northeastern tropical/subtropical parts of Australia, TWS trends were positive, varying from ~1-2 cm/year, despite the continental-scale 'big dry' period designation (Fig.2.2A, Fig.2.3B).

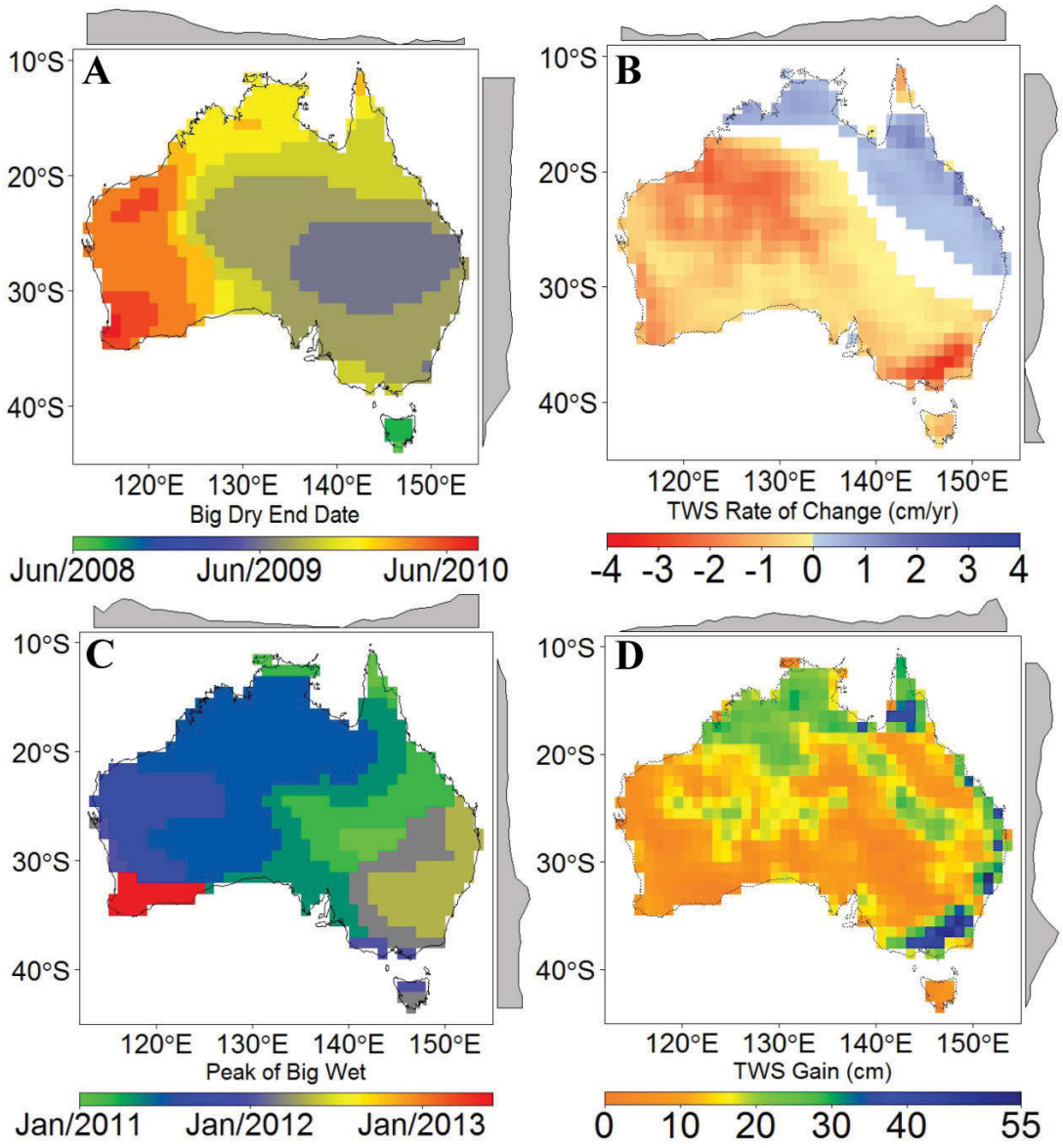

Figure 2.3. (A) Spatial patterns of the transition dates from drying phase ('big dry') to wetting phase ('big wet'), i.e., the 'big dry' end dates (or onset dates of the 'big wet'), over western and southeastern Australia or wet to wetter conditions in northern part of Australia; (B) Spatial patterns of the rates of change in TWS (cm/yr) during the 'big dry'. White areas represent pixels without a statistically significant ($p > 0.05$) trend in TWS; C) Spatial patterns of the timing date of the 'big wet' TWS peak (or end date of 'big wet'); and (D) TWS gains (cm) across the continent during the 'big wet'. The marginal graphics show the latitude and longitude average of each image.

2.3.3 Recovery of the continental total water storage during the 'big wet'

The spatial variability in the peak timings of the 'big wet' period is depicted in Fig.2.3C. The peak of the 'big wet' occurred first in central-east Australia (Jan 2011), and from there the peak timing lagged in a southeast to northwest diagonal manner, with a final, relatively weak 'big wet' pulse reaching southwest Australia in June 2013 (Fig.2.3C). By contrast, the longest wetting periods were encountered over southwestern and southeastern Australia, lasting approximately three years (Fig.2.3A,C).

The total water gained from the onset to the peak of the 'big wet', also revealed the highly variable wetting patterns across the continent (Fig.2.3D). The largest total water storage recoveries were limited to the eastern coast margins and northern Australia (Fig.2.3D). The southern part of MDB in southeastern Australia gained the largest quantity of water during the 'big wet' (55 cm). Weaker recoveries were encountered over central and western Australia, with very low TWS recovery (< 10 cm) in the Wheatbelt region of southwestern Australia (Fig.2. 3D).

2.3.4 Spatial partitioning of Australia's TWS across the 'big dry' and the 'big wet' periods

We further compared and quantified the relative changes in total water storage across both the 'big dry' and 'big wet' periods (Fig.2.4A). The per-pixel scatterplot of water loss during the 'big dry' and water gain during the 'big wet' revealed three distinct drought-wet response patterns (Fig.2.4A). Two distinct clusters plotted either above or below the 1:1 line, one indicating greater water storage gains during the 'big wet', relative to water losses during the 'big dry' (green colour), while the other cluster showed greater water losses than gains during the two hydroclimatic extreme periods (orange colour). The last cluster (blue colour) depicted areas that did not experience water loss but instead exhibited low water gains ('big dry') and high water gains ('big wet').

Spatially, these three clusters of TWS drying and recovery patterns formed three distinct geographic regions (Fig.2.4B) across Australia, which have a wide range of ecological, climatic, hydrological and geological conditions (Table 1). The first region (Zone I), in northern and northeastern Australia, showed no drought period (blue points in Fig.2.4A), while the second region (Zone II) experienced a greater water recovery during the “big wet” than water loss during the 'big dry' (green points above the 1:1 line

in Fig.2.4A). Zone II replenished the 'big dry' water loss by an average of 116% TWS recovery rate (Table 2). By contrast, the third region (Zone III) experienced the most severe water loss during the 'big dry' and weak water recovery that fell below the 1:1 line (Fig.2.4A). On average this zone only recovered 67% of the water loss during the 'big dry' (Table 2). In general, the intensity of human activities in Australia is much lower than those in other continents (Sanderson et al. 2002), with most impacts centred in urban and agricultural areas, primarily in Zones I and III. Even in large croplands, irrigation and river extraction activities are not intensive with rainfed cropland being more than 95% (NLWRA 2001).

At a continental scale, there was a reduction of Australia's water storage at a rate of -0.58 ± 0.06 cm/year, resulting in a total 3.89 ± 0.47 cm loss of water during the 'big dry' (Table 2). This water deficit was reflected by the severe droughts experienced in many parts of Australia (Fig.2.3B) and is equivalent to of 299 km^3 in volume or 2.29×10^{11} tons in mass. The 2010/11 wet pulse, however, replenished this water loss by adding an equivalent of 11.68 ± 0.52 cm water to the continent, a three-fold increase (compared with total water loss) of water poured into Australia within two years, the equivalent of 8.98×10^{11} tons (Table 2).

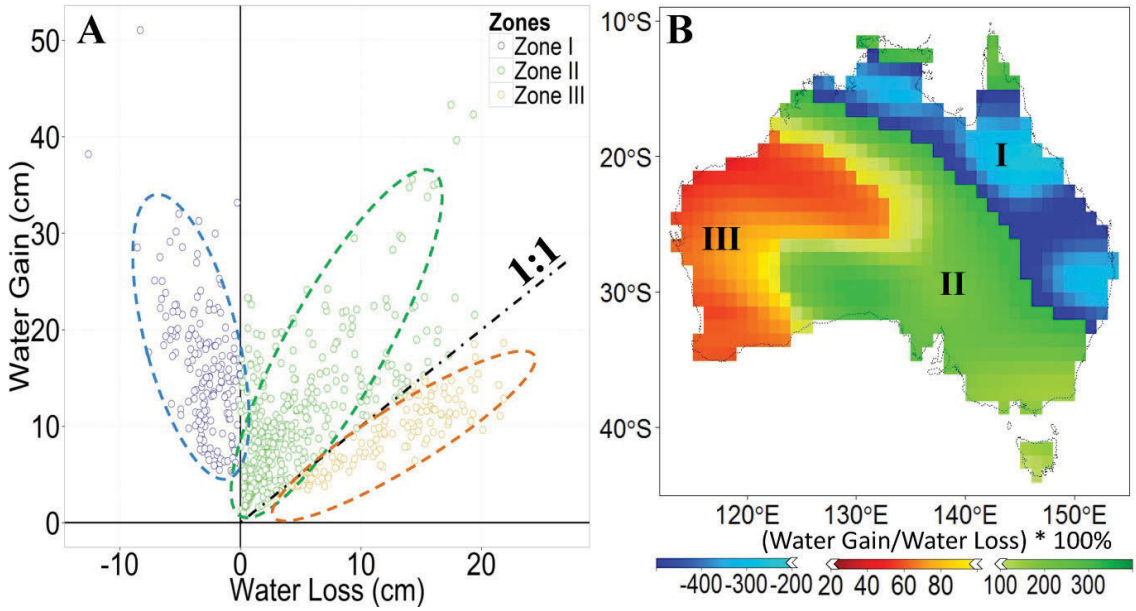

Figure 2.4. (A) Scatter plot of the water gain (cm) during the 'big wet' (y-axis) versus the water loss (cm) during the 'big dry' (x-axis) using all GRACE pixels in Australia; (B) Spatial clustering of the ratio between water gain and water loss (i.e.,TWS recovery rate) across the continent. Negative values indicate no TWS loss during the 'big dry'. The 0-100% means water storage is partially recovered, i.e., water loss is bigger than water gain, the value of 100% means water storage is fully recovered, i.e., water gain during the 'big wet' equals to the water loss during the 'big dry'. The values of >100% means the water gain is greater than the water loss.

Table 2.1. Summary of ecological, climatic, hydrological, geological and human conditions in Zone I, II and III

Zone	Area (km^2)	Major Land use[a]	Climate type[b]	Major climate drivers	Soil[c]	Hydrogeology[d]	Human activities[e]
Zone I	~ 1.96 × 10^6	Savanna, Forest	Aw,BSh	ENSO	Vertosol, Kandosol, Tenosol, Hydrosol	Palaoproterozoic basin, Cretaceous rocks; highly productivity aquifers	0-1
Zone II	~ 3.67 × 10^6	Shrubland, Agriculture, Forest, Grassland	BWh,BSh, BSk,Cfa, Cfb	ENSO,IOD, SAM	Rudosol, Sodosol, Kandosol, Calcarosol	Teritiary and Ordovician rocks; low to moderate productity aquifers	20-30 in crop area; 0-1(the rest)
Zone III	~ 1.99 × 10^6	Shrubland, Agriculture, Forest	BWh,Csa, Csb	IOD	Tenosol, Calcarosol, Rudosol, Sodosol	Yilgarn and Pilbara Craton, Cretaceous rocks; low productivity aquifers	20-30 in crop area; 0-1(the rest)

[a]Land use: Obtained from the Advanced Very High Resolution Radiometer (AVHRR) 1-km University of Maryland (UMD) land cover product.

[b]Climate type: World Map of Köppen−Geiger Climate Classification (Kottek et al. 2006). Aw = equatorial and winter dry, BSh = arid, steppe and hot arid, BWh=arid, desert and hot arid, BSk = arid, steppe and cold arid, Cfa = warm temperate, fully humid and hot summer, Cfb = warm temperate, fully humid and warm summer, Csa = warm temperate, summer dry and hot summer, Csb =warm temperate, summer dry and warm summer.

[c]Soil: Ausralian soil classification map from Australian Soil Resource Information System (ASRIS)

[d]Hydrogeology: Hydrogeology Map of Australia from Geoscience Australia

[e]Human activity: Human influence on the land surface across the globe (Sanderson et al. 2002) with human impact being rated on a scale of 0 (minimum) to 100 (maximum).

Table 2.2. Summary of the rates of change in TWS at the continental scale and for each geographic zone during both the dry and wet periods respectively with 95% CI.

Continental average	Dry / Wet trend (cm/yr)	Total water loss / gain (cm)	Recovery Rate (slope of points)
	-0.58 (±0.06)/7.49 (± 0.35)	-3.89 (±0.47)/11.68 (±0.52)	
Geographic Zone average			
Zone I	0.51 (±0.05)/ 9.82 (±0.70)	2.94 (±0.26)/ 15.85 (±1.00)	184% (±0.22)
Zone II	-0.66 (±0.07)/ 7.06 (±0.52)	-3.97 (±0.45)/ 11.10 (±0.78)	116% (±0.06)
Zone III	-1.24 (±0.09)/ 6.20 (±0.46)	-10.49 (±0.79)/ 8.64 (±0.58)	67% (±0.03)

2.3.5 Cumulative TWS and water-cycle intensification

The cumulative TWS flux from 2002 to 2014 for each of the 3 distinct geographic zones was computed to quantify the total loss or gain of water over the study period (Fig.2.5). The persistent increase in CTWS, from 2002, can be observed for Zone I with a maximum CTWS of 15.65 ± 1.04 cm in 2011, followed by a sharp decrease in CTWS in the subsequent 2012 and 2013 drying phase. Zone III, on the other hand, experienced a conspicuous water loss throughout 2002-2009 and despite some water gains during 2010-2011, the CTWS in this region never recovered to the 2002 level. Zone II, which is located between Zone I and Zone III, behaved in an intermediate manner as this area did not dry as rapidly as zone III and easily recovered all of its water losses during the 'big wet' period. Zone II experienced a seven-year continuous loss of water from 2002 to 2008, but readily recovered to its prior 2002 level during the 'big wet'. Figure 5 also corroborates the transition dates for the end timings of the 'big dry' (Fig.2.3A), with

Zone III having the longest 'big dry' period, followed by Zone II, while Zone I exhibited no drought at all.

Further, despite continent-wide drought during the 'big dry', a sizeable portion of northern Australia was still gaining water during the 'big dry' - a potential sign of spatial hydrologic cycle intensification (Fig.2.3B). Figure 5 shows that all three zones were divergent from 2002 up through 2011. Therefore, in particular zones I and III show short term signs of water cycle intensification, with the drier areas becoming drier while wet areas became wetter.

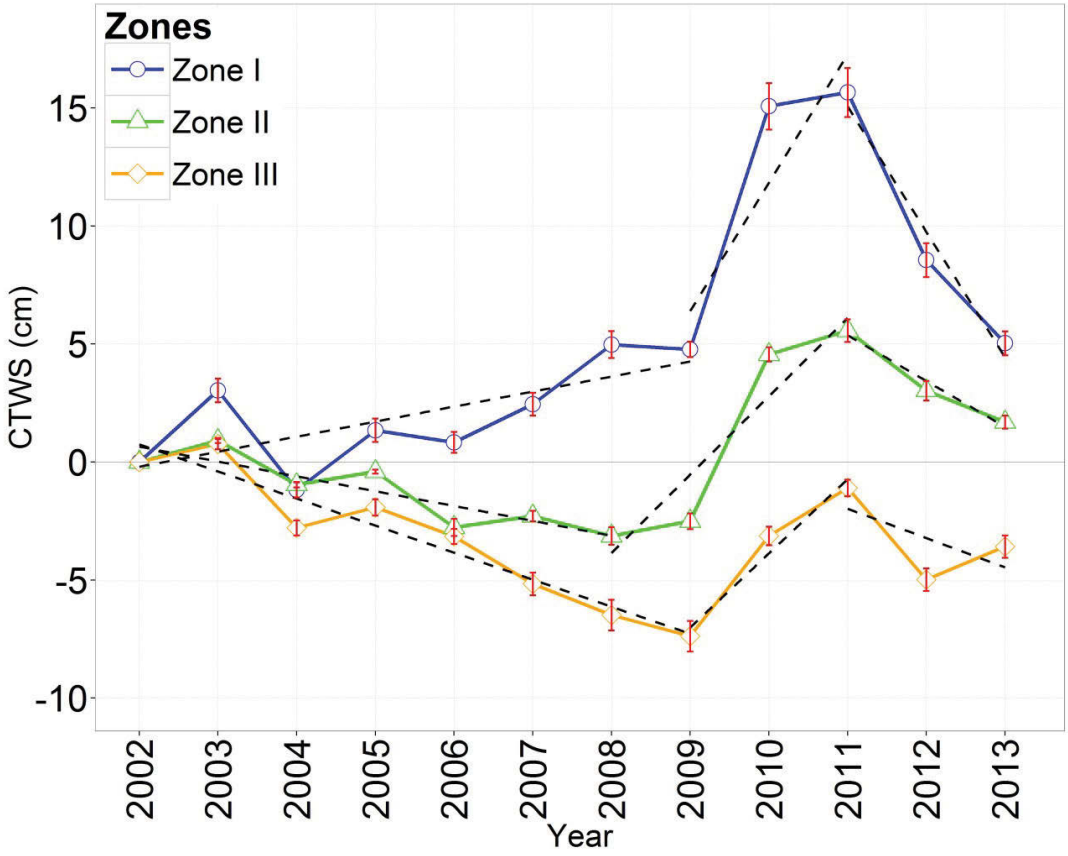

Figure 2.5. Cumulative TWS flux (CTWS) averaged over each geographic zone from 2002/03 to 2013/14 hydrological years, with error bars representing 95% CI. The black dashed lines are the linear trends of CTWS in each zone during the 'big dry', 'big wet', and second drying phase respectively ($p < 0.05$).

2.3.6 The varying importance of large-scale climate modes on the three geographic zones of TWS

We found close coupling between three climate modes and TWS during the study period with varying strength of relationships and lags at different areas across Australia (Fig.2.6A-F). The spatial patterns of the correlations between ENSO and TWS highlight three geographic clusters that are broadly similar as the TWS Zones I, II and III shown in Fig.4B (Fig.2.6A). Fig.2.6A shows MEI was highly related to TWSA over the continent and has the most extensive influence on TWS among three climate indices; in particular, the strongest correlation coefficients ($r > 0.4$) were observed in northern and northeastern Australia (Zone I), followed by much of Zone II. MEI versus TWSA had the weakest relationship within Zone III.

IOD represented by DMI was largely correlated with TWS across the western and southern portions of Australia (Fig.2.6B). By contrast with MEI, DMI was most significantly related to TWSA in Zone III and the southeastern tip of Zone II (southern part of the MDB).

Compared with ENSO and IOD, SAM was least correlated with TWS across Australia (Fig.2.6C). The correlations between SAMI and TWSA were not significant over most of the continent, with the exception of eastern Australia, where SAMI showed significant positive correlations with TWSA, increasing the springtime rainfall in that area (Fig.2.6C). These cross-correlation patterns between climate modes and TWS showed rough concurrence with the three TWS zones (cf. Figs.4B, 6A, B, C).

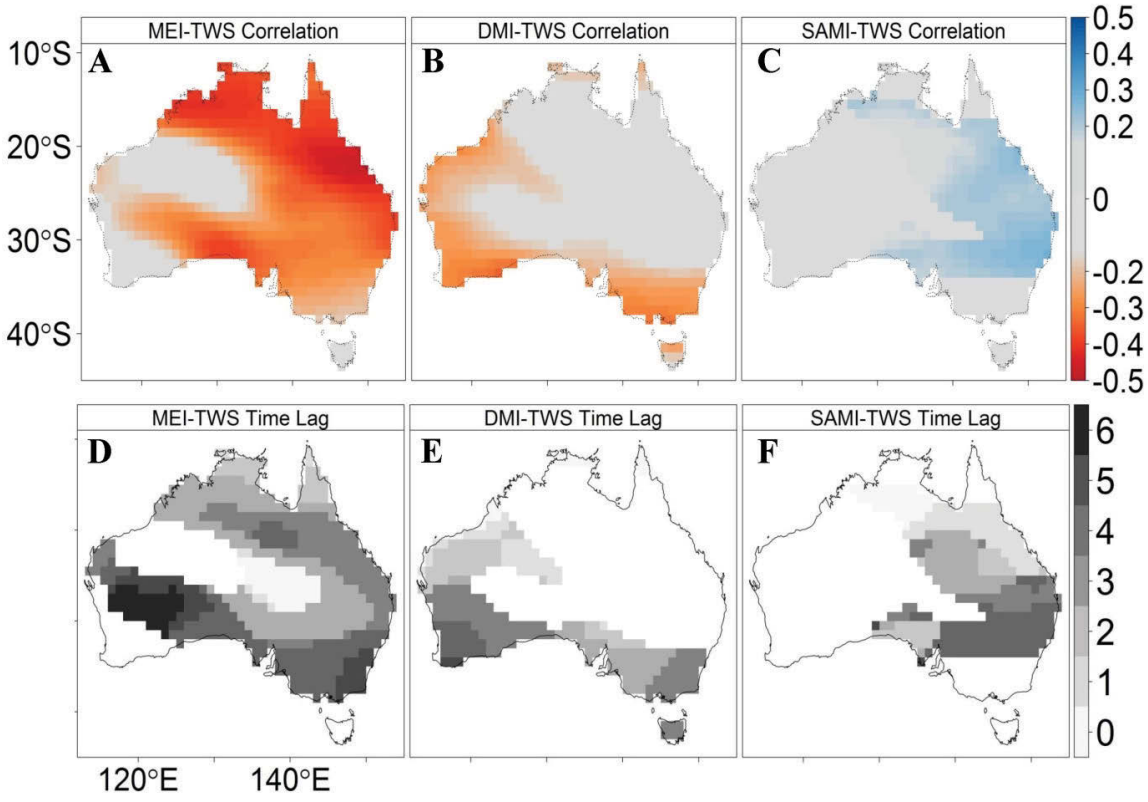

Figure 2.6. Pearson's coefficient (maximum r) and the time lag in months between (A,D) monthly MEI and TWSA; (B,E) DMI and TWSA; (C,F) SAMI and TWSA from July 2002 to December 2014. Only correlations significant at the 95% level are shown with non-significant pixels coloured as grey in A-C and white in D-F.

2.4 Discussion

2.4.1 Towards a more realistic characterisation of the water storage dynamics across time and space

We found the timing of the transition date between the 'big dry' and 'big wet', as defined from GRACE-TWSA, varied considerably across the continent. Our results demonstrate that a simplified characterisation of a single, continent-wide transition date between 'big dry' and 'big wet' is unrealistic and unable to provide accurate information about the hydrological dynamics over the continent. Our results are consistent with regional or basin-wide studies which found ambiguities in the 'big dry' end date (Bond et al. 2008; Heberger 2011; Hendon et al. 2014; Leblanc et al. 2011; Lim and Hendon 2015). In addition, as northern and north-eastern parts of Australia (Zone I) didn't experience water loss during the 'big dry', the dates provided in Fig.2.3A represent the

onsets of the 'big wet', or transition from low water gains to high water gains during the 'big wet' only.

Our findings also show that western Australia experienced the longest drying phase, which is in line with a climate change impacts report by the Climate Commission for Western Australia, which stated that western Australia experienced a longer 'big dry' period than other parts of Australia (Climate Commission 2011). Therefore, our results of a per-pixel characterisation of the drying and wetting phases, their duration and rate of change, refines previous studies and advances our understanding of the impacts of recent hydroclimatic variations on Australia's water storage dynamics.

2.4.2 Impacts of large-scale drought and wet events on Australia's water storage dynamics

We found the impacts of Australia's recent large-scale drought and wet extremes on water storage dynamics varied greatly across the continent, and in particular over south-eastern, north-western, and south-western Australia. Over south-eastern Australia, we found the largest fluctuations in TWSA during our study period, 2002-2014, which is consistent with previous region-scale assessments. For example, Leblanc et al. (2009) found that the MDB experienced one of the most severe and prolonged droughts on record during the 'big dry', that resulted in almost complete drying out of surface water storage with large scale groundwater depletion. This drought period was attributed to a significant lack of the "negative" phase of IOD in conjunction with increased air temperature (Ummenhofer et al. 2009). However, a complete replenishment of water in the basin was found during the 'big wet' (Hendon et al. 2014; Leblanc et al. 2011), which we found to be an average of 116% TWS recovery from our results. Consequently, the MDB was impacted the most by both droughts and floods during the early 21st-century in Australia, and will likely experience more of these extreme climatic events in coming decades (SEACI 2010).

We observed an extensive area over northwestern Australia that experienced a higher TWSA in 2002 than other parts of the continent (Fig.2.1B). This may be attributed to a substantial increase in rainfall induced by intensive cyclonic activity over northwestern Australia before our study began, which peaked in the year 2000 (Hassim and Walsh 2008; McGrath et al. 2012). However, a very strong TWS drying trend from 2002 to

the end of the 'big dry' was observed over this region associated with the decline in the frequency of tropical cyclones (McGrath et al. 2012; Nott 2011). Our research with GRACE data over northwestern Australia extended four more years as compared to previous studies (e.g. McGrath et al. 2012), and more importantly, we found that despite the 'big wet' pulse, TWS over most of this region was unable to recover water loss from the drought, indicating a severe risk in lack of water-availability (McGowan et al. 2012; McGrath et al. 2012).

The drying trend as indicated by GRACE-TWSA exerted significant impacts on Australia's agriculture production (Van Dijk et al. 2013), groundwater storage (Leblanc et al. 2011), and ecosystem function (Ma et al. 2015). For example, southwestern and southeastern Australia, the two crop-belts, experienced the most dramatic TWS declines during the big dry, which resulted in great reductions in crop production over irrigated and dryland agriculture (Ma et al. 2015; Van Dijk et al. 2013).

At the basin-level, we found that the water storage over MDB, the most important basin in Australia for crop production, wetlands, and biodiversity, to be highly sensitive to hydroclimatic variations as it exhibited the most dramatic swings in water loss/gain over the drought and wet periods, especially over the southern part of the basin (Fig.2.2B).

2.4.3 Three geographic zones and their relationships with large-scale climate modes

We showed a clustering tendency of drought-wet TWS responses across Australia, in which entire Australia can be grouped into three zones. These cluster areas reflected the fundamental influences from the interactions of the three major climate modes that affect Australia's climate (Behera et al. 2006; Cleverly et al. 2016a; Meyers et al. 2007). Overlap in the continental patterns of cross-correlations (Figs. 6 A,B,C) supports recent observations that ENSO, IOD and SAM interact to affect continental patterns of meteorology and productivity (Cleverly et al. 2016). Indeed, the TWS zones identified in this study are roughly co-located with the storm tracks affected by these climate modes (Cleverly et al. 2016).

We support the climate mode interpretation and the results from the cross correlation analysis with following discussions. First, Zone I is located at the northern and

northeastern tropical/subtropical Australia, where the climate is generally more humid with contrasting dry and wet seasons (Fig.2.4) (Williams et al. 2003). The climate of this region has been found strongly influenced by ENSO cycles, with periodic drought and wet periods associated with El Niño or La Niña phases (Tularam 2010). The extreme hydroclimatic variations as driven by the ENSO cycle is clearly reflected by GRACE measurements of TWSA, showing that Zone I has the largest pulse of TWSA during 2010-2011 (cf. Fig.2.4B, 5), which is associated with the strongest La Niña event in past ninety years (Cai and Rensch 2012).

By contrast, the formation of Zone III, which is located in western Australia, can be largely attributed to the influences exerted from the IOD cycle (Fig2.6). We noted that there was a persistent drying trend over Zone III, and its water storage did not recover to levels prior to the "big dry" period during the strong La Niña period. This further indicates the predominant influences from the IOD, and lower effects from the ENSO. Previous studies have found that the inter-annual variations in rainfall over western Australia are strongly governed by the IOD, but due to a sparsely distributed ground meteorological network over this region (Ashok et al. 2003a; England et al. 2006; Jones et al. 2009; Ummenhofer et al. 2008), less insights have been drawn at the regional scale. A persistent drying trend over Zone III is an interesting and important finding, which raises concerns on future water-availability over this region to support ecosystem function and human livelihood. Future studies are needed to address the pressing challenges that may arise from this potential further reduction of water storage over this region in the coming decades.

The climate of Zone II, which is located in between Zone I and Zone III, is most associated with complicated interactions among the influences from the east (ENSO), the west (IOD) and the south (SAM) (Jourdain et al. 2013; Keim and Verdon-Kidd 2009). Although this region experienced great reductions in water-storage during the 'big dry', we noted that the recovery of TWS during the 'big wet' was dramatic and was nearly 3 times that of the water loss during the 'big dry'. This level of high fluctuations in TWS is likely due to several explanations. For instance, the interactions among the three climate modes were found to strongly affect the climate over SE Australia (Murphy and Timbal 2008; Ummenhofer et al. 2009). A previous study found that the clearance and replacement of deep-rooted and highly-adapted native species (such as shrubland, woodlands) by shallow-rooted, less-adapted species (such as cropland,

pasture) over the SE Australia may make the naturally reoccurring drought and wet events even stronger, thus exerting much larger environmental and societal impacts (Leblanc et al. 2011; Walker et al. 1993).

A divergence in cumulative TWS flux between Zone I and Zone III was observed during the 'big dry' and 'big wet' periods (from 2002 to 2011). This pattern of a wetting trend over Zone I (northern and northeastern Australia) and a drying trend over Zone III (western Australia) provided evidence of potential spatial water cycle intensification, i.e., wet areas (Zone I) getting wetter, and dry areas (Zone III) becoming drier. Future studies are needed to understand the mechanisms behind this divergence, particularly the roles of various climate modes.

Previous studies have shown numerous connections of precipitation patterns over different parts of Australia associated with different climate modes (Cai et al. 2014b; He and Guan 2013; Meneghini et al. 2007; Risbey et al. 2009; Tularam 2010). This study utilized spatially consistent measures of total water storage anomaly and thus provided an alternative direct measure of the influences from large-scale climate modes on Australia's water storage dynamics. Furthermore, our finding of the correlations between the climate modes and GRACE-TWSA across the three geographic zones is a first step in providing insights into the control of large-scale climate patterns on Australia's vegetation and hydroclimatic dynamics, which have recently been found to significantly contribute to the global carbon and water cycles (Fasullo et al. 2013; Poulter et al. 2014). Future studies are needed to disentangle and quantify the relative importance of each climate mode from their complicated interactions on TWS dynamics over different parts of the continent.

2.5 Conclusion

In this study, we investigated the spatial patterns and temporal dynamics of terrestrial total water storage across Australia during the recent 'big dry' and 'big wet' events using GRACE observations. We focused on assessing the spatial partitioning and the loss and recovery of water storage under these extreme hydroclimatic events. Our results revealed a highly uneven distribution of water resources across space and time in Australia.

Across time, we observed large-scale reductions in water-storage during the prolonged 'big dry' period followed by a rainfall pulse-induced short-term recharge of water-storage during the 'big wet'. Across space, we found the trend in TWS during the study period varied greatly in direction, magnitude, and duration over different geographic regions. We further identified a strong clustering pattern in which Australia was grouped into three zones according to their distinct TWS responses to the 'big dry' and the 'big wet'. The clustering pattern of TWS trends provides the direct evidence of multi-climate mode interactions and control on Australia's water storage dynamics and delineates the extent of the influence of each major climate mode. Among three geographic zones, we found an overall drying trend over drier areas (western Australia) and an overall wetting trend over wetter areas (northern and northeastern Australia), i.e., dry gets drier and wet gets wetter, indicating a spatial intensification of water cycle.

Our results provide an improved understanding of the impacts of recent hydroclimatic extremes on Australia's water storage dynamics, and demonstrate the value of GRACE observations as an important indicator of hydrological system performance, and thus can be used for improving the management of water resources. Future studies are needed to understand the environmental and societal impacts of these extreme hydroclimatic events by integrating GRACE and other observational datasets.

2.6 References

AghaKouchak, A., Cheng, L., Mazdiyasni, O., & Farahmand, A. (2014). Global warming and changes in risk of concurrent climate extremes: Insights from the 2014 California drought. *Geophysical Research Letters, 41,* 8847-8852

Ahlström, A., Raupach, M.R., Schurgers, G., Smith, B., Arneth, A., Jung, M., Reichstein, M., Canadell, J.G., Friedlingstein, P., & Jain, A.K. (2015). The dominant role of semi-arid ecosystems in the trend and variability of the land CO2 sink. *Science, 348,* 895-899

Ashok, K., Guan, Z., & Yamagata, T. (2003a). Influence of the Indian Ocean Dipole on the Australian winter rainfall. *Geophysical Research Letters, 30,* 1944-8007

Ashok, K., Guan, Z., & Yamagata, T. (2003b). A Look at the Relationship between the ENSO and the Indian Ocean Dipole. *Journal of the meteorological society of Janpan, 81*, 41-56

Bastos, A., Running, S.W., Gouveia, C., & Trigo, R.M. (2013). The global NPP dependence on ENSO: La Niña and the extraordinary year of 2011. *Journal of Geophysical Research: Biogeosciences, 118*, 1247-1255

Behera, S.K., Luo, J.J., Masson, S., Rao, S.A., Sakuma, H., & Yamagata, T. (2006). A CGCM study on the interaction between IOD and ENSO. *Journal of climate, 19*, 1688-1705

Boening, C., J. K. Willis, F. W. Landerer, R. S. Nerem, and J. Fasullo (2012), The 2011 La Niña: So strong, the oceans fell, *Geophysical Research Letters, 39*, L19602

Bond, N.R., Lake, P., & Arthington, A.H. (2008). The impacts of drought on freshwater ecosystems: an Australian perspective. *Hydrobiologia, 600*, 3-16

Cai, W., Borlace, S., Lengaigne, M., Van Rensch, P., Collins, M., Vecchi, G., Timmermann, A., Santoso, A., McPhaden, M.J., & Wu, L. (2014a). Increasing frequency of extreme El Niño events due to greenhouse warming. *Nature Climate Change, 4*, 111-116

Cai, W., Purich, A., Cowan, T., van Rensch, P., & Weller, E. (2014b). Did Climate Change–Induced Rainfall Trends Contribute to the Australian Millennium Drought? *Journal of climate, 27*, 3145-3168

Cai, W., & Rensch, P. (2012). The 2011 southeast Queensland extreme summer rainfall: a confirmation of a negative Pacific Decadal Oscillation phase? *Geophysical Research Letters, 39,* L08702

Cai, W., Sullivan, A., & Cowan, T. (2011). Interactions of ENSO, the IOD, and the SAM in CMIP3 Models. *Journal of climate, 24*, 1688-1704

Castle, S.L., Thomas, B.F., Reager, J.T., Rodell, M., Swenson, S.C., & Famiglietti, J.S. (2014). Groundwater Depletion During Drought Threatens Future Water Security of the Colorado River Basin. *Geophysical Research Letters,41,* 5904-5911

Chen, J., Rodell, M., Wilson, C., & Famiglietti, J. (2005). Low degree spherical harmonic influences on Gravity Recovery and Climate Experiment (GRACE) water storage estimates. *Geophysical Research Letters, 32*, L14405

Chou, C., Chiang, J.C., Lan, C.-W., Chung, C.-H., Liao, Y.-C., & Lee, C.-J. (2013). Increase in the range between wet and dry season precipitation. *Nature Geoscience, 6*, 263-267

Cleveland, R.B., Cleveland, W.S., McRae, J.E., & Terpenning, I. (1990). STL: A seasonal-trend decomposition procedure based on loess. *Journal of Official Statistics, 6*, 3-73

Climate Commission. (2011). The Critical Decade: Western Australia climate change impacts. Department of Climate Change and Energy Efficiency, Commonwealth of Australia, Canberra, 16 pp.

Cleverly J, Eamus D, Luo Q, Restrepo Coupe N, Kljun N, Ma X, Ewenz C, Li L, Yu Q, Huete A. 2016. The importance of interacting climate modes on Australia's contribution to global carbon cycle extremes. *Scientific Reports 6*:23113.

Gent, P.R., Danabasoglu, G., Donner, L.J., Holland, M.M., Hunke, E.C., Jayne, S.R., Lawrence, D.M., Neale, R.B., Rasch, P.J., & Vertenstein, M. (2011). The community climate system model version 4. *Journal of climate, 24*, 4973-4991

Easterling, D.R., Meehl, G.A., Parmesan, C., Changnon, S.A., Karl, T.R., & Mearns, L.O. (2000). Climate extremes: observations, modeling, and impacts. *Science, 289*, 2068-2074

England, M.H., Ummenhofer, C.C., & Santoso, A. (2006). Interannual rainfall extremes over southwest Western Australia linked to Indian Ocean climate variability. *Journal of climate, 19*, 1948-1969

Famiglietti, J.S., & Rodell, M. (2013). Water in the Balance. *Science, 340*, 1300-1301

Fasullo, J.T., Boening, C., Landerer, F.W., & Nerem, R.S. (2013). Australia's unique influence on global sea level in 2010–2011. *Geophysical Research Letters, 40,* 4368-4373

Field C, Barros V, Dokken K, et al. (2014). Climate change 2014: impacts, adaptations, and vulnerability. *Intergovernmental panel on climate change report*. Cambridge, UK: Cambridge University Press, 2014.

Hassim, M.E., & Walsh, K.J. (2008). Tropical cyclone trends in the Australian region. *Geochemistry, Geophysics, Geosystems, 9,* 1525-2027

Heberger, M. (2011). Australia's Millennium Drought: Impacts and Responses. *In: Gleick, P.H. (Ed.), The World's Water: The Biennial Report on Freshwater Resources*. pp. 97–125.

He, X., & Guan, H. (2013). Multiresolution analysis of precipitation teleconnections with large-scale climate signals: A case study in South Australia. *Water Resources Research, 49*, 6995-7008

Hendon, H.H., Lim, E.-P., Arblaster, J.M., & Anderson, D.L. (2014). Causes and predictability of the record wet east Australian spring 2010. *Climate Dynamics, 42*, 1155-1174

Jiang, D., Wang, J., Huang, Y., Zhou, K., Ding, X., & Fu, J. (2014). The Review of GRACE Data Applications in Terrestrial Hydrology Monitoring. *Advances in Meteorology, 2014,* 1687-9309

Jones, D.A., Wang, W., & Fawcett, R. (2009). High-quality spatial climate data-sets for Australia. *Australian Meteorological and Oceanographic Journal, 58*, 233-248

Jourdain, N.C., Gupta, A.S., Taschetto, A.S., Ummenhofer, C.C., Moise, A.F., & Ashok, K. (2013). The Indo-Australian monsoon and its relationship to ENSO and IOD in reanalysis data and the CMIP3/CMIP5 simulations. *Climate Dynamics, 41*, 3073-3102

JPL (2012). GRACE product, Pasadena, CA [Available at http://podaacftp.jpl.nasa.gov/allData/tellus/L3/land_mass/RL05.]

Keim, A.S., & Verdon-Kidd, D.C. (2009). Climatic drivers of Victorian streamflow: Is ENSO the dominant influence? *Australian Journal of Water Resources, 13*, 17-29

Kirby, M., Connor, J., Bark, R., Qureshi, E., & Keyworth, S. (2012). The economic impact of water reductions during the Millennium Drought in the Murray-Darling Basin. In, *AARES conference* (pp. 7-10)

Kottek, M., Grieser, J., Beck, C., Rudolf, B., & Rubel, F. (2006). World map of the Köppen-Geiger climate classification updated. *Meteorologische Zeitschrift, 15*, 259-263

Landerer, F., & Swenson, S. (2012). Accuracy of scaled GRACE terrestrial water storage estimates. *Water Resources Research, 48,* W04531

Lawrence, D.M., Oleson, K.W., Flanner, M.G., Thornton, P.E., Swenson, S.C., Lawrence, P.J., Zeng, X., Yang, Z.L., Levis, S., & Sakaguchi, K. (2011). Parameterization improvements and functional and structural advances in version 4 of the Community Land Model. *Journal of Advances in Modeling Earth Systems, 3*, 1-27

Leblanc, M., Tweed, S., Ramillien, G., Tregoning, P., Frappart, F., Fakes, A., & Cartwright, I. (2011). Groundwater change in the Murray basin from long-term in situ monitoring and GRACE estimates. *Climate change effects on groundwater resources: A global synthesis of findings and recommendations CRC Press, November, 22*, 169-187

Leblanc, M.J., Tregoning, P., Ramillien, G., Tweed, S.O., & Fakes, A. (2009). Basin-scale, integrated observations of the early 21st century multiyear drought in southeast Australia. *Water Resources Research, 45*, W04408

Lim, E.-P., & Hendon, H.H. (2015). Understanding and predicting the strong Southern Annular Mode and its impact on the record wet east Australian spring 2010. *Climate Dynamics, 44*, 2807-2824

Long, D., Yang, Y., Wada, Y., Hong, Y., Liang, W., Chen, Y., Yong, B., Hou, A., Wei, J., & Chen, L. (2015). Deriving scaling factors using a global hydrological model to restore GRACE total water storage changes for China's Yangtze River Basin. *Remote Sensing of Environment, 168*, 177-193

Longuevergne, L., Scanlon, B.R., & Wilson, C.R. (2010). GRACE Hydrological estimates for small basins: Evaluating processing approaches on the High Plains Aquifer, USA. *Water Resources Research, 46*, W11517

Ma, X., Huete, A., Moran, S., Ponce-Campos, G., & Eamus, D. (2015). Abrupt shifts in phenology and vegetation productivity under climate extremes. *Journal of Geophysical Research: Biogeosciences, 120*, 2036-2052

McGowan, H., Marx, S., Moss, P., & Hammond, A. (2012). Evidence of ENSO mega-drought triggered collapse of prehistory Aboriginal society in northwest Australia. *Geophysical Research Letters, 39,* L22702

McGrath, G.S., Sadler, R., Fleming, K., Tregoning, P., Hinz, C., & Veneklaas, E.J. (2012). Tropical cyclones and the ecohydrology of Australia's recent continental-scale drought. *Geophysical Research Letters, 39,* L03404

Meneghini, B., Simmonds, I., & Smith, I.N. (2007). Association between Australian rainfall and the southern annular mode. *International journal of climatology, 27*, 109-121

Meyers, G., McIntosh, P., Pigot, L., & Pook, M. (2007). The years of El Niño, La Niña, and interactions with the tropical Indian Ocean. *Journal of climate, 20*, 2872-2880

Mo, K.C. (2000). Relationships between low-frequency variability in the Southern Hemisphere and sea surface temperature anomalies. *Journal of climate, 13*, 3599-3610

Murphy, B.F., & Timbal, B. (2008). A review of recent climate variability and climate change in southeastern Australia. *International journal of climatology, 28*, 859-879

Nicholls, N. (1991). The El Nino/southern oscillation and Australian vegetation. *Vegetation and climate interactions in semi-arid regions* (pp. 23-36): Springer

Nicholls, N. (2010). Local and remote causes of the southern Australian autumn-winter rainfall decline, 1958–2007. *Climate Dynamics, 34*, 835-845

Nicholls, N. (2011). What caused the eastern Australia heavy rains and floods of 2010/11. *Bull Aust Meteorol Oceanogr Soc, 24*, 33-34

Nott, J. (2011). A 6000 year tropical cyclone record from Western Australia. *Quaternary Science Reviews, 30,* 713-722

Poulter, B., Frank, D., Ciais, P., Myneni, R.B., Andela, N., Bi, J., Broquet, G., Canadell, J.G., Chevallier, F., & Liu, Y.Y. (2014). Contribution of semi-arid ecosystems to interannual variability of the global carbon cycle. *Nature, 509*, 600-603

Rayner, N., Parker, D.E., Horton, E., Folland, C., Alexander, L., Rowell, D., Kent, E., & Kaplan, A. (2003). Global analyses of sea surface temperature, sea ice, and night marine air temperature since the late nineteenth century. *Journal of Geophysical Research: Atmospheres, 108*, 4407

Risbey, J.S., Pook, M.J., McIntosh, P.C., Wheeler, M.C., & Hendon, H.H. (2009). On the remote drivers of rainfall variability in Australia. *Monthly Weather Review, 137*, 3233-3253

Rodell, M., Houser, P., Jambor, U.e.a., Gottschalck, J., Mitchell, K., Meng, C.-J., Arsenault, K., Cosgrove, B., Radakovich, J., & Bosilovich, M. (2004). The global land data assimilation system. *Bulletin of the American Meteorological Society, 85*, 381-394

Rodell, M., Velicogna, I., & Famiglietti, J.S. (2009). Satellite-based estimates of groundwater depletion in India. *Nature, 460*, 999-1002

Saji, N., Goswami, B.N., Vinayachandran, P., & Yamagata, T. (1999). A dipole mode in the tropical Indian Ocean. *Nature, 401*, 360-363

SEACI (2010). *Climate Variability and Change in South-eastern Australia: A Synthesis of Findings from Phase 1 of the South-eastern Australian Climate Initiative (SEACI)*. CSIRO Australia

Steffen, W.L., Hughes, L., Karoly, D.J., & Commission, C. (2013). *The Critical Decade: Extreme Weather*. Climate Commission Secretariat, Department of Industry, Innovation, Climate Change, Science, Research and Tertiary Education

Swenson, S., & Wahr, J. (2006a). Estimating large-scale precipitation minus evapotranspiration from GRACE satellite gravity measurements. *Journal of Hydrometeorology, 7*, 252-270

Swenson, S., & Wahr, J. (2006b). Post-processing removal of correlated errors in GRACE data. *Geophysical Research Letters, 33,* L08402

Thompson, D.W., & Solomon, S. (2002). Interpretation of recent Southern Hemisphere climate change. *Science, 296*, 895-899

Tregoning, P., McClusky, S., van Dijk, A., Crosbie, R., & Peña-Arancibia, J. (2012). Assessment of GRACE satellites for ground-water estimation in Australia. National Water Commission, Can-berra, 82, available at:archive.nwc.gov.au/library/waterlines/71

Trenberth, K.E. (2012). Framing the way to relate climate extremes to climate change. *Climatic change, 115*, 283-290

Tularam, G.A. (2010). Relationship between El Niño southern oscillation index and rainfall *Int.J. Sustain. Dev. Plann., 1*, 1-14

Ummenhofer, C.C., England, M.H., McIntosh, P.C., Meyers, G.A., Pook, M.J., Risbey, J.S., Gupta, A.S., & Taschetto, A.S. (2009). What causes southeast Australia's worst droughts? *Geophysical Research Letters, 36,* L04706

Ummenhofer, C.C., Sen Gupta, A., Pook, M.J., & England, M.H. (2008). Anomalous rainfall over southwest Western Australia forced by Indian Ocean sea surface temperatures. *Journal of climate, 21*, 5113-5134

Van Dijk, A.I., Beck, H.E., Crosbie, R.S., Jeu, R.A., Liu, Y.Y., Podger, G.M., Timbal, B., & Viney, N.R. (2013). The Millennium Drought in southeast Australia (2001–2009): Natural and human causes and implications for water resources, ecosystems, economy, and society. *Water Resources Research, 49*, 1040-1057

Wahr, J., Molenaar, M., & Bryan, F. (1998). Time variability of the Earth's gravity field: Hydrological and oceanic effects and their possible detection using GRACE. *Journal of Geophysical Research: Solid Earth (1978–2012), 103*, 30205-30229

Wahr, J., Swenson, S., & Velicogna, I. (2006). Accuracy of GRACE mass estimates. *Geophysical Research Letters, 33,* L06401

Walker, J., Bullen, F., & Williams, B. (1993). Ecohydrological changes in the Murray-Darling Basin. I. The number of trees cleared over two centuries. *Journal of Applied Ecology*,30, 265-273

Wen-Jian, H., & Hai-Shan, C. (2013). Impacts of regional-scale land use/land cover change on diurnal temperature range. *Advances in climate change research, 4*, 166-172

Williams, S.E., Bolitho, E.E., & Fox, S. (2003). Climate change in Australian tropical rainforests: an impending environmental catastrophe. *Proceedings of the Royal Society of London B: Biological Sciences, 270*, 1887-1892

Wolter, K. (1987). The Southern Oscillation in surface circulation and climate over the tropical Atlantic, Eastern Pacific, and Indian Oceans as captured by cluster analysis. *Journal of Climate and Applied Meteorology, 26*, 540-558

Wolter, K., & Timlin, M.S. (1998). Measuring the strength of ENSO events: how does 1997/98 rank? *Weather, 53*, 315-324

Wolter, K., & Timlin, M.S. (2011). El Niño/Southern Oscillation behaviour since 1871 as diagnosed in an extended multivariate ENSO index (MEI. ext). *International journal of climatology, 31*, 1074-1087

Yang, Y., Long, D., Guan, H., Scanlon, B.R., Simmons, C.T., Jiang, L., & Xu, X. (2014). GRACE satellite observed hydrological controls on interannual and seasonal variability in surface greenness over mainland Australia. *Journal of Geophysical Research: Biogeosciences, 119*, 2245-2260

Chapter 3: Spatial-temporal climate system drivers of Australia's total water storage and vegetation productivity under hydroclimatic extremes

Abstract

Extreme climate variability over Australia is driven by three dominant ocean-atmosphere climate systems including El Niño Southern Oscillation, Indian Ocean Dipole and Southern Annular Mode. In a previous study, we observed spatial clustering of Total Water Storage (TWS) responses to a Millennium drought ('big dry', 2001-09) and subsequent wet period ('big wet', 2010-11) across Australia. The entire continent partitioned into three geographic zones with diverse drying and wetting trends in rainfall, vegetation productivity, and total water storage, mimicking to varying extents, fundamental influences from the individual climate modes. We utilized Climate Index, satellite-based GRACE-Total Water Storage Anomaly (TWSA) and MODIS-Enhanced Vegetation Index (EVI) data to investigate the spatial-temporal responses, dynamics and trends of Australia's hydrologic and productivity patterns with the three climate systems. Three hydroclimatic extremes of a prolonged drought, a dramatic wet pulse and another anomalous El Niño event were analyzed from 2002 to 2015, using Partial Cross-Correlation Analyses to capture the controls of each climate driver on EVI, TWS, and rainfall. Our results confirmed the dominant influence of the climate modes and their geographic impacts on the continental scale ecohydrological patterns. Three distinct hydrologic zones in TWS patterns were observed across the hydroclimatic extremes study period, which were more pronounced than the spatial-temporal continental rainfall patterns. We further observed distinct changing patterns in surface greenness within the three zones, which were largely driven by respective Climate mode-TWS relationships, and less correlated with rainfall patterns. Moreover, the 2015 El Niño event, which caused severe declines in TWS and vegetation productivity over many parts of Australia, corroborated the three-zone-like influences from the climate modes. This study highlights the value of GRACE-TWSA for effectively linking the extreme climate variability with dynamics in Australia's vegetation productivity, which have recently been found to significantly contribute to the global carbon and water cycles.

3.1 Introduction

Climate variability across Australia is largely driven by three dominant ocean-atmosphere systems including the El Niño Southern Oscillation (ENSO), characterised by its two extreme phases: El Niño and La Niña in the tropical Pacific Ocean, the Indian

Ocean Dipole (IOD) in the tropical Indian Ocean and Southern Annular Mode (SAM) in the Southern Ocean (Holton et al. 1989; Saji et al. 1999a; Wallace and Thompson 2002; Webster et al. 1999). Here we refer ENSO, IOD and SAM as climate modes, of which influences on weather over Australia have varying levels of geographic impact at different times of year (Risbey et al. 2009). The principal climate driver is considered to be the ENSO (Bastos et al. 2013), with increasing frequencies of extreme El Niño and La Niña events due to global warming (Cai et al. 2014a). IOD and SAM have also been recognized to play important roles on climate variations especially during the recent hydroclimatic events in Australia.

Australia earned its reputation for "a land of climatic extremes" in the early 21st century by exhibiting three large-scale hydroclimatic extremes within the last 15 years (Cleverly et al. 2016). It first experienced a prolonged drought, commonly known as the 'Millennium Drought' (or 'big dry') from 2001 to 2009 (Leblanc et al. 2009; McGrath et al. 2012), which was then followed by an intensive wet pulse in 2010-2011 termed the 'big wet'(Heberger 2011; Nicholls 2011). Not long after the 'big wet', Australia switched into another drought in 2015 that eventually became one of the strongest El Niño events on record. These dry and wet extreme events exerted pronounced negative impacts on food production, water resources and ecosystems, with increased natural disasters such as bushfires, cyclones, droughts, flooding and severe declines in water availability over large areas (Kirby et al. 2012; Van Dijk et al. 2013).

Previous studies based on climate models suggested that the recent hydroclimatic events were largely caused by the variability and interactions of the three major climate modes (Cleverly et al. 2016; Ummenhofer et al. 2011). The 'big dry' event in south-eastern Australia was attributed to a significant lack of the ""negative"" phase of IOD in conjunction with increased air temperature (Ummenhofer et al. 2009) while that over south-western Australia was a result of the combination of positive IOD and an upward Southern Annular Mode (SAM) trend during winter (Cai et al. 2014b; Ummenhofer et al. 2008). Although the 'big wet' was mostly driven by one of the strongest La Niña events in the past nine decades (BOM 2012; Nicholls 2011), it was also influenced by a concurrent extreme positive excursion of SAM (Hendon et al. 2014; Lim and Hendon 2015) especially over eastern Australia. The 2015 dry event was found to be mainly explained by one of the 26 strongest El Niño events since 1900 (Scott Power 2016).

Numerous studies have been carried out on the effects of ENSO, IOD and SAM on rainfall across Australia. Risbey et al. (2009) examined the relative contributions of each climate mode to rainfall variability in different regions of Australia. They found climatic drivers have varying influence on rainfall depending on geographic locations and seasons, but generally interacted together to form rainfall patterns over the continent. Cleverly et al. (2016) further showed that synchronization of the three climate modes will often bring more than the effect of any single mode on rainfall, causing extreme dry or wet hydroclimatic events across Australia.

Despite these studies, it still remains a challenge to use rainfall to quantify the association between climate variability and hydrological dynamics across Australia. The resaons are 1) rainfall is highly variable across Australia, especially over arid/semi-arid regions where random rainfall pulse events are common; 2) rainfall records at any given location (over even long periods) can be skewed by weather contributions, such as individual storms, which are largely unrelated to climate modes (Risbey et al. 2009); 3) Australia has seen shifting rainfall patterns due to an intensified global water cycle with increasing hydroclimatic events (AghaKouchak et al. 2014; Xie et al. 2016). As a consequence, inconsistencies between climate modes and precipitation have been observed in historical records. For instance, rainfall was only significantly correlated with ENSO in around one third of the last 100 years, with absences occurring often during wet years (Cleverly et al. 2016).

As a measurement of variations in the integrated water, Total Water Storage Anomaly (TWSA) derived from the Gravity Recovery And Climate Experiment (GRACE) may be better than rainfall to examine the control of climate modes on Australian water resources, in particular, under hydroclimatic impacts. This is particularly important for Australia, which has so far faced increasingly common hydroclimatic extremes in the 21st century. GRACE-TWSA has been recognized as a valuable indicator for the water availability over large areas and widely used in hydrological and geodesic studies (Jiang et al. 2014; Tregoning et al. 2012). However, this information has not been fully realized in the area of climatology.

In our previous study (Xie et al. 2016), we observed a clustering tendency of Total Water Storage (TWS) responses to the 'big dry' and 'big wet' events across Australia, in which the entire continent could be partitioned into three zones. Specifically, a north to north-eastern subtropical region (zone I) exhibited persistent increasing trends in TWS

across both the dry and wet periods. A south-eastern region (zone II) that showed strong TWS drying and a subsequent complete recovery to previous TWS levels (2002) during the 'big wet'. By contrast, an extensive area in western Australia (zone III) had a continuous decline in TWS during the 'big dry' but only a subtle increase during the 'big wet', indicating a weak recovery of water storage. These geographic zones with diverse drying and wetting TWS trends, as quantified by GRACE-TWSA, may reflect the fundamental influences from various climate modes (Fig.2.4B).

In this chapter, we characterised and evaluated the spatial-temporal responses, dynamics and trends of Australia's hydrologic and productivity patterns with the three climate systems from 2002 to 2015, encompassing the recent hydroclimatic extremes of the prolonged 'big dry', dramatic 'big wet' pulse and anomalous 2015 El Niño event. Climate index, GRACE-TWSA, TRMM-rainfall and MODIS-EVI data were used to represent the variations in climate modes, hydrological conditions and vegetation productivity across Australia during the study period. As the relationships between the climate modes and TWS are expected to show significant and finite lags (Kirono et al. 2010; Schepen et al. 2012), a Partial Cross-Correlation Analysis (PCCA) technique was applied in this study, which enabled us to capture the control from each climate driver on TWS with the effects from the phase lags and other two drivers removed. In particular, we aimed to: (1) investigate the relative contributions of the three climate modes to the partitioning of the three TWS zones in Australia that were observed in our previous study; (2) examine the advantages of using GRACE-TWSA compared to rainfall in assessing the varying extents and fundamental influences from the climate modes on water resources and vegetation; (3) quantify the ecohydrological implications of the 2015 El Niño event and validate the three-zone-like influences from the climate modes.

This study is the first attempt to define the clear boundaries of the influences from various climate modes on Australian water storage dynamics. Our results herein can generate important knowledge that is highly valuable for understanding the hydrological impacts of climate dynamics over other global regions as well.

3.2 Data and Methods

3.2.1 Climate indices

We used three climate indices in this study to represent the dynamics in the coupled ocean-atmosphere systems (ENSO, IOD and SAM), which have been previously identified as the dominant drivers of climate variability across Australia (Cai et al. 2014b; Verdon-Kidd and Kiem 2009). These include the Southern Oscillation Index (SOI), the Indian Ocean Dipole Mode Index (DMI) and the Southern Annular Mode Index (SAMI).

SOI, representing the large-scale fluctuations in ENSO, is a measure of the difference in surface air pressure between the western and eastern tropical Pacific, i.e. between Tahiti and Darwin (Zhang and Casey 1992). This index (available from http://www.esrl.noaa.gov/psd/data/climateindices/list/) indicates the development and intensity of El Niño or La Niña events in the Pacific Ocean, which is best represented by monthly or longer averages as daily or weekly values can fluctuate markedly due to short-lived weather patterns and occurrence of tropical cyclones (Power et al. 1999). In general, a strongly and consistently negative SOI pattern is associated with a high probability of below long-term average rainfall for many areas of Australia, especially over northern and eastern Australia (termed the El Niño event). Conversely, deep and consistent positive SOI values often cause above average rainfall in Australia (termed the La Niña event).

DMI, derived from the Hadley Centre Sea Ice and Sea Surface Temperature (HadISST) dataset (Rayner et al. 2003), is an index of IOD represented by the anomalous zonal SST gradient between the western and south-eastern equatorial Indian Ocean (Saji et al. 1999b). A positive DMI often leads to less rainfall over the south-eastern and south-western areas of Australia while negative DMI values are likely to result in more rainfall in the same areas.

SAMI (also known as the Antarctic Oscillation Index) data were downloaded from the Climate Prediction Center. It represents the dynamics in SAM, which describes the north-south movement of the westerly wind belt that circles Antarctica, dominating the middle to higher latitudes of the southern hemisphere (Thompson and Solomon 2002). SAMI was constructed by projecting the monthly mean 700-hPa height anomalies onto the leading Empirical Orthogonal Function (EOF) mode (Mo 2000). Previous studies found positive SAMI values will often result in reduced rainfall over areas in southern Australia during the winter with an increased rainfall during the spring and summer but

is mostly confined to the southeast or central east coast (Hendon et al. 2014). The three climate indices used in this study are monthly time series data that extend from 2002 to 2015.

3.2.2 Total water storage anomaly

GRACE derived Total water storage anomaly data was described in Chapter 2.

3.2.3 Enhanced vegetation index

The Enhanced Vegetation Index (EVI) is widely used as a proxy of canopy "greenness", representing an integrative composite property of green leaf area, foliage cover, structure and leaf chlorophyll content (Glenn et al. 2008; Huete et al. 2002). EVI was developed as an alternative vegetation index to address some of the limitations in the Normalized Difference Vegetation Index (NDVI) such as an influence of atmospheric conditions, canopy background signals and in particular, saturation of high biomass (Huete et al. 2008; Huete et al. 2006). The formulation of EVI (Huete et al. 2002) is,

$$\text{EVI} = 2.5 \times \frac{\rho_{nir} - \rho_{red}}{\rho_{nir} + 6 \times \rho_{red} - 7.5 \times \rho_{blue} + 1} \quad (3.1)$$

where ρ_{nir}, ρ_{red}, and ρ_{blue} are surface reflectances in the near infrared (841–876 nm), red (620–670 nm) and blue (459–479 nm) bands respectively.

In this study we downloaded Moderate Resolution Imaging (MODIS) EVI data (MOD13C2, Collection 5) from 2000 to 2015 through the online Data Pool at the NASA Land Processes Distributed Active Archive Centre, USGS (https://lpdaac.usgs.gov). Global MOD13C2-EVI data are cloud-free spatial composites of the gridded 16-day 1 kilometre MOD13A2, and are provided monthly as a level-3 product projected on a 0.05 degree (5600-meter) geographic Climate Modelling Grid (CMG).

We further filtered the EVI data using the following criteria based on the Quality Assessment (QA) flags provided in MOD13C2 product: 1) used only highest quality of

VI usefulness for all bands; 2) performed atmospheric and adjacency corrections; 3) excluded observations with snow cover, high aerosol or climatology aerosol quantity, mixed or high clouds present, or water in the Land/Water Flag (Broich et al. 2014). Linear interpolation in the temporal dimension was used to fill the gaps remaining after QA filtering, but pixels with more than two consecutive gaps (2 months) were discarded from the analysis (Ma et al. 2013).

3.2.4 Rainfall

The Tropical Rainfall Measuring Mission (TRMM) was a joint endeavour between NASA and Japan's National Space Development Agency (JAXA). The mission was designed to monitor and study dynamics in the tropical/sub-tropical rainfall with a coverage of 40°N to 40°S from 1998 to present (Simpson et al. 1996). For this research, we utilized the TRMM 3B43 version 7 product that extends from 2002 to 2015, which combines the estimates generated by the TRMM satellite-derived precipitation and the Climate Anomaly Monitoring System (CAMS) global gridded rain gauge data. The resolution of the data is 0.25˚ grid pixels for each hour and we further composited the hourly observations into monthly values for comparison with other data used in this study.

3.2.5 Correlation analysis

The three climate modes are not independent. ENSO has a strong influence on, or mutually interacts with IOD and SAM at some areas of Australia during certain seasons (Cai et al. 2011). In particular, there are significant interactions between the development of the ENSO and IOD (Behera et al. 2006; Kug and Kang 2006; Kug et al. 2006). To address this issue and capture the impacts of individual climate mode on TWS, the Partial Correlation (PC) technique was developed in several earlier studies (Risbey et al. 2009). They used the PC technique to isolate the part of the rainfall explained by a given climate mode that is not correlated with other modes. However, this method cannot totally exclude the influences of other climate modes when they contain phase lags from the signal, which is often the case in Australia (Kirono et al. 2010; Schepen et al. 2012).

In this study, we used a Partial Cross Correlation Analysis (PCCA) to better quantify the relationships of two non-stationary signals (each climate mode and TWS) on different time lags. Based on methods developed in previous studies (Podobnik et al. 2009; Podobnik and Stanley 2008; Yuan et al. 2015; Zebende 2011), our PCCA method is designed at pixel level as below:

1). For each pixel on stacked GRACE-TWSA monthly images over a period, we have 3 climate time series and one TWSA time series, which all can be considered as random walks and defined as:

$$\sum_{i=1}^{k} t_i \tag{3.2}$$

where k is the length of the time series (e.g. 165 monhtly values of time series from April 2002 to December 2015).

2). The cross-correlation levels between TWSA(x) and each climate mode (y) can be estimated as,

$$\mathrm{cr} = \frac{\sum_i^k [(x(i)-mx)*(y(i-l)-my]}{\sqrt{\sum_i^k (x(i)-mx)^2}\sqrt{\sum_i^k (y(i-l)-my)^2}} \tag{3.3}$$

Where cr is the cross correlation coefficient, l is the time lag in months, mx and my are the means of the corresponding series. As the impact of climate modes on TWS is expected to show finite time lags (0 to 6 months), we only considered positive time lags when climate modes are leading the changes of TWS.

3). The optimal time lag (l) for each pixel was obtained when cr was the maximum. We then shifted the climate mode time series back to the corresponding time lags in order to quantify the partial correlations between them and TWS without the effects of the time lags. Finally the PCCA is determined as (Baba et al. 2004),

$$r_{xy.z} = \frac{r_{xy}-r_{xz}r_{yz}}{\sqrt{(1-r_{xz}^2)(1-r_{yz}^2)}} \tag{3.4}$$

Where $r_{xy.z}$ is the first-order partial correlation coefficient, x is one of the climate mode time series and y is the TWSA time series on each pixel and z is one of the other two

climate modes time series representing the first controlling variable, r_{xy}, r_{xz} and r_{yz} are the regular pearson correlation coefficients.

Partial correlation coefficient between one climate mode and TWSA time series with two controlling variables is calculated as second-order partial correlation (rxy.z1z2),

$$r_{xy.z1z2} = \frac{r_{xy.z1} - r_{xz2.z1} r_{yz2.z1}}{\sqrt{(1 - r^2_{xz2.z1})(1 - r^2_{yz2.z1})}} \quad (3.5)$$

Where $r_{xy.z1}$, $r_{xz2.z1}$ and $r_{yz2.z1}$ are first-order partial correlations among variables x, y, and controlling variables z2 and z1.

P-value for the Pearson partial correlations is computed as

$$p = \frac{\sqrt{(N-k-2)} * r}{\sqrt{(1-r^2)}} \quad (3.6)$$

as coming from a t distribution with (N – k - 2) degrees of freedom, where r is the partial correlation and N is sample size.

Semi Partial Cross Correlation Analysis (SPCCA) is used to quantify relative importance of each climate mode to TWS variance which is calculated based on equations of 1-3) and 6) below. Although the formula for SPCCA and PCCA are similar, they were used for different purposes as the Fig.3.1 shown.

$$sr_{x(yz1z2)} = \frac{r_{xy.z1} - r_{xz2.z1} r_{yz2.z1}}{\sqrt{1 - r^2_{yz2.z1}}} \quad (3.7)$$

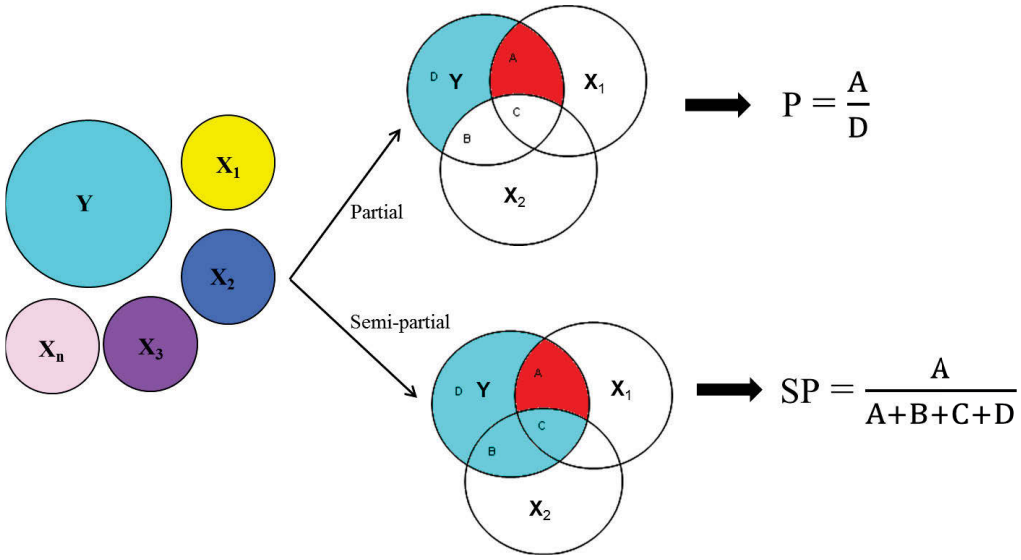

Figure 3.1. Illustration diagram for Partial and Semi-partial correlations

In order to assess the varying temporal impacts of climate modes on TWS across four seasons, we also calculated partial correlations between each climate mode and TWS without lag analysis. In addition, regular Cross Correlation Analysis (CCA) was applied to examine the spatial relationships between TWS, rainfall and EVI at pixel-level across Australia based on their monthly data.

3.2.6 Calculation for climate modes of TWS variance

We performed regression analysis between climate modes and TWSA time series on each pixel to evaluate the proportion of TWS variance explained by climate modes across Australia. Given multi-collinearity and interactions among the climate modes (Risbey et al. 2009), we chose not to use multiple regression of all three climatic variables. Instead, we achieved this by evaluating the R-square from the linear regression between TWSA and the climate driver with the highest correlation to monthly TWSA at each grid cell.

3.2.7 Spatio-temporal variability

Monthly values of three climate indices and continentally averaged TWSA over different periods were plotted to show their temporal variability and associations. The annual cumulative TWS flux described in Chapter 2 was calculated for the three TWS zones of Australia from 2002 to 2015 in this Chapter to represent the total TWS

loss/gain in each TWS zone under the three hydroclimatic impacts. Annual anomaly images of integrated EVI, rainfall and averaged TWSA were computed, relative to two time means (2002-14 and 2010-15) with the purpose of examining the spatial changing patterns in vegetation productivity, rainfall and TWS across Australia during the 'big dry' and 'big wet' events and 2015 El Niño event, respectively.

3.3 Results

3.3.1 Climate drivers of three distinct hydrologic zones in TWS patterns

Partial cross correlations between climate indices and GRACE-TWSA over 2002–2014 show the spatial influences from each climate driver on TWS across Australia with the effects from their phase lags and other two drivers removed (Fig.3.2). We found close coupling between the three climate modes and TWS during the study period in preferred but different geographic locations. These spatial patterns of climate-TWS associations suggest that the three geographic clusters are broadly similar as the TWS Zones I, II and III described in Chapter 2 (Fig. 3.2 and Fig.3.4B).

ENSO represented by SOI broadly influenced TWS over Zone I and II (eastern and northern Australia), with the strongest correlation coefficients ($r > 0.4$) observed in Zone I (Fig.3.2A). This shows ENSO is the dominant climate driver of TWS variability among the three but had weak influence on TWS over most of Zone III. DMI, representing IOD, was significantly correlated with TWSA in Zone II and III, spanning over much of the south-western and south-eastern areas of Australia (Fig.3.2B). Compared with ENSO and IOD, SAM influenced TWS the least across Australia (Fig.3.2C). During our study period, SAMI was only significantly correlated with TWSA over areas of eastern Australia (in parts of both Zone I and II), where its positive values could increase the springtime rainfall over that area.

Figure 3.2 presents varying geographic importance of individual climate mode on TWS across Australia, indicating TWS dynamics in Zone I is primarily controlled by ENSO while those in Zone III are largely influenced by IOD. TWS variations in Zone II, which is located in between Zone I and III, were driven by the combined interactions among ENSO, IOD and SAM.

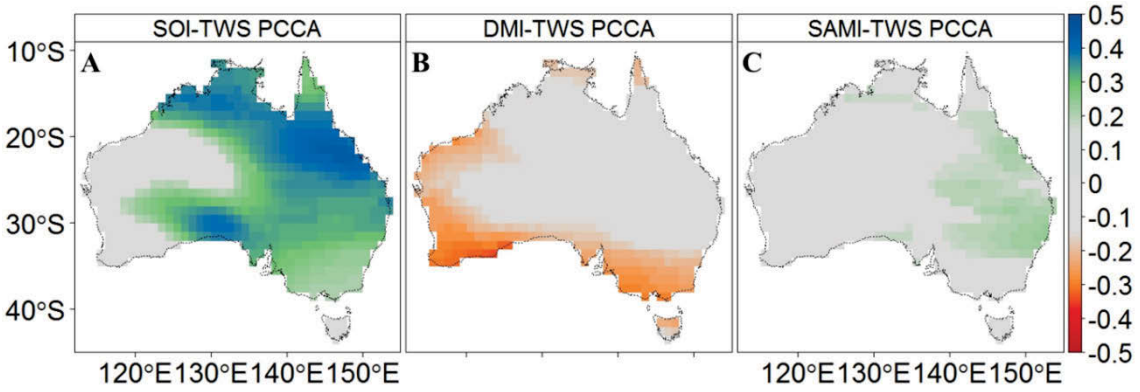

Figure 3.2. Partial cross correlation coefficients between monthly (A) SOI, (B) DMI, (C) SAMI and TWSA across Australia from April 2002 to December 2014. Only correlations significant at the 95% level are shown with non-significant pixels coloured as grey.

We observed that climate systems also exert varying influence on TWS by seasons (Fig.3.3). Our results showed ENSO modulates TWS over northern and eastern Australia through all seasons, with the strongest influence in summer and autumn (Fig.3.3A). IOD has the most pronounced effect on TWS also through summer and autumn, spanning over western and south-eastern regions of Australia (Fig.3.3B). The SAM tends to reduce TWS in spring over southern Australia while it increases TWS during summer but this increase is confined only to eastern coastal areas (Fig.3.3C). In contrast to the previous studies on climate drivers of rainfall seasonal variability (Risbey et al. 2009; Schepen et al. 2012), we found the influence of climate modes on TWS generally has a one season lag to that of rainfall. This indicates rainfall is the source of terrestrial water resources and partly leads TWS dynamics. However, due to the short temporal coverage of GRACE data (13 years), most of the pixels shown here don't have significant correlations. Therefore, Figure 3.3 here has to be interpreted with caution.

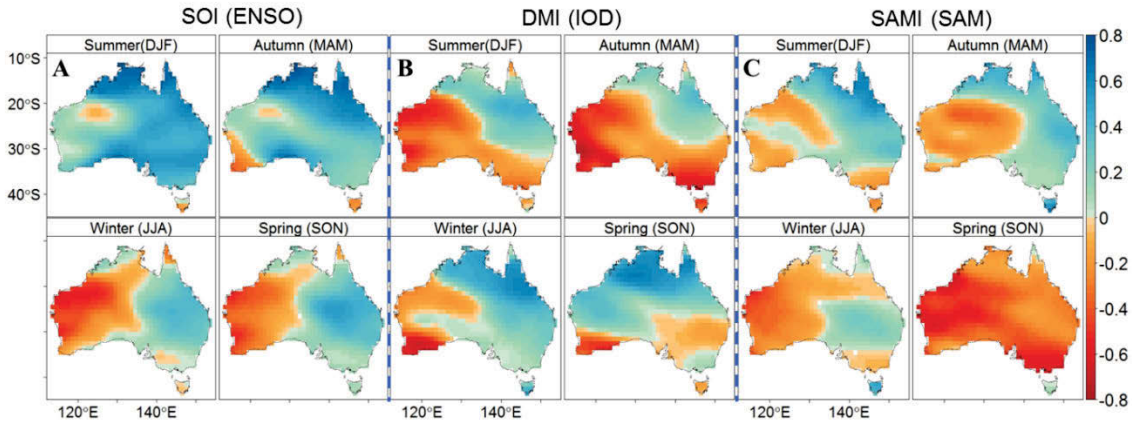

Figure 3.3. Partial correlation coefficients between (A) SOI, (B) DMI, (C) SAMI and TWSA for four seasons across Australia from 2002 to 2014. The confidence interval is (± 0.5).

We used SPCCA to calculate the relative importance of the three climate modes to TWS dynamics at any given location (1 degree pixel level) across Australia and further labelled them in a ternary plot (Fig.3.4A). ENSO is shown to be the most important climate driver of TWS variability, accounting for 76% of the highest importance pixels (highlighted in blue) across the continent (532 out of total 699 pixels). IOD was more important than ENSO and SAM over 22% of the country while SAM only accounted for around one percent. We further projected the ternary plot into a RGB composite map to show the spatial distributions of the relative importance in ENSO, IOD and SAM (Fig.3.4B). Similar to the partial cross correlations, ENSO has the most extensive influence on TWS, then IOD. There is a small area in north-western Australia, in which both of ENSO and IOD had a very weak influence on TWS, showing a higher importance of SAM represented in green (Fig.3.4B).

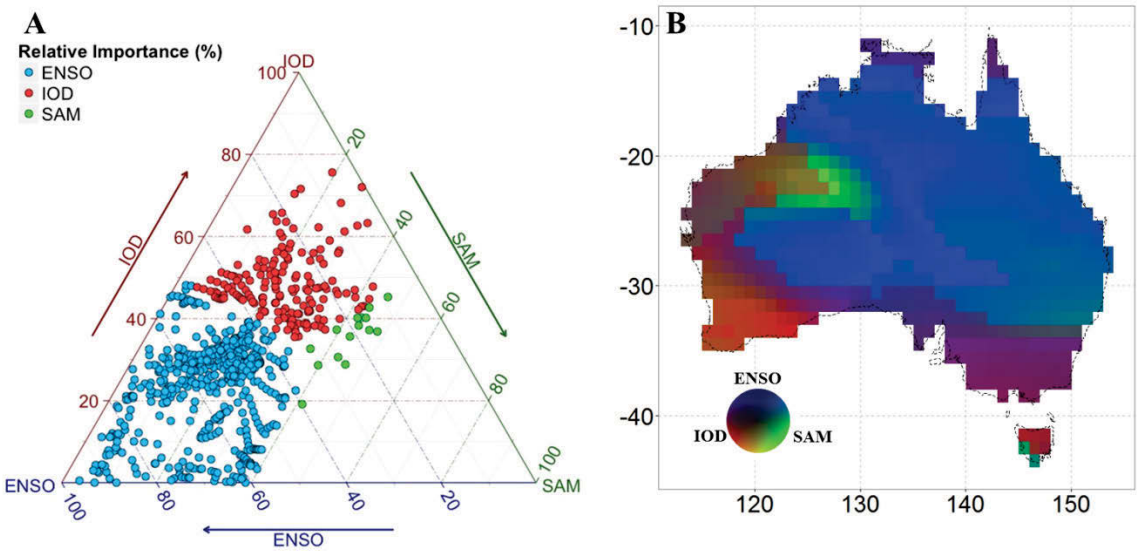

Figure 3.4. (A) Ternary plot of relative importance in three climate modes with blue colour representing ENSO has the highest importance, red for IOD and green for SAM. (B) RGB composite map of ternary plot on 1 degree pixel resolution.

TWS variance explained by the climate mode with the highest correlation at each pixel shows the importance of the leading drivers in each pixel region at any given location of Australia (Fig.3.5). We found that northern and eastern Australia has more TWS explained variance than other parts of Australia. In particular, the highest levels of explained variance are in Zone I, where TWS is mostly associated with ENSO. Areas of higher explained variance also include Zone II in association with ENSO, and south-western and south-eastern tips of Australia mostly in association with IOD and partly with SAM. TWS is poorly explained by any of the three climate drivers in Zone III especially in the north-western region of Australia, where TWS variation may be related to other climate drivers e.g. Madden–Julian oscillation (MJO). The amount of variance explained ranges from around 1% to 25%, but over most regions of the continent any given climate mode accounts for typically less than 20% of the variance in TWS (Fig.3.5). While Figure 3.5 shows in each case the amount of TWS variance explained is less than 25%, this is due to a single use of climate mode here that doesn't take into account the potential higher explanatory level through considering multiple modes and their interactions (Fig.3.5).

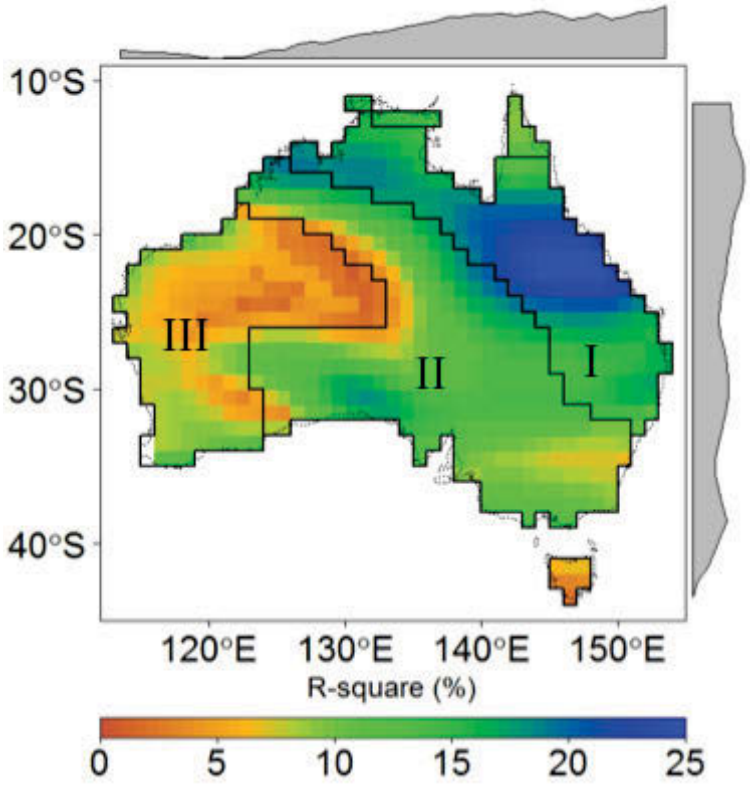

Figure 3.5. Amount of TWS variance explained by the climate mode with the highest correlation to monthly TWS (during 2002 – 2014) at each grid cell across Australia. The black lines denote the boundaries of the three TWS zones.

3.3.2 TWS-EVI vs rainfall-EVI patterns with climate variability

We also quantified the relationships between each climate mode and rainfall during the 'big dry' and 'big wet' periods (2002 – 2014) using the PCCA method. During the study time, ENSO was found to be the dominant climate driver for rainfall variations across the continent except over the south-western area of western Australia. We observed significant influence on rainfall from IOD and SAM as well but this was confined to small areas. Although rainfall is the input and main driver of TWS variability, we found the spatial-temporal continental rainfall patterns are much less pronounced to be the explanation for the three distinct TWS hydrologic zones observed in Chapter 2. This may indicate that the highly variable characteristics of rainfall in Australia especially over arid/semi-arid regions, makes it hard to use rainfall to link the climate variations and dynamics in water availability for ecosystems.

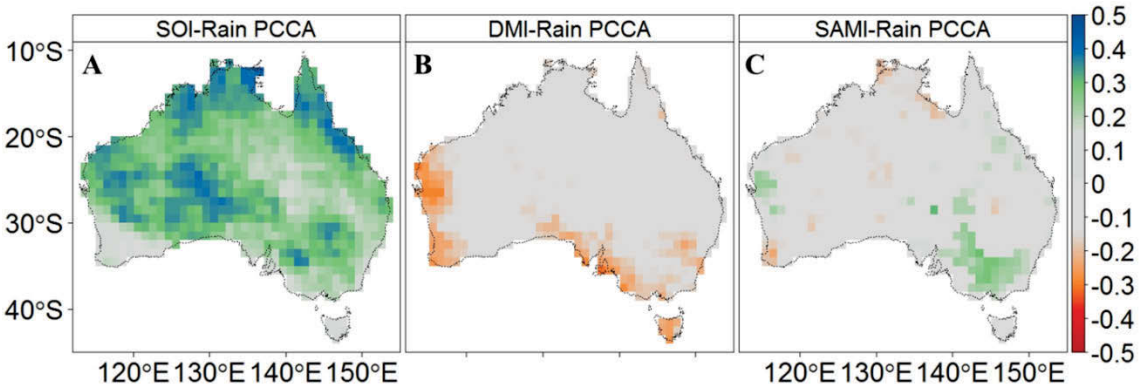

Figure 3.6. Partial cross correlation coefficients between monthly A) SOI, B) DMI, C) SAMI and Rainfall across Australia from April 2002 to December 2014. Only correlations significant at the 95% level are shown with non-significant pixels coloured as grey.

Annual anomalies of integrated EVI (iEVI) and total rainfall across Australia for hydrological years 2002 – 2013 were calculated to represent the dynamics in vegetation productivity and rainfall across the dry and wet hydroclimatic events. The end of the 'big dry' and 'big wet', representing also the driest year and the wettest year over our study period, were analysed to assess the links between TWS and vegetation/rainfall (Fig.3.7). We observed three distinct changing patterns in vegetation productivity over Zones I, II and III across the dry and wet years, largely following the TWS patterns (Fig.3.7A-B). By contrast, continental rainfall anomalies show similar three zone patterns as iEVI but inconsistencies exist between them, especially over Zone III, including the areas highlighted by the black circles in both dry and wet years (Fig.3.7C-D). This may indicate that GRACE-TWSA, as an integral measurement of water, is more directly linked with vegetation than rainfall, particularly under hydroclimatic impacts.

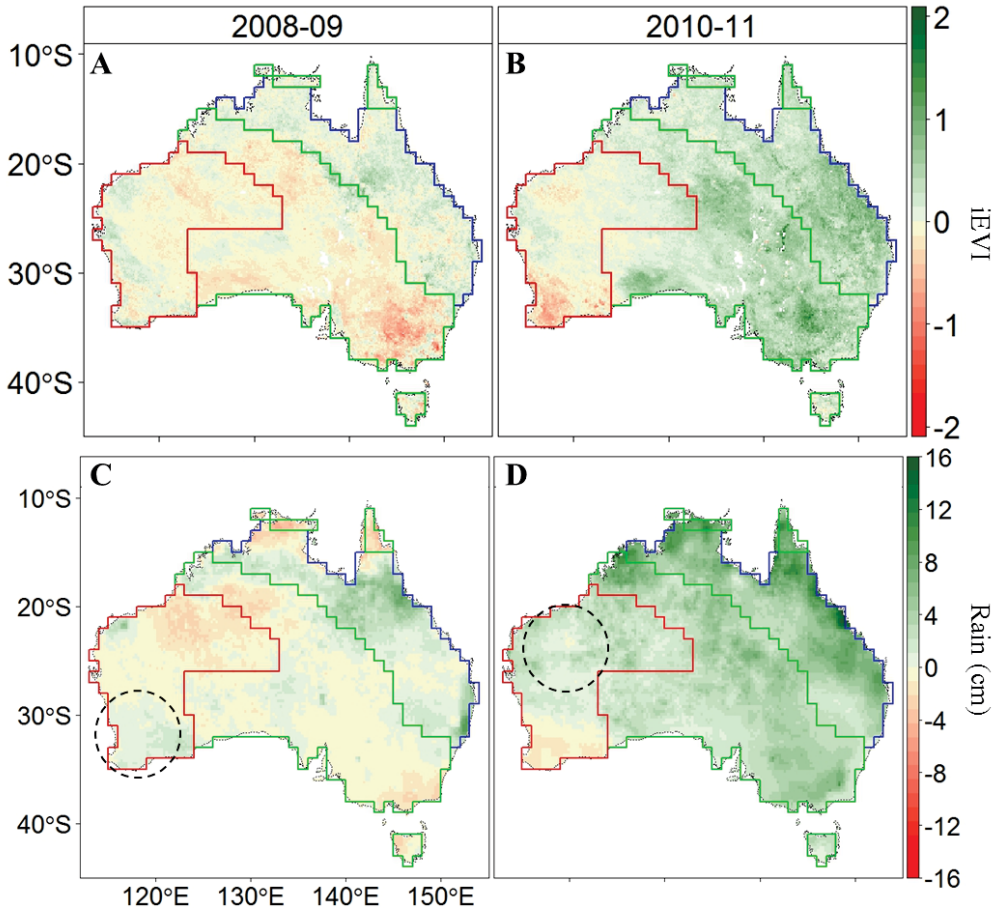

Figure 3.7. Anomalies of (A-B) annually integrated EVI and (C-D) summed rainfall across Australia over hydrological years for the end of the 'big dry' (2008-2009) and the end of the 'big wet' (2010-2011). The blue, green and red lines denote the boundaries of TWS Zones I, II and III respectively and dashed circles highlight the differences between figures A and C, B and D.

Results from cross correlation analysis show that TWS has better correlations overall (average r = 0.6) with surface greenness than rainfall (average r = 0.55) across Australia (Fig.3.8A, C). We also found the spatial distributions of correlation coefficients in the TWS-EVI relationship are more uniform than those in rainfall-EVI relationship, in which r is generally higher in northern Australia but lower in the southern parts (Fig.3.8A, C). Interestingly, the correlations between rainfall and TWS display a clear gradient, with high to low r spanning from northern to southern Australia (Fig.3.8E). Lag analysis shows that compared with rainfall, TWS is more directly related to EVI without lags over most parts of Australia, indicating TWS as a measure of final water availability on the land (Fig.3.8B, D). Rainfall is found to be leading TWS and EVI with general lags of 1 or 2 months (Fig.3.8D, F).

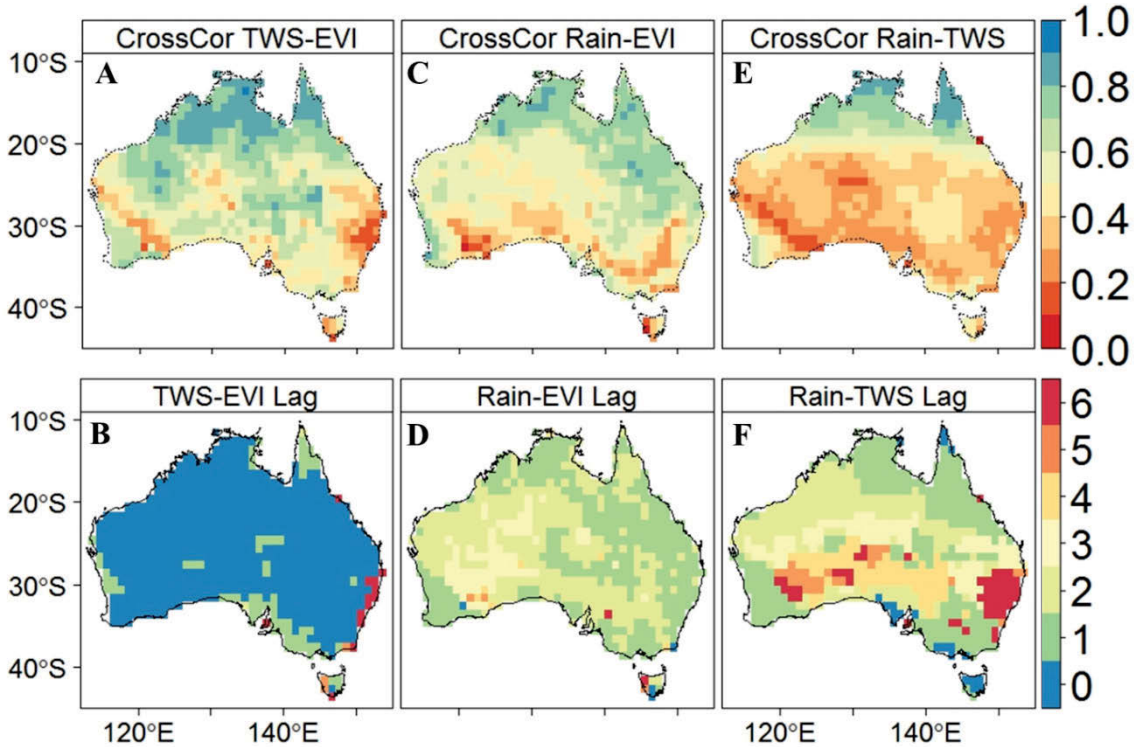

Figure 3.8. Pearson's coefficient (maximum r) and the corresponding time lag in months between (A-B) monthly TWSA and EVI; (C-D) rainfall and EVI; (E-F) rainfall and TWSA over April 2002 to December 2014.

3.3.3 Temporal evolution of TWS under variations in three climate modes and their interactions

Monthly TWSA averaged over the continent show both seasonal and inter-annual TWS fluctuations from 2002 to 2015, with generally higher values in autumn and lower ones in summer (Fig.3.9). The de-seasonalized time series of TWSA exhibited three distinct phases of dry, wet and another dry, demonstrating three recent hydroclimatic events in Australia (Fig.3.9). We observed an overall TWS drying trend from 2002 to October 2009, indicating the 'big dry' with a continent-wide rate of -0.58 cm/yr. The following 'big wet' caused a sudden wet pulse by adding the equivalent of a three-fold water increase compared to a total water loss into Australia within two years (2010-11). The continental TWSA showed a second drying trend commenced after the 'big wet' and stabilized during 2014, by the end of which TWSA values were nearly equivalent to those at the beginning of the study period in 2002 (Fig.3.9). However, the 2015 dry event, which has been identified as one of the strongest El Niño events since 1900, led Australia into another severe drought with a much sharper TWS decrease rate than that

of the 'big dry'. Eventually, the 2015 El Niño caused a continental equivalent water loss to a 'big dry' but over a much shorter time, with the de-seasonalized TWSA values being the lowest over the study period at the end of 2015. These drying and wetting trends in TWS may reflect the varying extent and fundamental influences from the three major climate modes.

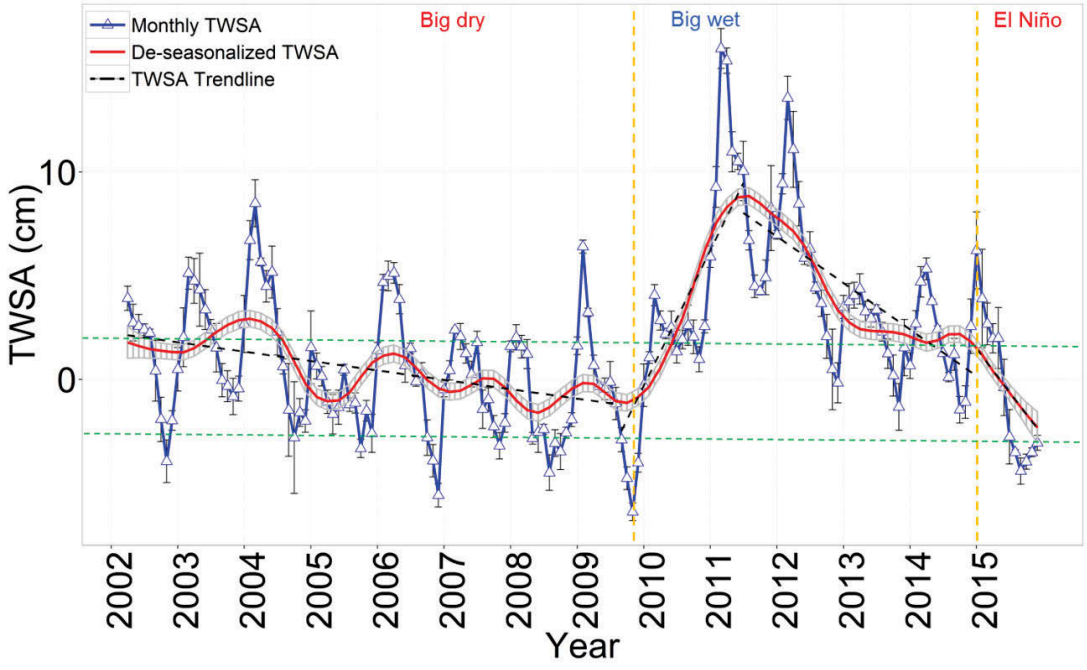

Figure 3.9. Monthly continental average TWSA from July 2002 to December 2015 (solid blue line) with the solid red line indicating the smoothed and de-seasonalized TWSA. The black dashed lines are the linear trends of the de-seasonalized TWSA during the 'big dry', 'big wet', 'after the big wet' and '2015 El Niño' respectively ($p < 0.05$). The error bars indicate the standard deviations among three GRACE datasets provided by JPL, CSR and GFZ, and the shaded area is 95% CI in the de-seasonalized TWSA.

We removed the seasonal component from the monthly data of the three climate indices (SOI, DMI and SAMI) and continental average TWSA, with the purpose of assessing their trends and the relationships between climate modes and TWS over 2002–2015. The de-seasonalized time series showed varying contributions of the three climate modes to the drying and wetting trends in TWS throughout the three hydroclimatic events (Fig.3.10). The positive DMI values during the 'big dry' indicated a persistent lack of a "negative" IOD phase, which was responsible for the decline in TWS across Australia during that period (Fig.3.10). There were no significant trends in SOI and SAMI during the drought, suggesting the 'big dry' was mostly attributed to IOD.

During the 'big wet', we found a quick TWS recovery, which resulted from the combined effects of a sharp increase in SOI, a decline in DMI and another jump of SAMI (Fig.3.10). Corroborating with previous studies (Hendon et al. 2014; Lim and Hendon 2015), our results demonstrated that the 'big wet' was mostly driven by a strong La Niña event in conjunction with a positive excursion of the SAM in Spring. After the 'big wet' until the end of 2014, SOI switched into a sharp decreasing trend, followed by a similar trend in continental TWS (Fig.3.10). It was also thought that the decreasing trend in the DMI may have partially neutralised the TWS loss. Australia experienced another severe drought in 2015, being forced by a strong El Niño event, positive phase of IOD and seasonal effects from SAM (Fig.3.10).

We observed that while a divergence of trends in SOI (positive) and DMI (negative) is likely to increase TWS in Australia, a convergence of those in SOI (negative) and DMI (positive) tend to decrease TWS. SAM only affects TWS over small parts of Australia during certain times of the year but is still important enough to make the condition better or worse (Fig.3.10). Therefore, a synchronization of the interaction amongst the three climate modes will often bring more than the effect of any single mode on TWS, causing extreme drought or flooding across Australia.

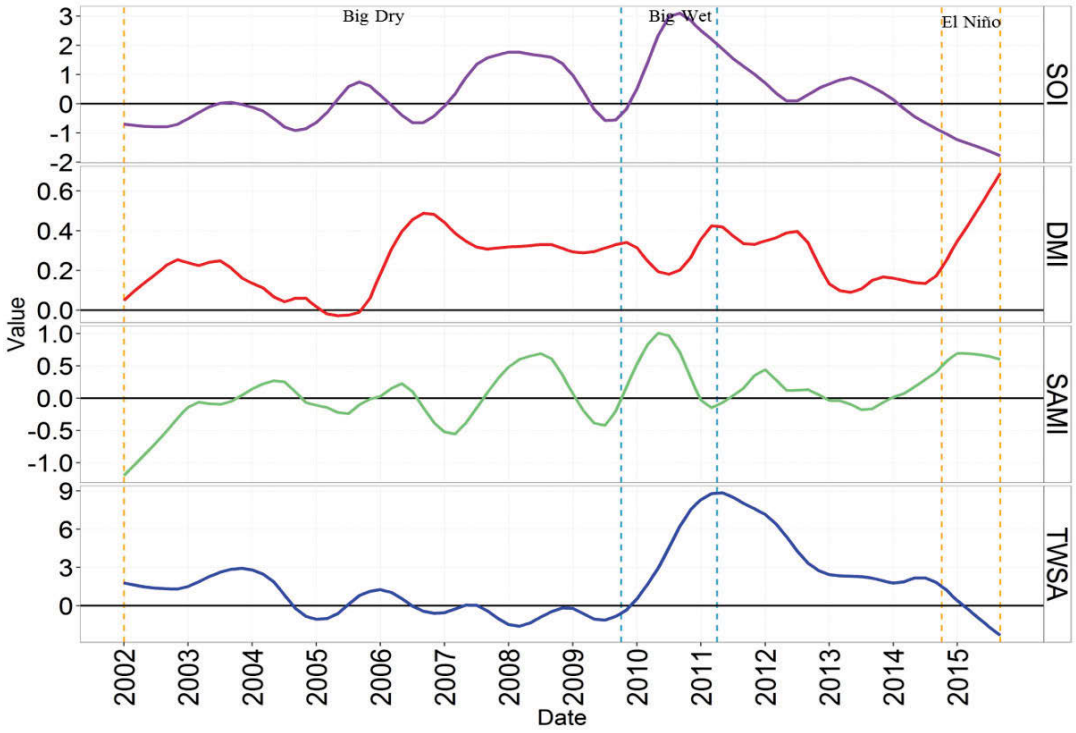

Figure 3.10. Monthly values of smoothed and de-seasonalized three climate indices (SOI, DMI and SAMI) and continental average TWSA from 2002 to 2015.

The annually Cumulative TWS (CTWS) fluxes from 2002 to 2015 for each of the three TWS geographic zones were computed to quantify the total loss or gain of water over the study period, in particular, under the hydroclimatic events driven by the three climate modes (Fig.3.11). Continental water loss or gain in each zone is shown to be highly related to the variations of the respective climate mode. For example, ENSO represented by SOI had the most dramatic changes in and after the 'big dry' (Fig.3.10), which was clearly reflected by the CTWS of Zone I with the sharpest wetting and drying trends during the periods (Fig.3.11). This is in line with the government climate reports (BOM) that showed north-eastern Australia had extensive flooding during the 'big wet' but experienced the most severe drought on record in 2015. We showed south-eastern Australia exhibited the most dramatic swings in water loss/gain over the drought and wet periods in chapter 2 and observed here that north-eastern Australia was another "land of extremes" over the 'big wet' and 2015 El Niño event, however this was due to different climatic reasons. Extreme climate variability of south-eastern Australia is attributed to the control of all three climate modes while that in north-eastern Australia is caused by the volatile El Niño-La Niña phases of ENSO. Figure 3.11 also shows that

2015 exhibited the lowest CTWS across all the TWS Zones after the 'big wet' period, indicating the El Niño event.

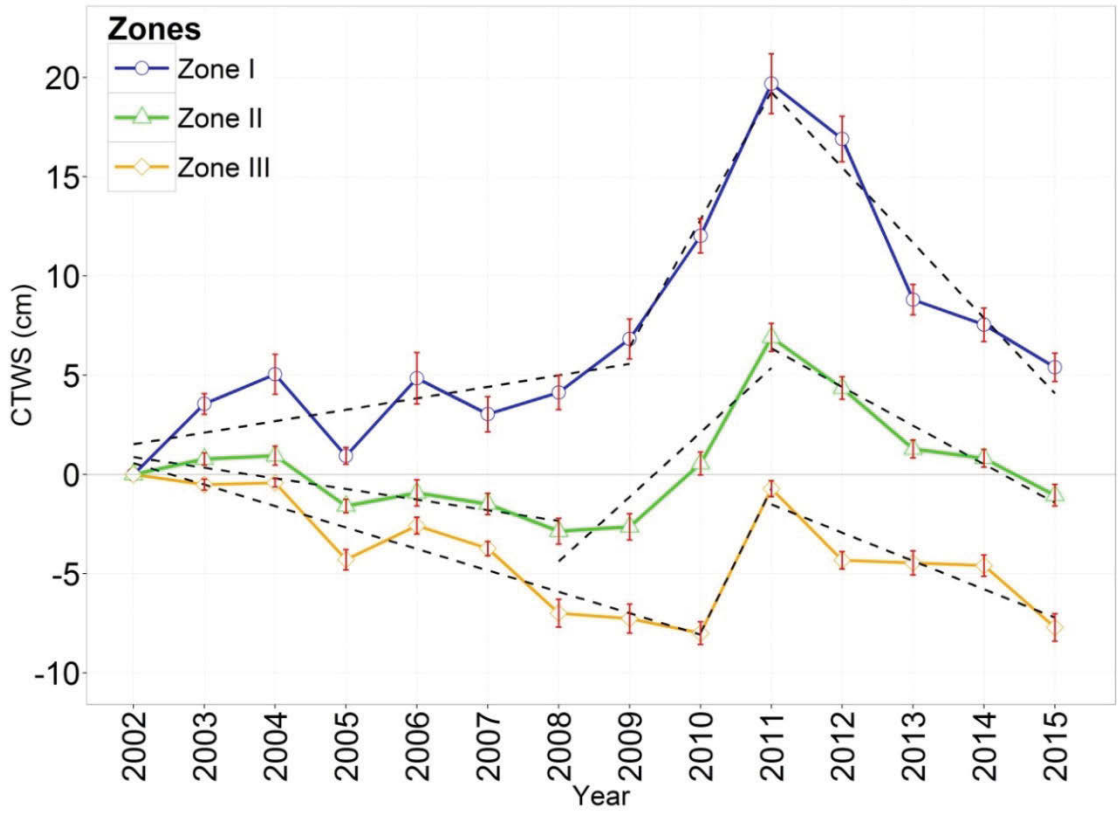

Figure 3.11. Cumulative TWS flux (CTWS) averaged over three TWS geographic zones (I-III) from 2002-2015, with error bars representing 95% CI. The black dashed lines are the linear trends of CTWS in each zone during the 'big dry', 'big wet', and second drying phase respectively ($p < 0.05$).

3.3.4 Ecohydrological implications of 2015 El Niño event

We plotted monthly values of SOI, DMI and SAMI and continental average TWSA from January to December 2015 to show the temporal evolutions of the three climate modes during this El Niño year and their impacts on continental TWS (Fig.3.12). Despite the short-term climatic analysis, our results still show interesting and solid findings that correspond with a recent Australian Bureau of Meteorology report (David Jones 2016). These include; 1) 2015 has been identified as one of the strongest El Niño events since 1900, which can be shown by our result of a consistent and sharp decline in TWS during the year (Fig.3.12); 2) we observed that the very dry conditions in Australia in 2015 were attributed to the synchronization of the interactions amongst the

three climate modes, including the strong El Niño phase of ENSO, the increasing trend of IOD in conjunction with positive SAM in Winter and negative SAM in Spring; 3) record 2015 average rainfall of just 17 mm over the continent has been found during September-October, in which our results show the peak convergence of SOI and DMI; 4) According to our results, the converging SOI and DMI plus the lowest SAMI are likely to make October the driest month in 2015 (Fig.3.12). Correspondingly, the BOM report showed October 2015 was recorded as the warmest and driest October in history. We have already shown TWS dynamics closely follow the variations in climate modes, so we expect to see the lowest TWSA in October. The reason Figure 3.12 shows the minimum TWSA in September instead of October is that there were GRACE data missing in October and November so the interpolated values for these two months may give biased results; 5) As IOD and SAM are largely driving the climate variability over south-western and south-eastern areas of Australia, the combined effects from IOD and SAM shown in Figure 3.12 may result in dry conditions across these two regions. This can also be validated by the BOM report, showing southwest and southeast Australia suffered serious droughts and bush fires in 2015; 6) BOM showed above-average rains to parts of Australia across November and December, which is in line with our result of a divergence of SOI and DMI after October, leading increases in TWS over the period.

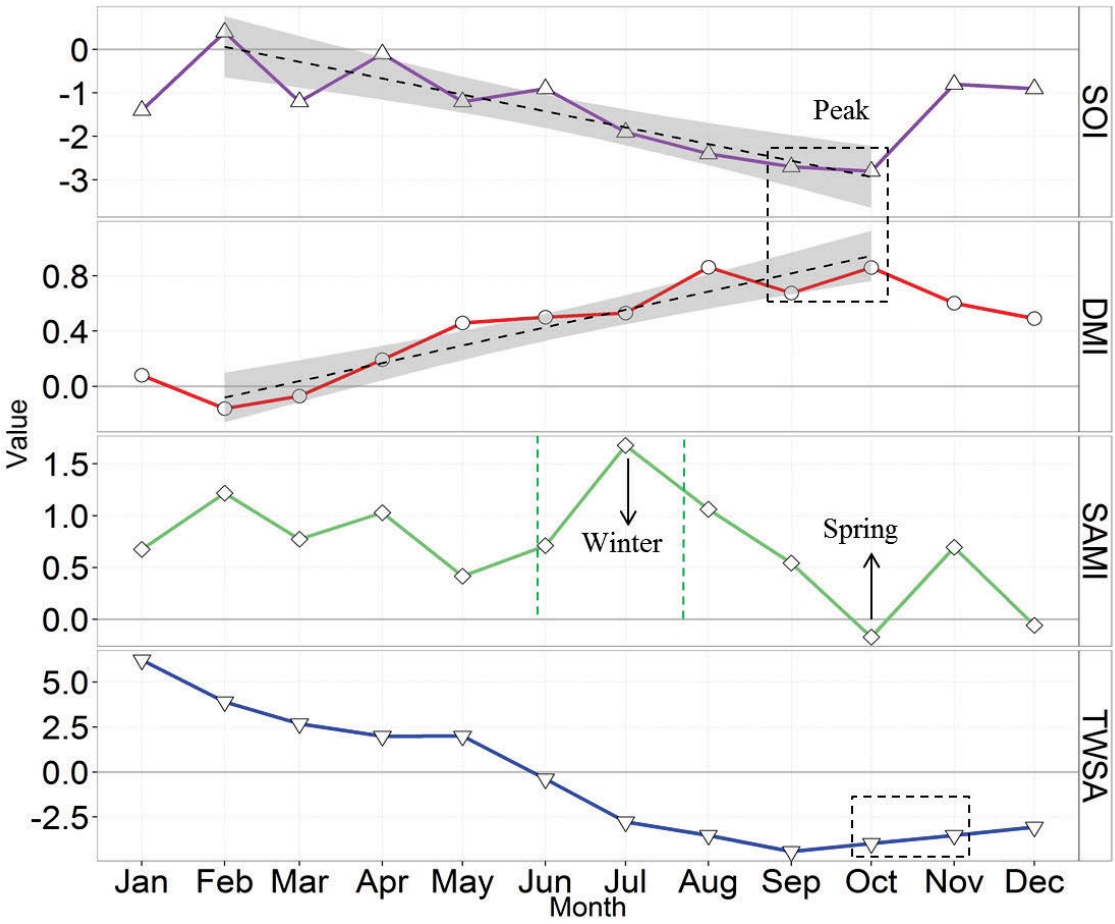

Figure 3.12. Monthly values of three climate indices (SOI, DMI and SAMI) and continental average TWSA over 2015.

Annual anomalies of integrated EVI and averaged TWSA for 2015 at the 1 degree level, relative to the mean over the period from the 'big wet' to the end of our analysis time (2010–2015), were computed to examine changes in spatial patterns of vegetation productivity and TWS under the 2015 El Niño impact (Fig.3.13). Overall, negative anomalies of iEVI and TWS were observed to account for more than 95 percent of Australia, indicating a continent-wide drought in 2015 (Fig.3.13). After the 'big wet', there was a consistent drying trend driven by ENSO (represented by the decreasing SOI) that eventually developed into a strong El Niño event in 2015 (Fig.3.10). This long-term effect from ENSO largely affected the vegetation and water in Zone I, with the most ecohydrological declines among the three zones (Fig.3.13). By contrast, the increasing DMI with the positive (in winter) and negative (in summer) SAMI were mostly responsible for the reduction in vegetation productivity over the south-western and south-eastern tips of Australia in Zone II and Zone III respectively (Fig.3.13A). There

are some inconsistencies between the anomaly patterns in iEVI and TWS over Zone II-III but overall the anomalies showed strong ecohydrological implications from the three-zone-like influences of the climate modes during this 2015 El Niño event.

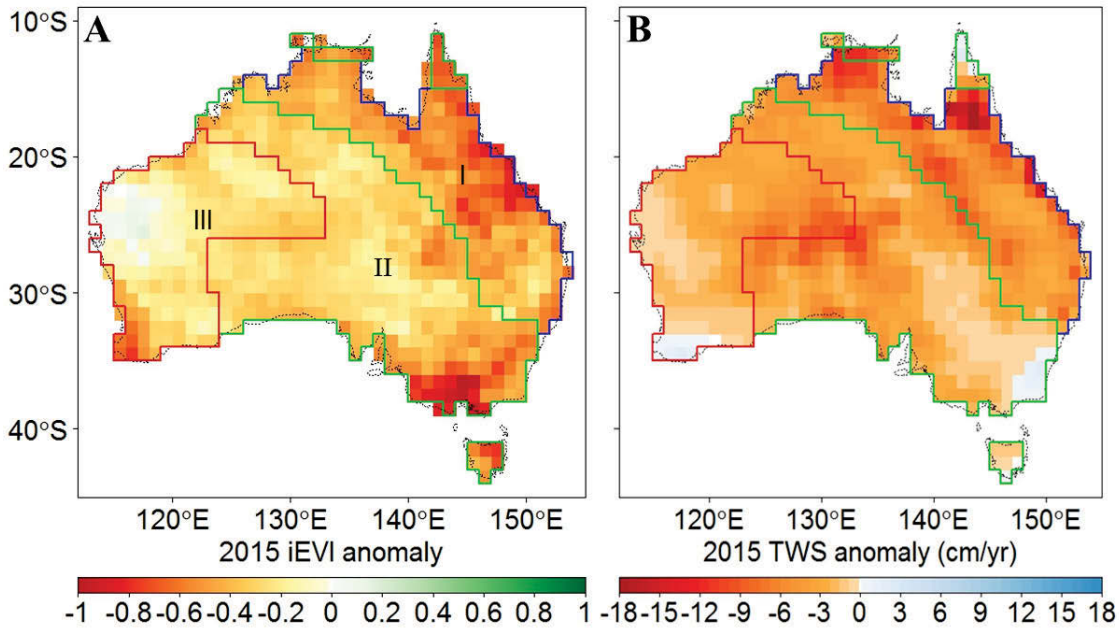

Figure 3.13. 2015 annual anomalies of (A) annually integrated EVI and (B) averaged TWSA across Australia over the period of 2010–2015. The blue, green and red lines represent the boundaries of TWS Zones I, II and III.

3.4 Discussion

3.4.1 Spatial-temporal associations between climate modes and TWS

The three major climate modes (ENSO, IOD and SAM) each have their preferred geographic and temporal varying importance on total water storage across Australia. In particular, our results showed that these climate-TWS spatial relationships mostly contributed to the observed partitioning of the three TWS zones in Australia across the dry and wet events in Chapter 2 (Xie et al. 2016).

Over the northern and north-eastern tropical/subtropical Australia (Zone I), TWS dynamics are mainly driven by ENSO especially in summer and autumn. Since the 'big wet', Zone I experienced dramatic swings of the largest increasing and decreasing TWS rates in Australia, which were associated with La Niña and El Niño phases. Therefore, ecosystems, agriculture and human beings over this region are facing extreme

fluctuations in water availability with periodic drought and flooding. south-eastern Australia, which is located in Zone II, was found to be another “land of extremes” but due to different climatic reasons. TWS there is significantly correlated to all three climate modes, which modulates TWS variability together or respectively across different seasons. As such, hydrological conditions in this region are expected to be particularly sensitive to any interactions among the climate drivers. By contrast, the far tip of south-western Australia (in Zone III) is the area that gets the least influence from ENSO. As another important agriculture land (wheat belt), TWS across this region is under control of both IOD and SAM. While IOD influences TWS during summer and autumn, SAM mainly takes effect during spring.

ENSO has been recognized as the principal driver of rainfall over Australia (Power et al. 1999), which as expected, was also shown to have the most extensive influences on TWS during most of the seasons. ENSO is characterized by its two extreme phases of El Niño and La Niña, which are often associated with hydroclimatic events in Australia. These two phases were found to have an asymmetrical effect on the hydrological conditions with La Niña being more related to Australian rainfall than El Niño (Risbey et al. 2009). IOD has similar polarized phases that are often associated with ENSO events. When IOD and ENSO are in phase, the impacts of El Niño and La Niña events on TWS are often at their most extreme over Australia, while when they are out of phase the impacts of the two events can be diminished. SAM appears to have the least influence on TWS and those effects are often confined to small areas. However, previous studies showed that SAM significantly attributed to both 'big dry' over south-western and south-eastern Australia and the 'big wet' along central-eastern coast (Cai et al. 2011; Hendon et al. 2014).

We found over most regions of the continent, any given climate mode accounts for less than 20% of the variance in TWS. Therefore, the three major climate modes considered here can provide a guide to TWS variations but are only a part of the story. However, we could still rely on them because they are partly predictable and thus provide a predictable component of TWS dynamics.

3.4.2 TWS vs rainfall for linking climate variability and vegetation productivity

GRACE derived TWSA has been recognized as a valuable and integral indicator of both ecological and hydrological performance over large-scale areas especially during hydroclimatic events (Xie et al. 2016; Yang et al. 2014). In this chapter, our results indicate GRACE-TWSA may have more advantages than rainfall for effectively linking the extreme climate variability with dynamics in Australia's vegetation productivity, which have recently been found to significantly contribute to the global carbon and water cycles (Ahlström et al. 2015; Poulter et al. 2014). We support this argument through following discussions.

First, rainfall is a product of complex global atmospheric phenomena, which is highly variable across Australia. For example, random rainfall pulse events are common over large arid/semi-arid regions of Australia. Shifting rainfall patterns due to an intensified global water cycle have also been found over the last few decades in Australia, with increasingly common hydroclimatic events since the beginning of the 21st century. Furthermore, previous studies showed that rainfall record at any given location (even over long periods) can be skewed by weather contributions such as individual storms, which are largely unrelated to climate modes (Risbey et al. 2009). Consequently, it is hard to estimate the relationships between climate modes and rainfall. Inconsistencies between them have been observed in historical records with significant ENSO-rainfall correlations only in around one third of the last 100 years (Cleverly et al. 2016). As a measurement of integrated water, TWS represents final water availability which may be more stable to indicate the hydrological conditions under climate variations. Although rainfall can provide a good explanation of inter-annual variability in surface greenness across Australia, it is unable to account for its variations at a monthly scale (Yang et al. 2014). As the strong relationships between monthly TWSA and EVI across Australia are mostly concurrent (Fig.3.8B), both our results and previous study demonstrated GRACE-TWSA is a more direct measure of water availability to vegetation than rainfall and, which can strongly connect Australia' extreme climate variability with ecosystems.

Many studies have used rainfall as a measure to quantify the associations between climate variability and ecohydrological dynamics. To the best of our knowledge, information on TWS has not been directly used for this purpose. Results of this chapter highlight the value of using GRACE-TWSA to estimate the spatial-temporal influence

from different climate modes on water resources and vegetation dynamics, and in particular, over arid and semi-arid land such as Australia.

3.4.3 2015 drought and future challenges in Australia

Australia's 2015 El Niño started in May and developed into one of the strongest such events on record, comparable to those of 1982 and 1997 (Jaci Brown et al. 2015). It was ranked as the fifth warmest on record, bringing widespread dry conditions. What's more, our results found this big El Niño event was very much strengthened by a positive IOD event and SAM effects during winter and summer (Fig.3.12). According to the BOM report, in the 2015 drought, three areas exhibited severe rainfall deficit, throughout an extensive part of north-eastern region as well as the south-western and south-eastern tips of Australia (Scott B. Power et al. 2016). These were clearly shown in our results of the declines in iEVI and TWSA anomalies (Fig.3.13). We found serious iEVI loss over several parts of Australia may correlate with bushfire events in 2015, with the largest iEVI loss over areas surrounding Melbourne where devastating bushfires were recorded in Victoria's southern coast on October (Fig.3.13). The 2015 El Niño impact validated the three climate-TWS zones across Australia, in which TWS and vegetation dynamics closely connect with variations in respective climate modes.

Climate models project an overall weakening of the Walker Circulation (Bjerknes 1969) over the early 21st century in the context of human-caused climate change, characterised by a faster warming in the eastern equatorial Pacific (favourable for extreme El Niño and in turn conducive to extreme La Niña) and a faster warming in the western Indian Ocean as well, which is likely to promote positive IOD events (Jaci Brown et al. 2015). Accordingly, the sequence of an El Niño preceded by a positive IOD and followed by a La Niña event is projected to occur more frequently, such as the three dry and wet continental hydroclimatic events that Australia has already experienced earlier this century. Therefore, consistent monitoring of climate modes and ecohydrological dynamics by integrating climate indices and remote sensing observations such as GRACE-TWSA is highly valuable for an improved management of risks in Agriculture, natural ecosystems and human well-being in the face of increasing hydroclimatic extremes. This study highlights the spatial varying influence of the three major climate modes on water resources and ecosystems across Australia,

which may provide a guide to decision makers for taking actions in various geographic areas according to the changes from different climate modes.

GRACE-TWSA observations have been widely used for assessing “hidden droughts” of subsurface groundwater depletion or soil drought, which are otherwise difficult to detect and monitor. Therefore, future studies would be valuable to explore and understand whether there is a connection between climate systems and groundwater across Australia or over the globe.

3.5 Conclusion

In this chapter, we used Climate Index data, satellite-based GRACE-TWSA, TRMM-rainfall and MODIS-EVI observations to investigate the spatial-temporal responses, dynamics and trends of Australia's hydrologic and vegetation productivity patterns with the three major climate modes (ENSO, IOD and SAM). Three hydroclimatic extremes of a prolonged drought, a dramatic wet pulse and another anomalous El Niño event were analysed from 2002 to 2015, using the PCCA method to capture the controls of each climate driver on EVI, TWS, and rainfall.

Our results confirmed the dominant influence of the climate modes and their geographic impacts on the continental scale ecohydrological patterns. These varying spatial influences from the climate modes during the 'big dry' and 'big wet' correspond with the three distinct hydrologic zones in TWS patterns observed in chapter 2, which were more pronounced than the continental rainfall patterns. We further observed distinct changing patterns in surface greenness within the three zones, which were largely driven by respective climate mode-TWS relationships, and less correlated with rainfall patterns. Moreover, the 2015 El Niño event, which caused severe declines in TWS and vegetation productivity over many parts of Australia, corroborated the three-zone-like influences from the climate modes. This study highlights the value of GRACE-TWSA, as a better hydrological factor than rainfall for effectively linking the extreme climate variability with Australia's ecosystems, which have recently been recognized to significantly contribute to the global carbon and water cycles (Ahlström et al. 2015; Poulter et al. 2014).

3.6 References

AghaKouchak, A., Cheng, L., Mazdiyasni, O., & Farahmand, A. (2014). Global warming and changes in risk of concurrent climate extremes: Insights from the 2014 California drought. *Geophysical Research Letters, 41*, 8847-8852

Ahlström, A., Raupach, M.R., Schurgers, G., Smith, B., Arneth, A., Jung, M., Reichstein, M., Canadell, J.G., Friedlingstein, P., & Jain, A.K. (2015). The dominant role of semi-arid ecosystems in the trend and variability of the land CO2 sink. *Science, 348*, 895-899

Baba, K., Shibata, R., & Sibuya, M. (2004). Partial correlation and conditional correlation as measures of conditional independence. *Australian & New Zealand Journal of Statistics, 46*, 657-664

Bastos, A., Running, S.W., Gouveia, C., & Trigo, R.M. (2013). The global NPP dependence on ENSO: La Niña and the extraordinary year of 2011. *Journal of Geophysical Research: Biogeosciences, 118*, 1247-1255

Behera, S.K., Luo, J.J., Masson, S., Rao, S.A., Sakuma, H., & Yamagata, T. (2006). A CGCM study on the interaction between IOD and ENSO. *Journal of Climate, 19*, 1688-1705

Bjerknes, J. (1969). Atmospheric teleconnections from the equatorial pacific. *Monthly Weather Review, 97*, 163-172

BOM, A.B.o.M. (2012). Record-breaking La Niña events: An analysis of the La Niña life cycle and the impacts and significance of the 2010–11 and 2011–12 La Niña events in Australia. In

Broich, M., Huete, A., Tulbure, M., Ma, X., Xin, Q., Paget, M., Restrepo-Coupe, N., Davies, K., Devadas, R., & Held, A. (2014). Land surface phenological response to decadal climate variability across Australia using satellite remote sensing. *Biogeosciences, 11*, 5181-5198

Cai, W., Borlace, S., Lengaigne, M., Van Rensch, P., Collins, M., Vecchi, G., Timmermann, A., Santoso, A., McPhaden, M.J., & Wu, L. (2014a). Increasing frequency of extreme El Niño events due to greenhouse warming. *Nat Clim Change, 4*, 111-116

Cai, W., Purich, A., Cowan, T., van Rensch, P., & Weller, E. (2014b). Did climate change–induced rainfall trends contribute to the Australian Millennium Drought? *Journal of Climate, 27*, 3145-3168

Cai, W., Sullivan, A., & Cowan, T. (2011). Interactions of ENSO, the IOD, and the SAM in CMIP3 Models. *Journal of Climate, 24*, 1688-1704

Cleverly, J., Eamus, D., Luo, Q., Restrepo-Coupe, N., Kljun, N., Ma, X., Ewenz, C., Li, L., & Yu, Q.H., Alfredo (2016). The importance of interacting climate modes on Australia's contribution to global carbon cycle extremes. *Scientific Reports*

David Jones, A.B.W., Karl Braganza, Scott B. Power (2016). Hasta la vista El Niño – but don't hold out for 'normal' weather just yet. In: The Conversion

Glenn, E.P., Huete, A.R., Nagler, P.L., & Nelson, S.G. (2008). Relationship between remotely-sensed vegetation indices, canopy attributes and plant physiological processes: what vegetation indices can and cannot tell us about the landscape. *Sensors, 8*, 2136-2160

Heberger, M. (2011). Australia's Millennium Drought: Impacts and Responses. *The World's Water* (pp. 97-125): Springer

Hendon, H.H., Lim, E.-P., Arblaster, J.M., & Anderson, D.L. (2014). Causes and predictability of the record wet east Australian spring 2010. *Climate Dynamics, 42*, 1155-1174

Holton, J.R., Dmowska, R., & Philander, S.G. (1989). *El Niño, La Niña, and the southern oscillation*. Academic press

Huete, A., Didan, K., Miura, T., Rodriguez, E.P., Gao, X., & Ferreira, L.G. (2002). Overview of the radiometric and biophysical performance of the MODIS vegetation indices. *Remote sensing of environment, 83*, 195-213

Huete, A., Restrepo-Coupe, N., Ratana, P., Didan, K., Saleska, S., Ichii, K., Panuthai, S., & Gamo, M. (2008). Multiple site tower flux and remote sensing comparisons of tropical forest dynamics in Monsoon Asia. *Agricultural and Forest Meteorology, 148*, 748-760

Huete, A.R., Didan, K., Shimabukuro, Y.E., Ratana, P., Saleska, S.R., Hutyra, L.R., Yang, W., Nemani, R.R., & Myneni, R. (2006). Amazon rainforests green-up with sunlight in dry season. *Geophysical Research Letters, 33*

Jaci Brown, Andrew B.Watkins, & Cahill, M. (2015). Odds keep rising for a big El Niño in 2015. In: The Conversation

Jiang, D., Wang, J., Huang, Y., Zhou, K., Ding, X., & Fu, J. (2014). The Review of GRACE Data Applications in Terrestrial Hydrology Monitoring. *Advances in Meteorology, 2014*

Kirby, M., Connor, J., Bark, R., Qureshi, E., & Keyworth, S. (2012). The economic impact of water reductions during the Millennium Drought in the Murray-Darling Basin. In, *AARES conference* (pp. 7-10)

Kirono, D.G., Chiew, F.H., & Kent, D.M. (2010). Identification of best predictors for forecasting seasonal rainfall and runoff in Australia. *Hydrological processes, 24*, 1237-1247

Kottek, M., Grieser, J., Beck, C., Rudolf, B., & Rubel, F. (2006). World map of the Köppen-Geiger climate classification updated. *Meteorologische Zeitschrift, 15*, 259-263

Kug, J.-S., & Kang, I.-S. (2006). Interactive feedback between ENSO and the Indian Ocean. *Journal of climate, 19*, 1784-1801

Kug, J.-S., Kirtman, B.P., & Kang, I.-S. (2006). Interactive feedback between ENSO and the Indian Ocean in an interactive ensemble coupled model. *Journal of climate, 19*, 6371-6381

Leblanc, M.J., Tregoning, P., Ramillien, G., Tweed, S.O., & Fakes, A. (2009). Basin-scale, integrated observations of the early 21st century multiyear drought in southeast Australia. *Water Resources Research, 45*, W04408

Lim, E.-P., & Hendon, H.H. (2015). Understanding and predicting the strong Southern Annular Mode and its impact on the record wet east Australian spring 2010. *Climate Dynamics, 44*, 2807-2824

Ma, X., Huete, A., Yu, Q., Coupe, N.R., Davies, K., Broich, M., Ratana, P., Beringer, J., Hutley, L.B., & Cleverly, J. (2013). Spatial patterns and temporal dynamics in savanna vegetation phenology across the North Australian Tropical Transect. *Remote Sensing of Environment, 139*, 97-115

McGrath, G.S., Sadler, R., Fleming, K., Tregoning, P., Hinz, C., & Veneklaas, E.J. (2012). Tropical cyclones and the ecohydrology of Australia's recent continental-scale drought. *Geophysical Research Letters, 39*

Mo, K.C. (2000). Relationships between low-frequency variability in the Southern Hemisphere and sea surface temperature anomalies. *Journal of Climate, 13*, 3599-3610

Nicholls, N. (2011). What caused the eastern Australia heavy rains and floods of 2010/11. *Bull Aust Meteorol Oceanogr Soc, 24*, 33-34

Podobnik, B., Horvatic, D., Petersen, A.M., & Stanley, H.E. (2009). Cross-correlations between volume change and price change. *Proceedings of the National Academy of Sciences, 106*, 22079-22084

Podobnik, B., & Stanley, H.E. (2008). Detrended cross-correlation analysis: a new method for analyzing two nonstationary time series. *Physical review letters, 100*, 084102

Poulter, B., Frank, D., Ciais, P., Myneni, R.B., Andela, N., Bi, J., Broquet, G., Canadell, J.G., Chevallier, F., & Liu, Y.Y. (2014). Contribution of semi-arid ecosystems to interannual variability of the global carbon cycle. *Nature, 509*, 600-603

Power, S., Casey, T., Folland, C., Colman, A., & Mehta, V. (1999). Inter-decadal modulation of the impact of ENSO on Australia. *Climate Dynamics, 15*, 319-324

Rayner, N., Parker, D.E., Horton, E., Folland, C., Alexander, L., Rowell, D., Kent, E., & Kaplan, A. (2003). Global analyses of sea surface temperature, sea ice, and night marine air temperature since the late nineteenth century. *Journal of Geophysical Research: Atmospheres, 108*, 4407

Risbey, J.S., Pook, M.J., McIntosh, P.C., Wheeler, M.C., & Hendon, H.H. (2009). On the remote drivers of rainfall variability in Australia. *Monthly Weather Review, 137*, 3233-3253

Saji, N., Goswami, B., Vinayachandran, P., & Yamagata, T. (1999a). A dipole mode in the tropical Indian Ocean. *Nature, 401*, 360-363

Saji, N., Goswami, B.N., Vinayachandran, P., & Yamagata, T. (1999b). A dipole mode in the tropical Indian Ocean. *Nature, 401*, 360-363

Sanderson, E.W., Jaiteh, M., Levy, M.A., Redford, K.H., Wannebo, A.V., & Woolmer, G. (2002). The Human Footprint and the Last of the Wild. *BioScience, 52*, 891-904

Schepen, A., Wang, Q., & Robertson, D. (2012). Evidence for using lagged climate indices to forecast Australian seasonal rainfall. *Journal of Climate, 25*, 1230-1246

Scott B. Power, Sophie Lewis, & Parton, K. (2016). BOM: 2015 Australia's fifth hottest year on record. In: Econews

Scott Power, S.L., Kevin Parton (2016). BOM: 2015 Australia's fifth hottest year on record. In: econews

Simpson, J., Kummerow, C., Tao, W.-K., & Adler, R.F. (1996). On the tropical rainfall measuring mission (TRMM). *Meteorology and Atmospheric physics, 60*, 19-36

Thompson, D.W., & Solomon, S. (2002). Interpretation of recent Southern Hemisphere climate change. *Science, 296*, 895-899

Tregoning, P., McClusky, S., van Dijk, A., Crosbie, R., & Peña-Arancibia, J. (2012). Assessment of GRACE satellites for groundwater estimation in Australia

Ummenhofer, C.C., England, M.H., McIntosh, P.C., Meyers, G.A., Pook, M.J., Risbey, J.S., Gupta, A.S., & Taschetto, A.S. (2009). What causes southeast Australia's worst droughts? *Geophysical Research Letters, 36*, L04706

Ummenhofer, C.C., Sen Gupta, A., Briggs, P.R., England, M.H., McIntosh, P.C., Meyers, G.A., Pook, M.J., Raupach, M.R., & Risbey, J.S. (2011). Indian and Pacific Ocean influences on southeast Australian drought and soil moisture. *Journal of Climate, 24*, 1313-1336

Ummenhofer, C.C., Sen Gupta, A., Pook, M.J., & England, M.H. (2008). Anomalous rainfall over southwest Western Australia forced by Indian Ocean sea surface temperatures. *Journal of Climate, 21*, 5113-5134

Van Dijk, A.I., Beck, H.E., Crosbie, R.S., Jeu, R.A., Liu, Y.Y., Podger, G.M., Timbal, B., & Viney, N.R. (2013). The Millennium Drought in southeast Australia (2001–2009): Natural and human causes and implications for water resources, ecosystems, economy, and society. *Water Resources Research, 49*, 1040-1057

Verdon-Kidd, D., & Kiem, A. (2009). On the relationship between large-scale climate modes and regional synoptic patterns that drive Victorian rainfall. *Hydrology and Earth System Sciences, 13*, 467-479

Wallace, J.M., & Thompson, D.W. (2002). The Pacific center of action of the Northern Hemisphere annular mode: Real or artifact? *Journal of Climate, 15*, 1987-1991

Webster, P.J., Moore, A.M., Loschnigg, J.P., & Leben, R.R. (1999). Coupled ocean–atmosphere dynamics in the Indian Ocean during 1997–98. *Nature, 401*, 356-360

Xie, Z., Huete, A., Restrepo-Coupe, N., Ma, X., Devadas, R., & Caprarelli, G. (2016). Spatial partitioning and temporal evolution of Australia's total water storage under extreme hydroclimatic impacts. *Remote Sensing of Environment*

Yang, Y., Long, D., Guan, H., Scanlon, B.R., Simmons, C.T., Jiang, L., & Xu, X. (2014). GRACE satellite observed hydrological controls on interannual and seasonal variability in surface greenness over mainland Australia. *Journal of Geophysical Research: Biogeosciences, 119*, 2245-2260

Yuan, N., Fu, Z., Zhang, H., Piao, L., Xoplaki, E., & Luterbacher, J. (2015). Detrended partial-cross-correlation analysis: A new method for analyzing correlations in complex system. *Scientific reports, 5*

Zebende, G. (2011). DCCA cross-correlation coefficient: quantifying level of cross-correlation. *Physica A: Statistical Mechanics and its Applications, 390*, 614-618

Zhang, X.-G., & Casey, T. (1992). Long-term variations in the Southern Oscillation and relationships with Australian rainfall. *Australian Meteorological Magazine*

Chapter 4: Landsat and GRACE observations of arid wetland dynamics in a dryland river system under multi-decadal hydroclimatic extremes

Abstract

Arid wetlands are important for biodiversity conservation, but are sensitive and vulnerable to climate variability and hydroclimatic events. Amplification of the water cycle, including the increasing frequency and severity of droughts and wet extremes, is expected to alter spatial and temporal hydrological patterns in arid wetlands globally, with potential threats to ecosystem services and their functioning. Despite these pressing challenges, the ecohydrological interactions and resilience of arid wetlands to highly variable water regimes over long time periods remain largely unknown. Recent broad-scale drought and floods over Australia provide unique opportunities to improve our understanding of arid wetland ecosystem responses to hydroclimatic extremes. Here we analysed the ecohydrological dynamics of the Coongie Lakes arid wetland in central Australia, one of the world's largest Ramsar-designated wetlands, using more than two decades (1988 – 2011) of vegetation and floodwater extent retrievals derived from Landsat satellite observations. To explore the impacts of large-scale hydrological fluctuations on the arid wetland, we further coupled Landsat measurements with Total Water Storage Anomaly (TWSA) data obtained from the Gravity Recovery and Climate Experiment (GRACE) satellites.

Pronounced seasonal and inter-annual variabilities of flood and vegetation activities were observed over the wetland, with variations in vegetation growth extent highly correlated with flood extent ($r = 0.64$, $p < 0.05$) that ranged from nearly zero to 3456 km^2. We reported the hydrological dynamics and associated ecosystem responses to be largely driven by the two phases (El Niño and La Niña) of the El Nino-Southern Oscillation (ENSO) ocean-atmosphere system. Changes in flood and vegetation extent were better explained by GRACE–TWSA ($r= 0.8$, lag = 0 month) than rainfall ($r = 0.34$, lag = 3 months) over the water source area, demonstrating that TWS is a valuable hydrological indicator for complex dryland river systems. The protracted Millennium Drought from 2001 to 2009 resulted in long-term absence of major flood events, which substantially suppressed wetland vegetation growth. However, the 2010-11 La Niña induced flooding events led to an exceptionally large resurgence of vegetation, with a mean vegetation growth extent anomaly exceeding the historical average (1988–2011) by more than 1.5 standard deviations, suggesting a significant resilience of arid wetland ecosystems to climate variability. This study showed the ecological functioning of arid wetlands is particularly sensitive to large-scale hydrological fluctuations and extreme

drought conditions, and vulnerable to future altered water regimes due to climate change. The methods developed herein can be applied to arid wetlands located in other dryland river systems across the globe.

4.1 Introduction

Wetlands around the world provide fundamental ecosystem services, such as climate regulation, carbon storage, groundwater recharge, water filtering and purification, and have scientific, cultural, economic and recreational values (Finlayson et al. 2005). They are rich in biodiversity, but highly sensitive to changes in climate due to their limited adaptive capacity (Kandus and Malvárez 2004). Drylands, covering around one-third of the Earth's surface with nearly 40% of the world's population, are characterised by highly limited water resources and extreme rainfall variability (Tooth 2000). This climate pattern often results in dryland river systems with complex hydro-geomorphology, including anabranching rivers, ephemeral lakes, and arid wetlands among other ecosystems (Knighton and Nanson 2001).

Arid wetlands are unique among wetland types, as they are situated in dryland environments and generally experience large fluctuations between flooding and drying phases (Puckridge et al. 2000; Yu et al. 2015). Recent studies have shown there is a wide distribution of wetland types in dryland environments with high biodiversity, but facing intensified pressure to their water resources (Brendonck and Williams 2000). These arid wetlands have already degraded or disappeared due to climate change and human impact (Jenkins et al. 2005; Williams 1999). A healthy ecohydrological functioning of such wetlands is critically required to provide vital water sources and life-support systems for the survival of endemic plants and animals as well as people inhabiting in dry regions. For example, the isolation and disconnection of water bodies in arid wetlands during the dry period between two flood events exert large impacts on vegetation communities, which are generally inactive with low photosynthetic activity before experiencing intense growth and reproduction when floods return (Puckridge et al. 2000).

Arid wetlands are particularly vulnerable to climate change, given their ephemeral characteristics associated with unstable water sources in harsh dryland environments (Capon 2003; Walker et al. 1995). Therefore, the increasingly common hydroclimatic

extremes (e.g. drought and flooding) together with intensified water cycles (Chou et al. 2013; Durack et al. 2012; Xie et al. 2016), will likely alter the hydrological regimes over drylands which, in turn, exert pronounced effects on the biodiversity and the integrity of arid wetland ecosystems worldwide (Hulme 2005; Roshier et al. 2001). In addition, anabranching rivers are common in drylands, which are characterised by numerous channels of various sizes in large floodplains, resulting in extremely variable streamflow (Puckridge 1998; Tooth and Nanson 1999). Since headwaters are transmitted by these rivers as flood pulses to downstream wetlands with high transmission losses, it is hard to use field observations or rainfall data to predict and evaluate the hydrological controls on ecohydrological processes of arid wetlands (Jarihani et al. 2015b). Moreover, the paucity of ecohydrological data of arid wetlands due to (i) remote locations with episodic flow regime; (ii) low levels of economic development; and (iii) sparse water gauging network, has limited our understanding of flood dynamics, ecological functions, and their interactions with large-scale climate modes (Jenkins et al. 2005).

Despite these pressing challenges, arid wetlands have attracted far less attention than other wetland types with relatively few relevant studies conducted (Williams 1999). Research on wetland ecosystems and hydrological dynamics in dryland environments have mostly been carried out by traditional approaches such as hydrological modelling based on small-scale field experiments (Fensham and Fairfax 2003; Fensham et al. 2005; Jenkins et al. 2005; Moiwo et al. 2010; Puckridge et al. 2000; Tooth et al. 2002; Tooth and McCarthy 2007; Walker et al. 1997; Walker et al. 1995; Yu et al. 2015). Remote Sensing (RS) technique, with multi-sensor systems of various spatial resolutions and physical properties, provides potentials and an unparalleled way to monitor important land surface dynamics and characteristics over data-sparse dryland regions (Adam et al. 2010).

Since the start of 21st century, satellite observations have been increasingly used for studying dryland water bodies and river floods including arid wetlands (Chen et al. 2013; Feyisa et al. 2014; Frazier et al. 2003; Frazier and Page 2000; Jarihani et al. 2013; Jarihani et al. 2014; Karim et al. 2011; Klemas 2011; Puckridge et al. 2010; Schumann et al. 2007; Tulbure et al. 2016; White and Lewis 2011). In addition, other relevant dryland hydrological studies about river flow variability and transmission losses, which exert considerable control on the water resource of downstream arid wetlands, have also

been undertaken through individual or combination of field data, satellite observations and hydrodynamic modelling (Bunn et al. 2006; Costelloe et al. 2003; Dunkerley and Brown 1999; Jarihani et al. 2015a; Jarihani et al. 2015b). Key papers for ecohydrological processes over arid wetland regions are summarised in Table 1. Although an increasing number of studies relevant to arid wetlands have been conducted, so far few have assessed their ecohydrological interactions and resilience to the highly variable water regimes, particularly hydroclimatic drought and wet extremes (Cleverly et al. 2016a).

Australia, on average the driest inhabited continent, features high climate variability (Finlayson and McMahon 1988; McMahon et al. 1992) and has a great number and variety of wetlands recognised by the Ramsar Convention for their ecohydrological significance (Kingsford 2000; Pittock et al. 2010; Woodward et al. 2014). In particular, arid wetlands in Australia are extensive, covering 70% of the continent, primarily distributed over south-eastern, central and northern arid regions of the country (Leigh et al. 2010). They are largely ecologically intact and can provide us with valuable insights into the intrinsic relationships between arid wetland functioning and environmental variations. Australia experienced a prolonged dry period with one of the worst droughts that commenced in 2001 and continued until 2009, commonly known as the “Millennium Drought” or 'big dry' (Van Dijk et al. 2013). This protracted dry period ended with an intensive wet pulse in 2010-2011 ('big wet'), attributed to one of the strongest La Niña events in the past century (Hendon et al. 2014). These events, which also largely affected central Australia (Cleverly et al. 2016b), provide an ideal 'natural experiment' to assess the dynamics and resilience of arid wetlands to intensified hydroclimatic extremes (Chen et al. 2016).

In this study we investigated the hydrological dynamics and ecosystem functioning of the Coongie Lakes arid wetland in central Australia, one of the world's largest Ramsar-designated wetlands, by integrating multi-sensor satellite observations over a 24-year period (1988-2011). Wetland vegetation growth and flood inundation extent derived from Landsat imagery were used to provide a long-term ecohydrological processes and their interactions over the wetland where there is scarcity of observational data. We also applied GRACE-derived TWS changes, as a surrogate of terminal water storage from the headwaters after transmission losses, to connect the wetland dynamics with water source variations. Specifically, we aimed to: (1) examine spatial-temporal

patterns of historical inundation in Coongie Lakes and their relationship with broad-scale climate modes; (2) quantify vegetation responses to multiple fluctuations between floods and drought conditions; (3) assess the resilience of this arid wetland to early 21st century hydroclimatic extremes; and (4) relate the variations in flooding and greening extent to large-scale hydrological dynamics (TWS/rainfall). Results from this research will generate a better understanding of underlying links between ecosystems and floods in arid wetlands, and how they respond to large-scale hydrological fluctuations and hydroclimatic extremes. This study will also provide scientific guidance for conservation strategies and management of arid wetland ecosystem resources worldwide to secure their sustainability through future climatic changes.

Table 4.1. Summary of relevant studies on ecological dynamics and hydrological processes of arid wetlands and river transmission losses in dryland environments worldwide (the current paper is added for completeness). In the 'Key findings' column, three components of studies are identified by the code: (i) arid wetland vegetation dynamics; (ii) arid wetland hydrological processes; and (iii) river flow variability and flood transmission losses. N/A represents 'not applicable' in the relevant research.

Study	Data & methods	Location/landscape/size	Key findings
1.Capon (2003)	Field surveys (2000-01) and historical data statistics analysis were used to investigate vegetation responses to variable flood regimes in a large arid floodplain.	Twelve sites in the Cooper Creek catchment/arid, low-gradient and large floodplains/50m × 50m quadrats	(i) Plant communities in arid catchments are primarily structured by flow regimes despite their inherent unpredictability (ii) Alterations in flood pulses through water extraction may result in a shift in community structure and an eventual loss of biodiversity (iii) Flows fluctuate unpredictably between long periods of drought and huge floods. In Cooper Creek catchment large floods can facilitate vast areas of inundation with considerable lengths of

			time (e.g. flood event of 1990)
2.Petus et al. (2013)	Satellite data of MODIS derived NDVI (250 m, 16 days) over 2002-10 were used to monitor temporal dynamics of wetland vegetation in an arid wetland.	Dalhousie Springs Complex in the Great Artesian Basin (GAB), Australia/largest discharge spring wetland among numerous others in hot and arid artesian groundwater basin/190 km^2	(i) Wetland vegetation activity can be discriminated from surrounding land responses. The extent of vegetated wetland areas declined during Australia's 'big dry' while increased in the 'big wet'. (ii) Close association was found between wetland vegetation and springs from groundwater flow. (iii) N/A
3.White et al. (2016)	NDVI computed from QuickBird and WorldView-2 satellite imagery with ground-based vegetation cover and spring discharge measurements were used to understand the relationship between groundwater outflows and the extent of wetlands they support.	Three spring complexes in southwest GAB, Australia/a diversity of spring forms, extents and hydrogeological settings among sites in hot and arid artesian groundwater basin/from 15 to 190 km^2	(i) A relatively consistent NDVI threshold (~ 0.3) can be used to differentiate wetland from dryland vegetation. (ii) Relationship between surface flow rate and wetland area is transferable to a range of GAB springs with different hydrogeological settings and vegetation composition. (iii) N/A
4.Puckridge et al. (2010)	AVHRR and Landsat-MSS satellite imagery, daily discharge data from water gauge and field observations were used to map the inundation patterns over an arid wetland. Sampling was applied to monitor the abundance and diversity of ecological responses.	Thirteen sites in the Coongie Lakes, Lake Eyre Basin, Australia/ freshwater arid wetland complex that consists of multiple water bodies connected by channels/ 20,000 km^2	(i) Reductions in the frequency of inundation and water-retention times will result in less dense and diverse vegetation communities (ii) Arid wetlands were exposed to long-term patterns of flooding and drying with resolution for flooding frequency

			being 1 year. (iii) Flood variability of the wetland was controlled by the water source area, Cooper Creek catchment
5.Jones (2015)	One candidate Dynamic Surface Water Extent (DSWE) algorithm with static thresholds was used to detect inundation in marsh with presence of vegetation based on Landsat imagery, which was evaluated and validated by in situ data from the Everglades Depth Estimation Network (EDEN)	The Everglades wetland region of South Florida, USA/subtropical, with long, hot summers and mild, dry winters; Wetlands are composed of mosaics of open water and wet prairie as well as herbaceous, shrub and forested wetlands /~5000 km^2	(i) N/A (ii) DSWE is relatively simple but efficient, requires no scene-based calibration data and can detect inundation in vegetated wetland environments with high accuracy (overall agreement is 0.73). DSWE was also found to have no significant trend or bias in its performance as a function of time or general hydrologic conditions, indicating a consistency for long-term monitoring (iii) N/A
6.Feyisa et al. (2014)	An Automated Water Extraction Index (AWEI) was proposed for surface water mapping using Landsat imagery	Sites of water bodies from five different countries ranging from wetlands to lakes	(i) N/A (ii) AWEI was shown to have a fairly stable optimal threshold value, which can be used for extracting water bodies in different environments especially in areas with shadows and urban backgrounds (iii) N/A
7.Chen et al. (2013)	Landsat data was used to compare and validate the inundation maps derived from daily and 8-day MODIS composite products with the methods of Open Water Likelihood	Narran Lakes wetland and Chowilla Riverland floodplain in Murray-Darling Basin, Australia/semi-arid/ around 4100 km^2 each	(i) N/A (ii) Both MODIS products provide a reasonable estimate of floodplain inundation across the two study sites. The accuracy of

	(OWL) and Modified Normalized Difference Water Index (MNDWI)		inundation mapping thus depends on the spatial and spectral characteristics of the MODIS imagery not the type of products. (iii) N/A
8.Knighton and Nanson (1994)	Input-output relationships were defined in terms of total flow volume and peak discharge from Gauge data of Currareva and Nappa Marrie	Cooper Creek, Lake Eyre Basin, Australia/ arid, low-gradient and large floodplains/420 km reach	(i) N/A (ii) Only ~ 30% of Cooper Creek flows reach Innamincka, hence the Coongie Lakes wetland with most water being retained in the "Channel Country". (iii) Transmission losses are high and vary non-linearly with stage, accounting for ~ 75% of total inflow over the Currareva-Nappa Merrie length.
9.Jarihani et al. (2015b)	Combine hydrodynamic modelling, satellite data and field measurements to quantify and understand the partitioning of flood transmissions losses in data-sparse dryland river system	Diamantina catchments, Lake Eyre Basin, Australia/arid, low-gradient and anabranching river system/180 km reach, 55,721 km^2	(i) N/A (ii) Terminal water storage was found to only receive ~ 11% of total inflow but critical for ecohydrological processes of downstream wetlands. (iii) Transmission losses of anabranching rivers in drylands were found to be high (~ 46% of total inflow), to which actual evapotranspiration contributed the most followed by infiltration. Remote sensing can be used in hydrodynamic model for dryland studies
10.This study	Wetland vegetation	Coongie Lakes, Lake Eyre	(i) Variations in

growth and flood inundation extent derived from Landsat imagery were used to provide a long-term ecohydrological dynamics and their interactions over an arid wetland. GRACE-TWSA time series was also applied as a surrogate of terminal water storage from the headwaters (after transmission losses), relating the wetland ecohydrological variations to large-scale hydrological fluctuations.	Basin, Australia/ freshwater arid wetland complex that consists of multiple water bodies connected by channels/ 20,000 km^2	wetland vegetation growth were highly correlated with flood extent. Arid wetlands exhibit strong ecological resilience to hydro-climate extremes, and are presumably sensitive to future altered water regions due to climate change (ii) Flood events over the Coongie Lakes showed extreme variability in extent across seasons and between years driven by ENSO (iii) GRACE-derived TWS changes are a valuable hydrological indicator for complex dryland river systems. As a surrogate of terminal water storage from the headwaters (after transmission losses), GRACE-TWSA can relate the ecohydrological variations in the arid wetland to the large-scale hydrological dynamics

4.2 Data and methods

4.2.1 Study area

Coongie Lakes is an approximately 20,000 km^2 freshwater arid wetland system located in the Strzelecki Desert of central Australia (Fig.4.1A), with annual rainfall

normally less than 200 mm/year and a reported annual potential evaporation larger than 2000 mm/year (Kotwicki 1986; Kotwicki and Allan 1998). It lies within the Lake Eyre Basin (LEB), which is the largest endorheic drainage basin in Australia (Fig.4.1B), covering one-sixth of the continent (Gibbs 2006). Coongie Lakes has been recognised both as a Ramsar Convention wetland (15/Jun/1987) and a wetland of national significance under the Directory of Important Wetlands in Australia.

Coongie Lakes wetland complex consists of serial permanent and intermittent lakes, waterholes, channels, numerous shallow floodplains, deltas, and several inter-dune swamps (Fig.4.1C). The channel banks and more frequently flooded areas of the wetland system are vegetated by coolibah and river red gum trees (*Eucalyptus* spp.), often with a dense understorey of lignum shrub thickets (Butcher and Hale 2011). Less frequently flooded parts of the floodplain are vegetated with sparser shrublands of chenopods and ephemeral herbs. The adjacent gibber plains are sparsely covered with perennial grasses (*Astrebla* spp.), while the dune country carries shrubs of *Dodonaea* sp., *Acacia* sp. and cane-grass *Zygochloa* sp. (Reid et al. 1988; Reid and Puckridge 2000). Major floods in the wetland initiate a period of rapid plant growth and an influx of wildlife, providing freshwater habitats and breeding grounds for wetland dependent flora and fauna (Puckridge et al. 2000).

The Cooper Creek catchment (purple polygon in Fig.4.1A), covering almost a quarter of the Lake Eyre Basin, has been identified as the water source area of Coongie Lakes (Puckridge 1998; Puckridge et al. 2010;). Around 80% of the catchment lies in Queensland, 18% in South Australia (where the wetland is) and the rest in New South Wales. Cooper Creek is one of the largest unregulated rivers in Australia, which has anastomosing river channels mainly concentrating on a wide floodplain named "Channel Country" (Knighton and Nanson 2001) (Fig.4.1A). The Cooper Creek catchment is fed by monsoonal rainfall in western Queensland (Walker et al. 1997), creating flood pulses which are the principal water supply of the Coongie Lakes arid wetland.

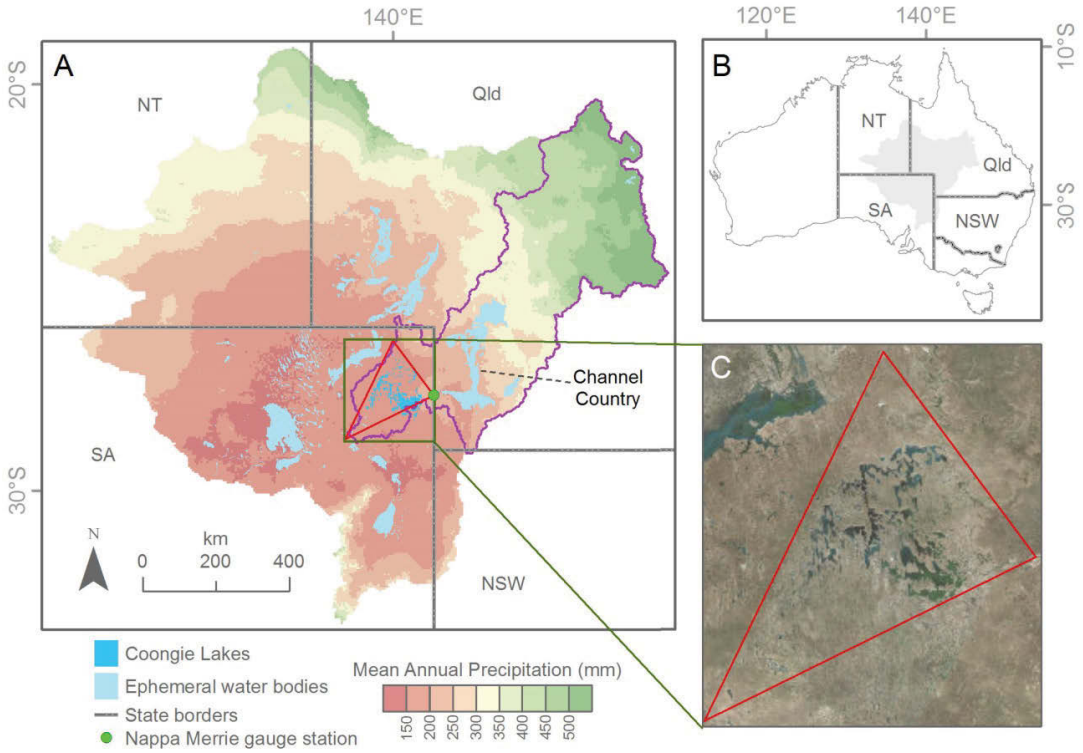

Figure 4.1. The location and climatic context of Coongie Lakes arid wetland. (A) Location of the study area with state boundaries; Coongie Lakes wetland extent in medium blue with Ramsar boundary highlighted by red triangle and Nappa Merrie gauge station (green point); Cooper Creek catchment outlined in purple; other major LEB ephemeral water bodies in pale blue including the "Channel Country". (B) Location of the Lake Eyre Basin (LEB) within Australia with state boundaries. (C) Natural colour image of Coongie Lakes during a period of inundation (image courtesy of Google Earth on 18/Apr/2004).

4.2.2 Landsat data

We downloaded Landsat data of Climate Data Record (CDR) surface reflectances (bands 1-7) from the Science Processing Architecture System of USGS Earth Resources Observation and Science (EROS) Centre (http://espa.cr.usgs.gov/). Data used in this study were acquired by the Landsat Thematic Mapper (TM, Landsat 4-5) and the Enhanced Thematic Mapper Plus (ETM+, Landsat 7) sensors with 16 days and 30 m resolutions. The Landsat scene of World Reference System path 98 and row 79 was chosen as it covers more than 90% of the inundation area within Coongie Lakes wetland. Thus, the valid image area within the Ramsar triangle boundary (black modified-rectangular shape) will be used as study area for all subsequent data analysis (Fig.4.2). Among all the available data from January 1988 to September 2011, we selected images

with less than 5% cloud cover for each month over the study area. As previous studies indicated four seasons over this wetland (Clarke et al. 2014; Clarke and Lewis 2015; Raja Segaran et al. 2015), we particularly looked for data in each austral season for following analyses. A total of 200 Landsat scenes were obtained, covering 70% of all months for the entire 24 years, and consisting of a minimum of one image for a season in each year. The residual cloud, cloud shadow and aerosol contamination were further filtered out from the surface reflectance data based on the quality assessment (QA) flags provided in CDR product (Zhu and Woodcock 2012; Zhu et al. 2015).

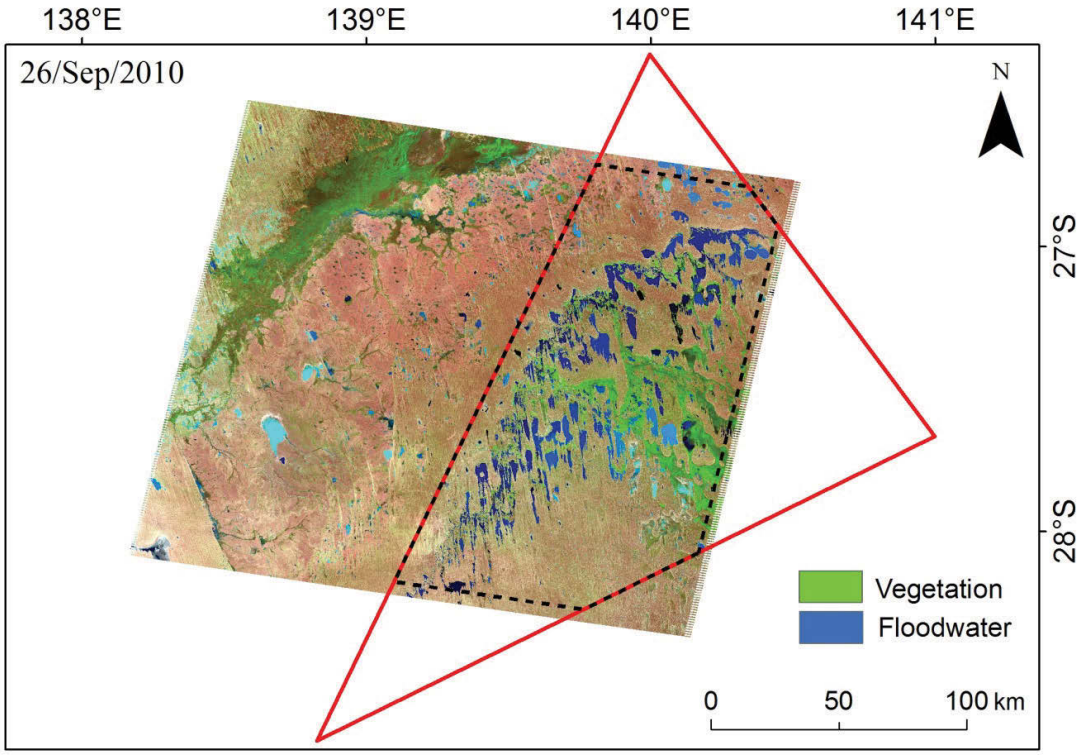

Figure 4.2. Landsat image (RGB 5-4-3 colour composite) indicating area (black modified-rectangular shape) for all subsequent data analysis and showing an extensive flooding event in the Coongie Lakes wetland (Ramsar site extent shown by the red triangle) on 26/Sep/2010.

4.2.3 GRACE-derived total water storage anomaly

To understand the impacts of large-scale hydrological processes on the Coongie Lakes wetland, we used a decade (April 2002 – September 2011) of Total Water Storage Anomaly (TWSA) data derived from the Gravity Recovery and Climate Experiment (GRACE) satellites. Launched by NASA and the German Aerospace Centre

(DLR) in March 2002, the GRACE system consists of twin satellites following one another at a distance of ~220 km in identical Earth orbits (Rodell et al. 2004). GRACE was designed to exploit the unique relationship between variations in the gravity field and changes in mass at the Earth's surface (Tapley et al. 2004; Wahr et al. 2006). As variations in land mass are mainly caused by shifting water storage, TWSA was obtained from the monthly GRACE data subtracted by a historical mean (2004-2009 time-mean as standard data format) (Chen et al. 2005; Tregoning et al. 2012). TWSA represents the changes in vertically integrated water storage, including groundwater, surface water, soil moisture, snow water and biological water (Famiglietti and Rodell 2013; Rodell et al. 2009). Different gravity-field solutions are produced by various institutions; for this study release-5, level-2 TWSA data from three independent GRACE research centres, Jet Propulsion Laboratory (JPL), University of Texas Centre for Space Research (CSR) and the GeoForschungsZentrum (GFZ) Potsdam were averaged to minimize the uncertainties associated with data processing. In addition, an appropriate scaling factor is crucial for restoring the GRACE signal losses during data process (e.g. truncation and filtering) before applying GRACE-TWSA to resolve any water-related issues. Previous studies found scaling factors derived from various Land Surface Models (LSMs) can show appreciable differences over arid and semiarid regions (Long et al. 2015a; Long et al. 2015b). Therefore, in this study we used an ensemble mean of scaling factors derived from six LSMs (Noah2.7, Mosaic, VIC, and CLM2.0 from GLDAS-1, WGHM2.2 and CLM4.0) described in Long et al. (2015a) to reduce the uncertainties in restoring the signals from GRACE data. Moreover, some of the LSMs such as CLM4.0 and WGHM also account for human activities (e.g. irrigation and river diversion) as well as the interactions between surface water and groundwater (Gent et al. 2011; Landerer and Swenson 2012; Long et al. 2015a). Eventually, the TWSA data used herein has 1° and monthly resolutions, representing Equivalent Water Height (EWH, in units cm).

4.2.4 Other observational data

To study the long-term rainfall patterns (1988-2011) over the Lake Eyre Basin, we used gridded monthly rainfall fields at 0.05° resolution from the Australian Bureau of Meteorology (BOM). The dataset was derived from several thousand ground meteorological station observations across Australia and the grids were computer-

generated using a sophisticated analysis technique as presented in Jones et al. (2009). The monthly BOM rainfall values have a root mean square error of 21.2 mm and a mean absolute error of 11.5 mm. As high uncertainties may exist in BOM data due to sparse rainfall stations across central Australia, we also used satellite observations of monthly rainfall from the 3B43 version-7 Tropical Rainfall Measuring Mission (TRMM) product for better correlation analysis between flood and rainfall across space over 2002-2011 (Chappell et al. 2013; Oke et al. 2009; Peña-Arancibia et al. 2013; Renzullo et al. 2011). TRMM was a joint endeavour between NASA and Japan's National Space Development Agency, and designed to monitor and study dynamics in the tropical/sub-tropical rainfall with a spatial resolution of 0.25° (Simpson et al. 1996). A comparison analysis between TRMM and ground-based (AWAP/BOM) rainfall data over the Cooper Creek catchment can be found in the Supplementary Material. Both BOM and TRMM rainfall data were further resampled to a 1° resolution to correspond with the GRACE data in the following analyses of this study.

The Digital Elevation Model (DEM) data of Cooper Creek catchment from Shuttle Radar Topography Mission (SRTM) was used in this study to show the topographical elevation patterns over the water source area of Coongie Lakes. We used version 4.1 of the seamless SRTM C-band DEM with 3-arc-second (~90 m) grid size, which is available from http://srtm.csi.cgiar.org (Jarihani et al. 2015a). Based on the version 2 of SRTM DEM released by NASA (also known as the "finished" version), version 4.1 is the result of a substantial editing effort by the National Geospatial Intelligence Agency and exhibits well-defined water bodies, coastlines and the absence of spikes and wells (single pixel errors). Furthermore, Jarvis et al. (2008) used a range of interpolation algorithms in conjunction with other sources of elevation data to effectively fill the voids on DEM across different size and terrain type areas, resulting in immediate use of DEM data for many applications (e.g. our case).

To explore the correlations between upstream runoff and floods/vegetation in Coongie Lakes wetland, we also obtained monthly stream flow data of Cooper Creek observed at the Nappa Merrie (003103A) gauge station from 1988 to 2011, through Queensland government website (https://water-monitoring.information.qld.gov.au/).

4.2.5 Vegetation Index calculation

Normalized Difference Vegetation Index (NDVI) was used as a proxy of canopy "greenness" in our analyses. NDVI has been shown to be closely associated with various vegetation biophysical parameters (e.g., canopy cover, leaf area index, fraction of absorbed photosynthetic radiation and biomass) across different ecosystems (Rouse Jr et al. 1974; Hwang et al. 2011; Johnson et al. 2005). In this study, we calculated 24 years (January 1988 to September 2011) of monthly NDVI using Landsat surface reflectance band 3 and band 4. The formulation of NDVI is,

$$\text{NDVI} = \frac{NIR - Red}{NIR + Red} \tag{4.1}$$

where NIR is the near-infrared surface reflectance (band 4,760-900 nm) and Red is the red surface reflectance (band 3, 630-690 nm).

Linear interpolation in the temporal dimension was used to fill the gaps remaining after QA filtering, but pixels with more than two consecutive gaps (+2 months) were excluded from the analysis. Values of NDVI for a given pixel range from -1 to +1 with 0 – 0.1 indicative of no vegetation (e.g., bare soil), while values close to 1 (0.8 – 0.9) indicate the highest possible density of vigorously growing green foliage, and values below zero (-1 – 0) indicating the presence of extensive open water (Myneni and Williams 1994).

4.2.6 Flood extent mapping

We mapped flood extent using the Dynamic Surface Water Extent (DSWE) algorithm described in Jones (2015), which with static thresholds was developed to detect inundation in wetlands based on Landsat observations from Thematic Mapper (TM, Landsats 4–5), Enhanced Thematic Mapper Plus (ETM+, Landsat7) and Operational Land Imager (OLI, Landsat 8). In particular, this algorithm focuses on mapping surface water in wetlands with open water and presence of vegetation, which has been evaluated and validated by comprehensive in situ data from the Everglades Depth Estimation Network (Conrads et al. 2014; Jones and Price 2007). DSWE was also found to have no significant trend or bias in its performance as a function of time or general hydrologic conditions, indicating a consistency for long-term surface water monitoring (Jones 2015). As cloud and cloud shadow have already been filtered out from the surface reflectance data, DSWE in this study was applied in cloud/shadow free

pixels. DWSE utilised the Modified Normalized Difference Wetness Index (MNDWI) proposed by Xu (2006) as a theoretical basis, which was demonstrated by previous studies to have a relatively strong performing metric compared to various water detection indices across a range of environments (Feyisa et al. 2014; Sun et al. 2012; Thomas et al. 2015; Tulbure et al. 2016; Zhang et al. 2011). The MNDWI is calculated as:

$$\text{MNDWI} = \frac{Green - MIR}{Green + MIR} \quad (4.2)$$

where Green is the green surface reflectance (band 2, 520–600 nm) and MIR is the middle infrared surface reflectance (band 5,1550–1750 nm).

The following two decision rules were uniformly applied to all Landsat pixels for presence of standing water (Jones 2015):

Floodwater if (MNDWI > 0.123) (4.3)

or:

(MNDWI > -0.5 and Band4 < 2000 and Band7 < 1000) (4.4)

Where MNDWI was calculated from equation 2; Band4 and Band7 are CDR band 4 (760 –900 nm) and band 7 (2080–2350 nm) surface reflectance.

Using this method, we mapped the historical coverage or extent of floods in the Coongie Lakes wetland from 1988 to 2011. Based on the annual flooding frequency of Coongie Lakes (Puckridge et al. 2010), we defined the years in which the maximum monthly flood extent ($flood_{max}$) was over 1500 km^2 as major flooding years, between 300 and 1500 km^2 as moderate flooding years, and below 200 km^2 as dry years.

4.2.7 Wetland vegetation growth extent extraction

In the Coongie Lakes wetland region (Figs. 1A and 2), the vegetation of the sand dunes and gibber plains and downs has much lower greenness as it is not influenced by flooding. Previous studies showed that a relatively consistent NDVI threshold of 0.3-0.35 can be used to discriminate arid wetland vegetation activity from surrounding dryland vegetation responses, which was fully validated by ground-based measurements (Petus et al. 2013; White and Lewis 2011; White et al. 2016). Based on the NDVI

threshold approaches applied in these studies, we defined a particular greenness value to differentiate wetland from non-wetland vegetation and extracted the growth extent in wetland vegetation based on NDVI images. NDVI thresholds of 0.30, 0.32, 0.34 and 0.35 were tested respectively to determine which was best associated with the vegetation directly adjoining the water bodies over Coongie Lakes. In this way, we excluded all the non-wetland vegetation and bare soil and focussed on the effects of floods on wetland ecosystems. We chose to use vegetation growth extent over the NDVI threshold instead of NDVI mean values for capturing the dynamic vegetated areas to avoid the confusion of high greenness within small extents, for example, around small permanent lakes in the dry years.

4.2.8 Spatio-temporal variability and correlation analysis

We calculated monthly values of flood and vegetation growth extent in the Coongie Lakes wetland area (Fig.4.2), as well as rainfall (BOM) amount over the Cooper Creek catchment (Fig.4.1A) for the period of January 1988 to September 2011. Mean monthly values of TWSA from GRACE over the Cooper Creek catchment were computed from April 2002 to September 2011. Images were processed to show the spatial patterns in inflow of floods, wetland vegetation growth dynamics, and changes of hydrological conditions. Cross-correlation analysis over April 2002 to September 2011 was carried out to obtain the maximum Pearson's correlation coefficient (r) and the corresponding time lag in months between monthly flood extent in Coongie Lakes and TWSA/rainfall (TRMM) of each pixel across the Lake Eyre Basin. As monthly rainfall amount is a flux variable, we calculated monthly accumulative rainfall with the long-term trend (2002-2011) removed as a state variable for this cross correlation analysis.

4.3 Results

4.3.1 Spatial-temporal flood patterns in Coongie Lakes from 1988 to 2011

The highly variable water regimes with episodes of long-term droughts and short intensive flood events over the Coongie Lakes were evident in our hydrologic analysis, where flood extent changed dramatically across seasons and between years, with ranges from near zero to 3456 km^2 (Fig.4.3). Over the 24-year study period, Coongie Lakes

wetland experienced a total of 10 flooding years, including five major flood events: two continuous floods in 1989 and 1990, one in 2000, and another two during 2010-2011 (blue semi-transparent areas at bottom of Fig.4.3). Five moderate flood events were recorded in 1988, 1991, 1995, 1998 and 2004, respectively (cyan semi-transparent areas at bottom of Fig.4.3). In 1997 and 2001, floods were restricted only to the north-eastern part of the wetland and in sizes between dry and moderate flooding years (Fig.4.3). The remaining 12 years were dry (flood extent < 200 km^2) with very little water apparent in Coongie Lakes (Fig.4.3). The data suggest that the dry periods between consecutive floods are increasing in length. Before 2000, the dry periods were 1 to 3 years long, while after 2000 the dry periods were 3 to 5 years (Fig.4.3).

We also observed that the flood events and drought periods at Coongie Lakes wetland were closely coupled with the large-scale climate system of El Niño Southern Oscillation (ENSO) events, or La Niña and El Niño years. In particular, five major flood events in the wetland, at decadal frequency, coincided with strong La Niña periods (blue colour bars at top of Fig.4.3). The disparity between low rainfall (< 200 mm/year) and high potential evaporation (> 2000/year mm) over the wetland area was balanced by water inflow from the upper Cooper Creek catchment. Rainfall amount averaged over the Cooper Creek catchment only weakly correlated with the flood events in the wetland ($r = 0.34$ with 3-month lag) during our study period (Fig.4.3).

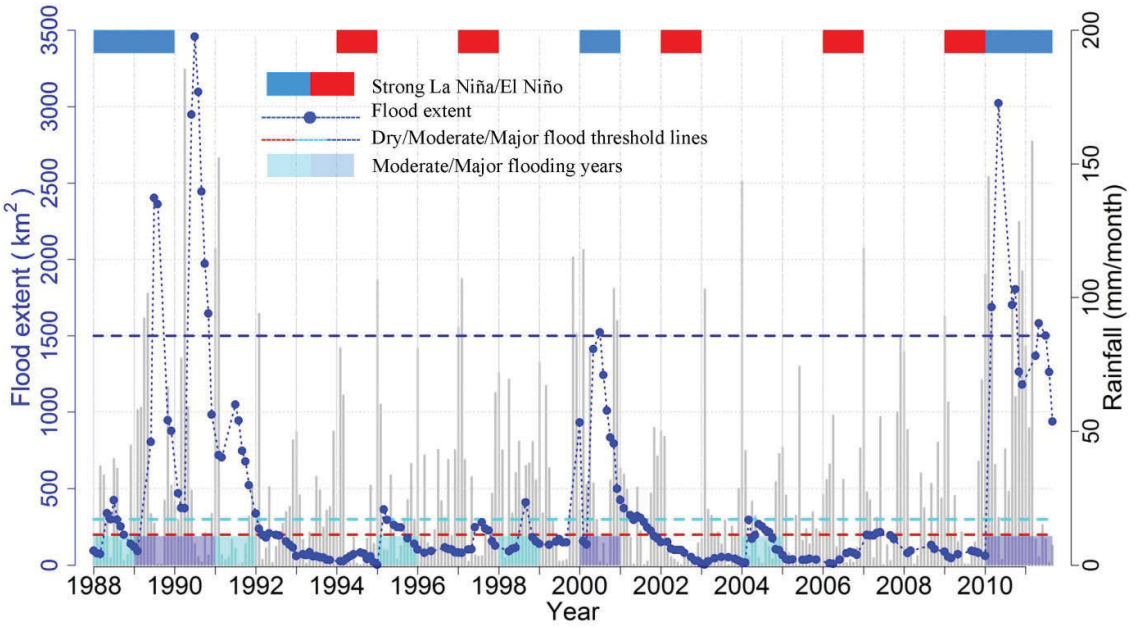

Figure 4.3. Monthly flood extent (blue points) in Coongie Lakes and monthly rainfall spatially averaged (grey histograms) over Cooper Creek catchment from January 1988 to September 2011, with blue and cyan semi-transparent areas at the bottom representing the years that had major ($flood_{max}$ > 1500 km^2 blue dashed line) and moderate (300 km^2 < $flood_{max}$ < 1500 km^2 cyan line) flooding events, while $flood_{max}$ under the red line (200 km^2 red dashed line) indicates the dry year. Colour bars on the top of the graph indicate periods of strong La Niña (blue)/El Niño (red) events (from Southern Oscillation Index analysis of Australian Bureau of Meteorology).

Spatially, flood extent images show that during wet years, floodwater was recharged to the east-central part of the study area from the downstream river of "Channel Country" (Fig.4.1A, 4). It then filled Coongie Lakes wetland sequentially from the northeast to southwest through river channels, flowing from one lake to another in succession (Fig.4.4). We found the frequency of flooding events to be no more than once per year over the 24-year study period (Fig.4.3), in which the Coongie Lakes wetland is often fully recharged in the wet season, then most of the floodwater will be evaporated or flow out during the following dry period (Fig.4.4). Flood extent in the wetlands had strong seasonal patterns, exhibiting peak inundation extent in June to August, before 2000, with a shift to March to May, after 2000 (e.g., Fig.4.4). During the dry periods, most of the water bodies in Coongie Lakes were empty but there were a few permanent small lakes located in the north-eastern part of the wetland (Fig.4.4 Summer).

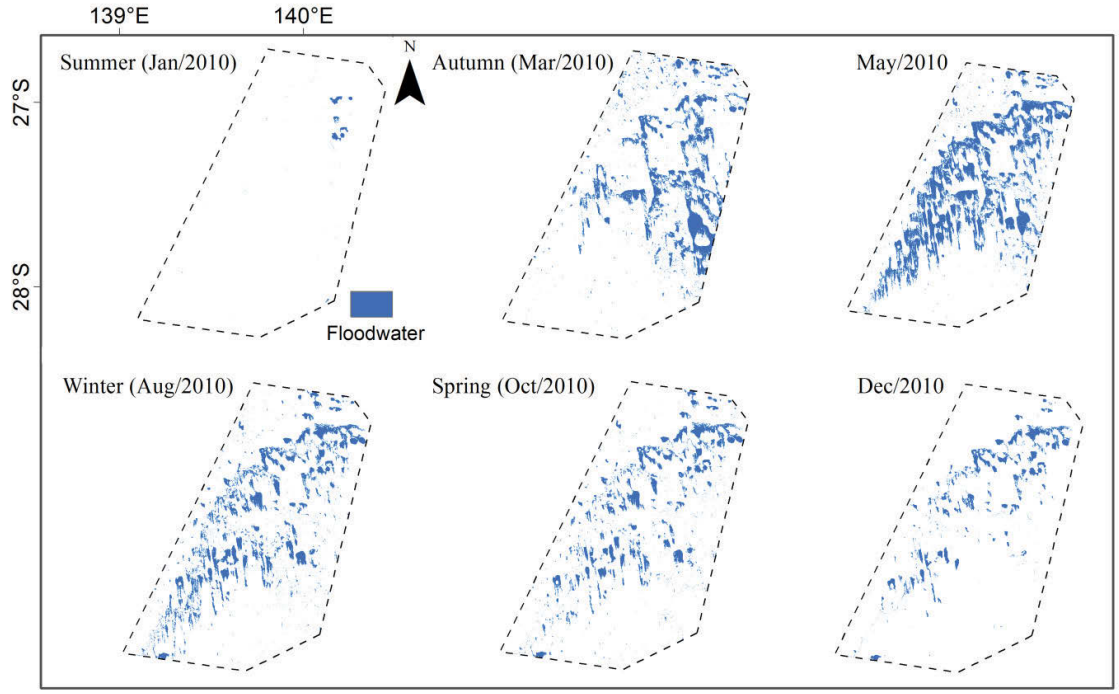

Figure 4.4. Spatial distribution of inundation over Coongie Lakes wetland for six monthly flood extent images across the four seasons of the 2010 major flooding year.

4.3.2 GRACE-TWSA identification of the water source area for Coongie Lakes wetland

The DEM data showed a clear northeast to southwest topographical elevation gradient over the Cooper Creek catchment, with Coongie Lakes wetland being located at the lowest area (0-50 m) while the upper catchment was > 250 m (Fig.4.5A). Within the catchment, in particular, over the "Channel Country" area adjacent to the wetland (Fig.4.1A), there is a complex dryland hydro-geomorphology, which is characterized by a gentle gradient and anastomosing river channels over wide floodplains that gradually transmit large, yet infrequent and slow-moving flood pulses (Jarihani et al. 2015b). Thus, the geomorphic setting (from high to low altitude) of Cooper Creek catchment as shown by the DEM illustrates the extent and location of the water source and enables water flowing from upper catchment south-westerly to feed the Coongie Lakes wetland (Fig.4.5A).

As reflected by the topographical pattern using the DEM data, the hydrological conditions over the Cooper Creek catchment will directly determine the magnitude and duration of the floods in Coongie Lakes, and in turn control the "boom and bust" dynamics of wetland vegetation. Therefore, choosing a good hydrological indicator of

the water source area is critical for monitoring and predicting the changes and health of this wetland. The spatial associations of the floods in the Coongie Lakes with the large-scale hydrological fluctuations, indicated by TWSA and rainfall, on per-pixel level are presented across the LEB over the 2002-2011 time period (Fig.4.5B–E). Cross-correlation analysis between flood extent in the wetland and GRACE-TWSA over the entire LEB confirmed that the Cooper Creek catchment region is the water source area of the Coongie Lakes wetland (Fig.4.5B). The spatial distribution of correlation coefficients across LEB reflects the local topography, with the highest correlations (r = 0.8, lag = 0 month) concentrating in the wetland's adjacent "Channel Country" area of Cooper Creek catchment (Fig.4.5B and C). By contrast, cross-correlation results between floods and detrended accumulative rainfall (TRMM) across the LEB show much weaker correlations between the flood extent in the wetland and rainfall amount over the Cooper Creek catchment (Fig.4.5Dand E).

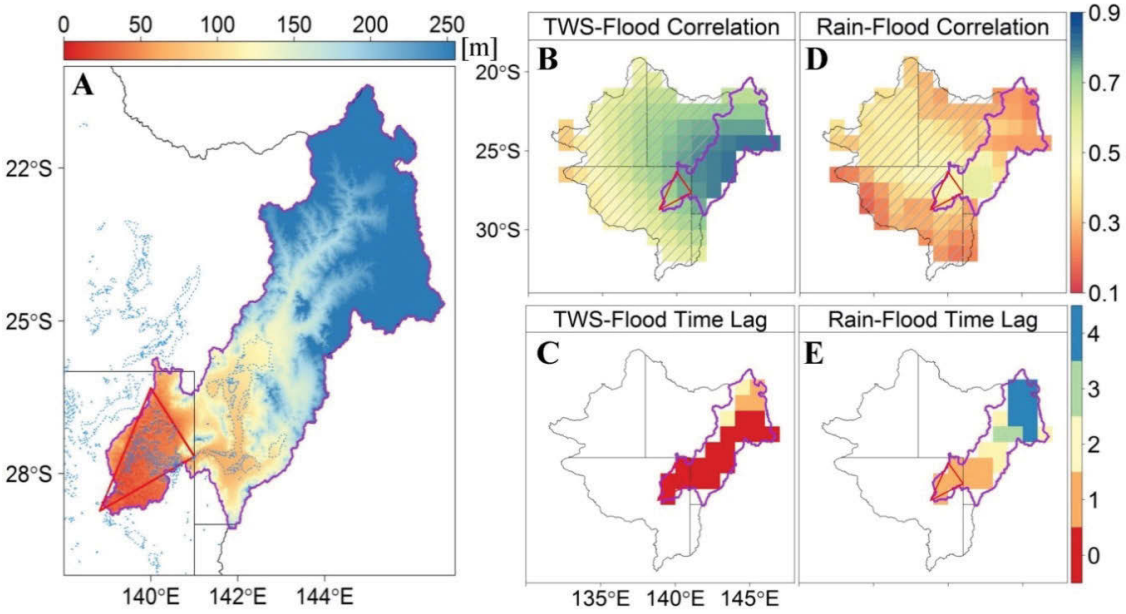

Figure 4.5. (A) Digital Elevation Model (DEM) of Cooper Creek catchment (purple line) with main water bodies (pale blue line), Ramsar boundary (red triangle); (B and C) Cross correlations and lag (unit: month) between monthly flood extent in Coongie Lakes and TWSA and (D and E) detrended accumulative rainfall (TRMM) across Lake Eyre Basin on 1× 1 degree pixel basis from April 2002 to September 2011. As the emphasis is Cooper Creek catchment, the outside pixels were either shaded (correlations) as a reference or excluded (lags).

4.3.3 Ecological responses of Coongie Lakes to hydrological variations

We found a threshold NDVI = 0.3 was optimal to map the wetland vegetation growth extent across the Coongie Lakes wetland. This threshold minimized the confounding effects of greening from surrounding rain-fed, non-wetland vegetation, which is expected to have a lower greenness due to the lack of water-availability than wetland vegetation. Our results showed strong seasonal and inter-annual variations in the spatial extent of vegetation growth (from 0.5 to 2625 km^2), which closely followed that of flood extent with peak values in austral winter and minimum values in summer (Fig.4.6). The relationship between flood and vegetation growth extent was the strongest and most significant with no lag ($r = 0.64$, $p < 0.05$) and 1 month lag ($r = 0.63$, $p < 0.05$). Such short time lags between flooding and vegetation extent suggest that the NDVI response is dominated by ephemeral and shrub species on the floodplains, which can react to increase in water-availability in a rapid manner, as is evident from the Figure 6. In addition, high correlations of 0.71 and 0.69 (lag = 0 month) were observed between monthly flood/vegetation growth extent and stream discharge records of Cooper Creek observed at the Nappa Merrie gauge station (Fig.4.6). This indicates the inconsistencies between the rainfall falling in the headwaters and the ecohydrological dynamics in the arid wetland downstream due to the high river transmission losses.

Our results revealed that the long dry periods were frequent and flood events were erratic during the 24 years, except major flooding that occurred at a decadal frequency (Fig.4.6). It is noteworthy that wetland vegetation in Coongie Lakes was able to tolerate droughts with low photosynthetic responses (vegetation growth extent between 0 and 300 km^2), but it was also very responsive to the floods with extensive increases in photosynthetic vegetation extent (over 500 km^2) (Fig.4.6). We also observed some peaks of vegetated area during the dry years of 1993, 2003, 2005. etc., which may indicate "carry-over" effects of floods on the arid wetland ecosystem and demonstrate ecological resilience of some perennial vegetation types (Fig.4.6).

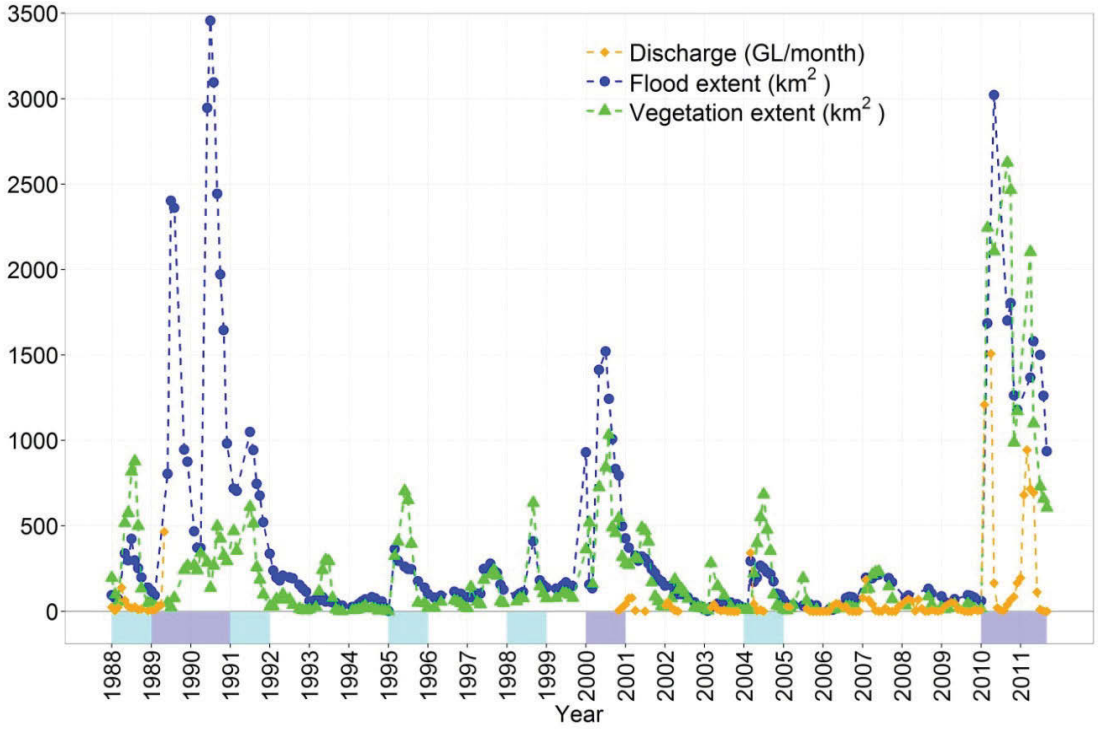

Figure 4.6. Monthly flood (blue points) and wetland vegetation growth (green points) extent in Coongie Lakes wetland and discharge (orange points) at Nappa Merrie station (Fig.4.1) from January 1988 to September 2011 with blue and cyan shaded areas at the bottom representing major and moderate flooding years.

Figure 7 exhibits the spatial distributions of wetland vegetation photosynthetic extent for particular months when the peak vegetation growth occurred, for a dry period, 1994, and for three major flood events in 1990, 2000 and 2010. Each panel of Figure 7 shows inundation as black, and wetland vegetation on a colour ramp from orange (low vigour) through green to blue (very vigorous). In dry periods, there was very little or no growth in wetland vegetation detected within the wetland area (e.g., 1994) (Fig.4.7). When the flood arrived, wetland vegetation grew vigorously in proximity to the water bodies, and particularly over the east-central portion of the study site that is the entry of the floodwaters from the Cooper Creek catchment (e.g., 1990, 2000 and 2010) (Fig.4.7).

Our results demonstrated that vegetation response to each flood event is unique with different extent despite the similar extent of flood. This is likely to be attributed to the different spatio-temporal characteristics of each flood event, such as the rates of rise and fall and the amplitude, duration and frequency of the flood events (Figs. 6 and 7). The floods generally had positive and cumulative effects on arid wetlands vegetation, as indicated by the tight coupling between flood extent and vegetation growth areas

(Fig.4.6 and Fig.4.7). However, our results also showed that extensive flooding over long periods may also preclude the development of wetland vegetation such as when the largest flood event of the entire study period occurred in 1990 (Fig.4.6). In 1990, the peak vegetation extent was even much smaller than those from some other moderate flood events such as in 1995, 1998, and 2004 (Fig.4.6).

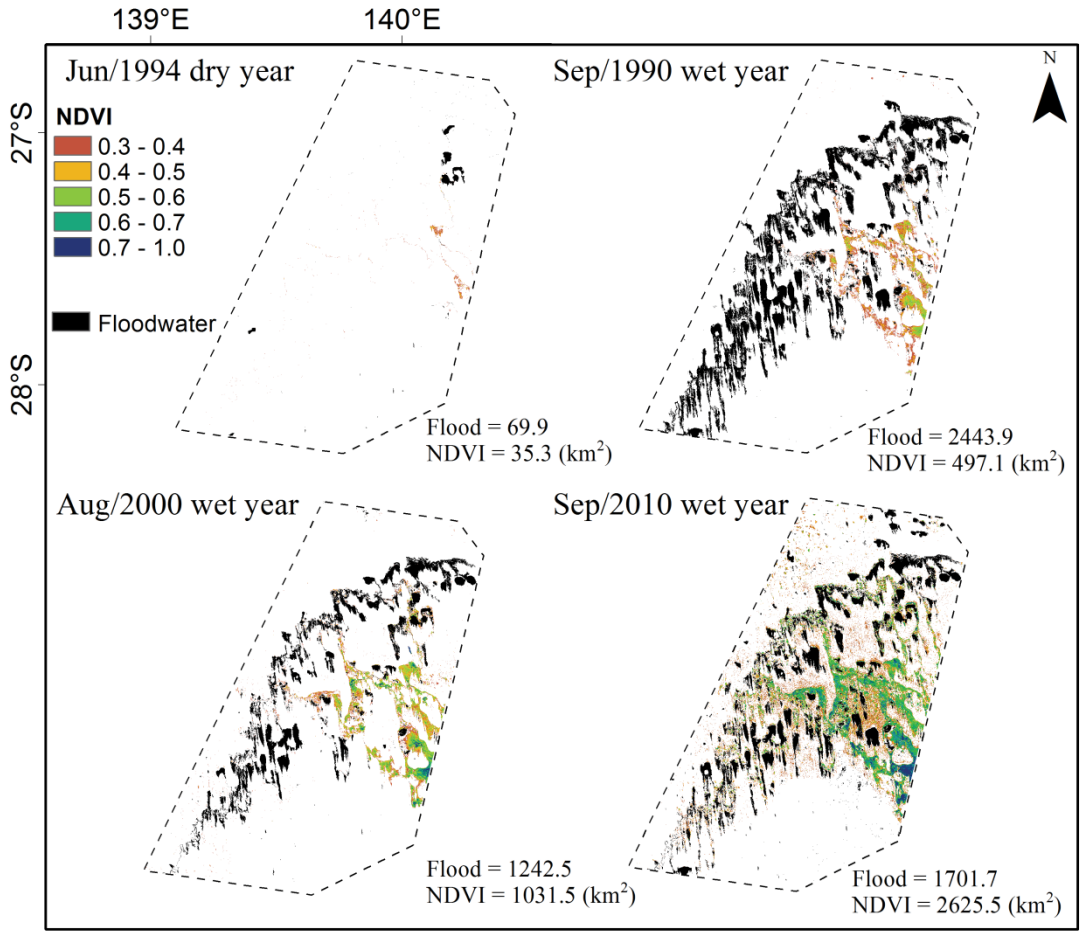

Figure 4.7. Maximum monthly growth extent in wetland vegetation over Coongie Lakes during a dry period (1994) and three major flood events (1990, 2000 and 2010). Black colour indicates inundation and colour ramp represents NDVI values from low (dark brown) through medium (light green) to high (dark blue).

4.3.4 The impacts of hydroclimatic extremes on ecohydrology in Coongie Lakes

Variations in TWSA over the Cooper Creek catchment clearly indicated the impacts from the recent Australia-wide 'big dry' and 'big wet' events (Fig.4.8). There was a significant decline in TWSA during the drought period (2002-2009) and an anomalous TWSA increase during the wet pulse (2010-11 La Niña) with drying and wetting rates

of -0.21 ± 0.09 and 5.17 ± 0.86 cm/year, respectively (Fig.4.8). Changes in TWSA over the water source area further largely drove the hydrological and ecological dynamics of Coongie Lakes, as indicated by the strong correlations between TWSA and flood extent ($r = 0.81$, $p < 0.05$) or vegetation extent ($r = 0.82$, $p < 0.05$).

During 2002-2009 'big dry' period, only one moderate flood with a concurrent vegetation growth was recorded, while the average flood and vegetation growth extent through the remaining years were only around 96 and 102 km^2, as compared to the historical average (1988-2011) of 392 and 252 km^2 respectively (Fig.4.8). This long-term dry anomaly represented by the conspicuous downward trend in TWSA, indicates the Coongie Lakes wetland was under increasing water stress during the protracted drought period (Fig.4.8). However, since the 'big wet' pulse arrived in early 2010, the parched wetland had received two major consecutive floods during 2010 – 2011 with an average flood extent of 1447 km^2 (Fig.4.8). These large floods resulted in two years of strong vegetation boom, which were the highest vegetation growth extent recorded over the 24-year study period (maximum vegetation extent = 2625 km^2 in 2010 and 2102 km^2 in 2011), with more than 1.5 standard deviations vegetation growth extent above 1988-2011 long-term average (Fig.4.8). The rapid recovery of vegetation growth in Coongie Lakes during the 'big wet' after the protracted 'big dry' suggests a strong ecological resilience of arid wetland vegetation.

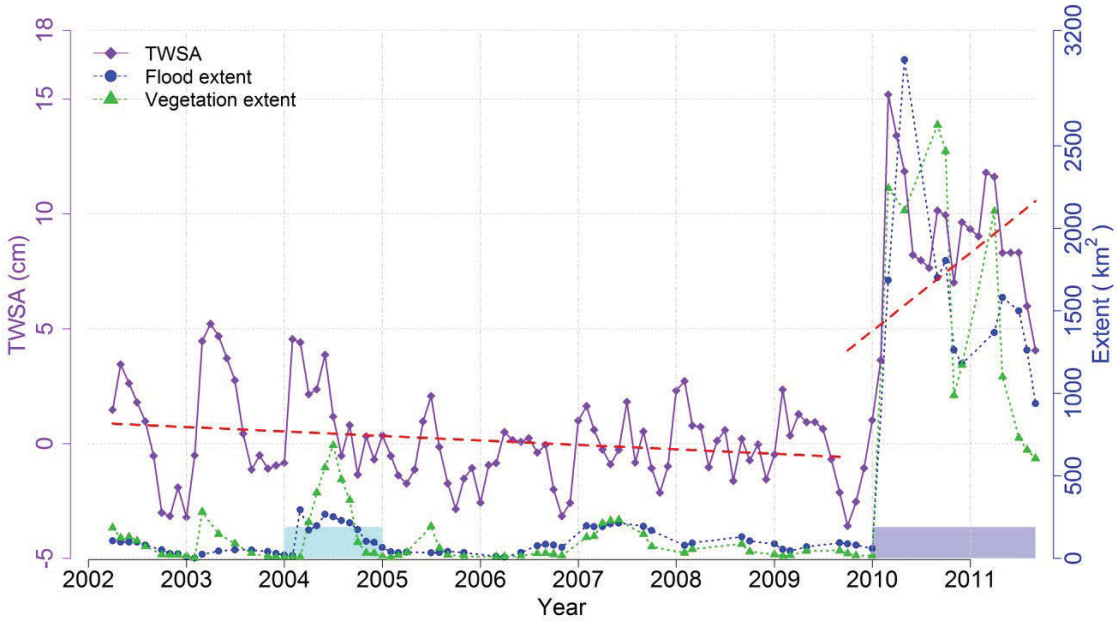

Figure 4.8. Monthly flood (blue points) and wetland vegetation growth (green points) extent in Coongie Lakes wetland and monthly TWSA (purple line) averaged over Cooper Creek catchment (Fig.4.1 A) from April 2002 to September 2011. The blue and cyan shaded areas indicate major and moderate flooding years. Two red dashed lines are the linear trends in TWSA during the 'big dry' (2002-2009) and the 'big wet' (2010-2011), respectively.

4.4 Discussion

In this study we investigated the dynamics and resilience of an arid wetland ecosystem in a dryland river system of Central Australia to multi-decadal spatial-temporal patterns of flood events and hydroclimatic extremes. First, our results revealed the tight coupling between flood and wetland vegetation dynamics, demonstrating the significance of periodic floods in driving arid wetlands ecosystem function. Meanwhile, we showed that GRACE-TWSA over the water source area is a better indicator than rainfall for monitoring hydrological dynamics in arid wetland area. Furthermore, we found a strong ecological resilience of arid wetland vegetation to extreme hydroclimatic events. Our results indicate the pronounced effect of hydrological variations on arid wetlands, suggesting that these ecosystems are particularly sensitive and vulnerable to a progression of alternating hydrological regimes due to climate change.

4.4.1 Ecological significance of periodic flood events over arid wetlands and their connection with large-scale climate systems

The emphasis of this study was to monitor the relative changes in floods and wetland vegetation within Coongie Lakes and their interactions across seasons and through years. Thus, the mapping methods used herein are well suited to achieve such purpose despite some uncertainties in the magnitudes of monthly Landsat derived inundation and wetland vegetation growth extent. This was also confirmed by high associations between flood, vegetation growth extent, stream discharge and GRACE-TWSA over study areas that were derived from independent sources. Our results demonstrated that periodic flood events in arid wetland areas have specific ecological significance and play a crucial role in sustaining wetland vegetation, upon which many other species are dependent (Sheldon et al. 2010). Despite a close coupling between floods and vegetation growth, we found that during the 24-year study period, vegetation within the wetland did not always benefit from the flood events, especially when the floods were persistent and over-extensive (such as in 1990, Fig.4.6 and Fig.4.7). This might be due to oxygen depletion of submerged plants from prolonged and extreme extensive floodwaters, which consequently lower the richness and biomass of plant communities (Casanova and Brock 2000; Vervuren et al. 2003).

We also observed an alternation of temporal hydrological regimes over the Coongie Lakes wetland during the study period, indicated by the increases in the duration of dry periods between each two floods after 2000 relative to 1988-1999 (Fig.4.3). Meanwhile, we noted that the peak timing of the inundation extent in the wetland shifted about three months ahead since 2000. This may potentially lead to an earlier peak of wetland vegetation growth, which is likely to reduce the ecosystem production due to a shorter growing season.

Without the interference from human activities such as regulation and diversion of the water source, the interactions between floods and vegetation in Coongie Lakes directly mirror the recent climate variability. Our results demonstrated that flood events and dry periods of Coongie Lakes arid wetland can be linked to the fluctuations between El Niño dry phases and La Niña wet phases of ENSO. This is in line with previous studies that showed the rainfall variability over the Cooper Creek catchment is primarily affected by ENSO, which is fed by the monsoonal rains from western Queensland in the tropical zone (Reid et al. 1988; Timms 2001). The frequency of extreme ENSO events due to greenhouse warming has been increasing over the last four decades, and is likely

to enhance in future, which will exert substantial ecological and hydrological impacts on arid wetlands (Cai et al. 2014; IPCC 2014).

4.4.2 GRACE-TWSA as a valuable and integrative indicator of arid wetland ecohydrological dynamics

Using GRACE-derived TWSA across LEB, we identified the location and extent of the water source region for Coongie Lakes arid wetland. Our results revealed that GRACE-TWSA over the Cooper Creek catchment can explain a large fraction of the variations in flood and vegetation growth extent both seasonally and inter-annually, with strong correlations higher than 0.8 (Fig.4.8). By contrast, the much weaker relationships between rainfall amounts over the water source area and the ecohydrological dynamics in the wetland showed the limitation of using rainfall data to understand the hydrological controls on arid wetland ecosystems (Fig.4.5).

This finding reflects the complexity of the hydrological processes over dryland areas. Australian dryland river systems are known to have one of the most variable flow regimes in the world (Puckridge et al. 1998), with ENSO contributing significantly to this variability (Chiew et al. 1998; Walker et al. 1995). A successful flood pulse delivery of rainfall falling in the headwaters downstream to arid wetlands is crucial for the ecosystems inside, which is largely determined by the complicated hydro-geomorphology in dryland anabranching river systems that features extreme spatial and temporal variability in streamflow (Jarihani et al. 2013). As a result, the variable flow in anabranching rivers with large transmission losses (actual evaporation, infiltration to the soil and groundwater and terminal water remaining after floods) make it extremely hard to monitor and predict the dynamics of arid wetland ecosystems based on the rainfall alone (Jarihani et al. 2015b). Although such issues were partly addressed in this study by applying detrended accumulative rainfall, future work is needed to explore the relationship between effective rainfall (rainfall minus transmission losses) and floods using hydrodynamic modelling (Jarihani et al. 2015b).

As an integrative measure of vertical changes in total water storage, GRACE gravitational observations have been identified as a valuable proxy of water availability over large areas, with consistent data free from cloud effects (Guan et al. 2015; Penatti et al. 2015;Reager and Famiglietti 2009; Yang et al. 2014). GRACE-TWSA thus can be

used as a surrogate of terminal water storage from the headwaters, after transmission losses, at various pixel-level locations along the Cooper Creek, which is a better hydrological indicator than rainfall to monitor the ecohydrological performance over arid wetland areas. Climate change is predicted to markedly alter current hydrological regimes later this century (Fischer et al. 2013; IPCC 2014), exerting great threats to arid wetland ecosystems. Therefore, a continuous and proper hydrological indicator such as GRACE-TWSA will not only guide the design of Australia's arid wetland management strategies to a changing climate, but also generate important knowledge that is highly valuable for understanding arid wetlands over other global regions.

4.4.3 Ecological resilience of arid wetlands despite high hydrological variations and hydroclimatic extremes

Australia's early 21st century 'big dry' and 'big wet' events provide an ideal natural experiment to understand the ecological resilience of arid wetlands to the hydroclimatic extremes. The recovery of ecological functioning of Coongie Lakes wetland indicates the ability of arid wetland ecosystems to absorb the disturbances associated with drought and retained the sensitivity to water availability during the wet period.

The high ecological resilience of arid ecosystems (e.g. arid wetland ecosystems) to hydroclimatic extremes can be attributed to their drought-adapted hydraulic architecture to a highly variable climate through a combination of different species that promote the resilience at the ecosystem-level (Ma et al. 2015; Ponce Campos et al. 2013). For example, ephemeral and shrub species respond rapidly to changes in water availability with shallow root systems to take advantage of increase in soil moisture (Chen et al. 2016). By contrast, perennial vegetation types within the wetland such as Eucalypts may respond to flooding events with longer lags (up to 4-6 months) (Lawley et al. 2016; Petus et al. 2013). Therefore, the variations in wetland vegetation growth extent observed in this study should be dominated by the recurrent vegetation types on the floodplain, lagging 0-1 months to the changes in flood extent. By contrast, the observed 'carry-over' effects of vegetation boom during the dry years (e.g.1993, 2003, 2005) might be mostly attributed to the seasonal growth of the deeper-rooted persistent shrubs and trees, which could benefit from the previous year's flood. Consequently, these factors contribute to the resilience of arid wetlands to the high hydrological variations

and climatic variability. However, as this study focuses on satellite observations of arid wetlands, there is limited knowledge of detailed species composition and new species assemblages (e.g. invasive species) over Coongie Lakes, which might partly contribute to the increase in wetland vegetation greenness during the 'big wet' period (Moran et al. 2014). Future field work is needed to collect more ground data on this aspect.

The dramatic effects of hydrological variations on ecological functioning of the arid wetlands suggest these are highly adapted and resilient ecosystems, which are particularly sensitive to future altered spatial and temporal water regimes due to climate change. Hydroclimatic extremes are projected to be increasing in frequency over the coming decades (AghaKouchak et al. 2014; Cai et al. 2014), however, previous studies have shown little change in global drought over the past 60 years (Sheffield et al. 2012) and more physically-based studies of potential evapotranspiration have been suggested to predict potential drought climatic extremes in future (McVicar et al. 2012; Yin et al. 2014).Thus, consistent observations from multiple sources particularly satellites over long-term period, are highly valuable to monitor arid wetlands and detect their potential loss world-wide.

4.5 Conclusion

We have shown that periodic flood and drought events in the Coongie Lakes arid wetland, an arid wetland in central Australia, produced "boom and bust" ecological responses that are primarily driven by the large-scale ENSO climate mode. We further found that GRACE-TWSA over the water source area provides a better way than rainfall to monitor ecohydrological dynamics (flood extent and vegetation growth) in the wetland. The recent hydroclimatic extremes exerted dramatic impacts on the ecological functioning of the wetland, and the rapid recovery of vegetation growth in 2010-11 wet year, after the protracted dry period, demonstrated a strong ecological resilience of arid wetlands to hydroclimatic variations.

Amplification of the hydrological cycle as a consequence of climate change is predicted to increase climate variability and the frequency and severity of droughts and wet extremes. In the meantime, proposals for water extraction from dryland rivers like Cooper Creek continue to be promoted. These pose great challenges for the conservation of arid wetlands in Australia and around the world, suggesting that

consistent monitoring of these wetlands by integrating data from multiple space-borne sensors is urgently needed for effective conservation and sustainable management of arid wetland resources.

4.6 References

Adam, E., Mutanga, O., & Rugege, D. (2010). Multispectral and hyperspectral remote sensing for identification and mapping of wetland vegetation: a review. *Wetlands Ecology and Management, 18*, 281-296

AghaKouchak, A., Cheng, L., Mazdiyasni, O., & Farahmand, A. (2014). Global warming and changes in risk of concurrent climate extremes: Insights from the 2014 California drought. *Geophysical Research Letters, 41*, 8847-8852

Brendonck L, Williams WD. (2000). Biodiversity in wetlands of dry regions (drylands). *Biodiversity in Wetlands: Assessment, Function and Conservation,1*, 181–194

Bunn, S.E., Thoms, M.C., Hamilton, S.K., & Capon, S.J. (2006). Flow variability in dryland rivers: boom, bust and the bits in between. *River Research and Applications, 22*, 179-186

Butcher, R., & Hale, J. (2011). Coongie Lakes Ramsar Site Ecological Character Description. In: Report to the Department of Sustainability, Environment, Water, Population and Communities, Canberra < https://www.environment.gov.au/water/wetlands/publications/coongie-lakes-ramsar-site-ecological-character-description>

Cai, W., Borlace, S., Lengaigne, M., Van Rensch, P., Collins, M., Vecchi, G., Timmermann, A., Santoso, A., McPhaden, M.J., & Wu, L. (2014). Increasing frequency of extreme El Niño events due to greenhouse warming. *Nature Climate Change, 4*, 111-116

Capon, S.J. (2003). Plant community responses to wetting and drying in a large arid floodplain. *River Research and Applications, 19*, 509-520

Casanova, M.T., & Brock, M.A. (2000). How do depth, duration and frequency of flooding influence the establishment of wetland plant communities? *Plant Ecology, 147*, 237-250

Chappell, A., Renzullo, L.J., Raupach, T.H., & Haylock, M. (2013). Evaluating geostatistical methods of blending satellite and gauge data to estimate near real-time daily rainfall for Australia. *Journal of Hydrology, 493*, 105-114

Chen, J., Rodell, M., Wilson, C., & Famiglietti, J. (2005). Low degree spherical harmonic influences on Gravity Recovery and Climate Experiment (GRACE) water storage estimates. *Geophysical Research Letters, 32*, L14405

Chen, T., McVicar, T.R., Wang, G., Chen, X., de Jeu, R.A., Liu, Y.Y., Shen, H., Zhang, F., & Dolman, A.J. (2016). Advantages of Using Microwave Satellite Soil Moisture over Gridded Precipitation Products and Land Surface Model Output in Assessing Regional

Vegetation Water Availability and Growth Dynamics for a Lateral Inflow Receiving Landscape. *Remote Sensing, 8*, 428-440

Chen, Y., Huang, C., Ticehurst, C., Merrin, L., & Thew, P. (2013). An evaluation of MODIS daily and 8-day composite products for floodplain and wetland inundation mapping. *Wetlands, 33*, 823-835

Chiew, F. H. S., Piechota, T. C., Dracup, J. A. and McMahon, T. A. (1998). El Niño/Southern Oscillation and Australian rainfall, streamflow and drought: links and potential forecasting. *Journal of Hydrology, 204*, 138-149

Chou, C., Chiang, J.C., Lan, C.-W., Chung, C.-H., Liao, Y.-C., & Lee, C.-J. (2013). Increase in the range between wet and dry season precipitation. *Nature Geoscience, 6*, 263-267

Clarke, K., Lawley, E., Raja Segaran, R., & Lewis, M. (2014). Spatially-explicit environmental indicators for regional NRM planning for climate change. In: Report for Natural Resources SA Arid Lands <https://www.researchgate.net/profile/Kenneth_Clarke2>

Clarke, K., & Lewis, M. (2015). Desert Jewels Remote Sensing: Inundation dynamics. In: Report for the Department of Environment, Water and Natural Resources <https://www.researchgate.net/profile/Kenneth_Clarke2>

Cleverly, J., Eamus, D., Van Gorsel, E., Chen, C., Rumman, R., Luo, Q., Coupe, N.R., Li, L., Kljun, N., & Faux, R. (2016a). Productivity and evapotranspiration of two contrasting semiarid ecosystems following the 2011 global carbon land sink anomaly. *Agricultural and Forest Meteorology, 220*, 151-159

Cleverly J, Eamus D, Luo Q, Restrepo Coupe N, Kljun N, Ma X, Ewenz C, Li L, Yu Q, Huete A. (2016b). The importance of interacting climate modes on Australia's contribution to global carbon cycle extremes. *Scientific Reports 6*:23113

Conrads, P.A., Petkewich, M.D., O'Reilly, A.M., & Telis, P.A. (2014). Hydrologic record extension of water-level data in the Everglades Depth Estimation Network (EDEN), 1991-99. In: Technical Report for US Geological Survey: Reston, VA, USA < pubs.usgs.gov/sir/2014/5226/pdf/sir2014-5226.pdf>

Costelloe, J.F., Grayson, R.B., Argent, R.M., & McMahon, T.A. (2003). Modelling the flow regime of an arid zone floodplain river, Diamantina River, Australia. *Environmental Modelling & Software, 18*, 693-703

Dunkerley, D., & Brown, K. (1999). Flow behaviour, suspended sediment transport and transmission losses in a small (sub-bank-full) flow event in an Australian desert stream. *Hydrological Processes, 13*, 1577-1588

Durack, P.J., Wijffels, S.E., & Matear, R.J. (2012). Ocean salinities reveal strong global water cycle intensification during 1950 to 2000. *Science, 336*, 455-458

Famiglietti, J.S., & Rodell, M. (2013). Water in the Balance. *Science, 340*, 1300-1301

Fensham, R., & Fairfax, R. (2003). Spring wetlands of the Great Artesian Basin, Queensland, Australia. *Wetlands Ecology and Management, 11*, 343-362

Fensham, R., Fairfax, R., Pocknee, D., & Kelley, J. (2005). Vegetation patterns in permanent spring wetlands in arid Australia. *Australian Journal of Botany, 52*, 719-728

Feyisa, G.L., Meilby, H., Fensholt, R., & Proud, S.R. (2014). Automated Water Extraction Index: A new technique for surface water mapping using Landsat imagery. *Remote Sensing of Environment, 140*, 23-35

Finlayson, B., & McMahon, T. (1988). Australia vs the world: a comparative analysis of streamflow characteristics. In: *Fluvial geomorphology of Australia (Ed.R.F.Warner)*, pp.17-40. Academic Press, Sydney.

Finlayson, M., Cruz, R., Davidson, N., Alder, J., Cork, S., de Groot, R., Lévêque, C., Milton, G., Peterson, G., & Pritchard, D. (2005). Ecosystems and Human Well-being: Wetlands and Water Synthesis. *Millennium Ecosystem Assessment Report*,World Resources Institute, Washington, DC

Fischer, E., Beyerle, U., & Knutti, R. (2013). Robust spatially aggregated projections of climate extremes. *Nature Climate Change,3*, 1033-1038

Frazier, P., Page, K., Louis, J., Briggs, S., & Robertson, A. (2003). Relating wetland inundation to river flow using Landsat TM data. *International Journal of Remote Sensing, 24*, 3755-3770

Frazier, P.S., & Page, K.J. (2000). Water body detection and delineation with Landsat TM data. *Photogrammetric Engineering and Remote Sensing, 66*, 1461-1468

Gent, P.R., Danabasoglu, G., Donner, L.J., Holland, M.M., Hunke, E.C., Jayne, S.R., Lawrence, D.M., Neale, R.B., Rasch, P.J., & Vertenstein, M. (2011). The community climate system model version 4. *Journal of Climate, 24*, 4973-4991

Gibbs, L.M. (2006). Valuing water: variability and the Lake Eyre Basin, central Australia. *Australian Geographer, 37*, 73-85

Guan, K., Pan, M., Li, H., Wolf, A., Wu, J., Medvigy, D., Caylor, K.K., Sheffield, J., Wood, E.F., & Malhi, Y. (2015). Photosynthetic seasonality of global tropical forests constrained by hydroclimate. *Nature Geoscience, 8*, 284-289

Hendon, H.H., Lim, E.-P., Arblaster, J.M., & Anderson, D.L. (2014). Causes and predictability of the record wet east Australian spring 2010. *Climate Dynamics, 42*, 1155-1174

Hulme, P.E. (2005). Adapting to climate change: is there scope for ecological management in the face of a global threat? *Journal of Applied Ecology, 42*, 784-794

Hwang, T., Song, C., Bolstad, P.V., & Band, L.E. (2011). Downscaling real-time vegetation dynamics by fusing multi-temporal MODIS and Landsat NDVI in topographically complex terrain. *Remote Sensing of Environment, 115*, 2499-2512

IPCC (2014). Climate change 2014: impacts, adaptation, and vulnerability. Contribution of Working Group II to the Fifth Assessment Report of the Intergovernmental Panel on Climate Change

Jarihani, A.A., Callow, J.N., Johansen, K., & Gouweleeuw, B. (2013). Evaluation of multiple satellite altimetry data for studying inland water bodies and river floods. *Journal of Hydrology, 505*, 78-90

Jarihani, A.A., Callow, J.N., McVicar, T.R., Van Niel, T.G., & Larsen, J.R. (2015a). Satellite-derived Digital Elevation Model (DEM) selection, preparation and correction for hydrodynamic modelling in large, low-gradient and data-sparse catchments. *Journal of Hydrology, 524*, 489-506

Jarihani, A.A., Larsen, J.R., Callow, J.N., McVicar, T.R., & Johansen, K. (2015b). Where does all the water go? Partitioning water transmission losses in a data-sparse, multi-channel and low-gradient dryland river system using modelling and remote sensing. *Journal of Hydrology, 529*, 1511-1529

Jarihani, A.A., McVicar, T.R., Van Niel, T.G., Emelyanova, I.V., Callow, J.N., & Johansen, K. (2014). Blending Landsat and MODIS data to generate multispectral indices: A comparison of "Index-then-Blend" and "Blend-then-Index" approaches. *Remote Sensing, 6*, 9213-9238

Jarvis, A., Reuter, H.I., Nelson, A., Guevara, E., 2008. Hole-filled seamless SRTM data V4. International Centre for Tropical Agriculture (CIAT). Available from the CGIAR-CSI SRTM 90 m Database, <http://srtm.csi.cgiar.org>

Jenkins, K.M., Boulton, A.J., & Ryder, D.S. (2005). A common parched future? Research and management of Australian arid-zone floodplain wetlands. *Hydrobiologia, 552*, 57-73

Johnson, W.C., Millett, B.V., Gilmanov, T., Voldseth, R.A., Guntenspergen, G.R., & Naugle, D.E. (2005). Vulnerability of northern prairie wetlands to climate change. *BioScience, 55*, 863-872

Jones, D.A., Wang, W., & Fawcett, R. (2009). High-quality spatial climate data-sets for Australia. *Australian Meteorological and Oceanographic Journal, 58*, 233

Jones, J.W. (2015). Efficient wetland surface water detection and monitoring via Landsat: Comparison with in situ data from the Everglades Depth Estimation Network. *Remote Sensing, 7*, 12503-12538

Jones, J.W., & Price, S.D. (2007). Conceptual design of the Everglades Depth Estimation Network (EDEN) grid. US Geological Survey: Reston, VA, USA, 2007

Kandus, P., & Malvárez, A.I. (2004). Vegetation patterns and change analysis in the lower delta islands of the Paraná River (Argentina). *Wetlands, 24*, 620-632

Karim, F., Petheram, C., Marvanek, S., Ticehurst, C., Wallace, J., & Gouweleeuw, B. (2011). The use of hydrodynamic modelling and remote sensing to estimate floodplain inundation and flood discharge in a large tropical catchment. In:Proceedings of MODSIM2011: The 19th International Congress on Modelling and Simulation, Perth, Australia

Kingsford, R.T. (2000). Ecological impacts of dams, water diversions and river management on floodplain wetlands in Australia. *Austral Ecology, 25*, 109-127

Klemas, V. (2011). Remote sensing of wetlands: case studies comparing practical techniques. *Journal of Coastal Research, 27*, 418-427

Knighton, A.D., & Nanson, G.C. (1994). Flow transmission along an arid zone anastomosing river, Cooper Creek, Australia. *Hydrological Processes, 8*, 137-154

Knighton, A.D., & Nanson, G.C. (2001). An event-based approach to the hydrology of arid zone rivers in the Channel Country of Australia. *Journal of Hydrology, 254*, 102-123

Kotwicki, V. (1986). Floods of Lake Eyre. Engineering and Water Supply Department, Adelaide, South Australia

Kotwicki, V., & Allan, R. (1998). La Nina de Australia-contemporary and palaeo-hydrology of Lake Eyre. *Palaeogeography, Palaeoclimatology, Palaeoecology, 144*, 265-280

Landerer, F., & Swenson, S. (2012). Accuracy of scaled GRACE terrestrial water storage estimates. *Water Resources Research, 48*, W04531

Lawley, E.F., Lewis, M.M., & Ostendorf, B. (2016). A remote sensing spatio-temporal framework for interpreting sparse indicators in highly variable arid landscapes. *Ecological Indicators, 60*, 1284-1297

Leigh, C., Sheldon, F., Kingsford, R.T., & Arthington, A.H. (2010). Sequential floods drive'booms' and wetland persistence in dryland rivers: a synthesis. *Marine and Freshwater Research, 61*, 896-908

Long, D., Longuevergne, L., & Scanlon, B.R. (2015a). Global analysis of approaches for deriving total water storage changes from GRACE satellites. *Water Resources Research, 51*, 2574-2594

Long, D., Yang, Y., Wada, Y., Hong, Y., Liang, W., Chen, Y., Yong, B., Hou, A., Wei, J., & Chen, L. (2015b). Deriving scaling factors using a global hydrological model to restore GRACE total water storage changes for China's Yangtze River Basin. *Remote Sensing of Environment, 168*, 177-193

Ma, X., Huete, A., Moran, S., Ponce-Campos, G., & Eamus, D. (2015). Abrupt shifts in phenology and vegetation productivity under climate extremes. *Journal of Geophysical Research: Biogeosciences, 120*, 2036-2052

McMahon, T., B. Finlayson, A. Haines, and R. Srikanthan (1992), Global Runoff: Continental Comparisons of Annual Flows and Peak Discharges, Catena Verlag, Cremlingen-Dested, West GermanyMcVicar, T.R., Roderick, M.L., Donohue, R.J., Li, L.T., Van Niel, T.G., Thomas, A., Grieser, J., Jhajharia, D., Himri, Y., & Mahowald, N.M. (2012). Global review and synthesis of trends in observed terrestrial near-surface wind speeds: Implications for evaporation. *Journal of Hydrology, 416*, 182-205

Moiwo, J.P., Lu, W., Zhao, Y., Yang, Y., & Yang, Y. (2010). Impact of land use on distributed hydrological processes in the semi-arid wetland ecosystem of Western Jilin. *Hydrological processes, 24*, 492-503

Moran, M.S., Ponce-Campos, G.E., Huete, A., McClaran, M.P., Zhang, Y., Hamerlynck, E.P., Augustine, D.J., Gunter, S.A., Kitchen, S.G., & Peters, D.P. (2014). Functional response of US grasslands to the early 21st-century drought. *Ecology, 95*, 2121-2133

Myneni, R., & Williams, D. (1994). On the relationship between FAPAR and NDVI. *Remote Sensing of Environment, 49*, 200-211

Oke, A., Frost, A., & Beesley, C. (2009). The use of TRMM satellite data as a predictor in the spatial interpolation of daily precipitation over Australia. In: Proceedings of the 18th World IMACS/MODSIM Congress

Peña-Arancibia, J.L., van Dijk, A.I., Renzullo, L.J., & Mulligan, M. (2013). Evaluation of precipitation estimation accuracy in reanalyses, satellite products, and an ensemble method for regions in Australia and South and East Asia. *Journal of Hydrometeorology, 14*, 1323-1333

Penatti, N.C., de Almeida, T.I.R., Ferreira, L.G., Arantes, A.E., & Coe, M.T. (2015). Satellite-based hydrological dynamics of the world's largest continuous wetland. *Remote Sensing of Environment, 170*, 1-13

Petus, C., Lewis, M., & White, D. (2013). Monitoring temporal dynamics of Great Artesian Basin wetland vegetation, Australia, using MODIS NDVI. *Ecological Indicators, 34*, 41-52

Pittock, J., Finlayson, M., Gardner, A., & McKay, C. (2010). Changing character: the Ramsar Convention on Wetlands and climate change in the Murray-Darling Basin, Australia. *Environmental and Planning Law Journal, 24*, 401-425

Ponce Campos, G.E., Moran, M.S., Huete, A., Zhang, Y., Bresloff, C., Huxman, T.E., Eamus, D., Bosch, D.D., Buda, A.R., & Gunter, S.A. (2013). Ecosystem resilience despite large-scale altered hydroclimatic conditions. *Nature, 494*, 349-352

Puckridge, J., Walker, K., & Costelloe, J. (2000). Hydrological persistence and the ecology of dryland rivers. *Regulated Rivers: Research & Management, 16*, 385-402

Puckridge, J.T. (1998). Wetland management in arid Australia. The Lake Eyre Basin as an example. In: Williams, W.D. (Ed.), Wetlands in a Dry Land: Understanding for Management. Environment Australia, Canberra, pp. 85–96.

Puckridge, J.T., Costelloe, J.F., & Reid, J.R.W. (2010). Ecological responses to variable water regimes in arid-zone wetlands: Coongie Lakes, Australia. *Marine and Freshwater Research, 61*, 832-841

Raja Segaran, R., Clarke, K., White, D., & Lewis, M. (2015). Spatial Indicators of Ecological Condition for Lake Eyre Basin. In: Report for Goyder Institute for Water Research <https://www.researchgate.net/profile/Kenneth_Clarke2/publications>

Reager, J., & Famiglietti, J. (2009). Global terrestrial water storage capacity and flood potential using GRACE. *Geophysical Research Letters, 36*, L23402

Reid, J., Gillen, J., Pty, A.G., & Australia, S. (1988). The Coongie Lakes Study. Department of Environment and Planning, Adelaide

Reid, J.R.W. and Puckridge, J.T. (2000). The Seasonal Ecology of the Coongie Lakes System and Cooper Creek Floodplain, Central Australia. A report to the South Australian Department of Environment and Heritage and the Australian Heritage Commission undertaken with assistance from the National Estates Grants Program. Arid Lands Environment Centre, Alice Springs

Renzullo, L., Chappell, A., Raupach, T., Dyce, P., Ming, L., & Shao, Q. (2011). An assessment of statistically blended satellite-gauge precipitation data for daily rainfall analysis in Australia. In: Proceedings of the 34th International Symposium on Remote Sensing of Environment (ISRSE)

Rodell, M., Famiglietti, J., Chen, J., Seneviratne, S., Viterbo, P., Holl, S., & Wilson, C. (2004). Basin scale estimates of evapotranspiration using GRACE and other observations. *Geophysical Research Letters, 31*, L20504

Rodell, M., Velicogna, I., & Famiglietti, J.S. (2009). Satellite-based estimates of groundwater depletion in India. *Nature, 460*, 999-1002

Roshier, D., Whetton, P., Allan, R., & Robertson, A. (2001). Distribution and persistence of temporary wetland habitats in arid Australia in relation to climate. *Austral Ecology, 26*, 371-384

Rouse, J.W., Haas, R.H., Scheel, J.A., & Deering, D.W. (1974). Monitoring Vegetation Systems in the Great Plains with ERTS. *Proceedings, 3rd Earth Resource Technology Satellite (ERTS) Symposium, 1*, 48-62.

Schumann, G., Hostache, R., Puech, C., Hoffmann, L., Matgen, P., Pappenberger, F., & Pfister, L. (2007). High-resolution 3-D flood information from radar imagery for flood hazard management. *IEEE Transactions on Geoscience and Remote Sensing, 45*, 1715-1725

Sheffield, J., Wood, E.F., & Roderick, M.L. (2012). Little change in global drought over the past 60 years. *Nature, 491*, 435-438

Sheldon, F., Bunn, S.E., Hughes, J.M., Arthington, A.H., Balcombe, S.R., & Fellows, C.S. (2010). Ecological roles and threats to aquatic refugia in arid landscapes: dryland river waterholes. *Marine and Freshwater Research, 61*, 885-895

Simpson, J., Kummerow, C., Tao, W.-K., & Adler, R.F. (1996). On the tropical rainfall measuring mission (TRMM). *Meteorology and Atmospheric physics, 60*, 19-36

Sun, F., Sun, W., Chen, J., & Gong, P. (2012). Comparison and improvement of methods for identifying waterbodies in remotely sensed imagery. *International journal of remote sensing, 33*, 6854-6875

Tapley, B.D., Bettadpur, S., Ries, J.C., Thompson, P.F., & Watkins, M.M. (2004). GRACE measurements of mass variability in the Earth system. *Science, 305*, 503-505

Thomas, R.F., Kingsford, R.T., Lu, Y., Cox, S.J., Sims, N.C., & Hunter, S.J. (2015). Mapping inundation in the heterogeneous floodplain wetlands of the Macquarie Marshes, using Landsat Thematic Mapper. *Journal of Hydrology, 524*, 194-213

Timms, B.V. (2001). Large freshwater lakes in arid Australia: A review of their limnology and threats to their future. *Lakes & Reservoirs: Research & Management, 6*, 183-196

Tooth, S. (2000). Process, form and change in dryland rivers: a review of recent research. *Earth-Science Reviews, 51*, 67-107

Tooth, S., McCarthy, T., Brandt, D., Hancox, P., & Morris, R. (2002). Geological controls on the formation of alluvial meanders and floodplain wetlands: the example of the Klip River, eastern Free State, South Africa. *Earth Surface Processes and Landforms, 27*, 797-815

Tooth, S., & McCarthy, T.S. (2007). Wetlands in drylands: geomorphological and sedimentological characteristics, with emphasis on examples from southern Africa. *Progress in Physical Geography, 31*, 3-41

Tooth, S., & Nanson, G.C. (1999). Anabranching rivers on the Northern Plains of arid central Australia. *Geomorphology, 29*, 211-233

Tregoning, P., McClusky, S., van Dijk, A., Crosbie, R., & Peña-Arancibia, J. (2012). Assessment of GRACE satellites for ground-water estimation in Australia. *National Water Commission*, Can-berra, 82, available at:archive.nwc.gov.au/library/waterlines/71

Tulbure, M.G., Broich, M., Stehman, S.V., & Kommareddy, A. (2016). Surface water extent dynamics from three decades of seasonally continuous Landsat time series at subcontinental scale in a semi-arid region. *Remote Sensing of Environment, 178*, 142-157

Van Dijk, A.I., Beck, H.E., Crosbie, R.S., Jeu, R.A., Liu, Y.Y., Podger, G.M., Timbal, B., & Viney, N.R. (2013). The Millennium Drought in southeast Australia (2001–2009): Natural and human causes and implications for water resources, ecosystems, economy, and society. *Water Resources Research, 49*, 1040-1057

Vervuren, P., Blom, C., & De Kroon, H. (2003). Extreme flooding events on the Rhine and the survival and distribution of riparian plant species. *Journal of Ecology, 91*, 135-146

Wahr, J., Swenson, S., & Velicogna, I. (2006). Accuracy of GRACE mass estimates. *Geophysical Research Letters, 33*, L06401

Walker, K.F., Puckridge, J., & Blanch, S.J. (1997). Irrigation development on Cooper Creek, central Australia- prospects for a regulated economy in a boom-and-bust ecology. *Aquatic Conservation: Marine and Freshwater Ecosystems, 7*, 63-73

Walker, K. F., Sheldon, F. and Puckridge, J. T. (1995). A perspective on dryland river ecosystems. *Regulated Rivers: Research and Management, 11*, 85-104.

White, D.C., & Lewis, M.M. (2011). A new approach to monitoring spatial distribution and dynamics of wetlands and associated flows of Australian Great Artesian Basin springs using QuickBird satellite imagery. *Journal of Hydrology, 408*, 140-152

White, D.C., Lewis, M.M., Green, G., & Gotch, T.B. (2016). A generalizable NDVI-based wetland delineation indicator for remote monitoring of groundwater flows in the Australian Great Artesian Basin. *Ecological Indicators, 60*, 1309-1320

Williams, W.D. (1999). Conservation of wetlands in drylands: a key global issue. *Aquatic Conservation: Marine and Freshwater Ecosystems, 9*, 517-522

Woodward, C., Shulmeister, J., Larsen, J., Jacobsen, G., & Zawadzki, A. (2014). The hydrological legacy of deforestation on global wetlands. *Science, 346*, 844-847

Xie, Z., Huete, A., Restrepo-Coupe, N., Ma, X., Devadas, R., & Caprarelli, G. (2016). Spatial partitioning and temporal evolution of Australia's total water storage under extreme hydroclimatic impacts. *Remote Sensing of Environment, 183*, 43-52

Xu, H. (2006). Modification of normalised difference water index (NDWI) to enhance open water features in remotely sensed imagery. *International Journal of Remote Sensing, 27*, 3025-3033

Yang, Y., Long, D., Guan, H., Scanlon, B.R., Simmons, C.T., Jiang, L., & Xu, X. (2014). GRACE satellite observed hydrological controls on interannual and seasonal variability in surface greenness over mainland Australia. Journal of Geophysical Research: *Biogeosciences, 119*, 2245-2260

Yin, D., Roderick, M.L., Leech, G., Sun, F., & Huang, Y. (2014). The contribution of reduction in evaporative cooling to higher surface air temperatures during drought. *Geophysical Research Letters, 41*, 7891-7897

Yu, L., García, A., Chivas, A.R., Tibby, J., Kobayashi, T., & Haynes, D. (2015). Ecological change in fragile floodplain wetland ecosystems, natural vs human influence: The Macquarie Marshes of eastern Australia. *Aquatic Botany, 120*, 39-50

Zhang, F., Zhang, B., Li, J., Shen, Q., Wu, Y., & Song, Y. (2011). Comparative analysis of automatic water identification method based on multispectral remote sensing. *Procedia Environmental Sciences, 11*, 1482-1487

Zhu, Z., Wang, S., & Woodcock, C.E. (2015). Improvement and expansion of the Fmask algorithm: cloud, cloud shadow, and snow detection for Landsats 4–7, 8, and Sentinel 2 images. *Remote Sensing of Environment, 159*, 269-277

Zhu, Z., & Woodcock, C.E. (2012). Object-based cloud and cloud shadow detection in Landsat imagery. *Remote Sensing of Environment, 118*, 83-94

Chapter 5: Impacts of the dry and wet hydroclimatic events on water resources and ecosystem functioning across Australia

This chapter is a compilation of studies undertaken during the course of my PhD research rather than an integrative journal style chapter as in the previous chapters. The inclusion of this chapter is aimed to provide an unique way to describe the results of multiple small and interesting experiments that yielded ideas for future ecohydrological proposals, analyses and validation.

Abstract

Australia has already experienced multiple large-scale dry and wet hydroclimatic extremes in this century. These extremes have been exerting pronounced ecohydrological stress across the continent and are expected to continue in the future. The aim of this chapter is to conduct a compilation of studies on ecohydrological impacts of the recent hydroclimatic events for improved management and protection of water resources and ecosystems in Australia. Based on a combination of multi-sensor satellite observations, modelling and ground truth data, we used remote sensing and statistical methods to investigate spatial-temporal responses, dynamics, trends and interactions of ecohydrology on continental, regional and biome scales under extreme hydroclimatic impacts.

Our results revealed variable drying and wetting patterns in different water resources across Australia which, in turn, resulted in the changes in the ecosystems. We found a significant increase in continental ET during the 'big dry', which may partly explain the disparity between the continental decreasing TWS and increasing rainfall during the same period. We also observed that soil moisture across Australia largely drives the seasonal variations in TWS while groundwater contributes to its long-term trends. TWS is generally driven by rainfall but can detect drought better especially "hidden drought" such as groundwater depletion. Moreover, TWS has overall better, spatially more uniform and temporally more direct correlations with surface greenness than rainfall across Australia. GRACE-TWSA thus can be used as a valuable indicator for ecohydrological system performances particularly under extreme hydroclimatic events. This study will provide scientific guidance for conservation strategies and management of Australian water and ecosystem resources to secure their sustainability through future climatic changes.

5.1 Introduction

Around the world, pressures on water resources as well as their dependent ecosystems are increasing, mostly as a result of human activities such as population expansion, urbanisation, increased industrialisation, growing demands for water, pollution and so on (UN WWAP 2003; Vörösmarty et al. 2000). Meanwhile, these are being aggravated by recent climate change. In particular, the intensifying water cycle

due to global warming, characterized by dry seasons and locations getting drier and wet areas and periods becoming wetter, results in reduced available water resources and a decline in critical ecosystems (Chou et al. 2013; Chou and Lan 2012; Chou et al. 2009; Xie et al. 2016c). Therefore, integrated, scalable and system-level monitoring and management of water resources and surrounding ecosystems are needed more than ever to maintain their sustainability in the face of human development and a changing climate (Harris et al. 2006; Pahl-Wostl 2007).

Remote Sensing (RS), with mutiple earth observation satellites, has provided one of the most important tools in analysing the land surface dynamics and characteristics over long-term periods and on broad spatial scales. It thus offers comprehensive information on ecohydrological dynamics and processes (Kumar and Reshmidevi 2013; Pietroniro and Prowse 2002). By contrast, traditional methods applied in hydrological and ecological studies such as ground observations and modelling are hampered by a lack of gauge stations and detailed information about the physical and ecohydrological parameters of study sites over large regions (Su 2000). Satellite-based RS methods have been widely used to measure the quantity or quality of water resources and ecosystems, detect the spatial-temporal variations in the hydro-meteorological characteristics and evaluate the corresponding ecological responses etc. This leads to a significant improvement in both hydrological and ecological research which, in return, supports the operational water resources and ecosystems community for management practices and decisions (Jong et al. 2008; Kerr and Ostrovsky 2003; Schmugge et al. 2002).

As climate change is predicted to markedly alter current hydroclimatic conditions later this century (Ponce-Campos et al. 2013; Yang et al. 2014), it is essential to monitor the water resources, as represented by various hydrological factors such as rainfall, soil moisture, groundwater, ET, runoff etc, for a better understanding of hydrological conditions and associated ecosystem performance. This is particularly important for Australia, which consists of a vast continent with most parts of its mainland being desert or semi-arid areas. Ecosystems in Australia are generally water-limited in various climate zones across the continent (Pickett-Heaps et al. 2014).

Australia has already experienced three hydroclimatic events in this century, including a prolonged drought commonly known as the 'Millennium Drought' (or 'big dry') from 2001 to 2009, followed by an intensive wet pulse during 2010 and 2011

termed the 'big wet'. These dry and wet extreme events exerted pronounced negative impacts on food production, water resources, natural ecosystems and agriculture, with increased forest die-back, bushfires and flooding over large areas. In facing such high climate variability and increasing hydroclimatic events, scientists have been asking themselves what would happen to the mostly water-limited ecosystems across Australia? By using 14 years of satellite observations, a recent study of ecological resilience showed eastern Australia's dry woodlands and semi-arid grasslands are among ecosystems that are the most sensitive to extreme climatic events (Seddon et al. 2016). The authors also observed that vegetation in central Australia's desert and arid lands exhibited slow responses to climate variability, which may indicate these ecosystems have strong adaptations to prevent boom and bust. Crops in Australia, as agricultural ecosystems, are found to be highly sensitive to changes in climate too. This means it is difficult and challenging to manage sustainable livestock and crop production in the face of hydroclimatic extremes, especially under Australia's intensifying conditions of abrupt dry and wet periods (Huete and Ma 2016). Ecosystems, if forced to cross a critical threshold will be transformed into new states, often with losses in biodiversity, exotic species invasions, and sudden forest die-off events (Allen et al. 2010; Ponce Campos et al. 2013; Walker et al. 2004). As a consequence, it is important to monitor the temporal dynamics and spatial patterns in water resources and associated ecosystems, and assess their interactions across Australia under these dry and wet hydroclimatic extremes.

In this chapter, our main aim is to conduct a compilation of multiple small experiments on hydrological dynamics, the associated changes in ecosystems and their interactions during the 'big dry' and 'big wet' events. This study was based on multi-sensor satellite data of various spatial resolutions and physical properties (surface reflectance, microwave and gravitational anomaly), integrating with modelling datasets and field observations from 2002 to 2014. We focussed on multi assessments on the effects that hydroclimatic extremes brought to Australian water resources and ecosystems for future improved ecohydrological management and protection across space and time. Essentially, we aimed to: (1) confirm the spatial intensification of Australian water storage observed in Chapter 2 using various geostatistics methods; (2) investigate the spatio-temporal patterins of rainfall during the study period and its relationship with TWS; (3) estimate ET, groundwater variations from GRACE-TWSA

time series data; (4) monitor the drying and wetting patterns of various water resources; and (5) evaluate the ecological responses to hydrological variations at continental, regional and biome scales.

5.2 Data and Methods

5.2.1 Data

a. Hydrological datasets

1) AWAP hydro-meteorological data

The Australian Water Availability Project (AWAP) is a joint effort by The Commonwealth Scientific and Industrial Research Organisation (CSIRO), Marine and Atmospheric Research (CMAR), the Bureau of Meteorology (BOM) and the Bureau of Rural Science (BRS). This project is aimed at monitoring the dynamics of Australian terrestrial water balance, using model-data fusion methods to combine both modelling and field observations (Raupach et al. 2009). The AWAP project provides the past history and present state of all water fluxes contributing to changes in soil moisture (rainfall, soil evaporation, transpiration, surface runoff and deep drainage, etc) across the whole continent at a spatial resolution of 5 km, in three forms: 1) weekly/monthly near-real-time measurements, 2) monthly/annual historical time series since 1900, and 3) monthly climatologies. The goal of AWAP is to achieve long-term monitoring and improve our understanding of the dynamics and trends of Australian hydrological systems, particularly their responses to climate variability and change, and thus to assist adaptive, system-wide management.

In this chapter, we utilized two AWAP datasets – Total Evapotranspiration (Soil + Vegetation) and Surface Runoff with resolutions of 5 km and monthly, respectively. They were produced by the WaterDyn model (Raupach et al. 2012), on which the key inputs and constraints are the meteorology (precipitation, solar radiation, minimum and maximum daily temperatures) and continental parameter maps (e.g. soil characteristics, albedo, seasonality of vegetation greenness). The meteorological fields were generated by the BOM, which provided both daily products (near-real time) and reprocessed products (including quality control and incorporating data that arrived too late for

inclusion in the near-real time product). By integrating AWAP ET and Runoff products with GRACE- TWSA and rainfall, we were able to monitor the dynamics of the terrestrial water balance across Australia during the recent hydroclimatic events.

2) GLDAS soil moisture data

The Global Land Data Assimilation System (GLDAS) was developed jointly by Goddard Space Flight Centre (GSFC) in NASA and National Centers for Environmental Prediction (NCEP) in NOAA, with purpose of producing optimal fields of global land surface states and fluxes in various time resolutions (Rodell et al. 2002). Parallelized and streamlined by the sister project - the Land Information System (LIS), the GLDAS drives multiple, offline land surface models (the Noah, CLM, VIC, and Mosaic land surface models etc) that integrate both satellite data and a huge amount of field observations to simulate a comprehensive archive of modelled and observed surface meteorological data and parameter maps with 0.25 to 1 degree resolutions from 1979 to date (Rodell et al. 2004d).

As reliable and high resolution measured soil moisture over a large area is limited, in this chapter we used a GLDAS soil moisture product derived from the Noah Model in order to extract changes in groundwater from the GRACE observed total water storage anomalies. There are four layers in the soil moisture data (2 metres deepest), with resolutions of 1° and monthly, respectively. (Berg et al. 2003; Kumar et al. 2006).

b. Ecological datasets

1) Fraction of Photosynthetically Active Radiation (fPAR)

The Fraction of Photosynthetically Active Radiation (fPAR) data, produced by the CSIRO Land and Water, describes the Australia-wide monthly fraction of Photosynthetically Active Radiation absorbed by vegetation. They were derived from Advance Very High Resolution Radiometer data, spanning from July 1981 to Oct 2011. fPAR is linearly related to fractional foliage cover and split into those of persistent vegetation and of recurrent vegetation, which represents non-deciduous perennial vegetation and annual, ephemeral and deciduous vegetation, respectively. Data were processed using the invariant-cover-triangle method (Donohue et al. 2009) to remove

the majority of errors introduced by sensor calibration and change-over effects. fPAR products have been in the form of monthly grids of a 0.08 degree cell size from July 1981 and of 0.01 degree from Feb 1995, and are suited to the analysis of long-term dynamics (trends) in vegetation cover (Donohue et al. 2008).

In this chapter, we used fPAR Version4 data of 0.01 degree monthly to monitor the changes in trees and grasses during the 'big dry' and 'big wet' events, and evaluate their relationships with variations in hydrological factors such as groundwater, soil moisture and so on.

2) Land cover map of Australia

In this chapter, we used the Dynamic Land Cover Dataset (DLCD) from Geoscience Australia and Bureau of Agricultural and Resource Economics and Sciences as the reference of the land cover classifications over Australia (http://www.ga.gov.au/scientific-topics/earth-obs/landcover) (Lymburner et al. 2011).

The DLCD was developed from an analysis of a 16-day EVI composite collected at 250 metres resolution using the Moderate Resolution Imaging Spectroradiometer (MODIS) satellite for the period from 2000 to 2008 (Huete et al. 2002; Zhang and Foody 1998). This Australian land cover classification system is nationally consistent and thematically comprehensive and can be used to assess the land cover types of forests, woodlands, rangelands and cropping systems in Australia (Lymburner et al. 2011). The accuracy of this dataset has been validated through a comparison with more than 25,000 field sites and shows a high degree of consistency with field based information about land cover (Lymburner et al. 2011).

Other Data used in this chapter, including GRACE-TWSA, MODIS-EVI and TRMM-rainfall, were described in Chapters 1–3. Some data were further resampled to a 1° resolution in accordance with the GRACE data and the observations here extended from July 2002 to June 2014. We selected to work in hydrological years rather than calendar years (July to June in the following year instead of January to December in the same year), as it is most appropriate for a hydrological study in the Southern Hemisphere. To avoid ambiguities, we add "Hydro" in front of the hydrological years to differentiate it from the calendar years to describe the results.

5.2.2 Geostatistics methods

Geostatistics is a powerful tool to quantitatively study spatial structure of hydrology, which is a combination of the traditional earth science and statistical methods (Matheron 1963). Geostatistical analysis has been proven to be one of the most effective ways to study the spatial distributions and heterogeneity of various hydrological variables (Xiaoning et al. 2009). In this study, besides the traditional geostatistics methods such as the standard deviation, density curve and histogram, we also utilized the variogram and Moran's Index to study the characteristics of spatial variability of TWS across Australia during the 'big dry' and the 'big wet' periods.

Spatial heterogeneity of annual TWSA was analysed by variogram calculated from the variation analysis function (Fig.5.1 A). The nugget (C0) on the variogram shows the spatial heterogeneity of the random part, caused by a small sampling scale and experimental error. The sill (C + C0) stands for the degree of spatial heterogeneity, which shows how much variation there is overall in the data. The ratio C0/(C0+C) reflects the random variation size of the total variation. The higher it is, the greater the spatial heterogeneity extent arising from the spatial autocorrelation part (Xiaoning et al. 2009).

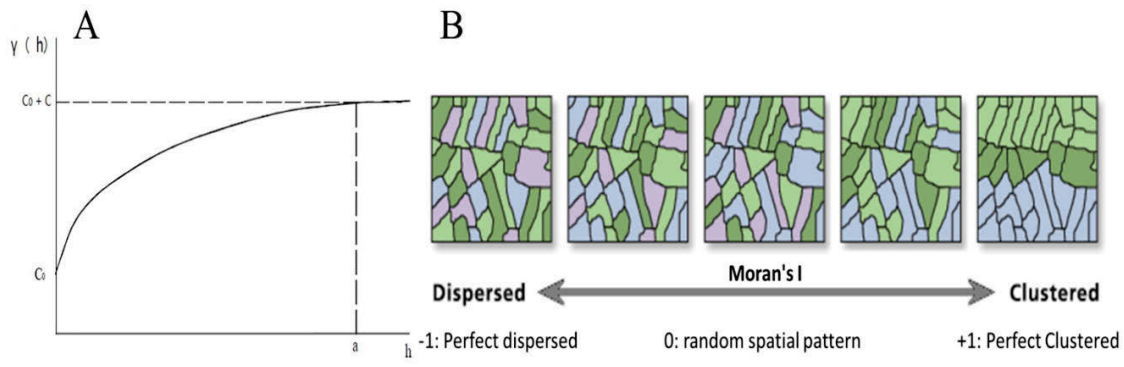

Figure 5.1. (A) Typical image of variogram and (B) Illustration of Moran's Index

Moran's Index (Moran's I) is a measure of spatial autocorrelation developed by Patrick Alfred Pierce Moran (Moran 1950). When the z-score or p-value indicates statistical significance, a positive Moran's I index value indicates tendency toward clustering while a negative Moran's I index value indicates tendency toward dispersion (Fig.5.1 B). Values range from -1 (indicating perfect dispersion) to +1 (perfect

correlation). We used Moran's I of annual cumulative TWS flux to measure the degree of TWS clustering across Australia through the study period. Data processing, statistical analysis and visualization in this chapter were conducted in R scientific computation environment (R Core Team 2015). Student's t-test was used to evaluate the confidence level of all analyses in this study (*p-value*).

5.2.3 Time series analysis of rainfall

One simple model was used in this chapter to separate 'dry' and 'wet' rainfall months in each year based on TRMM data, which helps in identifying the temporal-spatial rainfall patterns in Australia. The flow chart of the model is shown below:

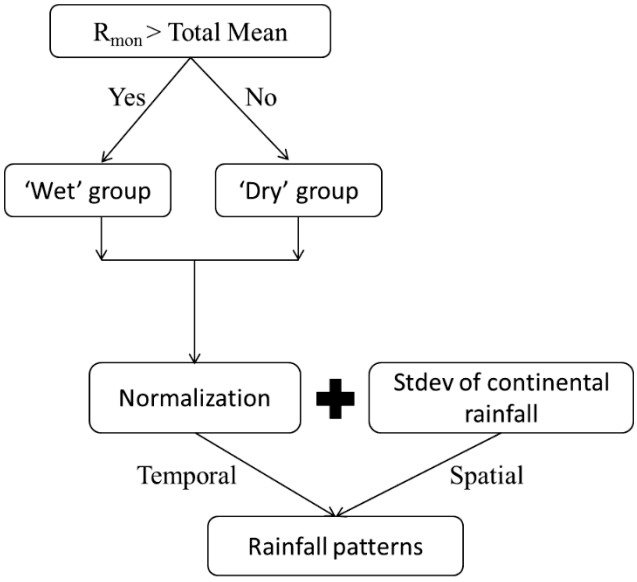

Figure 5.2. Flow chart for the separation model of 'dry' and 'wet' rainfall months

Bureau of Meteorology (BOM) rainfall data of over one century (1900 to 2013) was processed into annual anomalies to characterise the long-term change in rainfall patterns in Australia.

Here we also applied the same relevant methods described in Chapter 1-2 to deseasonalize rainfall and GRACE-TWSA data, produce their monthly time series, calculate the rainfall 'big dry' and 'big wet' trend maps and cross correlation map between rainfall and TWS.

5.2.4 Australian continental ET estimate based on the water balance equation

Empirical models based on satellite observations were widely used by previous studies to estimate large-scale ET over long time periods (Rodell et al. 2004a; Swenson and Wahr 2006; Szilagyi et al. 2001; Wan et al. 2015; Zeng et al. 2012). According to the water balance budget, ET can be expressed as the residual of total precipitation (P) minus net runoff (Q) and terrestrial total water storage change (ΔS), i.e. ET = P – Q – ΔS (Verstraeten et al. 2008). ΔS shows the variations in total water storage (TWS), which stands for the vertically integral water storage including soil moisture, groundwater, surface water, snow water and biological water (Rodell et al. 2004d; Yeh et al. 2006). ΔS is difficult to estimate at large scales and was mostly neglected in previous studies. However, recently the available GRACE derived TWSA data provides a great potential to reassess the estimation of ET by considering ΔS over large spatial scale based on the water balance approach (Rodell et al. 2004a; Swenson and Wahr 2006; Zeng et al. 2012).

In this study we assumed that across Australia, surface drainage divides coincide with groundwater flow divides, thus inputs and outputs of groundwater can be ignored. Accordingly, the monthly Australian continental ET can be computed at a pixel level as:

$$\Delta S = (TWSA(n) - TWSA(n\text{-}1)) \tag{5.1}$$

$$ET_{wb}(n) = P(n) - Q(n) - \Delta S \tag{5.2}$$

Where n is the month, and TWSA is the monthly Total Water Storage Anomaly for each pixel (cm/mon). P and Q are monthly precipitation (cm/mon) and runoff (cm/mon). The change in terrestrial water storage ΔS was estimated from GRACE-TWSA as the difference between one month observation and the previous observation.

Uncertainty in the ET derived from water balance approach was estimated as its relative error (Rodell et al. 2004a). Assuming that measurement errors of P, Q, and ΔS are independent and normally distributed about their true values,

$$\sigma^2_{\overline{ET}} = \sigma^2_{\overline{P}} + \sigma^2_{\overline{Q}} + \sigma^2_{\overline{\Delta S}} \tag{5.3}$$

where σ is the standard deviation; and

$$\sigma^2_{\overline{X}} = \frac{\mu_{\overline{X}}}{2} \tag{5.4}$$

where μ is the relative uncertainty in mean flux accumulation $\overline{X}$. Thus,

$$\mu_{\overline{ET}} = \frac{\sqrt{\mu^2_{\overline{P}} + \mu^2_{\overline{Q}} + \mu^2_{\overline{\Delta S}}}}{\overline{P} - \overline{Q} - \overline{\Delta S}} \tag{5.5}$$

Given $\mu_{\overline{ET}}$, the relative error for $\overline{ET}$, the 95% confidence limits on ET were computed as absolute error $\pm\overline{ET}$.

5.2.5 GRACE-based estimation of groundwater storage changes

GRACE-based Total Water storage Anomalies (TWSA) can be vertically divided into changes in Groundwater (GW), Soil Moisture (SM), Snow Water, Surface Water (SW) and Biological Water (BW). As more than 70% of Australian mainland is classified as arid and semi-arid, snow and biological water variations in Australia can generally be ignored, each of which only makes a modest (<10 mm) contribution to regional scale mass variations across Australia (Tregoning and McClusky 2011; Tregoning et al. 2012). Therefore, removing surface water, soil moisture and groundwater signals from the total water storage variations to evaluate the changes of groundwater is reasonably accurate and this method has been widely used in many previous studies for both Australia and other countries.

Given GRACE derived TWSA, GLDAS numerically modelled soil moisture anomalies (SMA) and AWAP modelled Runoff anomalies (QA), monthly groundwater storage variations (GWA) can be computed at per pixel level as:

GWA = TWSA - SMA – QA (5.6)

As the GLDAS SMA data used in the equation contains modelled soil moisture values to a depth of 2 meters below the ground, GWA here also includes the water storage change within the intermediate zone (the soil zone below 2 m and above the water table) (Yeh et al. 2006).

5.2.6 Trend Analysis

Using the temporal trend analysis method and the auto-defined 'big dry' timing map (based on TWSA) presented in Chapter-1, decadal time series change was assessed per-pixel in the monthly grids of Rainfall, ET, SMA and GWA, EVI to examine their geographic distributions of changing trends as well as Australian average trends. Based on the pixels of the stacked monthly images, the magnitude and significance of trends in the three variables were quantified by linear (ordinary least squares) regression and nonlinear seasonal regression (Xu et al. 2005). As both analyses gave similar results, only the trends from the linear regressions are presented here. As we determined the annual trends in the three variables for every terrestrial pixel with the units of cm/yr, the trends for Australia-wide and regional study areas were calculated as the spatial averages of these trend grids.

5.2.7 Spatio-temporal variability and correlation analysis

For the period of Hydro 2002 to 2012, mean values of monthly ecohydrological variables (EVI, TWSA, rainfall, SM, GW, ET, etc.) at both continental and regional scales were calculated and some monthly images were processed to show the spatio-temporal variability of vegetation and water across Australia or over regional sites. Multiple linear regressions of distinct temporal segments were assessed to show magnitude and significance of the trends in various variables during drying and wetting phases. The seasonality of each variable was computed as the monthly climatological mean from Hydro 2002 through 2012. Cross-correlation analysis was carried out to obtain the maximum Pearson's correlation coefficient (r) and the corresponding time lag in months among ecohydrological variables across the Australian continent. The time series of the variables were processed in different ways including 1) deseasonalizing and smoothing the time series using the 'Seasonal Decomposition of Time Series by LOESS' (STL) method (Cleveland et al. 1990); and 2) detrending the time series based on the method used in Wu et al. (2007).

5.3 Results

5.3.1 Spatial and temporal variations in water resources under hydroclimatic extremes

5.3.1.1 Geostatistics of water cycle intensification

Multiple geostatistics methods were applied to TWSA data in this section to characterise the spatial structure and dynamics of TWS across Australia during the dry and wet periods. Our geostatistics results show that the spatial heterogeneity of TWS was increasing during the 'big dry' and 'big wet' events and confirmed the short-term sign of water cycle intensification indicated in Chapter 2, with the dry areas in Australia getting drier while wet areas were becoming wetter.

a. Variations and convergence of TWSA in the three TWS zones

In Chapter 2, we partitioned the Australian continent into three TWS zones based on the distinct GRACE-TWSA clusters, which were formed from the TWS recovery rates during the 'big wet', relative to water losses during the 'big dry' (Fig.2.4). In this section, mean annual TWSA of the three zones was calculated to represent the regional TWS variations across the zones; in particular, to show the changes in TWS difference between the wet (Zone I) and dry (Zone III) contrasting areas (Fig.5.3A).

At the beginning of our study time (year of 2002), the TWSA in Zone III was positive and bigger than that in Zone I. This is in agreement with previous studies which showed a substantial increase in rainfall over northwest Australia before 2002 – start of GRACE data collection (Rotstayn et al. 2007; Shi et al. 2008). Thereafter, TWS decreased dramatically in dry areas while increasing in wet areas during the 'big dry' with TWSA of Zone I and Zone III intercepting in the Calendar year of 2007. The TWSA difference between dry and wet areas showed a sharp and consistent increase during the 'big dry' and this continued until the end of the 'big wet' (Fig.5.3B). During the 'big wet', even though the TWS increased in the dry areas as well, the increasing TWS difference was driven by the larger TWS gain in Zone I (Fig.5.3B). Zone II, which is located between Zone I and Zone III, behaved in an intermediate manner as this area did not dry as rapidly as zone III and easily recovered its water losses during the 'big wet' period but it gained less water than Zone I.

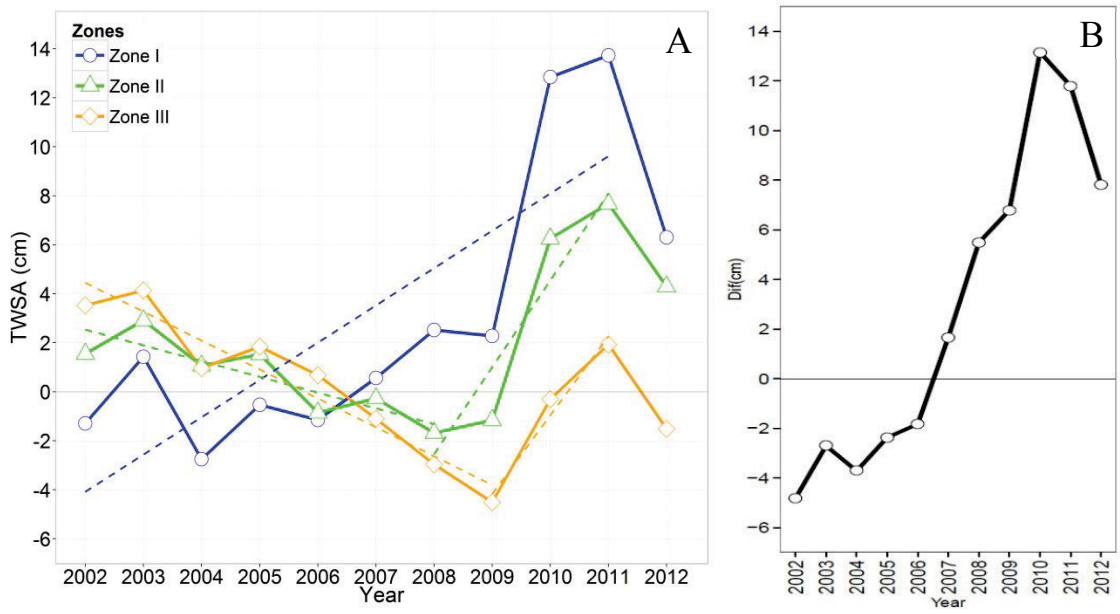

Figure 5.3. (A) Annual mean TWSA in the three TWS zones across Australia from Hydro 2002 to 2012 (p-value < 0.05); (B) Annual TWSA difference between wet (Zone I) and dry (Zone III) contrasting areas in Australia during Hydro 2002 and 2012.

We also drew two transects on the TWS change of rate map in Hydro 2002 to 2012 that cross three zones (Fig.5.4), with one going from southwest to northeast and the other heading from northwest to southeast. The two profiles on the margins represent the TWS trends on each pixel along the two transects. Figure 5.4 indicates a clear TWS gradient during the 'big dry' and 'big wet' across the three zones, with increasing TWS from southwestern (Zone III) to northeastern Australia (Zone I).

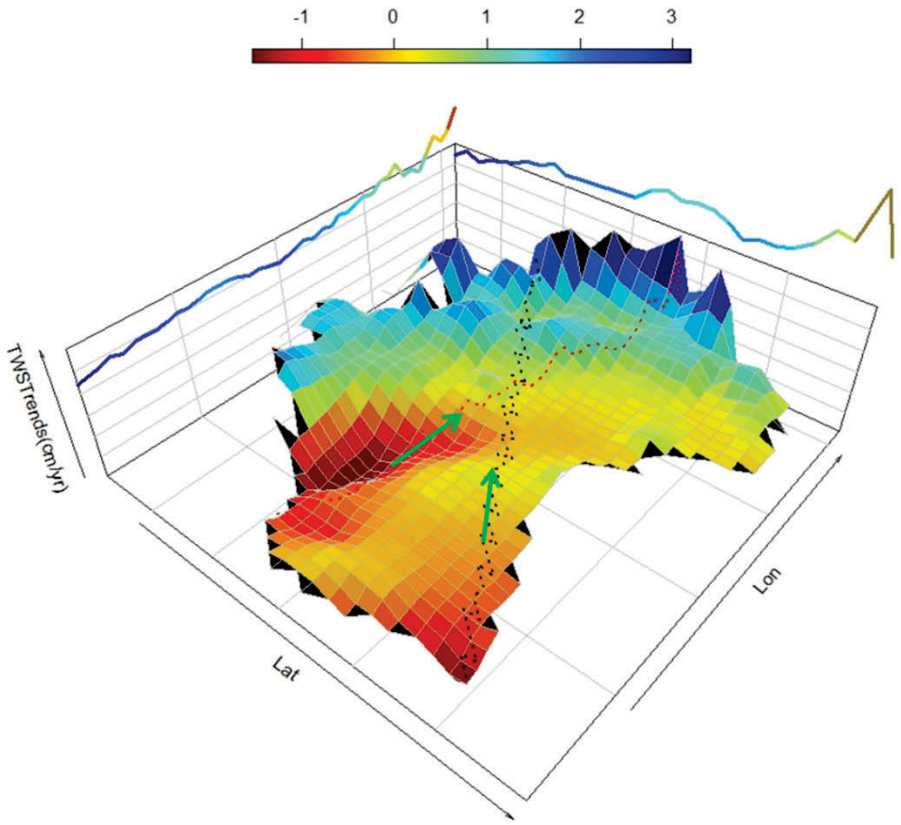

Figure 5.4. 3D plot of TWS trends from Hydro 2002 to 2012 with two transects.

b. Standard deviation changes of continental TWSA

Standard deviation (Stdev) of all TWSA pixels across Australia exhibited two distinct temporal segments (Fig.5.5), a sharp downward trend from 2002 to 2007 and a dramatic increasing trend from 2007 till the end of the 'big wet' (2011). The significant trends in Stdev indicate the general convergence of TWSA in Australia during the first segmental period and the fast dispersion of TWSA across the continent afterwards.

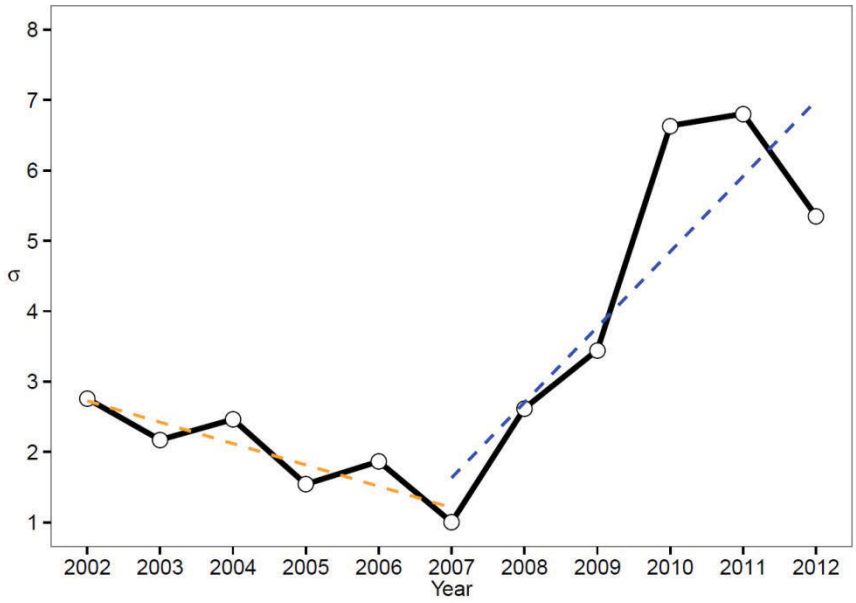

Figure 5.5. Changes in the standard deviation of annual TWSA across Australia from Hydro 2002 to 2012.

c. The TWS difference between the extreme dry and wet areas in Australia

Figure 5.6 shows the temporal changes in the distributions of annual TWSA density from Hydro 2002 to 2012. The peak density of TWSA in most of the years during the 'big dry' was smaller than 0 but moved right and became positive during the 'big wet', indicating the general water distribution patterns in Australia during the dry and wet periods (Fig.5.6). The subplot in the Figure 5.6 stands for the range of TWSA density in each year and it showed a Stdev-like pattern with TWSA density range decreasing from 2002 to 2007 while increasing sharply from 2007 to 2011. This corroborates the results from the Stdev analysis but from a density distribution point of view, it shows the TWS distribution imbalance among dry and wet areas might get more extreme during the 'big dry' and the 'big wet'. Thus, a further study focusing on 10% of the maximum and minimum TWSA pixels from the annual images was investigated to check the TWS difference evolution in the 'extreme' dry and wet areas in Australia.

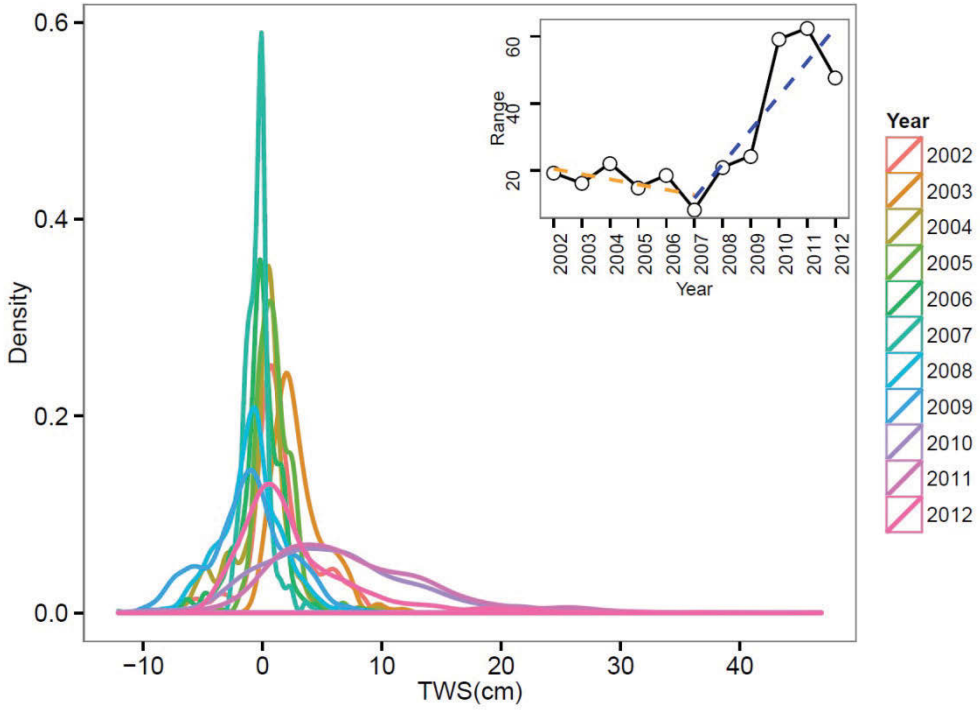

Figure 5.6. The density distribution plot of annual TWSA from Hydro 2002 to 2012; The subplot represents the density range changes among continental TWSA from Hydro 2002 to 2012 with piecewise trend lines (Range = $Density_{max}$ – $Density_{min}$).

The top and bottom 10% of TWSA pixels were chosen from each annual TWSA image, which vary from year to year, indicating the TWS changes in the 'extreme' dry and wet areas across the Australian continent over the study period. The density histograms of all TWSA pixels were plotted with the 10% pixels in shade (Fig.5.7A) and the TWSA difference between the mean values of 10% top and bottom TWSA got smaller at first and then became larger (Fig.5.7B). In addition, a ribbon graph of the dry and wet 10% pixels was plotted to show the TWSA changes in the 'extreme' dry and wet areas of Australia separately, relative to the total mean over the study time (Fig.5.7C). Hydro 2007 was the year when TWS in the 'extreme' dry and wet areas were the closest; thereafter, the grey shade areas became thicker and thicker through the time, indicating that the extreme dry regions of Australia became even drier, and vice versa.

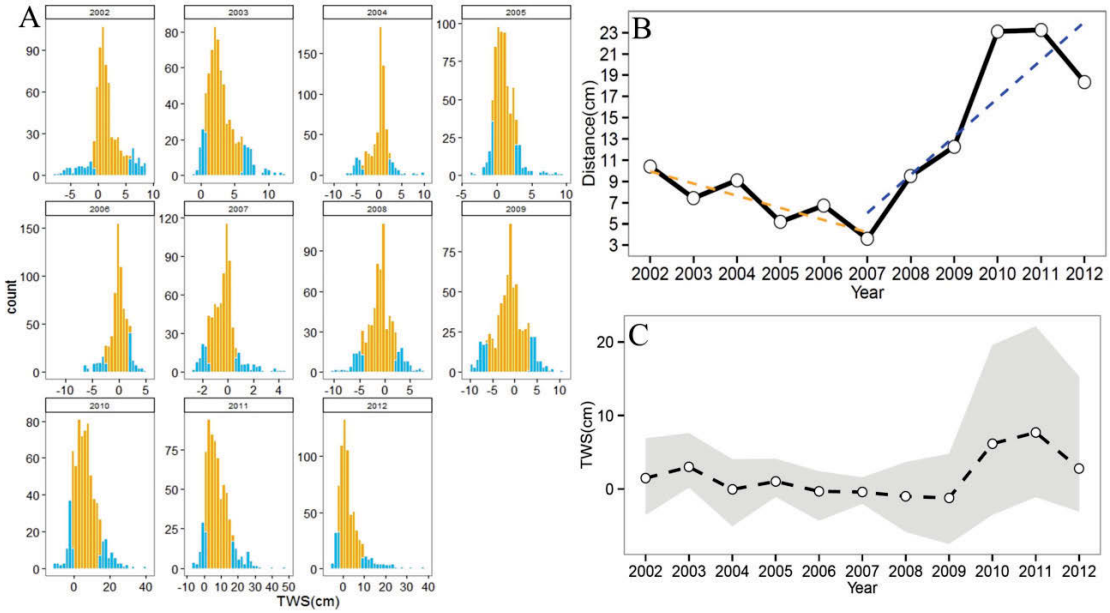

Figure 5.7. (A) Density histograms of all annual TWSA pixels with the max and min 10% pixels in shade; (B) Difference between the mean values of the max and min 10% TWSA; (C) Ribbon plot of the top and bottom 10% TWSA pixels (shade area) with the line representing the total mean of annual TWSA in Australia from Hydro 2002 to 2012.

d. TWSA variogram

A variogram of annual TWSA was calculated and plotted by using the variation analysis function to show the spatial heterogeneity of TWSA across Australia (Fig.5.8A). The significant downward and upward trends in the sill of the TWSA variogram indicate the decline and increase in the spatial heterogeneity of TWSA across Australia during the study period (Fig.5.8B). Moreover, the small magnitudes of the ratio C0/(C0+C) suggest that the variogram result is not affected by the spatial autocorrelation (Table.5.1). Hence, the variogram method in geostatistics provides another spatial evidence for the TWS intensification in Australia.

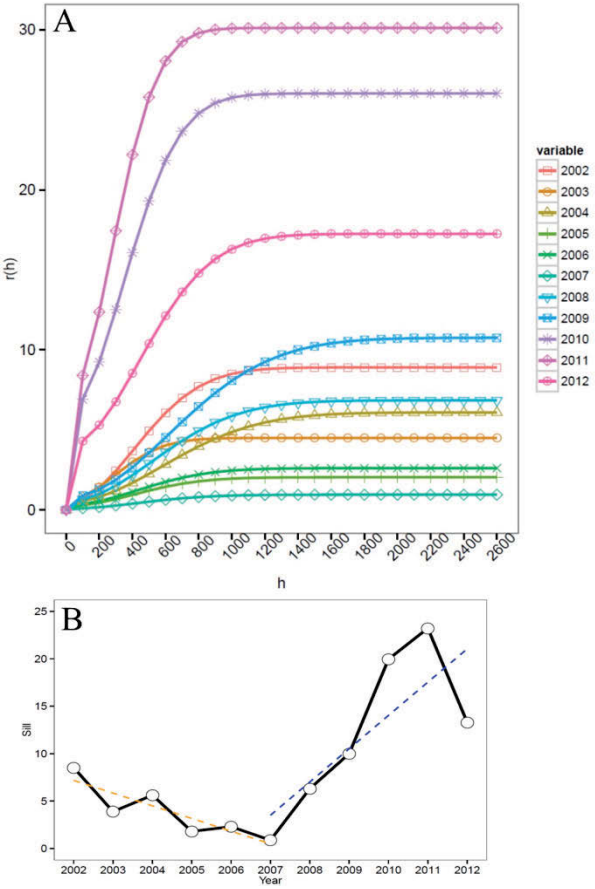

Figure 5.8. The (A) variogram scatter and (B) its sill of annual TWSA during Hydro 2002 and 2012

Table 5.1. Summary of TWSA variogram

Year	2002	2003	2004	2005	2006	2007	2008	2009	2010	2011	2012
Nugget (C0)	0.38	0.61	0.47	0.24	0.31	0.08	0.53	0.76	6.05	6.89	3.95
Sill (C0+C)	8.52	3.89	5.62	1.80	2.30	0.87	6.31	9.99	19.96	23.23	13.29
C0/(C0+C) (%)	4.48	15.60	8.40	13.21	13.41	8.63	8.47	7.64	30.33	29.65	29.74

e. The Moran's Index of TWS clustering

The different geostatistics methods mentioned above all gave similar results that suggest a short-term sign of TWS intensification. Here another geostatistics method named Moran's I was applied on the annual cumulative TWS flux data with the purpose of evaluating the degree of spatial TWSA clustering (Fig.5.9). Figure 5.9 shows a

consistent increase in Moran's index during the 'big dry' and 'big wet', indicating the TWS was getting increasingly clustered through these periods. Indeed this finding, along with the results from all other geostatistics methods used in this study, provides strong evidence of water cycle intensification during the recent two hydroclimatic events, with the dry areas becoming drier while the wet areas became wetter.

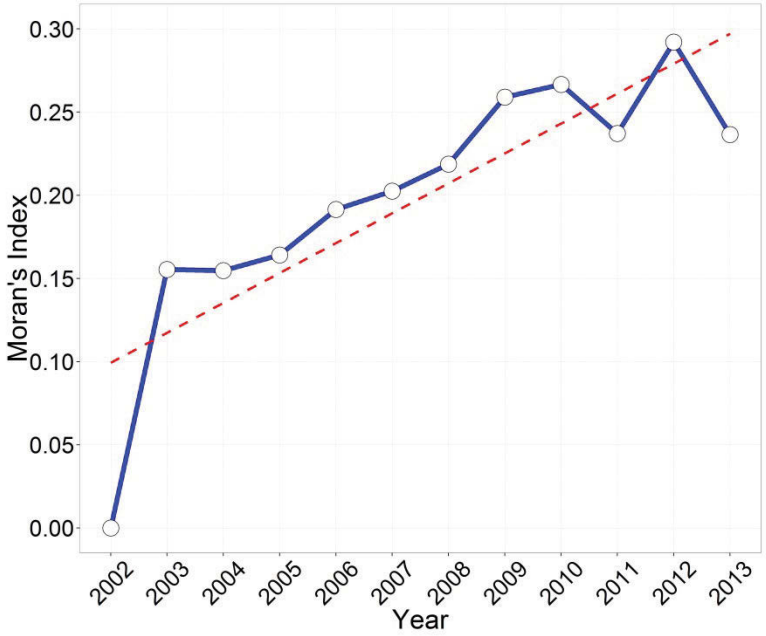

Figure 5.9. The Moran's Index of annual cumulative TWS flux from hydro 2002 to 2013

5.3.1.2 Rainfall patterns and its relationship with TWS

a. Uneven temporal-spatial distributions of rainfall

Results from the rainfall time series analysis method show that temporally the rainfall in the 'dry' months and 'wet' months was getting more extreme through the time studied, with less rain in 'dry' months while more fell during the 'wet' months (Fig.5.10A). In the spatial domain, the standard deviation of all annual rainfall pixels across Australia significantly increased from Hydro 2002 up to 2010 (Fig.5.10B). This indicates the TWS intensification might be translated from the more extreme rainfall patterns in Australia during the 'big dry' and 'big wet'.

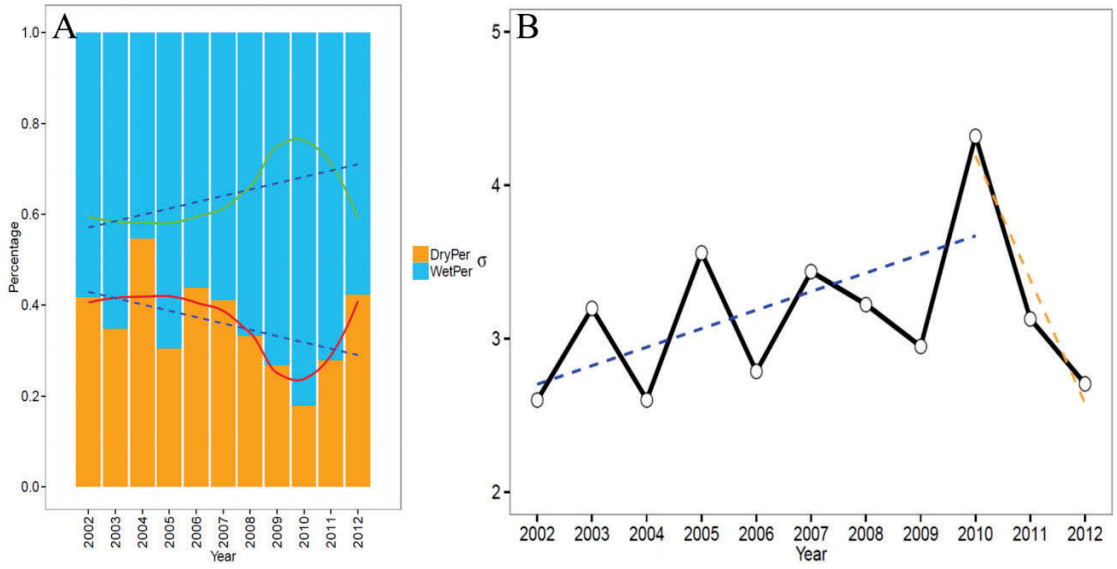

Figure 5.10. (A) Ratio of rainfall in dry (orange) and wet (blue) months of each year during Hydro 2002 and 2012 ($p < 0.05$). (B) Standard deviation of all annual rainfall pixels during Hydro 2002 and 2012 ($p < 0.05$).

A rainfall rate of change map during the 'big dry' (Fig.5.11A) was created to show the drying trend of rainfall in Australia on a pixel level and the rainfall gain map (Fig.5.11B) was produced for the 'big wet' event, where each pixel represents rainfall gains (cm) during the wet pulse. The rainfall 'big dry' trend map corroborates its variance mentioned above and indicates the intensifying spatial distributions of rainfall across Australia (Fig.5.11A). It shows that during the 'big dry' there was a reduction in rain in the western regions, while the east experienced increasing levels of precipitation. Similar uneven rainfall patterns occurred during the 'big wet' period, even though we observed a positive anomaly in precipitation on a continental scale. It was mostly driven by eastern Australia and there were not many rainfall gains in the western part (Fig.5.11B). We found various TWS recovery patterns from the interior to the eastern margins of the continent, in which the anomalous rain gained in eastern Australia during the 'big wet' can be linked to the recent devastating floods over northern and eastern Australia.

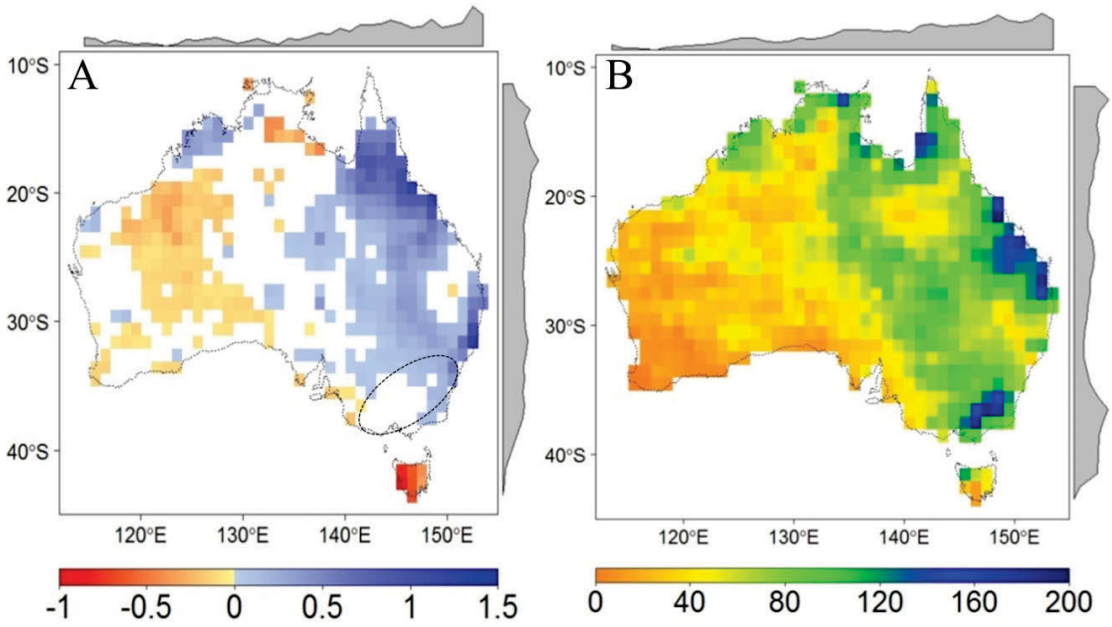

Figure 5.11. (A) Rainfall rate of change during the 'big dry': slope between 2002 and the end of the 'big dry' based on the TWS timing map for the end of the 'big dry' and pixels with statistically non-significant slopes excluded from the analysis (white). (B) Rainfall gains (cm) across the continent during the 'big wet'. The marginal graphics show the latitude and longitude mean summaries of each image.

b. The relationship between rainfall and TWS

We observed a continent-wide TWS anomaly profile followed rainfall changes with a two-month lag ($R^2 = 0.63$) during our study period (Fig.5.12A). The continental 'big dry' end timing derived from rainfall (Aug-2009) was two months earlier than that (Oct-2009) from TWS and rainfall 'big wet' ended around a half year earlier than the TWS. However, once the seasonality was removed from the time series, TWS exhibits a significant decline (p-value < 0.05) while rainfall slightly increased during the 'big dry' (Fig.5.12A). This may indicate that the mean annual precipitation (MAP) could remain constant or increase through the years, yet its temporal-spatial distributions might become more uneven, resulting in a reduction of TWS.

The long-term rainfall time series (BOM: 1900 to 2014 annual anomalies) shows an increase in precipitation during the 'big dry' (red rectangle in Fig.5.12B). However, the average rain for this period is below the long-term meteorological mean (Fig.5.12B). This is reflected in the recent governmental climate report, showing average continental-rainfall has increased in Australia since 1900, with above-average

precipitation in Australia's north offsetting a drop in annual rainfall in the south (CSIRO and BOM 2014). The 'big dry', also known as the Millennium drought, is considered to be one of the worst recorded droughts in Australia since European settlement (Van Dijk et al. 2013). Nevertheless, previous studies showed that it is hard to distinguish the severity of this drought solely based on rainfall anomalies (Ummenhofer et al. 2009). Our TWS trend map indicates a clear severe drought in south-eastern Australia during the 'big dry' (Fig.2.3B) but the rainfall 'big dry' trend map missed this important information (black circle on Fig.5.11A).

We present spatial cross correlations between deseasonalized TWS and rainfall across Australia (Fig.5.12C) and found they correlated well in northern, eastern and some parts of western Australia with a 1 or 2-month lag (rainfall antecedent). However, in many water limited areas of western Australia, the coefficient of determination decreases indicating a lower correlation, which may be due to the low and variable rainfall and high evapotranspiration over these regions. Therefore, combining GRACE derived TWSA with Rainfall can provide better understanding of hydrological events like droughts and floods.

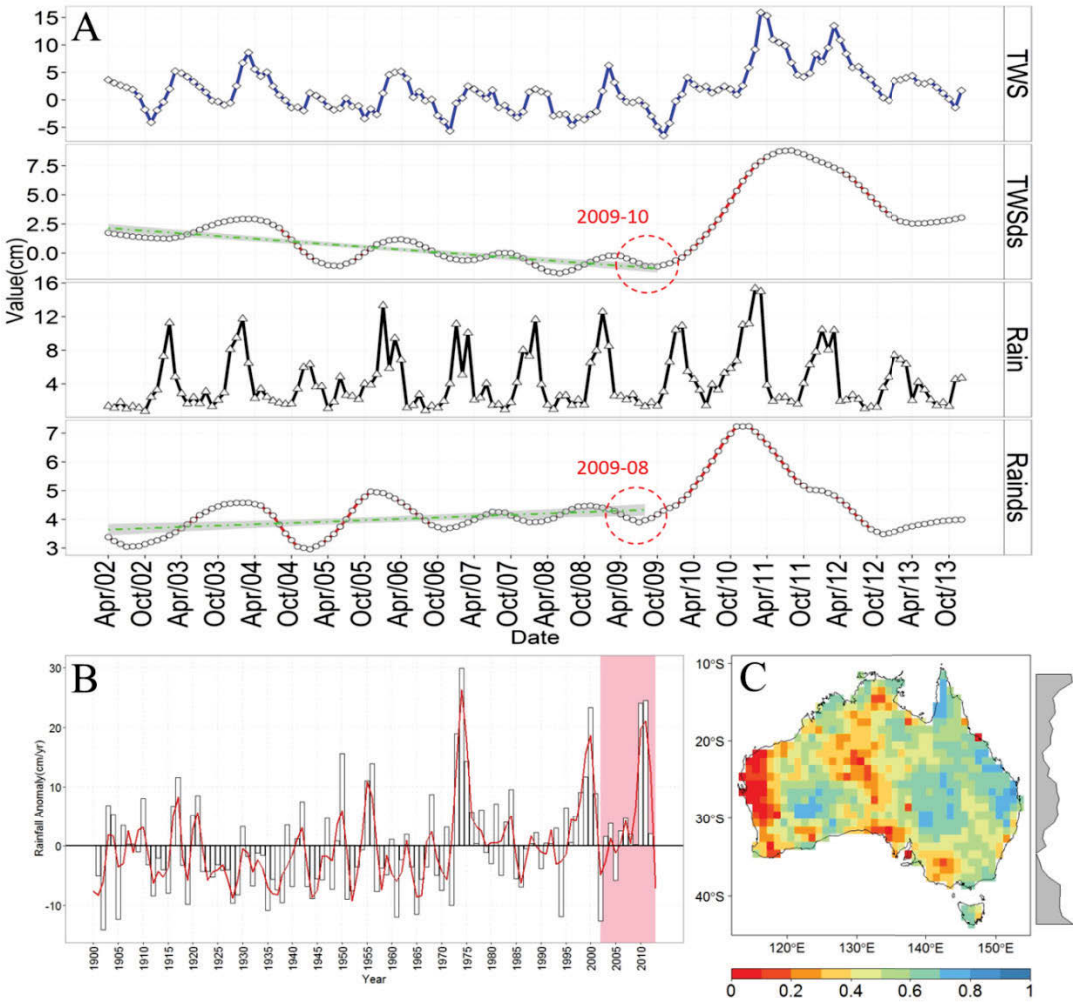

Figure 5.12. (A) Monthly mean values of total water storage anomalies (TWSA), deseasonalized TWSA, rainfall and deseasonalized rainfall in cm for continental Australia from 2002 to 2013; (B) Time series of annual BOM precipitation anomalies (cm year^{-1}), with 5-year running mean superimposed in red curve (1900-2013). (C) Cross Pearson's correlation coefficients between rainfall and TWS from 2002-2013.

5.3.1.3 ET changes during the 'big dry' and 'big wet'

Due to the linear water balance approach we used and the random characteristics of the monthly precipitation data, the estimated monthly ET (ET_{WB}) image tends to have sharp and negative values in some pixels. To reduce the sharp noises and avoid the negative values, we smoothed the ET_{WB} time series for each pixel on the stacked monthly ET_{WB} images using the Savitzky-Golay smoothing method, with a 3-month moving average window (Savitzky and Golay 1964).

a. Temporal changes in ET through the dry and wet events

The time series of continental-scale averaged TWSA, rainfall and ET, from Hydro 2002 to 2012, show fluctuations at both seasonal and inter-annual temporal scales. We observed the TWSA followed rainfall patterns in a two-month lag while monthly ET had concurrent variations as rainfall, with a correlation (r) of 0.72 (Fig.5.13). As mentioned in section 5.3.1.2, once the seasonality was removed from the time series, TWS changes exhibited a significant decline ($p < 0.05$) but rainfall increased during the 'big dry' ($p < 0.05$). Figure 5.13 may partly explain these conflicting trends in TWS and rainfall by showing a significant upward trend in deseasonalized ET ($p < 0.05$). Overall the 'big dry' trends in the linear regression of deseasonalized TWSA, rainfall and ET time series are -0.039, 0.0066 and 0.0034, respectively. This indicates that the decreasing trend in TWS was larger than the rate of ET consuming the rainfall. Therefore, ET should be only one of the reasons for the TWS decline, which might also be attributed to other factors such as more extreme spatial-temporal rainfall patterns during the 'big dry'. Future work is needed to study this by analysing more relevant meteorological data.

During the 'big wet', the three variables went up dramatically but with different intensities and durations. ET tightly followed with rainfall, and both of them peaked half year earlier than TWS before all three plunged with sharper trends in their second dry phase. Moreover, rainfall started increasing from December 2012 while ET still decreased, which seemed to stop the TWS from continuing to decline.

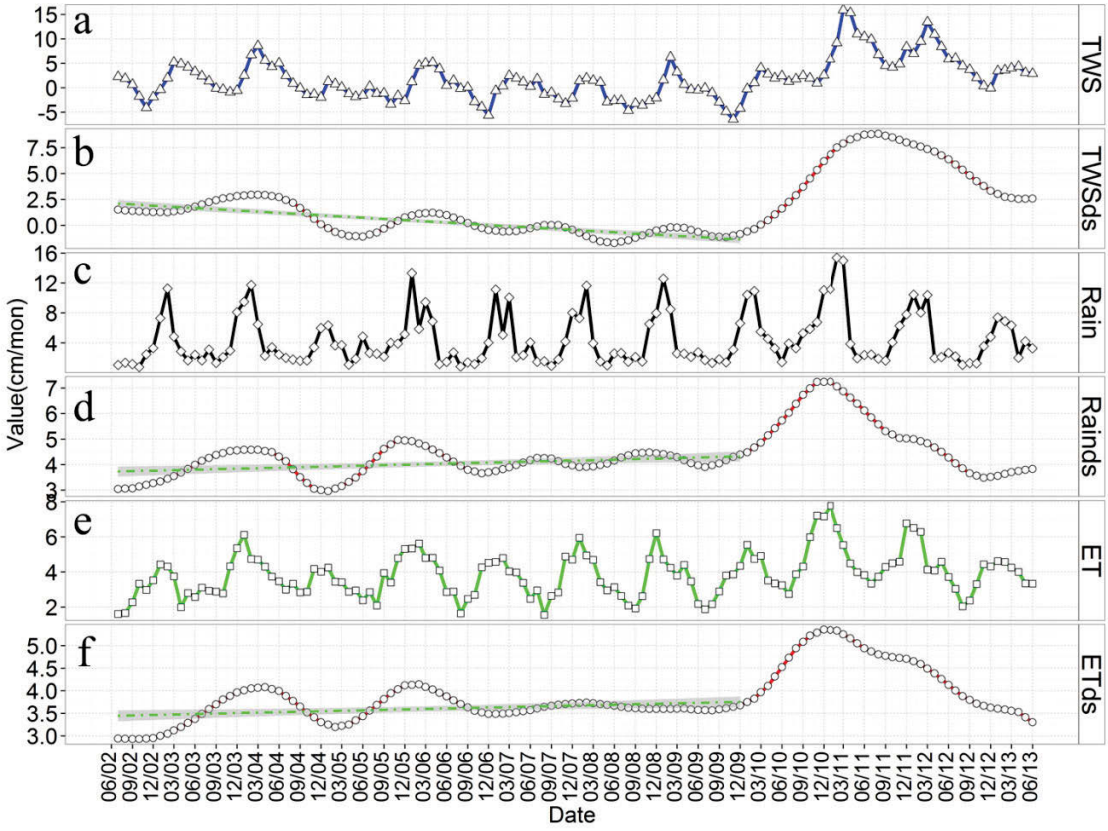

Figure 5.13. Monthly mean of (a) total water storage anomalies (TWS), (b) smoothed and deseasonalized TWSA (TWSds), (c) rainfall (Rain), (d) smoothed and deseasonalized rainfall (Rainds), (e) Evapotranspiration (ET) and (f) smoothed and deseasonalized ET (ETds) all in cm for continental Australia from Hydro 2002 to 2012.

b. Spatial patterns of ET across the continent

ET rates of change in the 'big dry' (Hydro 2002-2008) and for the combined 'big dry' and 'big wet' period (Hydro 2002-2011) were calculated to see the impacts of the dry and wet events on spatial ET patterns across the Australian continent (Fig.5.14). An east to west ET rate of change pattern in the 'big dry' was observed with ET increasing in eastern Australia but decreasing in western Australia (Fig.5.14A), which is in line with rainfall patterns in the 'big dry' period (Fig.5.11A).

When the 'big wet' arrived associated with the increased rainfall, an increase in ET was found across most of the continent except for some areas in western Australia and the southwestern tip of Australia (Fig.5.14B). However, after the pixels with statistically non-significant ET trends were excluded ($p > 0.05$), we found very few

negative trends left in western Australia and some positive pixels in eastern part on the ET 'big dry' trend map while the combined 'big dry' and 'big wet' trend map showed only significant positive ET trends in eastern Australia.

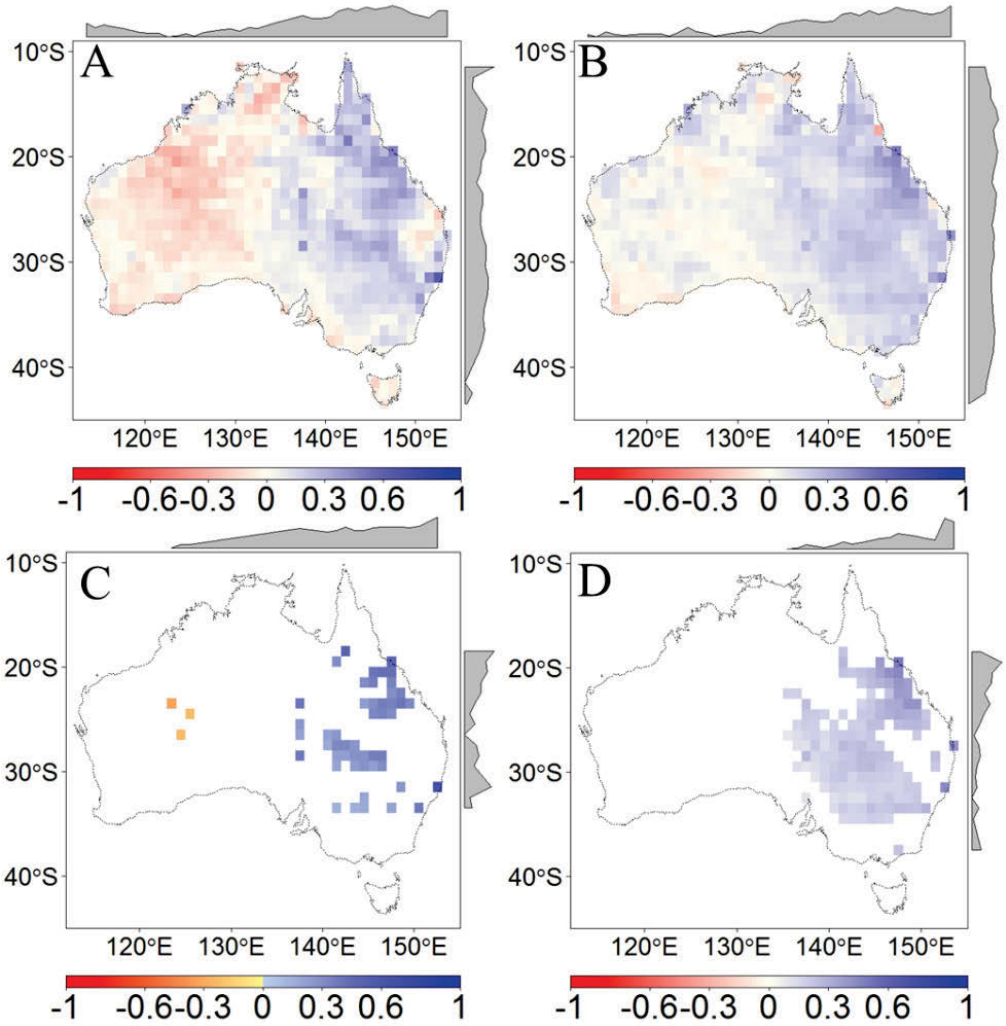

Figure 5.14. (A) ET rate of change in the 'big dry' (Hydro 2002-2008); and (B) for the combined 'big dry' and 'big wet' period (Hydro 2002-2012) over Australia with all pixels (cm/yr); (C) ET rate of change in the 'big dry'; and for the (D) combined 'big dry' and 'big wet' period over Australia (cm/yr) with statistically non-significant pixels excluded.

5.3.1.4 Soil moisture and groundwater on drying and wetting

a. The contributions of SM/GW to variations in TWS through time

Figure 5.15 depicts decadal variations (from Hydro 2002 to 2012) in the monthly averaged GLDAS Soil Moisture Anomaly (SMA), GRACE derived Ground Water Anomaly (GWA) and TWSA over the Australian continent. Seasonal trends in SMA and TWSA follow each other fairly well, with the seasonal amplitude both being about 8 cm (Fig.5.15). GWA shows seasonality as well but with a much smaller amplitude that is less than half of those in TWSA and SMA (< 4 cm). In general, all three variables exhibit higher values during Austral autumn and lower values in Austral spring. TWSA, soil moisture and groundwater also had strong inter-annual variations during the study period, which encompasses the 'big dry' and 'big wet' periods. Similar to TWSA, both soil moisture and groundwater showed two dramatic peaks during the 2-year 'big wet' pulse. However, there was a significant decreasing trend in groundwater during the 'big dry' ($p < 0.05$) while soil moisture stayed relatively stable (Fig.5.15). This may indicate that the decline in the TWS during the dry period was mostly attributed to the decrease of groundwater.

SMA and GWA are all highly correlated with TWSA, with correlation coefficients being 0.9 and 0.8 respectively. A linear regression analysis method was applied in this study to model the variations in TWS that can be explained by SM and GW. The fitted linear equation was found below:

$$TWSA = 1 * SMA + 0.98 * GWA \ (r^2=0.99, p < 0.01)$$

The relative importance of SMA and GWA to the variations in TWSA are 0.57 and 0.43. As shown by Fig.5.15, SMA showed similar seasonal changes and amplitudes with those in TWSA through the years, which may indicate the seasonal changes in TWS were primarily a function of soil moisture.

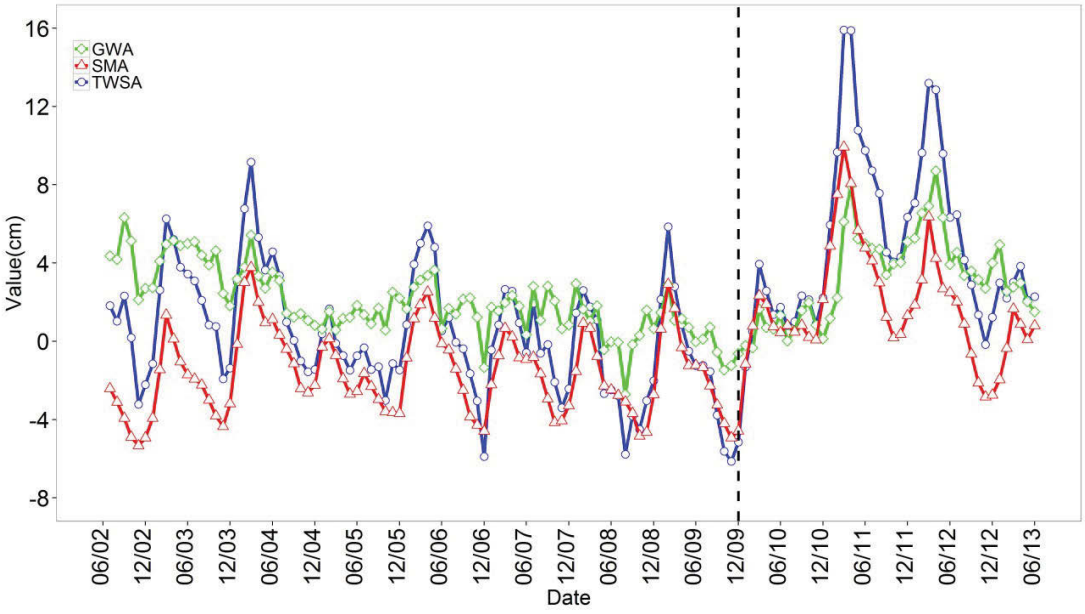

Figure 5.15. Monthly continental average TWSA (blue), SMA (red) and GWA (green) from Hydro 2002 to 2012 with the dashed black vertical line representing the continental end timing of the 'big dry' or the onset of the 'big wet'.

b. Spatial drying and wetting patterns of SM and GW across Australia

Rates of change in soil moisture and groundwater were calculated at pixel level by using the temporal trend analysis method to show the geographic distributions of their changing trends across Australia (Fig.5.16). During the 'big dry' period, decreasing trends in soil moisture mainly concentrated in a large area spanning from northwestern to central Australia, with the rest of the continent, especially the northeastern part having increases in SM (Fig.5.16A). By contrast, GW showed more extensive loss across Australia during the dry period. In particular, GW had similar drying patterns as those in TWS, exhibiting not only GW loss in the northwest area but also in the southeastern and southwestern tips of Australia where the two main areas of agricultural land are located (three black circles in Fig.5.16C). However, the soil moisture 'big dry' trend map did not catch the serious dry information in these two agricultural areas with SM trends either showing non-significant or positive values (Fig.5.16A). When the 'big wet' pulse arrived, soil moisture was fully recharged in most of Australia especially in the southeastern part (Fig.5.16B) while GW in western and southeastern Australia was hardly affected much by the wet period, with GW loss continuing after the 'big wet' (three black circles in Fig.5.16D).

Through the entire study time (both the dry and wet periods), groundwater became intensified with similar patterns of TWS intensification, increasing in wet areas (north-eastern Australia) while decreasing in dry areas (western Australia). This is also indicated by the marginal plots of Figure 5.16 D. Results from SM and GW rates of change maps revealed that in southeastern parts of Australia especially in the Murray-Darling Basin (also known as the 'Australian breadbasket'), the recovery of the total water storage during the two years' wet pulse described in Chapter 2 should be mainly attributed to the increases in SM, as the groundwater in the basin was not recharged much by rainfall and was still decreasing after the 'big wet', corresponding with the previous studies (Leblanc et al. 2011; Leblanc et al. 2009). Therefore, the GW loss in both southeastern and southwestern areas might be attributed to the substantive irrigation of agriculture during the long millennium drought. Groundwater loss is often easily neglected and may cause irreversible damage to local agriculture and the natural ecosystem.

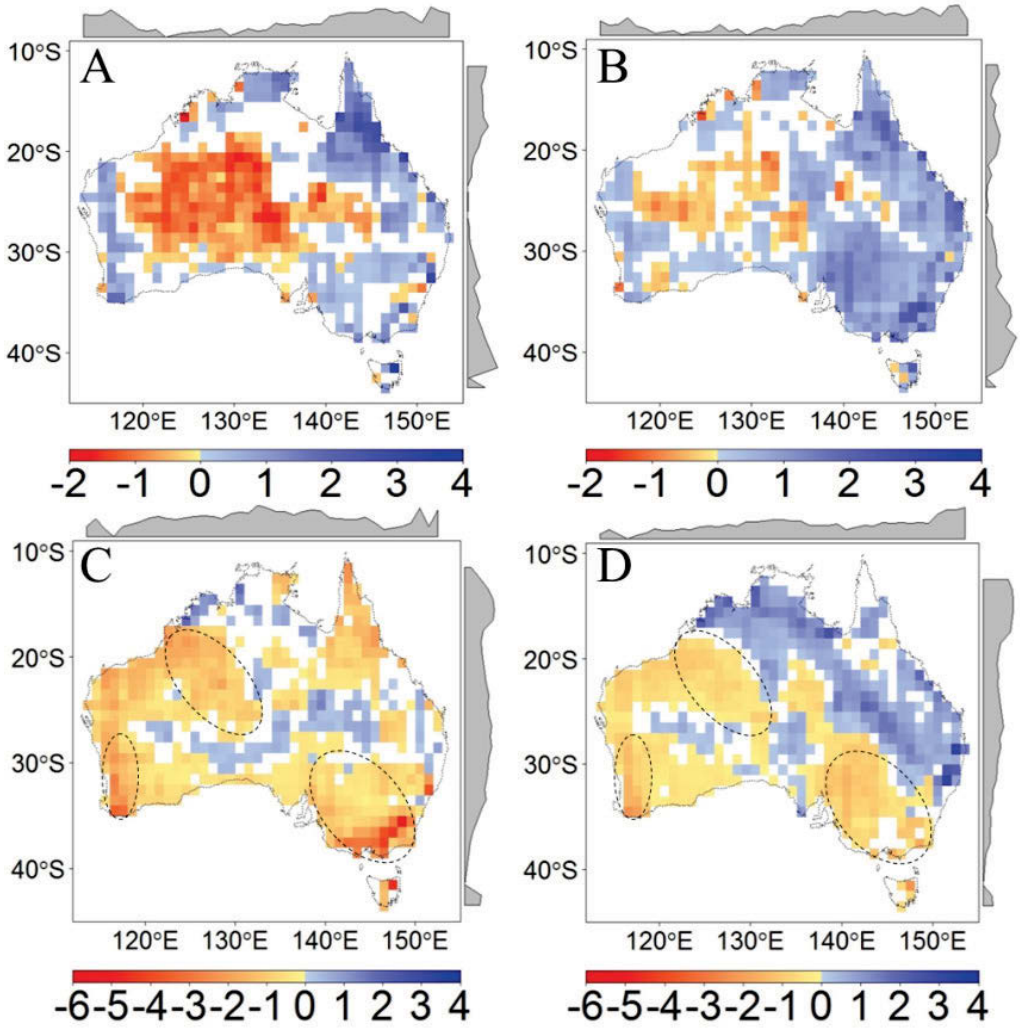

Figure 5.16. (A) Soil moisture rate of change in the 'big dry' (Hydro 2002-2008); and (B) for the combined 'big dry' and 'big wet' periods (Hydro 2002-2012) over Australia (cm/yr); (C) Groundwater rate of change in the 'big dry'; and (D) for the combined 'big dry' and 'big wet' periods over Australia (cm/yr). Statistically non-significant pixels were excluded.

5.3.2 Response of ecosystem to hydrological variations under hydroclimatic extremes

5.3.2.1 Ecohydrological interactions over Australian continent

a. The relationships between vegetation and hydrological factors

Seasonality in hydrological (TWSA and rainfall) and ecological (EVI) variables during the 'big dry' and 'big wet' events over Australian continent is depicted in Fig.5.17. Seasonal patterns in TWSA and EVI closely followed each other during the dry and wet periods, with both variables exhibiting peak values in Austral autumn (March) and

minimum values in Austral spring (November). By contrast, the seasonal cycle of rainfall is distinct from those of TWSA and EVI, indicating a general summer peak and winter trough (Fig.5.17). We found TWSA and EVI showed a bigger seasonal magnitude during the 'big wet' than that in the 'big dry' but kept the same shape in profile. However, a shift in peak values of rainfall seasonal patterns was observed, with higher values moving from summer during the 'big dry' to autumn in the 'big wet'.

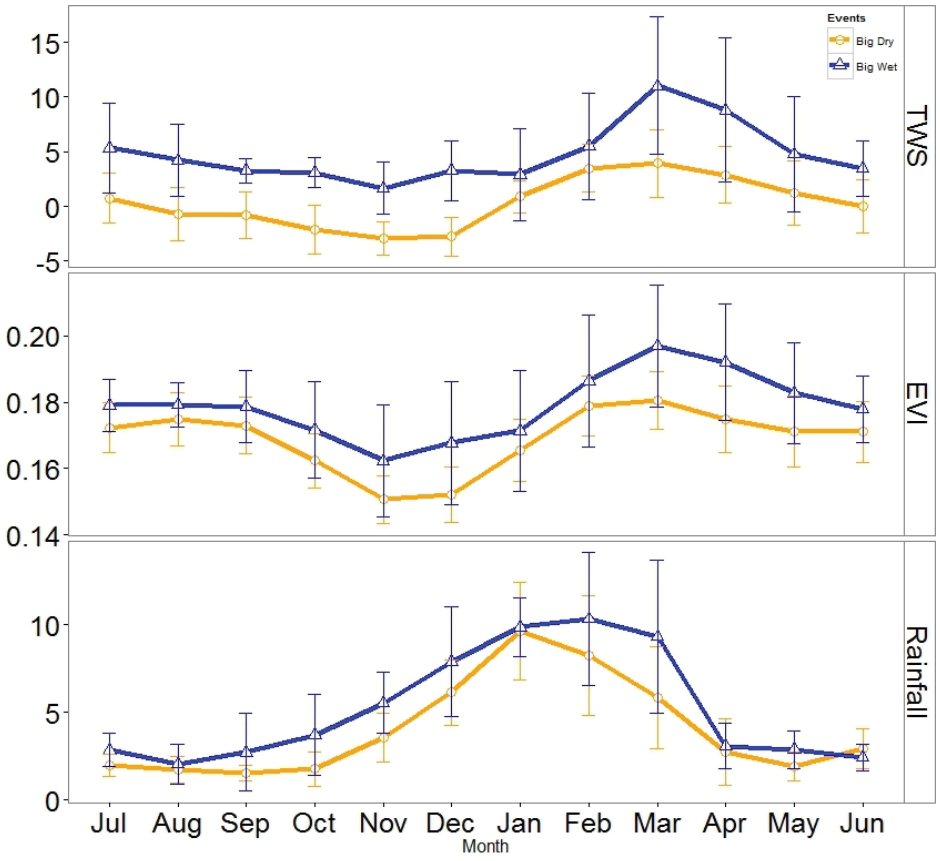

Figure 5.17. Hydrological seasonality (July to June) of continentally averaged (a) total water storage anomaly, (b) EVI, and (c) rainfall over Australia. Each point represents the monthly climatological mean from the 'big dry' and 'big wet' periods during the hydro 2002 to 2012, and error bars indicate one standard deviation.

The relationships between hydrological and ecological variables across the Australian continent during the entire study time (Hydro 2002-2012) were evaluated by the cross correlation analysis method based on the analysed variables (TWSA, Rainfall and EVI) that were constrained by three different methods (Fig.5.18). Firstly, we investigated the spatial patterns of correlations among the original monthly time series of TWSA, Rainfall and EVI (Fig.5.18 A1-3). Monthly TWSA and EVI are positively

correlated over most of the continent with the exception of some weak associations between them in southwestern and southeastern Australia where the agricultural lands are located (Fig.5.18 A1). As the impact of TWS, as well as precipitation, on EVI is expected to show some time lag due to the variability in the temporal response of vegetation to water availability, the maximum correlation coefficients (r) obtained by the cross correlation analysis method were based on different time lags that vary across Australia (Fig.5.19). Correlations between original monthly rainfall and EVI (continental average r = 0.56) are generally weaker than those between TWS and EVI (r = 0.6) throughout the country (Table.5.2), with significant correlations mainly concentrated in northern and northeastern Australia (Fig.5.18 A2). Rainfall precedes EVI by 1 month in these areas and 2-3 months in central and western Australia (Fig.5.19 A2).

We also accessed the correlations between the deseasonalized time series of TWSA, rainfall and EVI to evaluate the relationships between them without the effect of seasonal variations. Results showed that the correlations between rainfall and EVI were greatly improved throughout the entire country after their seasonal components were removed, with a r of 0.79 while those between TWSA and EVI became slightly worse (r = 0.56 in Table.5.2) especially in the southwestern and southeastern agricultural areas. However, the lags between rainfall and EVI in western Australia changed from around 2 to more than 4 months (Fig.5.19 B2).

A time series can be broken down into three components: seasonal component, trend, and remainder. After deseasonalization, the correlations between variables above show the relationship between the trends + reminders in two variables. As non-stationary data, TWSA, rainfall and EVI time series contain deterministic trends, as a result, detrending the time series of these variables may provide more reliable relationship evaluation among them (Kaufmann et al. 2000). Detrended TWSA and EVI show improved correlations coefficients across Australia with a spatially averaged r of 0.65 (Fig.5.18C1 and Table.5.2) and similar lag patterns to those between the original monthly TWSA and EVI. By contrast, much weaker correlations between detrended rainfall and EVI were found (r = 0.53), with high correlation coefficients found only in northern and northeastern Australia (Fig.5.18 C2).

Strong correlations between monthly rainfall and TWSA through the study time concentrated in northern Australia with a lag of 1 month (Fig.5.18 A3, B3, C3 and Fig.5.19 A3, B3, C3). Moreover, the larger time lags between rainfall and EVI than those between TWSA and EVI suggest that rainfall may lead the behaviour of TWS (Fig.5.19).

In summary, the results presented above reveal that the spatial correlations in the TWSA-EVI relationship are more uniform and stronger than those in the rainfall-EVI relationship where rainfall is generally better connected with EVI in eastern Australia but less correlated with EVI in the western parts of the continent. This indicates that TWS patterns were the primary drivers of EVI dynamics, rather than rainfall and GRACE observed TWSA is a robust and valuable predictor of seasonal surface greenness over Australia. However, the strong relationship between deseasonalized rainfall and EVI also indicates that rainfall may make a potential contribution to the long-term trend of the vegetation across Australia.

Table 5.2. Spatially averaged optimal correlations and corresponding lags (in months) between TWSA, rainfall and EVI over Australian continent.

Cor/Lag (months)	Original	Deseasonal	Detrended
TWS-EVI	0.60/0	0.56/0	0.65/0
Rain-EVI	0.56/2	0.79/3	0.53/2
Rain-TWS	0.42/2	0.62/3	0.42/2

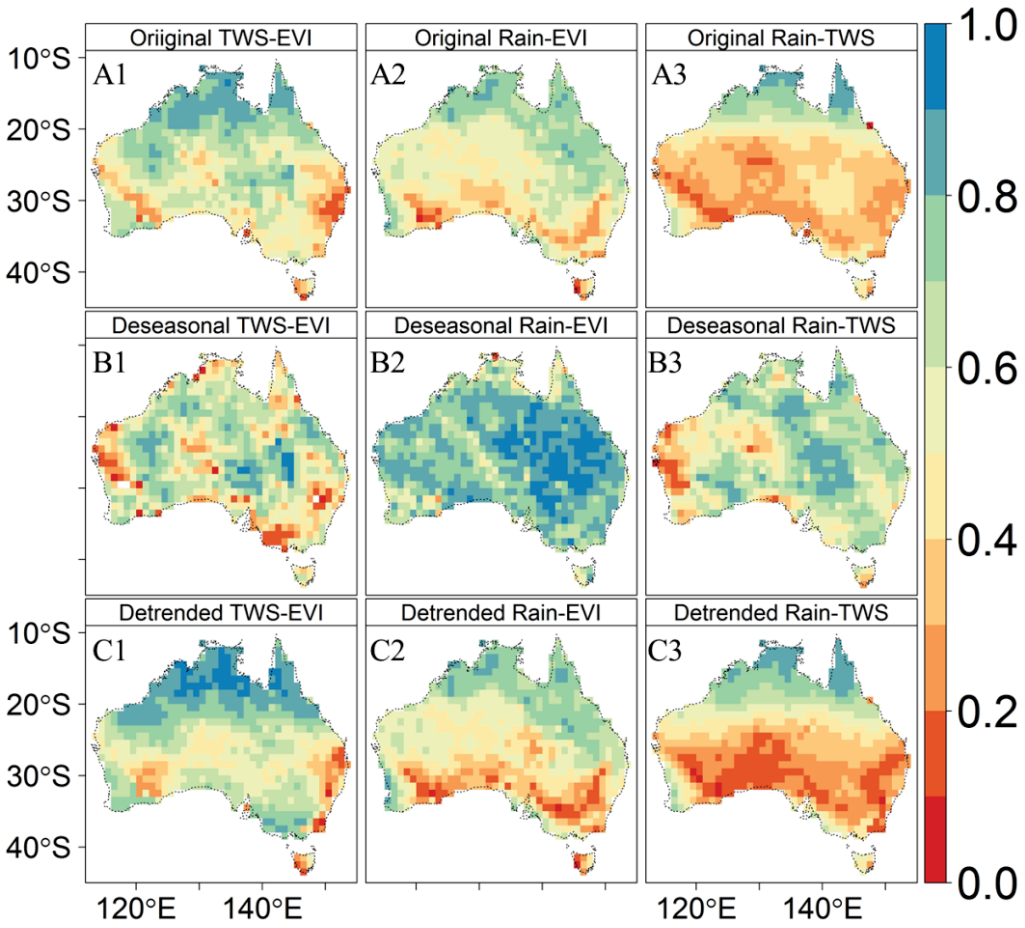

Figure 5.18. Spatial cross correlation coefficients (maximum r) across Australian continent during Hydro 2002 - 2012 between (A 1-3) original monthly TWSA, rainfall and EVI; (B 1-3) deseasonalized monthly TWSA, rainfall and EVI; (C 1-3) detrended monthly TWSA, rainfall and EVI.

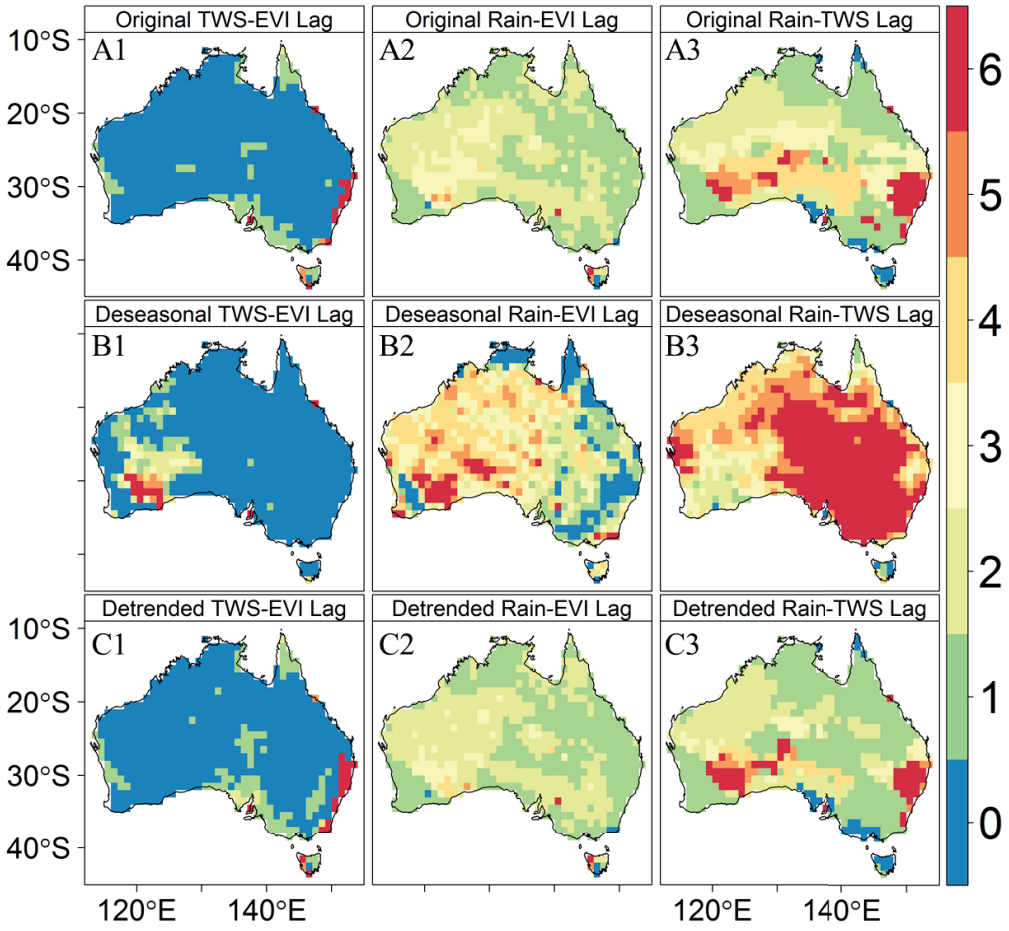

Figure 5.19. Spatial lags in months across Australian continent during Hydro 2002 - 2012 between (A 1-3) original monthly TWSA, rainfall and EVI; (B 1-3) deseasonalized monthly TWSA, rainfall and EVI; (C 1-3) detrended monthly TWSA, rainfall and EVI.

b. Spatial-temporal vegetation greening and browning

Monthly continental averaged ecological (EVI) and hydrological (TWSA, rainfall, soil moisture, groundwater) variable anomalies, from Hydro 2002 to 2012, show fluctuations at both intra and inter-annual temporal scales with differences in the direction, magnitude, and duration of their responses to the 'big dry' and 'big wet' events (Fig.5.20). During the drought period (2002 - 2009), hydrological stress was indicated by continental scale decreases in TWS and GW while there were slight increases and decreases in the long-term trends of rainfall and soil moisture respectively. Despite the significant decline in continental TWS, it was mainly expressed in the groundwater loss rather than soil moisture. Vegetation greenness, represented by EVI, showeda non-significant decline in its continual average trend during this dry period. There were dramatic increases in all the hydrological variables during the two-year wet extreme

period shown in Figure 5.20, which resulted in a large boom of vegetation across Australia (Fig.5.20). However, the switch from high national rainfall to very dry conditions was rapid. As a consequence, EVI time series then reversed a second time, with a sharp downward trend, bringing large-scale vegetation browning and by the end of the analysis period, continent-wide EVI values were nearly equivalent to those before the 'big wet'.

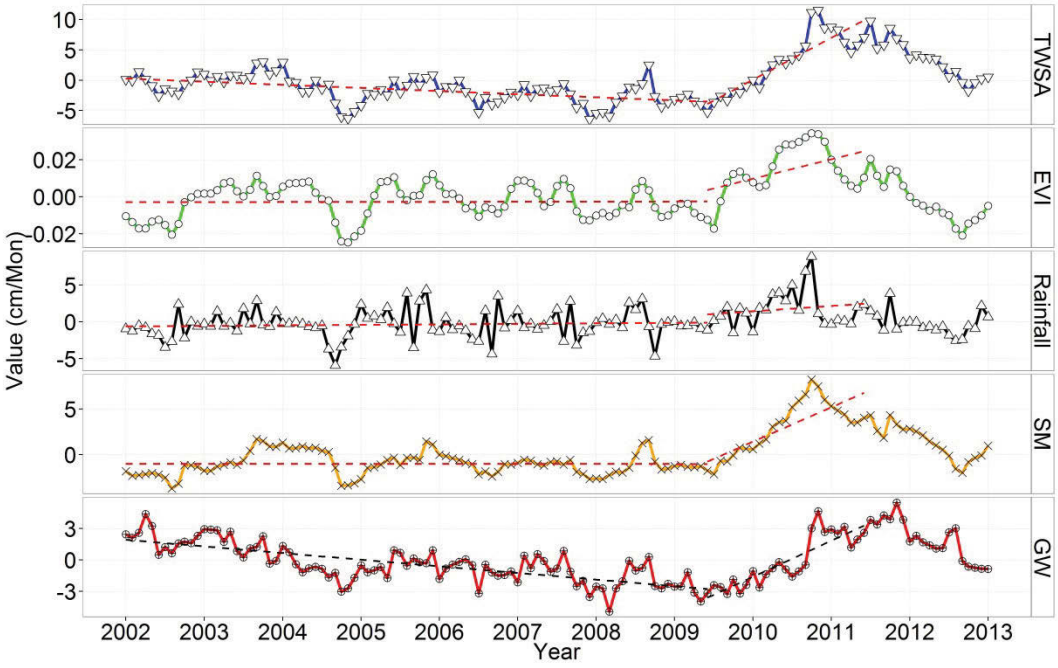

Figure 5.20. Time series of monthly EVI, TWSA, rainfall, soil moisture, groundwater over Australian continent during Hydro 2002-2012, with dashed lines representing 'big dry' and 'big wet' trends in all the variables.

Spatial EVI rates of change maps were calculated to illustrate the geographic distribution of changing trends in vegetation across Australia under general dry and wet conditions. The time series of continental average EVI showed no significant changes during the 'big dry' (Fig.5.20). However, spatially we found a strong decline in EVI over western, central and southeastern parts of Australia while there were some increases in northeastern regions (Fig.5.21 A). This divergence of EVI trends offset each other, resulting in the stable EVI trend during the dry period. The intensifying EVI trends continued after the 2 year wet pulse, with an east-west pattern, showing EVI decreases in western and increases in eastern Australia (Fig.5.21 B). The spatial greening and browning patterns of vegetation in Australia during the 'big dry' and 'big wet' showed

strong similarity to the TWS trends in the three TWS zones observed in Chapter-1, indicating a close connection between GRACE-TWS and EVI, both of which are primarily driven by the three key climates modes of Australia (ENSO, IOD, SAM).

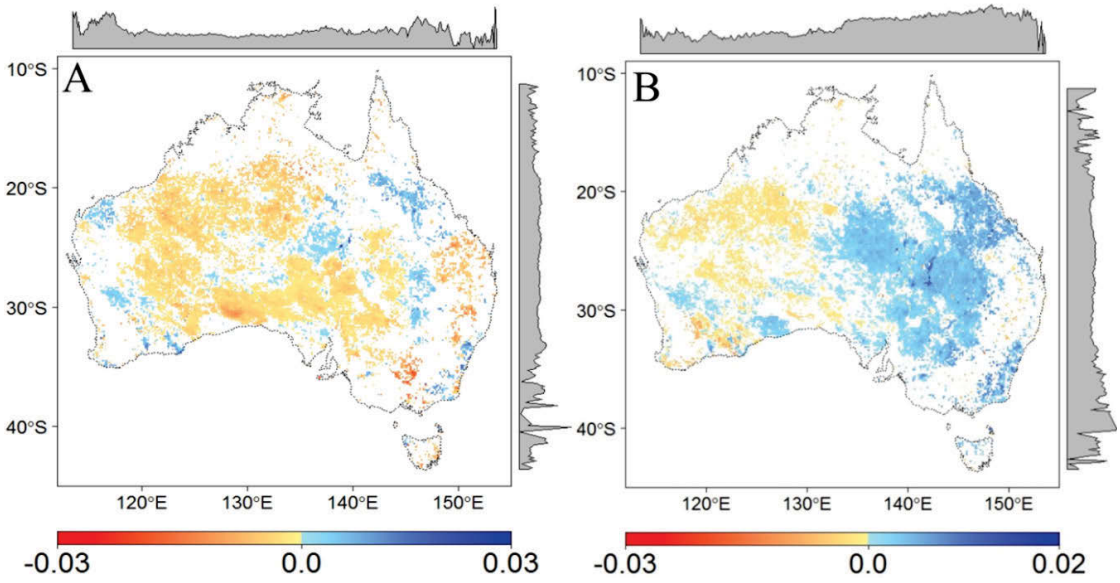

Figure 5.21. (A) EVI rate of change in the 'big dry'; and (B) for the combined 'big dry' and 'big wet' period (Hydro 2002-2012) over Australia (cm/yr) with statistically non-significant pixels excluded.

c. Associations between GRACE-derived TWSA and EVI constrained by rainfall

The X-Y scatter points of Mean Annual Precipitation (MAP) and EVI over Hydro 2002-2012 were plotted with each pixel coloured to represent various correlation between TWS and EVI (Fig.5.22). We observed that the relationship between rainfall and EVI across Australia exhibits a shape of a two-branch "fork" with the trend line of the entire points being the division boundary. Interestingly, we also found that most of the points (pixels) with lower TWS-EVI correlation ($r < 0.5$) centred in two blocks; either 1) in the areas with MAP being less than 500 mm/yr; 2) or in the section of the upper branch of the "fork". These two dot clusters show that with the same amount of rainfall, vegetation in different grid boxes (1x1 degree area) show various EVI values, indicating different bioregions.

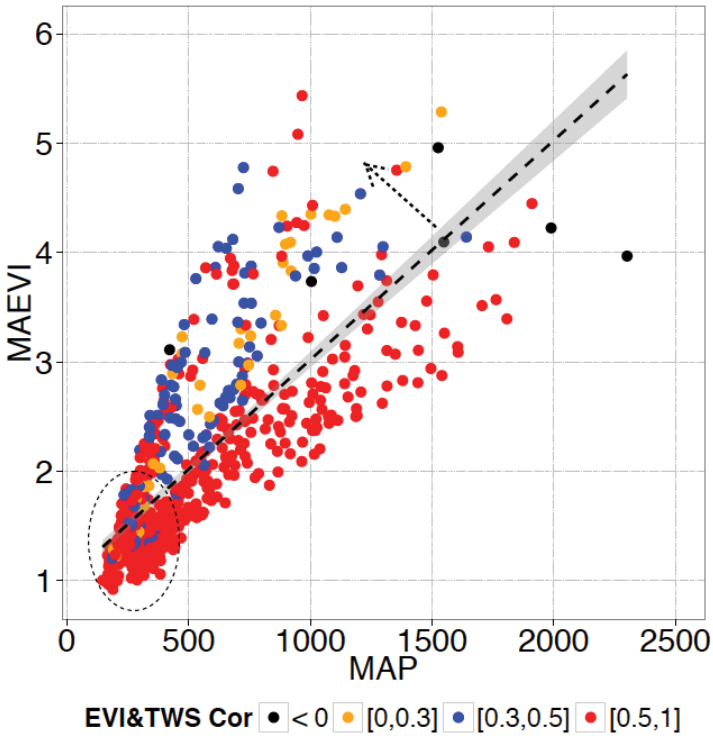

Figure 5.22. Scatter points of Mean Annual Precipitation and EVI over Hydro 2002 - 2012. Each point stands for one pixel, which is colored by the correlation coefficients between EVI and TWS.

A scatter diagram of annual rainfall and EVI for each individual year was also plotted to see the associations between TWS and EVI under the constraint of different year by year annual rainfall (Fig.5.23). Throughout the years from Hydro 2002 to 2012, similarly as expressed in mean annual scatter points (Fig.5.22), when the points of all years were added up together (Fig.5.23 A), pixels with low TWS-EVI correlations were still found in two regions (less than 500mm/yr and upper branch of "fork" areas).

Under different hydroclimatic conditions, the patterns of annual rainfall-EVI scatter points varied from year to year but still kept the format as a 'fork', with low correlations between TWS and EVI staying in the upper branch of the 'fork' (Fig.5.23 B). Moreover, we also found the Hydro years of 2005, 2008 and 2010 had the most pixels with low correlations, in which the hydroclimatic conditions were more extreme than other years (Fig.5.23 B).

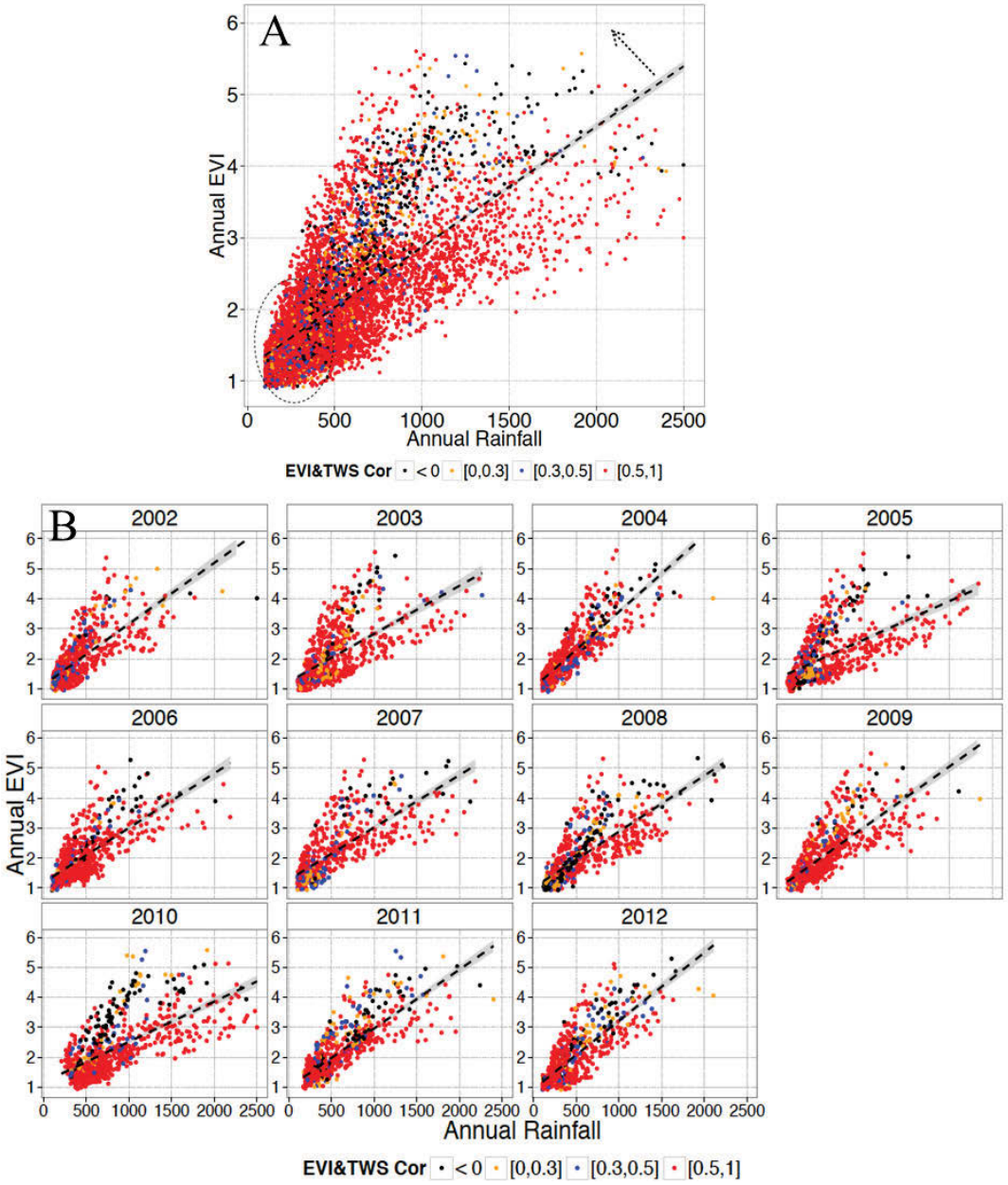

Figure 5.23. (A) All scatter points of Mean Annual Precipitation and EVI for 11 years of Hydro 2002 - 2012. Each point stands for one pixel, which colored by the correlation coefficients between EVI and TWS. (B) Scatter points of Mean Annual Precipitation and EVI for each individual year during Hydro 2002 – 2012.

5.3.2.2 Hydrological variations and their ecological implications at regional scale

a. Ecohydrological dynamics in three TWS zones

Chapter 2 showed that Australia can be partitioned and grouped into three geographic zones according to their distinct TWS responses to the 'big dry' and the 'big

wet' (Fig.2.4). In this section, we explicitly investigated the hydrological variations and corresponding ecological responses across these three TWS zones.

1) Total Water Storage

The time series of continental average ecological variable (EVI) and hydrological variables (TWS and GW anomalies, rainfall, soil moisture) over TWS Zone I, II and III with overall trends in the deseasonalized variables were depicted in Figure.5.24. We found during the study period, TWS was highly related to soil moisture, groundwater and EVI across the three zones (Table.5.3) with expectation of low correlation between TWS and GW in Zone II. TWS followed rainfall fairly well in Zone I with one month lag (r = 0.7), both of which showed similar strong seasonal and inter-annual patterns (Fig.5.24 A). Due to the high variations of rainfall in south-eastern and western Australia, TWS had relatively lower correlations with rainfall in Zone II and III being 0.42 (lag = 1 month) and 0.51 (lag = 2 months), respectively (Fig.5.24 B-C). However, the deseasonalized trends in TWSA and rainfall showed a close connection over all the three zones (Fig.5.24), indicating the leading role of rainfall in the variations in TWS.

2) Soil Moisture

Soil moisture across the three zones had good connections with TWS and EVI, and low correlations with groundwater (Table.5.3, Fig.5.24). Results showed that soil moisture closely followed rainfall with correlations of 0.78 and 0.55 respectively in Zone I and II with a general 1 month lag (Fig.5.24 A-B). The irregular and intensive rainfall across most of the central and western Australia plus the high evaporation caused large uncertainties in its relationship with soil moisture in Zone III (Fig.5.24 C). During the 'big dry', Zone II exhibited the most dramatic soil moisture loss among the three zones, with a consistent low profile showing nearly no seasonality (Fig.5.24 B). The 'big dry' amplitude of the variations in Zone II SM was less than 1/3 of those in Zone I (around 20 cm) and Zone III (around 18 cm), indicating a complete drying out of surface water and soil moisture in this region (Fig.5.24 B). However, the soil moisture fully recharged during the 'big wet' in all three zones including Zone II (Fig.5.24).

3) Vegetation

Vegetation showed strong correlations (r ~ 0.75) with TWS and SM across the three zones, with no lag or a 1 month lag (Table.5.3). Compared with TWS and SM, rainfall was well related to EVI but had lower correlations with longer lags (rainfall antecedent) in the three zones.

Over the decadal time period, the magnitude of EVI variations in Zone I was 0.115 (0.161, 0.276), which was twice that of Zone III (Fig.5.24 A, C). The high EVI values in Zone III were nearly equivalent to the low EVI values in Zone I, indicating the low vegetation cover in western and central Australia (Zone III) with most plants being of sparse woodland and shrubland type. north-eastern and northern Australia (Zone I) have large woody vegetation such as topical forests. Vegetation in Zone I stayed stable during the drought period and increased during the 'big wet' (Fig.5.24 A) while there was a growing mortality of trees over Zone III indicated by the decline in the baseline of the EVI profile, but vegetation recovered during the wet period (Fig.5.24 C). EVI in Zone II stayed vigorous with clear seasonal patterns regardless of the consistent low surface water and soil moisture in the region (Fig.5.24 B). This stable greenness over Zone II may be partly explained by the fact that crop lands, in which agricultural activities such as irrigation occur, account for one third of this zone.

EVI showed the lowest values in Oct-Dec 2009 across the three zones, which was around the end of the 'big dry' when the minimum TWS and SM occurred. The following 'big wet' replenished the water in most of Australia, causing the increases in vegetation, which nevertheless reversed again due to another dry phase of Australia right after this 'big wet'.

Table 5.3. Correlations among all the ecohydrological variables during Hydro 2002 and 2012.

Zone I	TWS	SM	GW	EVI	Rainfall
TWS	1.00	0.90	0.84	0.84	0.42
SM	0.90	1.00	0.52	0.94	0.47
GW	0.84	0.52	1.00	0.47	0.23
EVI	0.84	0.94	0.47	1.00	0.59
Rainfall	0.42	0.47	0.23	0.59	1.00
Zone II					
TWS	1.00	0.80	0.27	0.63	0.33
SM	0.80	1.00	-0.36	0.57	0.48
GW	0.27	-0.36	1.00	0.06	-0.25
EVI	0.63	0.57	0.057	1.00	0.32
Rainfall	0.33	0.48	-0.25	0.32	1.00
Zone III					
TWS	1.00	0.89	0.83	0.76	0.15
SM	0.89	1.00	0.49	0.82	0.24
GW	0.83	0.49	1.00	0.44	0.01
EVI	0.76	0.82	0.44	1.00	-0.06
Rainfall	0.15	0.24	0.01	-0.06	1.00

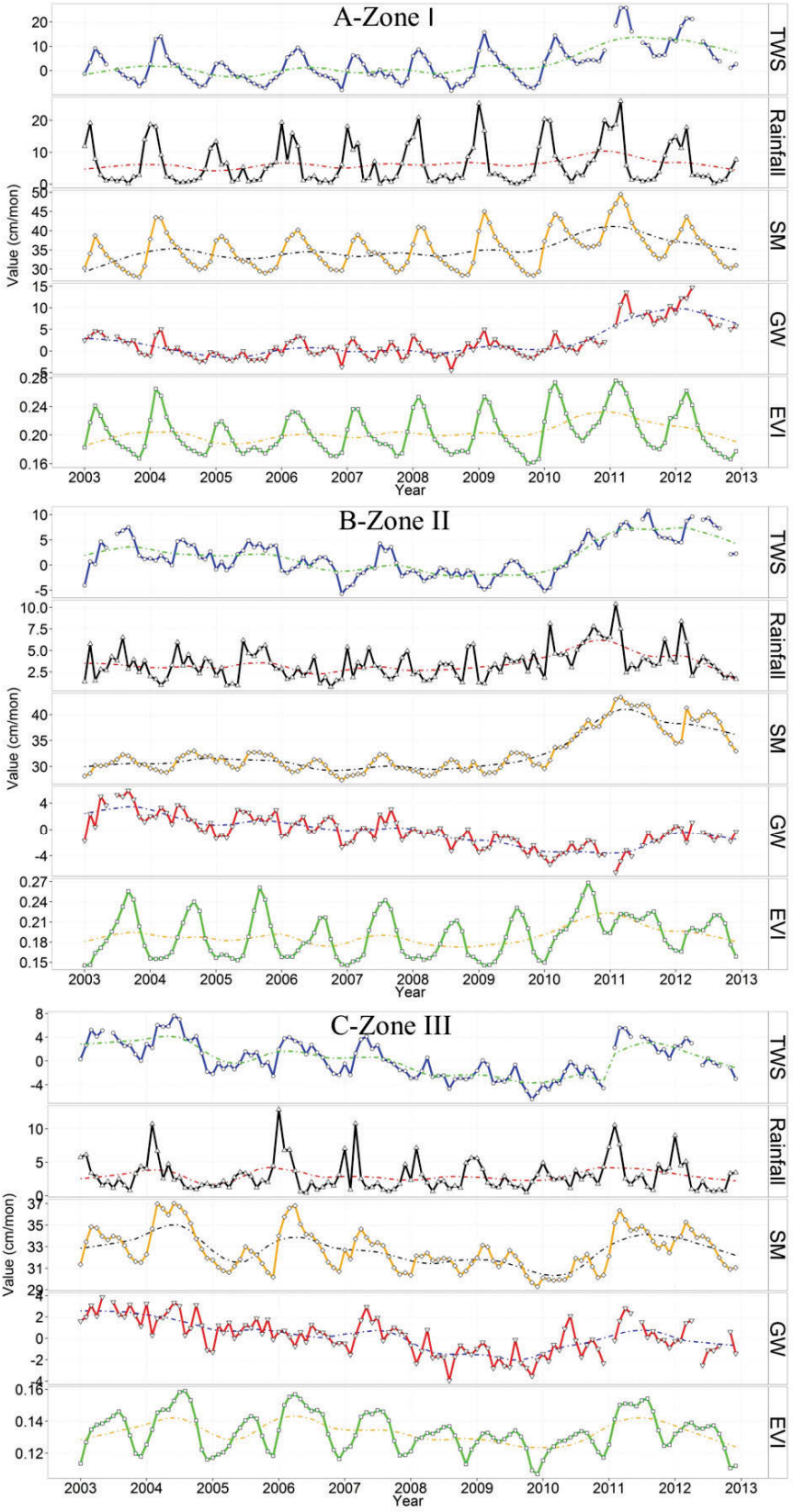

Figure 5.24. Monthly values of spatially averaged TWS and GW anomalies, rainfall, soil moisture and EVI over zone I, II and III with dashed lines representing the overall trend in each variable, of which the oscillating seasonal component has been removed.

The ecohydrological variables in Zone I, II and III, being controlled by the different climate systems, showed various seasonal patterns through the two hydroclimatic events (Fig.5.25). There was smooth and clear seasonality in TWS, EVI and rainfall over Zone I during both the 'big dry' and the 'big wet', with TWS and EVI having similar seasonal patterns which were following those of rainfall with a one month lag (Fig.5.25 A). EVI seasonal patterns in Zone II and III largely matched each other but had opposite phenology to those in Zone I (Fig.5.25 B-C). The rainfall seasonal patterns were similar across the three zones, which consequently may indicate rainfall seasonal variations did not favour those in EVI much in Zone II and III (Fig.5.25 B-C). Unlike rainfall, TWS showed double seasonal peaks in both Zone II and III in Austral spring and autumn respectively which supported vegetation growth during the spring season in these two zones (Fig.5.25 B-C). Therefore, TWS seasonal profiles showed much higher correlation with EVI across the three zones than those between rainfall and EVI. In general, the magnitudes of the three variables descends from Zone I to Zone III and from the 'big wet' to 'big dry' (Fig.5.25). However, the EVI profile in Zone III during the 'big wet' was equivalent to that in the 'big dry' (Fig.5.25 C), indicating that Zone III did not receive much more rainfall during the 2010-11 wet pulse. Moreover, the signals of variables in Zone I mostly drive the patterns of continental averaged seasonal patterns of these three variables (Fig.5.25 A).

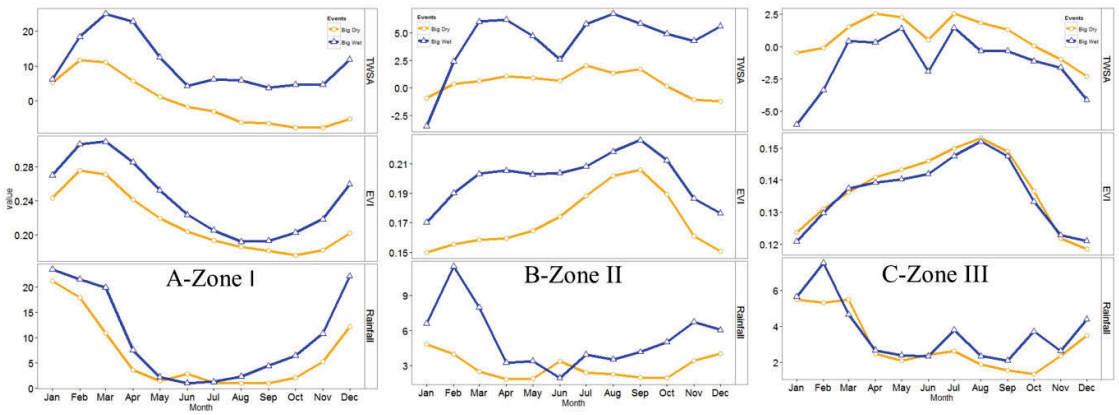

Figure 5.25. Seasonality of spatially averaged total water storage anomaly, EVI, and rainfall across (A) Zone I, (B) Zone II and (C) Zone III. Each point represents the monthly climatological mean from the 'big dry' and 'big wet' periods during the hydro 2002 to 2012.

b. Various responses of biome classes to hydroclimatic extremes across river basins

TWS drying and wetting patterns varied greatly across Australia's main river basins (Fig.5.26). The Murrary Darling Basin (MDB) was found to be the most sensitive basin to the recent hydroloclimatic extremes, exhibiting the most dramatic swings in water loss/gain over the drought and wet periods (Fig.5.26 B-d). In particular, the most severe drying and wetting hydrologic dynamics occurred in the southern part of the MDB. The south-western Coast basin had both the longest drought and wetting periods (Fig.5.26 B-k). The Gulf of Carpentaria (Fig.5.26 B-b), Northeast Coast (Fig.5.26 B-e) and Timor Sea (Fig.5.26 B-i) Basins were not affected by the 'big dry', while the Indian Ocean (Fig.5.26 B-j), south-western Coast and most of the Western Plateau (Fig.5.26 B-h) basins did not recover the water lost during the 'big dry' from the 'big wet' pulse. Moreover, The Western Plateau basin had the most extensive water depletion area spanning from the north-western to south-eastern boundaries during the 'big dry'. In general, the patterns of the 'big wet' peak timings shown in Chapter 2 (Fig.2.3) were similar to the river basin boundary maps (Fig.5.26), which may indicate the wet pulse terminated on a basin-scale order.

In addition, six sub sites across the river basins with significant TWS drying and wetting trends through the 'big dry' and 'big wet' were chosen to conduct a cross-site study with regard to the impacts of hydroclimatic extremes on various biome classes at different geographic areas of Australia (Fig.5.26). We named them based on their corresponding locations as Site-1:Northwest; Site-2:Central; Site-3:MDB; Site-4:Southwest; Site-5:Northeast ; Site-6:North.

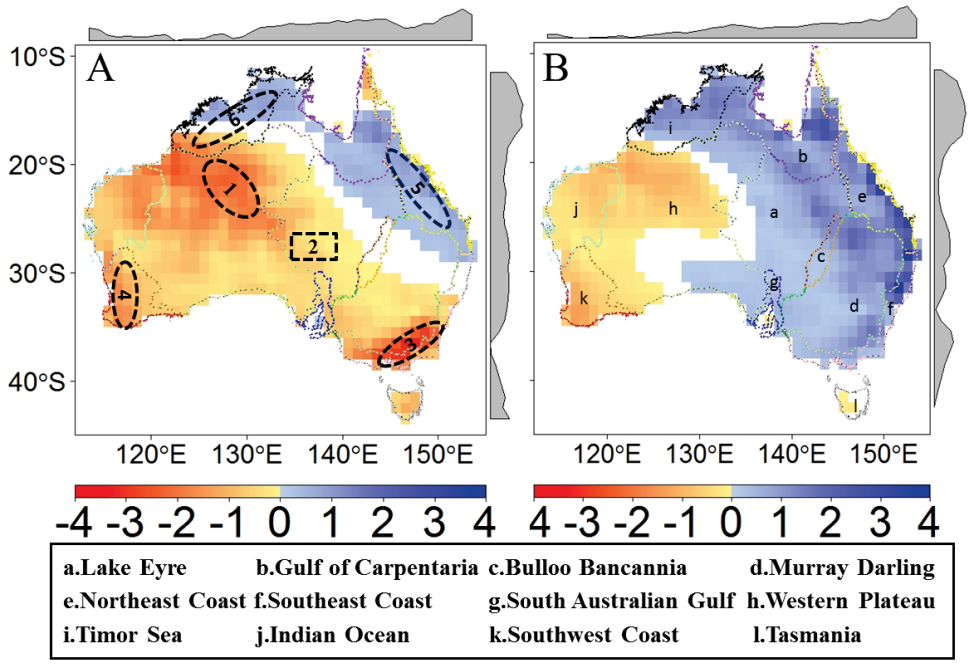

Figure 5.26. TWS rates of change in the (A) 'big dry' and (B) for the combined 'big dry' and 'big wet' period, with labelled boundaries of Australian major river basins and the selected six study sites.

1) Biome level ecological responses to dry and wet events across sites

There is a large diversity of biome classes across the six sub study sites, ranging from grass and shrublands to woodlands, from farmlands to natural forests, and from land vegetation to wetland ecosystems located across various river catchments and climatic zones (Table.5.4). Annual values of spatially averaged TWSA and EVI over the six sites, from 2003 to 2012, show fluctuations through the years, involving differences in the direction, magnitude, and duration of water sources and ecosystem (biome classes) responses to drought and wet periods (Fig.5.27). During the dry period, EVI across all the sites closely followed the trends in TWS, with vegetation declining in 3 sites (Northwest, Southwest and MDB) and increasing in the sites of the Northeast and North (Fig.5.27 B). Sparse vegetation in the central Australia site stayed relatively stable despite the large reduction in TWS occurring there but with very low EVI values during this period. When the 'big wet' arrived, there was broad vegetation revival across most of the sites due to the dramatic increases in TWS except in the Southwest site where the drought was still occurring on (Fig.5.27 A-B). Vegetation growth in these sites continued until 2012 when the EVI decreased again after the 2010-11 wet period

(Fig.5.27 B). In general, the six study sites showed a strong relationship between TWS and EVI across all biome types. However, we found that TWS was the most related to sparse vegetation, grass and shrublands with an average correlation of 0.7 while there were relatively lower correlations with forest and agricultural ecosystems (r = 0.42). This may suggest the strong resilience and sensitivity of semi-arid and arid ecosystems in Australia.

Table 5.4. Summary of the six sub study areas

Site	Center Longitude (°E)	Center Latitude (°S)	Major Vegetation Group (MVG)
Northwest	125.18	21.40	•Hummock Grasslands
Central	133.10	24.10	•Hummock Grasslands •Acacia Shrublands •Acacia Open Woodlands •Tussock Grasslands •Eucalypt Open Woodlands •Other sparse woodlands
MDB	146.20	36.60	•Agriculture farmlands •Eucalypt Open Forests (trees 10 to 30m tall) •Heathlands
Southwest	117.52	32.24	•Agriculture farmlands •Eucalypt Open Forests (trees 10 to 30m tall) •Mallee woodlands and shrublands
Northeast	145.25	19.53	•Eucalypt Woodlands •Eucalypt Open Woodlands •Rainforests and Vine Thickets •Melaleuca Forests and Woodlands •Other Open Woodlands
North	129.60	15.14	•Tropical Eucalypt Woodlands/ Grasslands •Eucalypt Woodlands •Eucalypt Open Woodlands •Rainforests and Vine Thickets

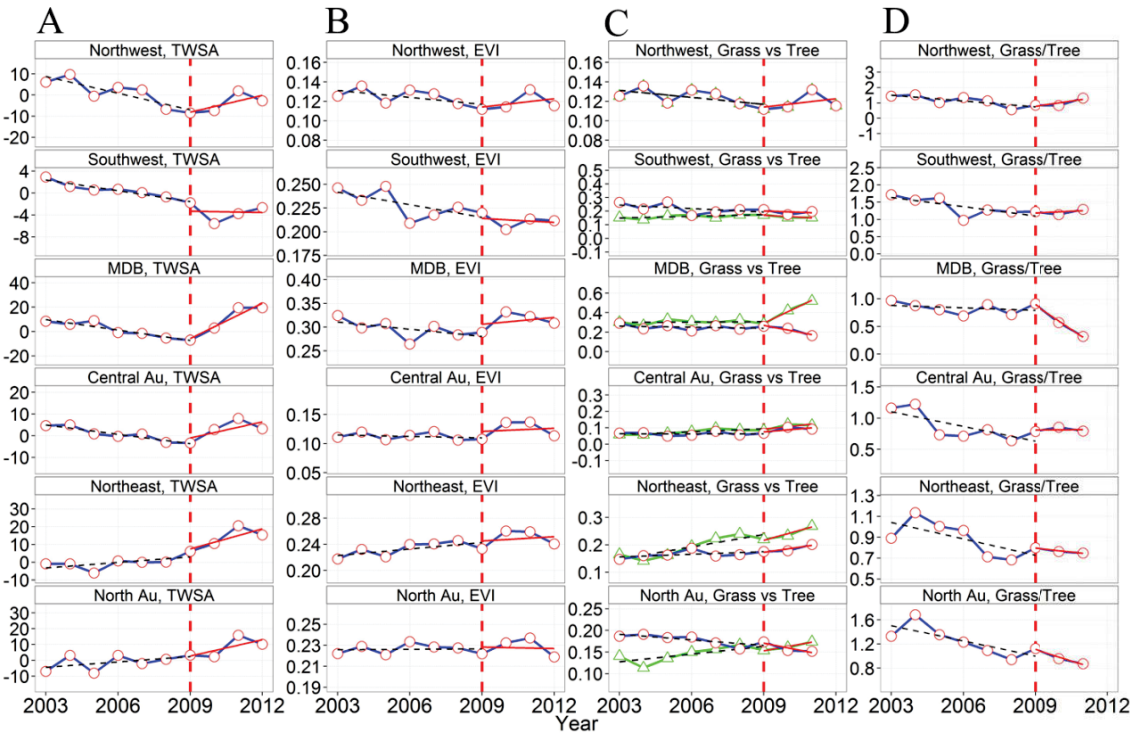

Figure 5.27. (A) Annually averaged TWSA; (B) EVI; (C) Persistent (green) and recurrent (blue) fPAR; and (D) ratio between Persistent and recurrent fPAR over the six sites across Australia during 2003 and 2012.

2) Grasses and Trees on drying and wetting across sites

Previous studies have shown that there was a differential response of vegetation functional types (perennial woody and ephemeral herbaceous vegetation types) to recent climatic changes in Australia (Donohue et al. 2009; Lu et al. 2003; Ma et al. 2013). The Australian Persistent and Recurrent fPAR datasets (described as the fraction of Photosynthetically Active Radiation absorbed by vegetation) provided by CSIRO, representing non-deciduous perennial vegetation and deciduous ephemeral deciduous vegetation respectively, were used in this section to study the separate responses of trees and grasses across the six sites to the recent dry and wet hydroclimatic extremes. There is only one herbaceous vegetation type (Hummock grasslands) in our Northwest Site-1, for which we only used EVI data.

We observed distinct impacts of hydrological variations on persistent vegetation types (trees) and recurrent vegetation types (grasses) across the study sites through the dry and wet hydroclimatic events (Fig.5.27 C). Grasses across most of the study sites, encompassing both water-limited and energy-limited areas, were found to be

significantly browning during the 'big dry', even in the North site where TWS was increasing during that period (Fig.5.27 C). The 'big wet' did not seem to favour the grasses much, with recurrent vegetation in four sites not being able to recover to the previous drought level (Northwest, Southwest, MDB and North). By contrast, trees stayed stable in the Southwest site and had overall significant increases in the rest of the sites regardless of the dry conditions during the 'big dry' (Fig. 5.27 C). The persistent greenness of perennial woody types suggests that the decreasing signal presented in the EVI profile may be mostly contributed by the recurrent vegetation types (Fig.5.27 B).

We also calculated the grass/tree ratios for the six sites and found all of the ratios went consistently down from 2002 to 2012, which indicated that grasses declined during these two hydroclimatic events relative to trees (Fig.5.27 D). Our results revealed that woody and herbaceous types have different inter-annual responses to the dry and wet events with recurrent vegetation types (grass) being more sensitive and fragile to the hydroclimatic extremes. The persistent vegetation type (trees) was shown in this study to have higher stability and resilience to the extreme hydrological variations, which reflects the ability of woody plants to increase their rooting depths and competitively suppress grass growth. This corroborates the previous studies that showed without changing the total amount of precipitation, increases in precipitation intensity can push soil water deeper into the soil, increase aboveground woody plant growth and decrease aboveground grass growth in systems like Australian arid and semi-arid ecosystems (Donohue et al. 2009; Kulmatiski and Beard 2013).

c. Macro-hydroclimatic impacts on micro-ecology at specific sites

Australia's recent large-scale but unevenly distributed drought and intensive wet pulse also provide unique opportunities and an ideal natural setting to assess the impacts of macro-hydroclimatic extremes on micro-ecology at specific sites. In this section, mangrove forests, one of the most important ecosystems for Australia were studied to evaluate the local ecohydrological processes under the large-scale hydroclimatic contexts, which will lead to advances in ecological research of local-scale specific plant species and improve our understanding of how they will respond to global climate change.

Three mangrove study sites were chosen in the Dampier Peninsula, northwest Australia where a serious water loss in the 'big dry' and insufficient water recharge during the wet period were observed (Fig.5.28). For contrast, we selected another three mangrove sites (at a similar latitude) in the Gulf of Carpentaria, west Queensland that showed no drought during the dry period and dramatic increases in TWS during the 'big wet' (Fig.5.28).

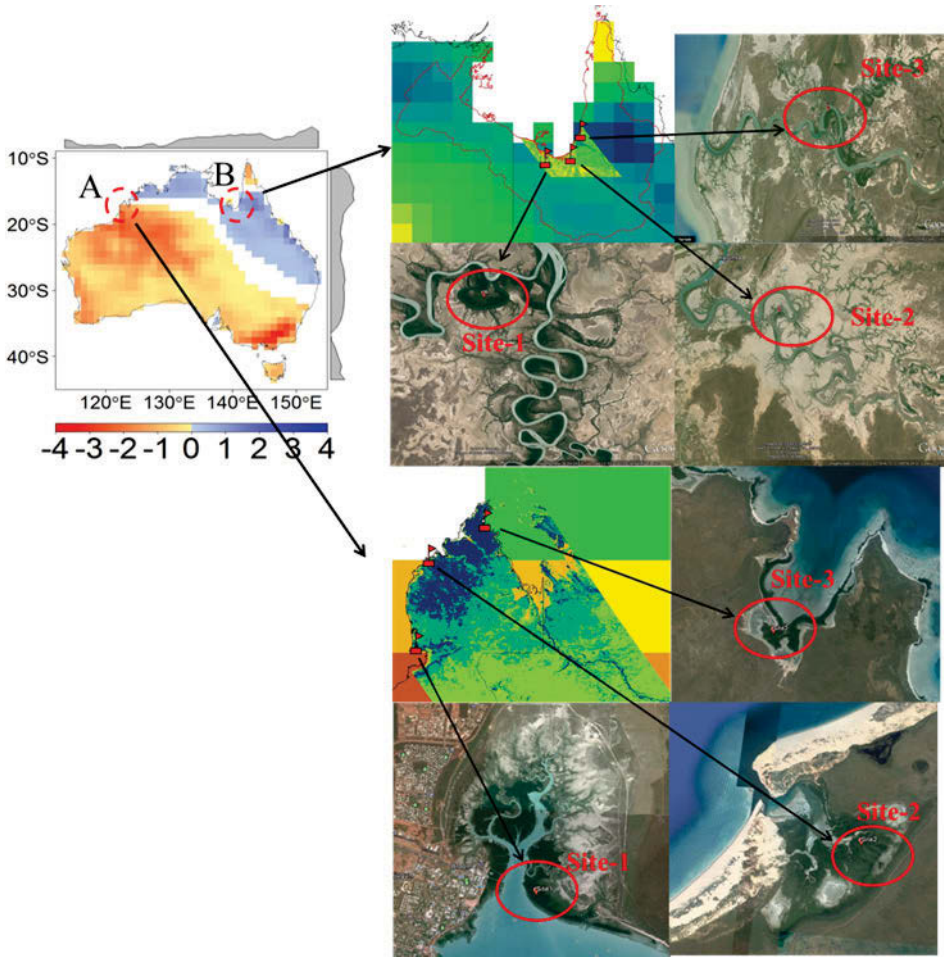

Figure 5.28. Six mangrove study sites with three in (A) Dampier Peninsula, northwest Australia and (B) another three in the Gulf of Carpentaria, west Queensland.

1) Connections between macro-hydrology and micro-ecology at specific sites

The monthly EVI values of mangroves over the six sites in Dampier and Queensland, from 2000 to 2014, exhibited greenness fluctuations in mangrove forests on both seasonal and inter-annual temporal scales (Fig.30). Our mangrove study sites in both Dampier and Queensland are located in the tropical zone of Australia, in which mangroves in all sites showed similar seasonality with EVI values peaking in dry

seasons (between April and October) and low values in wet seasons (between November and March). Another mangrove boom with smaller magnitude around February was also observed in some of the sites (Fig.30).

A deseasonalized time series of spatially averaged EVI over the sites in Dampier and Queensland, and the corresponding deseasonalized TWS values at pixel-site where the mangrove study sites were located during 2000 - 2014 were calculated and plotted in Figure.5.29. We found EVI over the mangrove forests in Dampier sites closely followed TWS variations, which significantly decreased during the 'big dry', and recovered during the wet period, then declined again when TWS reversed into another dry phase (Fig.5.29 A). The three sites in Dampier had overall downward trends in EVI with the mangrove forest in site-3 showing the sharpest loss trend (Fig.5.20 A). By contrast, through the entire study period, Queensland mangrove sites all showed increases in EVI, following the strong upward trends in the TWSA values at the corresponding pixel-sites ($p < 0.05$). In addition, the magnitude of the trends in mangrove EVI across the three sites is connected to those in TWS, with bigger trends in TWS at the pixel-site causing sharper EVI increasing growth rates (site-2 EVI in Fig.5.29 B).

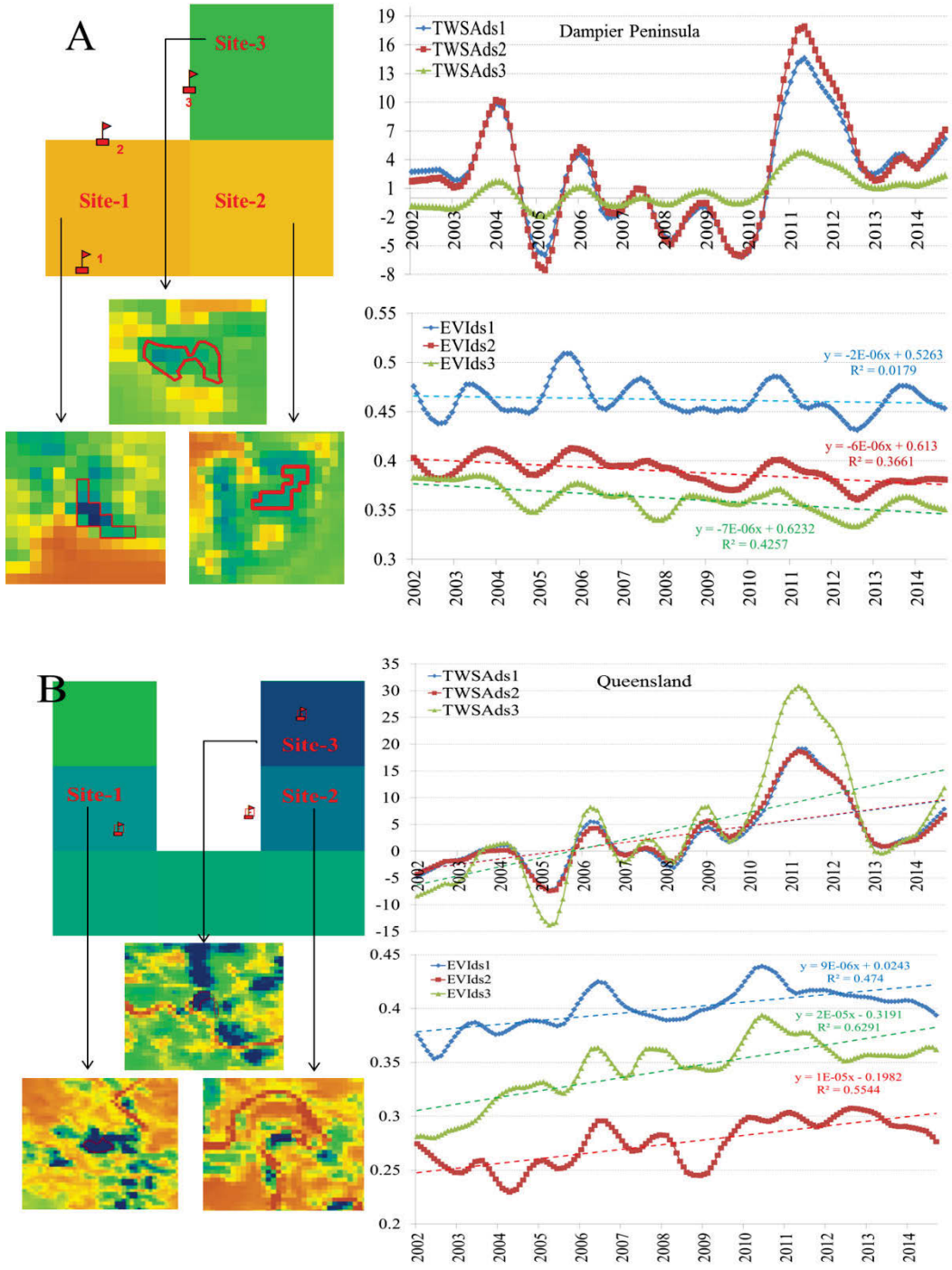

Figure 5.29. Deseasonalized time series of spatially averaged EVI over the sites in (A) Dampier and (B) Queensland, and the corresponding deseasonalized TWS values at pixel-site where the mangrove study sites are located from 2000 to 2014.

2) The impacts of the 'big wet' pulse on mangroves

Interestingly, we found similar patterns in the response of mangroves across both Dampier and Queensland sites to the 2010-11 'big wet' pulse, with TWS increasing for

the 1.5 to 2 years but mangrove EVI only followed for around one year and then started declining (Fig.5.30). More fresh water in the coastal waterways going from inland to sea, indicated by the increase in TWS, could be the reason for the mangrove boom. However, the earlier reversal of mangrove EVI increases might be due to several reasons. For example, 1) the 2010 sea level fall increased the salinity along the coast which led to a decline in mangroves; 2) flooding along the waterways or the coast resulted in anoxic environment, causing the decrease in mangroves. Further studies are needed to untangle this phenomenon.

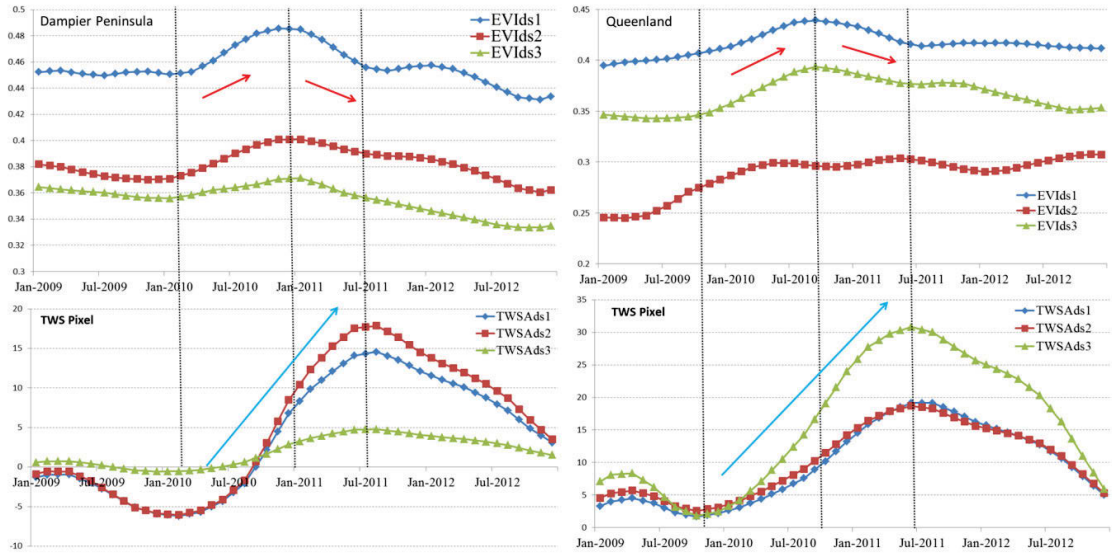

Figure 5.30. Deseasonalized time series of spatially averaged EVI over the sites in (A) Dampier and (B) Queensland, and the corresponding TWS values at pixel-site where the mangrove study sites during the ending year of the 'big dry'(2009) and the 'big wet' period (2010 and 2011).

We also further explored the changes in Chlorophyll-a and Salinity near our mangrove sites which are supposed to be closely connected with fluctuations in the photosynthetic activity of mangroves. We found the Chlorophyll-a along the coast is higher in the Austral winter (July) and relatively lower in the Austral summer (Jan) as cold water tends to have more nutrients than warm water and brings a Chlorophyll-a boom. This may result in the observed mangrove winter boom across the six selected study sites in Dampier and Queensland. In addition, sea surface salinity around our mangrove sites was found to be higher during the summer than that in winter. This also corresponded to the observed higher mangrove greenness during the winter which may be attributed to the low salinity that relieved the stress of mangroves.

5.4. Discussion

5.4.1. Water resources in the balance under hydroclimatic extremes

5.4.1.1 A land of more extreme droughts and flooding rains

Based on a range of climate models, the Intergovernmental Panel on Climate Change (IPCC) identifies that among the important consequences of climate change, a shift in location, magnitude and frequency of various precipitation, temperature and other extreme events are likely to happen in future climate scenarios (AghaKouchak et al. 2014; Cai et al. 2014; IPCC 2014). In particular, recent remote sensing research, model studies and empirical evidence suggest that precipitation regimes, as a result of global warming, have become more extreme at global-scale levels, defined as dry seasons and locations are getting drier and wet areas and periods are becoming wetter (Chou et al. 2013; Chou and Lan 2012; Durack et al. 2012; Easterling et al. 2000). This effect is often termed as the "rich-get-richer mechanism" (Emori and Brown 2005; Held and Soden 2006) or the "thermodynamic contribution" (Chou and Neelin 2004; Chou et al. 2009). Studies show this intensification of the hydrological cycle has been observed to increase during the last few decades around the world in both spatial and temporal domains with negative consequences to production and rain use efficiency of terrestrial ecosystem (Famiglietti and Rodell 2013; Trenberth and Dai 2007; Zhang et al. 2013). These changes in hydroclimatic events such as droughts and flooding among other anomalies have a clear adverse effect on human comfort and health, ecosystem resilience, and food security (Wheeler and von Braun 2013).

Australia is a land of extremes, and famously of 'droughts and flooding rains'. That's been truer than ever in the 21st century, and since 2000 the country has see-sawed from drought to deluge with surprising speed (Cleverly et al. 2016b). Observed increases in monsoonal rainfall in northern and northeastern Australia and decreases in rainfall across southern and western areas since 1900 are consistent with a generalised wetter tropics and drier mid-latitudes scenario (CSIRO and BOM 2014). The recent severe and prolonged Millennium drought and an immediate record wet pulse also hit Australia with a strong spatial variation, which was indicated by our GRACE-TWSA results based on geostatistics, revealing a short-term intensification of the water cycle in Australia.

Too little or too much rain can each be problematic, and when both happen in quick succession, it will bring larger negative impacts. In natural ecosystems, bushfires across Australia will become more likely as the plants swing between exceptional growth and subsequent drying and death, leaving behind large amounts of fuel. To provide extra resilience to the changing conditions, farmers, in particular, may need to diversify their livestock numbers and crop types (Cleverly et al. 2016a). Studying the responses of Australia to hydroclimatic extremes is essential for farmers and everyone else on the land to adapt to Australia's droughts as well as floods.

5.4.1.2 GRACE satellite observed hydrological performance

Corroborating with the spatial patterns of our TWS intensification, recent precipitation studies showed a 10~20% loss of autumn and winter rainfall over both the southwestern and southeastern tips of the Australia. This systematically reduced inflows to dams and led to progressive depletion of water storage over these areas (Gergis et al. 2012). For the southeast, rainfall during 2010 and 2011 brought meaningful relief after 15 dry years while the southwest received the rainfall pulse much later with a smaller amount. In the meantime, eastern Australia as a whole (the states of Queensland, New South Wales, and Victoria) received the highest springtime rainfall on record since 1900, resulting in widespread floods (Heberger 2011; Hendon et al. 2014; Lim and Hendon 2015).

Our study indicates a west to east spatial intensifying pattern in rainfall across the 'big dry' and 'big wet', with rainfall decline in the drought and there was insufficient supplementation during the wet period over western Australia. In comparison, increasing and large gains in rainfall were observed over eastern Australia during the dry and wet events (Fig.5.11). Despite the similarities between the dry-wet patterns in rainfall and TWS, we found GRACE derived TWSA was more sensitive to hydroclimatic extremes than rainfall, which sometimes cannot capture the severe dry conditions. We also observed that in contrast to the random and intensive characteristics of rainfall, the TWSA time series is relatively stable with a buffering changing rate. Given the dynamics and complexity of water cycles in Australia, the observed total water storage anomaly (TWSA) from GRACE can provide a good

indicator of hydrological performance over large-scale areas during the drought and flooding periods.

5.4.1.3 Water balance derived ET_{WB} vs AWAP modelled ET_{AWAP}

Monthly Australia-wide ET data over 2002 - 2013 were estimated based on the water balance approach. AWAP ET (ET_{AWAP}) and TRMM rainfall products with higher resolutions (5 km and 25 km respectively) were used in this section to validate this ET product (ET_{WB}) over Australia.

Averaged annual ET_{WB}, ET_{AWAP} and rainfall from 2002 to 2013 exhibited analogous spatial patterns across the continent (Fig.5.31). Being primarily driven by rainfall, ET_{WB} and ET_{AWAP} had consistent distribution patterns, both showing higher ET in northern Australia, along the eastern coast and in the southwestern tip with lower ET in the Australian outback. The continental averages of the mean annual ET_{WB}, ET_{AWAP} and rainfall are 46.13, 41.62, 54.03 cm/yr respectively, indicating the high evapotranspiration across Australia with more than 80% of rainfall returned back to the atmosphere.

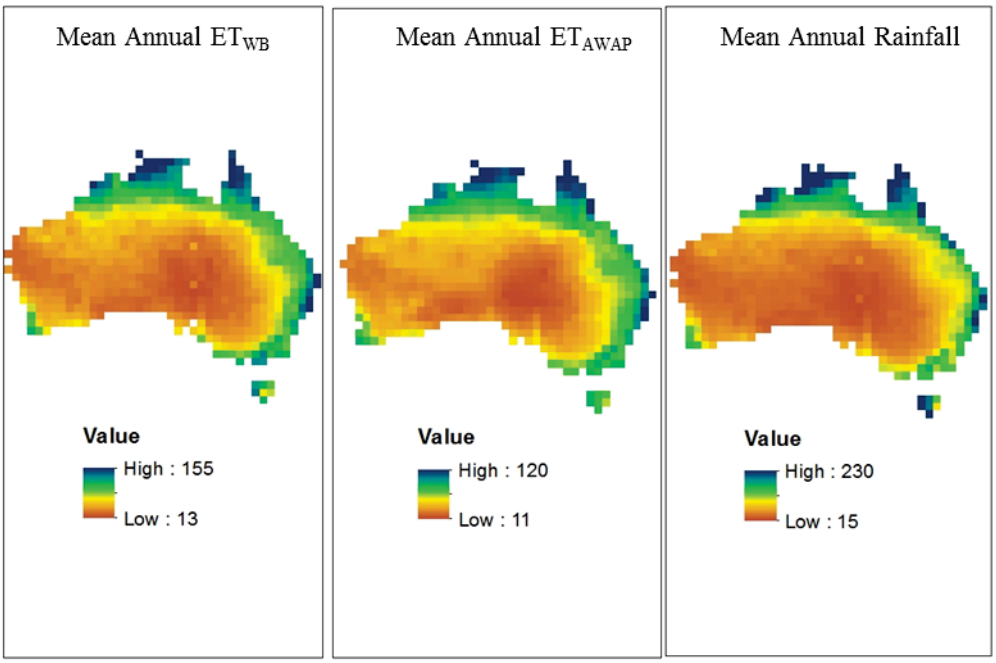

Figure 5.31. Spatial distributions of mean annual ET (ET_{WB} and ET_{AWAP}) and rainfall during Hydro 2002 - 2012 (cm/yr) across Australia.

Spatial correlation coefficients between monthly ET_{WB}, ET_{AWAP} and rainfall during Hydro 2002 - 2012 were calculated to show their relationships across Australia (Fig.5.32). In general, ET_{WB} and ET_{AWAP} are well correlated over the continent with a mean correlation of 0.45. ET_{WB} followed rainfall well, and the correlation coefficient between them at most of the locations over the continent is higher than 0.7, indicating rainfall as the major driver of ET in Australia. However, we observed a low correlation between ET_{WB} and rainfall in the two main Australian agricultural regions (southeastern and southwestern corners). This may indicate that even though 95% of the crop lands in Australia are rain-fed, human management still exerts a big impact on these areas which in turn changes the natural patterns of terrestrial ET.

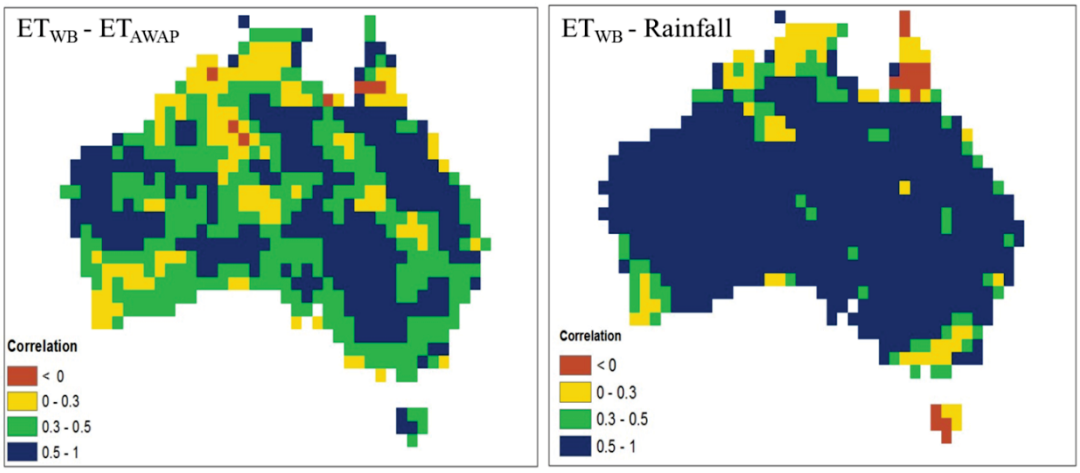

Figure 5.32. Pearson's correlation coefficients (r) between monthly (A) ET_{WB} and ET_{AWAP} , (B) ET_{WB} and rainfall from Hydro 2002 to 2012.

Temporally, the monthly time series of ET_{WB} and ET_{AWAP} highly matched each other during the study period (Fig.5.33). We investigated the relationships among ET_{WB}, ET_{AWAP} and rainfall on both monthly and annual scales and found a strong correlation of 0.54 between monthly ET_{wb} and ET_{AWAP}, both of which are all highly related to rainfall (Table.5.5). In addition, correlations among the three annual data were even stronger (Table.5.5).

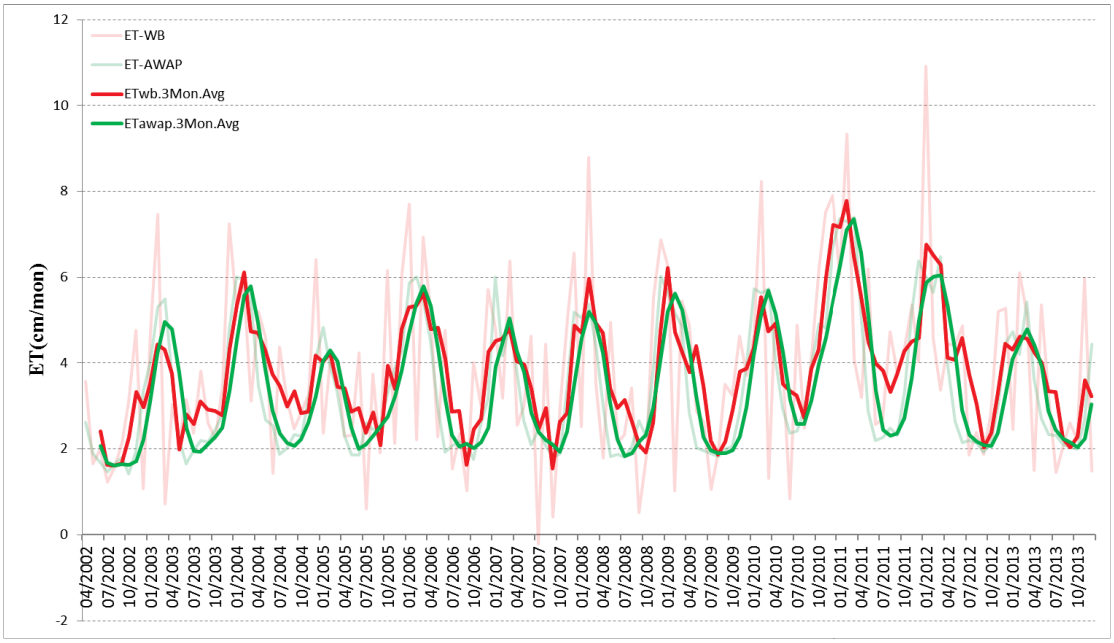

Figure 5.33. Time series of monthly mean ET_{WB} and ET_{AWAP} over the Australian continent with their 3-month running means.

Table 5.5. Pearson's correlation coefficients (r) between a) monthly ET_{WB}, ET_{AWAP} and rainfall; and between b) annual ET_{WB}, ET_{AWAP} and rainfall during Hydro 2002 - 2012.

a)	GET	AET	Rainfall
GET	1	0.54	0.65
AET	0.54	1	0.89
Rainfall	0.65	0.89	1

b)	GET	AET	Rainfall
GET	1	0.962833	0.918042
AET	0.962833	1	0.977762
Rainfall	0.918042	0.977762	1

Comparison between the two ET products was also evaluated on a pixel level between the mean annual ET_{wb} and ET_{AWAP} over Hydro 2002 - 2012. We found a near 1:1 trend among all the ET_{wb} and ET_{AWAP} 1 °x 1 ° pixels, indicating a good match between these two ET datasets (Fig.5.34A).

Relative error in the annual ET_{wb} during the decadal period was computed to estimate the overall uncertainty of the water balance approach derived ET. We found the 95% confidence interval is ± 1.9 cm/yr and around 4% of ET_{wb} product (Fig.5.34 B). Biases in the model estimates were consistent over time and on the same order as the GRACE uncertainty. It thus demonstrates the high accuracy of the ET_{wb} product.

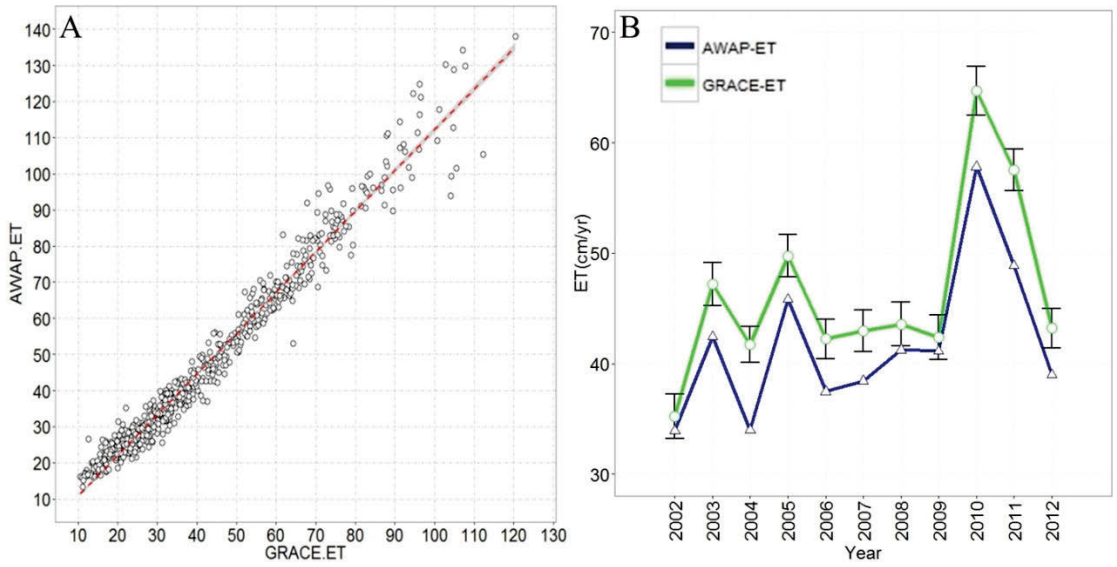

Figure 5.34. (A) Scatter diagram of mean annual ET_{wb} and ET_{AWAP} from Hydro 2002 to 2012, with dots representing pixel values of ET_{wb} and ET_{AWAP}; (B) Annual profiles of ET_{wb} and ET_{AWAP} during Hydro 2002 - 2012 with Y error bars standing for the 95% confidence interval of ET_{wb}.

In summary, according to all the analyses mentioned above, it is reasonable to draw the conclusion that monthly ET products estimated by our water balance approach, using input terrestrial water storage anomaly (TWSA) data from the GRACE satellites, precipitation and in situ runoff measurements, are accurate, easy to update and consistent with the Australian AWAP modelling ET dataset which has already been validated (Raupach et al. 2009). Moreover, a previous study has demonstrated the importance of using GRACE-TWSA for ET estimation based on the water balance equation, as using the methods ignoring total water storage changes, will significantly bias ET estimation, especially in regions of low ET (Zeng et al. 2012).

5.4.2. Impacts of the two hydroclimatic events on ecosystem functioning

5.4.2.1 Low association between vegetation and TWS indicates the potential stress of ecosystem under extreme hydrolicmatic impacts

Figures 5.22 and 5.23 showed that the scatter diagrams between rainfall and EVI across Australia exhibited a shape of a two-branch "fork", with pixels of lower TWSA-EVI correlation ($r < 0.5$) centred on the upper branch of the "fork". We further

investigated the ecohydrological dynamics in the pixels where TWSA was not well correlated with EVI during our study period and found TWS in these areas showed weaker recovering capacity than EVI to hydroclimatic extremes. During the 'big dry', TWS in these pixel areas kept decreasing even when rainfall had started increasing while it continued to increase for a while during the wet period regardless of the drop in rainfall. This lagged recovery of TWS may indicate its high sensitivity to hydroclimatic events, of which variations and seasonality can be easily disturbed by the dry and wet extremes. In addition, we observed a strong adaption of vegetation in the low TWSA-EVI correlation points on the upper branch during the 'big dry' and 'big wet'. These are mostly crops which are managed by farmers with irrigation etc and a few vegetation types associated with Groundwater Dependent Ecosystems (GDEs) that have long roots to get water from deep soil water and groundwater. As a result, the low correlations between TWSA and EVI were mostly attributed to the disagreement between the trends in TWS and vegetation over agricultural and GDEs areas. For example, the Murray-Darling Basin in southeastern Australia experienced the most dramatic swings during the dry and wet periods, with TWS over this region showing a consistent decline, followed by a sharp jump. However, as most of this region is covered by agricultural lands with some GDEs, broad weak correlations between TWSA and EVI were recorded across MDB. By contrast, the pixels that showed the strongest TWS and EVI correlations were located in areas where either 1) no big climatic events occurred during the study time and both TWS and vegetation stayed stable or 2) there were extreme hydroclimatic events but the vegetation inside was very sensitive to the changing climate (e.g. herbaceous plants), which closely followed the variations in TWS.

The largest number of pixels with weak TWSA and EVI correlations were found in the Hydro years of 2008 and 2010 (Fig 5.23), which were identified to be the driest and wettest years during our study period. Thus, this may indicate that the more extreme hydroclimatic events the year experienced, the more areas with low TWSA and EVI correlations might be found on the upper branch of the "fork", which to some extent can reflect the impacts of hydroclimatic extremes on vegetation over areas. Our results, revealing low associations between TWSA and EVI, may indicate potential stress of an ecosystem under extreme hydroclimatic events. Plants have a certain degree of tolerance to water deficiency and some can live on groundwater when it is dry such as GDEs. However, continuing hydroclimatic events like droughts or flooding may cross the

threshold and make vegetation collapse due to the rising mortality rates. Although detrending TWSA and EVI datasets can largely improve their correlation over agricultural areas, using the original data is still a good way for us to achieve the early warnings for the risks to ecosystems across Australia under hydroclimatic extremes.

5.4.2.2 GRACE satellite observed hydrological controls on vegetation over mainland Australia

Corroborating with previous studies (McGrath et al. 2012; Yang et al. 2014), in general we found a closer correlation between vegetation and TWS than that between vegetation and precipitation across the continent. Of all the ecosystems studied, TWSA has the strongest relationship with EVI in savanna, shrub land and grassland, which are very sensitive to altered hydroclimatic conditions (Fig 5.27). In addition, we also observed that monthly EVI has larger time lags with precipitation than with TWS over the continent, suggesting precipitation may not be a direct measure of water availability to vegetation while GRACE-TWSA data can be used to monitor the water available for terrestrial ecosystems, agriculture and human consumption.

Over areas without large surface water bodies such as big reservoirs, lakes or rivers, variations in TWS are mainly driven by groundwater storage (GW) and soil moisture (SM) changes. Given the lack of groundwater and soil moisture data for extensive regions, there is great potential in using GRACE-TWSA data to evaluate hydrological controls on vegetation dynamics across large areas. GRACE observations have been widely used in hydrological and geodesic studies (Chen et al. 2010; Di Long 2013; Leblanc et al. 2009; Velicogna and Wahr 2006) and have recently also been used as a highly valuable measurement in ecological or ecohydrological research (Guan et al. 2015; Jones et al. 2014; Xie et al. 2016a; Xie et al. 2016b).

We studied ecological responses to the 'big dry' and 'big wet' events across the continent and found that TWS patterns were the primary drivers of EVI dynamics, rather than rainfall. EVI temporal patterns, although highly correlated with TWS, showed less significant changing trends, which may suggest buffering mechanisms and vegetation resilience. This chapter highlights the GRACE derived TWSA observations as a valuable indicator for both hydrological and ecological systems performance, and shows GRACE as an important tool for achieving a better understanding of impacts of

the hydroclimatic extremes on water resources and ecosystem functioning across Australia.

5.4.2.3 Future study on macroecology of mangroves in Australia

Mangroves are uniquely adapted trees and larger shrubs that inhabit the tidal sea edge, which offer many benefits to both natural systems and humans including coastal erosion prevention, provision of nursery areas for fish and shrimp, water filtration, medicinal ingredients and the attraction of tourists, amongst many other factors. Nearly a fifth of the coast of Australia is surrounded by mangrove-lined coast, being the third largest area of mangroves in the world after Indonesia and Brazil. In 2015, a dramatic, pronounced extreme level of mangrove dieback occurred in Australia, with close to 10,000 hectares of mangroves having across a stretch of coastline reaching from Queensland to the Northern Territory. Concurrent with Great Barrier Reef coral bleaching, these recent natural disasters may result from a combination of extreme temperatures, drought and lowered sea levels that were associated with a strong 2015 El Niño event (Duke and van Oosterzee 2017).

Most of the previous studies on mangrove forests focused on their local ecological dynamics (e.g. tolerance to salinity and hypoxia, litter fall, zonation and production etc), with little attention to the historical and evolutionary and especially large-scale hydrological environmental contexts that can exert strong influences on local ecohydrological processes (Ellison 2002). Recent studies suggested that studying large-scale hydrological contexts that constrain local processes (i.e. a "macroecology of mangroves") can provide us with new insights of the dynamics in the function and structure of mangrove ecosystems (Ellison 2002). Moreover, such analyses can test whether general rules that have been identified for upland forest ecosystems also apply to the mangrove ecosystems.

Future studies based on multi-sensor satellite observations with various spatial resolutions and physical properties (surface reflectance, microwave and gravitational anomaly), integrating with other ground observational datasets, are needed to better understand the large-scale hydrological impacts on local ecological process. This, in turn, will advance the ecological research of mangrove forest and better protect them from the changing climate.

5.5. Conclusion

In this study we investigated spatial patterns and temporal dynamics of water resources and ecosystems across Australia during the recent 'big dry' and 'big wet' events, by integrating GRACE and other satellite observations with field and modelling data. We focused on conducting a compilation of small experiments on monitoring and analysing changes in various hydrological factors (TWS, rainfall, ET, soil moisture, groundwater and runoff etc) and ecological components (e.g. grass and trees), and their interactions under these extreme hydroclimatic events.

First, 1) results based on geostatistics confirmed the temporary sign of water cycle intensification in Australia during the study period, with water storage increasing in dry areas (western Australia) while decreasing in wet areas (north and northeastern tropical/semi-tropical region); 2) meanwhile, we observed a general close relationhip between rainfall and TWS (rainfall antecedent) but demonstrated that GRACE-TWSA is better than rainfall in detecting drought especially "hidden drought", groundwater depletion; 3) moreover, monthly ET and groundwater variations derived from water balance equation based on GRACE observations were found to be reasonable; 4) we observed ET significantly increased during the 'big dry', which may partly explain the conflict between the continent-wide decreasing TWS and increasing rainfall during the dry period; 5) we also found that soil moisture across Australia largely drives the seasonal variations in TWS while groundwater contributes to its long-term trends; 6) our results showed that TWS has overall better, spatially more uniform and temporally more direct correlations with surface greenness than rainfall across Australia, indicating GRACE-TWSA as a valuable indicator for ecological system performance particularly under hydroclimatic events.

Future studies are needed to conduct a comprehensive program, involving a combination of remote sensing techniques, ground observations, ecohydrological models and climate systems imitation etc, in order to better understand the environmental and economic impacts of climate change, and in particular, the increasing frequency and intensity of extreme weather events. This kind of project will help decision-makers make safe decisions about infrastructure, health, water management, agriculture, biodiversity and housing that will have lasting effects on future generations.

5.6. References

AghaKouchak, A., Cheng, L., Mazdiyasni, O., & Farahmand, A. (2014). Global warming and changes in risk of concurrent climate extremes: Insights from the 2014 California drought. *Geophysical Research Letters, 41*, 8847-8852

Allen, C.D., Macalady, A.K., Chenchouni, H., Bachelet, D., McDowell, N., Vennetier, M., Kitzberger, T., Rigling, A., Breshears, D.D., & Hogg, E.T. (2010). A global overview of drought and heat-induced tree mortality reveals emerging climate change risks for forests. *Forest ecology and management, 259*, 660-684

Atkinson, P.M., & LLoyd, C.D. (2007). Non-stationary variogram models for geostatistical sampling optimisation: An empirical investigation using elevation data. *Computers & Geosciences, 33*, 1285-1300

Berg, A.A., Famiglietti, J.S., Walker, J.P., & Houser, P.R. (2003). Impact of bias correction to reanalysis products on simulations of North American soil moisture and hydrological fluxes. *Journal of Geophysical Research: Atmospheres (1984–2012), 108*

Briffa, K., & Jones, P. (1990). Tree-ring standardization and growth-trend estimation. *Methods of Dendrochronology: Applications in the Environmental Sciences*, 137-152

Cai, W., Borlace, S., Lengaigne, M., Van Rensch, P., Collins, M., Vecchi, G., Timmermann, A., Santoso, A., McPhaden, M.J., & Wu, L. (2014). Increasing frequency of extreme El Niño events due to greenhouse warming. *Nat Clim Change, 4*, 111-116

Chen, J., Wilson, C.R., & Tapley, B.D. (2010). The 2009 exceptional Amazon flood and interannual terrestrial water storage change observed by GRACE. *Water Resources Research, 46*

Chou, C., Chiang, J.C., Lan, C.-W., Chung, C.-H., Liao, Y.-C., & Lee, C.-J. (2013). Increase in the range between wet and dry season precipitation. *Nature Geoscience, 6*, 263-267

Chou, C., & Lan, C.-W. (2012). Changes in the annual range of precipitation under global warming. *Journal of climate, 25*, 222-235

Chou, C., & Neelin, J.D. (2004). Mechanisms of global warming impacts on regional tropical precipitation*. *Journal of climate, 17*, 2688-2701

Chou, C., Neelin, J.D., Chen, C.-A., & Tu, J.-Y. (2009). Evaluating the "rich-get-richer" mechanism in tropical precipitation change under global warming. *Journal of climate, 22*, 1982-2005

Cleveland, R.B., Cleveland, W.S., McRae, J.E., & Terpenning, I. (1990). STL: A seasonal-trend decomposition procedure based on loess. *Journal of Official Statistics, 6*, 3-73

Cleverly, J., Eamus, D., Luo, Q., Restrepo-Coupe, N., Kljun, N., Ma, X., Ewenz, C., Li, L., & Yu, Q.H., Alfredo (2016a). The importance of interacting climate modes on Australia's contribution to global carbon cycle extremes. *Scientific Reports*

Cleverly, J., Eamus, D., Van Gorsel, E., Chen, C., Rumman, R., Luo, Q., Coupe, N.R., Li, L., Kljun, N., & Faux, R. (2016b). Productivity and evapotranspiration of two contrasting semiarid ecosystems following the 2011 global carbon land sink anomaly. *Agricultural and Forest Meteorology, 220*, 151-159

Cook, E.R., & Peters, K. (1997). Calculating unbiased tree-ring indices for the study of climatic and environmental change. *The Holocene, 7*, 361-370

CSIRO, & BOM (2014). State of the Climate 2014 *http://www.csiro.au/en/Outcomes/Climate/Understanding/State-of-the-Climate-2014/References.aspx*

Dardel, C., Kergoat, L., Hiernaux, P., Grippa, M., Mougin, E., Ciais, P., & Nguyen, C.-C. (2014). Rain-use-efficiency: What it tells us about the conflicting Sahel greening and Sahelian paradox. *Remote Sensing, 6*, 3446-3474

Di Long, B.R.S., Laurent Longuevergne,Alexander Y. Sun,D. Nelun Fernando,Himanshu Save (2013). GRACE satellite monitoring of large depletion in water storage in response to the 2011 drought in Texas. *Geophysical Research Letters, 40*, 3395-3401

Donohue, R.J., McVICAR, T., & RODERICK, M.L. (2009). Climate-related trends in Australian vegetation cover as inferred from satellite observations, 1981–2006. *Global Change Biol, 15*, 1025-1039

Donohue, R.J., Roderick, M.L., & McVicar, T.R. (2008). Deriving consistent long-term vegetation information from AVHRR reflectance data using a cover-triangle-based framework. *Remote Sensing of Environment, 112*, 2938-2949

Duke, N., & van Oosterzee, P. (2017). Extreme weather likely behind worst recorded mangrove dieback in northern Australia. In: The conversation

Durack, P.J., Wijffels, S.E., & Matear, R.J. (2012). Ocean salinities reveal strong global water cycle intensification during 1950 to 2000. *Science, 336*, 455-458

Easterling, D.R., Meehl, G.A., Parmesan, C., Changnon, S.A., Karl, T.R., & Mearns, L.O. (2000). Climate extremes: observations, modeling, and impacts. *science, 289*, 2068-2074

Eichler, T., & Higgins, W. (2006). Climatology and ENSO-related variability of North American extratropical cyclone activity. *Journal of Climate, 19*, 2076-2093

Ellison, A.M. (2002). Macroecology of mangroves: large-scale patterns and processes in tropical coastal forests. *Trees, 16*, 181-194

Emori, S., & Brown, S. (2005). Dynamic and thermodynamic changes in mean and extreme precipitation under changed climate. *Geophysical Research Letters, 32*, L17706

Famiglietti, J.S., & Rodell, M. (2013). Water in the Balance. *Science, 340*, 1300-1301

Gergis, J., Gallant, A.J.E., Braganza, K., Karoly, D.J., Allen, K., Cullen, L., D'Arrigo, R., Goodwin, I., Grierson, P., & McGregor, S. (2012). On the long-term context of the 1997–

2009 'Big Dry'in South-eastern Australia: insights from a 206-year multi-proxy rainfall reconstruction. *Climatic Change, 111*, 923-944

Guan, K., Pan, M., Li, H., Wolf, A., Wu, J., Medvigy, D., Caylor, K.K., Sheffield, J., Wood, E.F., & Malhi, Y. (2015). Photosynthetic seasonality of global tropical forests constrained by hydroclimate. *Nature Geoscience, 8*, 284-289

Harris, J.A., Hobbs, R.J., Higgs, E., & Aronson, J. (2006). Ecological restoration and global climate change. *Restor Ecol, 14*, 170-176

Heberger, M. (2011). Australia's Millennium Drought: Impacts and Responses. *The World's Water* (pp. 97-125): Springer

Held, I.M., & Soden, B.J. (2006). Robust responses of the hydrological cycle to global warming. *Journal of climate, 19*, 5686-5699

Hendon, H.H., Lim, E.-P., Arblaster, J.M., & Anderson, D.L. (2014). Causes and predictability of the record wet east Australian spring 2010. *Climate Dynamics, 42*, 1155-1174

Huete, A., Didan, K., Miura, T., Rodriguez, E.P., Gao, X., & Ferreira, L.G. (2002). Overview of the radiometric and biophysical performance of the MODIS vegetation indices. *Remote sensing of environment, 83*, 195-213

Huete, A., & Ma, X. (2016). Rising extreme weather warns of ecosystem collapse: study. In: The Conversion

IPCC (2014). Climate change 2014: impacts, adaptation, and vulnerability. *Contribution of Working Group II to the Fifth Assessment Report of the Intergovernmental Panel on Climate Change*

Jones, M.O., Kimball, J.S., & Nemani, R.R. (2014). Asynchronous Amazon forest canopy phenology indicates adaptation to both water and light availability. *Environmental Research Letters, 9*, 124021

Jong, S.d., Kwast, H., Addink, E., Su, B., Bierkens, M., Dolman, A., & Troch, P. (2008). Remote sensing for hydrological studies. *Climate and the hydrological cycle*, 297-320

Kaufmann, R.K., Zhou, L., Knyazikhin, Y., Shabanov, N.V., Myneni, R.B., & Tucker, C.J. (2000). Effect of orbital drift and sensor changes on the time series of AVHRR vegetation index data. *Geoscience and Remote Sensing, IEEE Transactions on, 38*, 2584-2597

Kerr, J.T., & Ostrovsky, M. (2003). From space to species: ecological applications for remote sensing. *Trends Ecol Evol, 18*, 299-305

Kulmatiski, A., & Beard, K.H. (2013). Woody plant encroachment facilitated by increased precipitation intensity. *Nat Clim Change*

Kumar, D.N., & Reshmidevi, T. (2013). Remote sensing applications in water resources. *Journal of the Indian Institute of Science, 93*, 163-188

Kumar, S.V., Peters-Lidard, C.D., Tian, Y., Houser, P.R., Geiger, J., Olden, S., Lighty, L., Eastman, J.L., Doty, B., & Dirmeyer, P. (2006). Land information system: An

interoperable framework for high resolution land surface modeling. *Environ Modell Softw, 21*, 1402-1415

Leblanc, M., Tweed, S., Ramillien, G., Tregoning, P., Frappart, F., Fakes, A., & Cartwright, I. (2011). Groundwater change in the Murray basin from long-term in situ monitoring and GRACE estimates. *Climate change effects on groundwater resources: A global synthesis of findings and recommendations CRC Press, November, 22*, 169-187

Leblanc, M.J., Tregoning, P., Ramillien, G., Tweed, S.O., & Fakes, A. (2009). Basin-scale, integrated observations of the early 21st century multiyear drought in southeast Australia. *Water Resources Research, 45*, W04408

Lim, E.-P., & Hendon, H.H. (2015). Understanding and predicting the strong Southern Annular Mode and its impact on the record wet east Australian spring 2010. *Climate Dynamics, 44*, 2807-2824

Lu, H., Raupach, M.R., McVicar, T.R., & Barrett, D.J. (2003). Decomposition of vegetation cover into woody and herbaceous components using AVHRR NDVI time series. *Remote Sensing of Environment, 86*, 1-18

Lymburner, L., Tan, P., Mueller, N., Thackway, R., Thankappan, M., Islam, A., Lewis, A., Randall, L., & Senarath, U. (2011). Land Cover Map of Australia, 1st ed., Scale 1:5 000 000. In. Canberra: GeoScience Australia

Ma, X., Huete, A., Moran, S., Ponce-Campos, G., & Eamus, D. (2015). Abrupt shifts in phenology and vegetation productivity under climate extremes. *Journal of Geophysical Research: Biogeosciences, 120*, 2036-2052

Ma, X., Huete, A., Yu, Q., Coupe, N.R., Davies, K., Broich, M., Ratana, P., Beringer, J., Hutley, L.B., & Cleverly, J. (2013). Spatial patterns and temporal dynamics in savanna vegetation phenology across the North Australian Tropical Transect. *Remote Sensing of Environment, 139*, 97-115

Matheron, G. (1963). Principles of geostatistics. *Economic geology, 58*, 1246-1266

McGrath, G.S., Sadler, R., Fleming, K., Tregoning, P., Hinz, C., & Veneklaas, E.J. (2012). Tropical cyclones and the ecohydrology of Australia's recent continental-scale drought. *Geophysical Research Letters, 39*

Moran, P.A. (1950). Notes on continuous stochastic phenomena. *Biometrika, 37*, 17-23

Pahl-Wostl, C. (2007). Transitions towards adaptive management of water facing climate and global change. *Water resources management, 21*, 49-62

Piao, S., Fang, J., Zhou, L., Guo, Q., Henderson, M., Ji, W., Li, Y., & Tao, S. (2003). Interannual variations of monthly and seasonal normalized difference vegetation index (NDVI) in China from 1982 to 1999. *Journal of Geophysical Research: Atmospheres, 108*

Pickett-Heaps, C.A., Canadell, J.G., Briggs, P.R., Gobron, N., Haverd, V., Paget, M.J., Pinty, B., & Raupach, M.R. (2014). Evaluation of six satellite-derived Fraction of Absorbed

Photosynthetic Active Radiation (FAPAR) products across the Australian continent. *Remote Sensing of Environment, 140*, 241-256

Pietroniro, A., & Prowse, T.D. (2002). Applications of remote sensing in hydrology. *Hydrological processes, 16*, 1537-1541

Pinzon, J.E., & Tucker, C.J. (2014). A non-stationary 1981–2012 AVHRR NDVI3g time series. *Remote Sensing, 6*, 6929-6960

Ponce-Campos, G.E., Moran, M.S., Huete, A., Zhang, Y., Bresloff, C., Huxman, T.E., Eamus, D., Bosch, D.D., Buda, A.R., & Gunter, S.A. (2013). Ecosystem resilience despite large-scale altered hydroclimatic conditions. *Nature, 494*, 349-352

Ponce Campos, G.E., Moran, M.S., Huete, A., Zhang, Y., Bresloff, C., Huxman, T.E., Eamus, D., Bosch, D.D., Buda, A.R., & Gunter, S.A. (2013). Ecosystem resilience despite large-scale altered hydroclimatic conditions. *Nature, 494*, 349-352

R Core Team (2015). R: A language and environment for statistical computing (Available at):www.r-project.org. In. Vienna, Austria R Foundation for Statistical Computing

Raupach, M.R., Briggs, P., Haverd, V., King, E., Paget, M., & Trudinger, C. (2009). *Australian water availability project (AWAP): CSIRO marine and atmospheric research component: final report for phase 3*. Bureau of Meteorology and CSIRO

Raupach, M.R., Briggs, P., Haverd, V., King, E., Paget, M., & Trudinger, C. (2012). Australian Water Availability Project. In: CSIRO Marine and Atmospheric Research,Canberra, Australia

Rodell, M., Famiglietti, J., Chen, J., Seneviratne, S., Viterbo, P., Holl, S., & Wilson, C. (2004a). Basin scale estimates of evapotranspiration using GRACE and other observations. *Geophysical Research Letters, 31*, L20504

Rodell, M., Houser, P., Jambor, U., Gottschalck, J., Meng, J., Arsenault, K., DiGirolamo, N., & Hall, D. (2002). Use of MODIS-derived snow fields in the Global Land Data Assimilation System. In, *Proceedings GAPP Mississippi River Climate and Hydrology Conference*

Rodell, M., Houser, P., Jambor, U.e.a., Gottschalck, J., Mitchell, K., Meng, C., Arsenault, K., Cosgrove, B., Radakovich, J., & Bosilovich, M. (2004d). The global land data assimilation system. *Bulletin of the American Meteorological Society, 85*, 381-394

Roderick, M.L., Noble, I.R., & Cridland, S.W. (1999). Estimating woody and herbaceous vegetation cover from time series satellite observations. *Global Ecology and Biogeography, 8*, 501-508

Rotstayn, L.D., Cai, W., Dix, M.R., Farquhar, G.D., Feng, Y., Ginoux, P., Herzog, M., Ito, A., Penner, J.E., & Roderick, M.L. (2007). Have Australian rainfall and cloudiness increased due to the remote effects of Asian anthropogenic aerosols? *Journal of Geophysical Research: Atmospheres (1984–2012), 112*

Savitzky, A., & Golay, M.J. (1964). Smoothing and differentiation of data by simplified least squares procedures. *Analytical chemistry, 36*, 1627-1639

Schmugge, T.J., Kustas, W.P., Ritchie, J.C., Jackson, T.J., & Rango, A. (2002). Remote sensing in hydrology. *Advances in water resources, 25*, 1367-1385

Seddon, A.W., Macias-Fauria, M., Long, P.R., Benz, D., & Willis, K.J. (2016). Sensitivity of global terrestrial ecosystems to climate variability. *Nature*

Shi, G., Cai, W., Cowan, T., Ribbe, J., Rotstayn, L., & Dix, M. (2008). Variability and trend of North West Australia rainfall: observations and coupled climate modeling. *Journal of climate, 21*, 2938-2959

Silvertown, J., Dodd, M.E., McConway, K., Potts, J., & Crawley, M. (1994). Rainfall, biomass variation, and community composition in the Park Grass Experiment. *Ecology*, 2430-2437

Su, Z. (2000). Remote sensing of land use and vegetation for mesoscale hydrological studies. *International Journal of Remote Sensing, 21*, 213-233

Swenson, S., & Wahr, J. (2006). Estimating large-scale precipitation minus evapotranspiration from GRACE satellite gravity measurements. *Journal of Hydrometeorology, 7*, 252-270

Szilagyi, J., Katul, G.G., & Parlange, M.B. (2001). Evapotranspiration intensifies over the conterminous United States. *Journal of Water Resources Planning and Management, 127*, 354-362

Tregoning, P., & McClusky, S. (2011). Deriving groundwater estimates in Australia from Graviety Recovery and Climate Experiment(GRACE) observations. In, *WIRADA Science Symposium*. Melbourne, Australia

Tregoning, P., McClusky, S., van Dijk, A., Crosbie, R., & Peña-Arancibia, J. (2012). Assessment of GRACE satellites for groundwater estimation in Australia

Trenberth, K.E., & Dai, A. (2007). Effects of Mount Pinatubo volcanic eruption on the hydrological cycle as an analog of geoengineering. *Geophysical Research Letters, 34*

Ummenhofer, C.C., England, M.H., McIntosh, P.C., Meyers, G.A., Pook, M.J., Risbey, J.S., Gupta, A.S., & Taschetto, A.S. (2009). What causes southeast Australia's worst droughts? *Geophysical Research Letters, 36*, L04706

UNWWAP, U.N.W.W.A.P. (2003). Water in a Changing World. In. The United Nations World Water Development Report 3, Paris and London: Unesco Pub.

Van Dijk, A.I., Beck, H.E., Crosbie, R.S., Jeu, R.A., Liu, Y.Y., Podger, G.M., Timbal, B., & Viney, N.R. (2013). The Millennium Drought in southeast Australia (2001–2009): Natural and human causes and implications for water resources, ecosystems, economy, and society. *Water Resources Research, 49*, 1040-1057

Velicogna, I., & Wahr, J. (2006). Measurements of time-variable gravity show mass loss in Antarctica. *science, 311*, 1754-1756

Verón, S.R., Oesterheld, M., & Paruelo, J.M. (2005). Production as a function of resource availability: slopes and efficiencies are different. *J Veg Sci, 16*, 351-354

Verstraeten, W.W., Veroustraete, F., & Feyen, J. (2008). Assessment of evapotranspiration and soil moisture content across different scales of observation. *Sensors, 8*, 70-117

Vörösmarty, C.J., Green, P., Salisbury, J., & Lammers, R.B. (2000). Global water resources: vulnerability from climate change and population growth. *science, 289*, 284-288

Walker, B., Holling, C.S., Carpenter, S.R., & Kinzig, A. (2004). Resilience, adaptability and transformability in social-ecological systems. *Ecology and society, 9*, 5

Wan, Z., Zhang, K., Xue, X., Hong, Z., Hong, Y., & Gourley, J.J. (2015). Water balance-based actual evapotranspiration reconstruction from ground and satellite observations over the conterminous United States. *Water Resources Research, 51*, 6485-6499

Wheeler, T., & von Braun, J. (2013). Climate change impacts on global food security. *Science, 341*, 508-513

Wu, Z., Huang, N.E., Long, S.R., & Peng, C.-K. (2007). On the trend, detrending, and variability of nonlinear and nonstationary time series. *Proceedings of the National Academy of Sciences, 104*, 14889-14894

Xiaoning, S., Xia, Z., Xiaotao, L., & Xinhui, L. (2009). Spatial Heterogeneity Analysis of Soil Moisture Based on Geostatistics. In, *Information Science and Engineering (ICISE), 2009 1st International Conference on* (pp. 5134-5137): IEEE

Xie, Z., Huete, A., Ma, X., Restrepo-Coupe, N., Devadas, R., Clarke, K., & Lewis, M. (2016a). Landsat and GRACE observations of arid wetland dynamics in a dryland river system under multi-decadal hydroclimatic extremes. *Journal of Hydrology*

Xie, Z., Huete, A., Restrepo-Coupe, N., Ma, X., Devadas, R., & Caprarelli, G. (2016b). Spatial partitioning and temporal evolution of Australia's total water storage under extreme hydroclimatic impacts. *Remote Sensing of Environment, 183*, 43-52

Xie, Z., Huete, A., Restrepo-Coupe, N., Ma, X., Devadas, R., & Caprarelli, G. (2016c). Spatial partitioning and temporal evolution of Australia's total water storage under extreme hydroclimatic impacts. *Remote Sensing of Environment*

Xu, Z., Takeuchi, K., Ishidaira, H., & Li, J. (2005). Long-term trend analysis for precipitation in Asian Pacific FRIEND river basins. *Hydrological Processes, 19*, 3517-3532

Yang, Y., Long, D., Guan, H., Scanlon, B.R., Simmons, C.T., Jiang, L., & Xu, X. (2014). GRACE satellite observed hydrological controls on interannual and seasonal variability in surface greenness over mainland Australia. *Journal of Geophysical Research: Biogeosciences, 119*, 2245-2260

Yeh, P.J.F., Swenson, S., Famiglietti, J., & Rodell, M. (2006). Remote sensing of groundwater storage changes in Illinois using the Gravity Recovery and Climate Experiment (GRACE). *Water Resources Research, 42*, W12203

Zeng, Z., Piao, S., Lin, X., Yin, G., Peng, S., Ciais, P., & Myneni, R.B. (2012). Global evapotranspiration over the past three decades: estimation based on the water balance equation combined with empirical models. *Environmental Research Letters, 7*, 014026

Zhang, J., & Foody, G. (1998). A fuzzy classification of sub-urban land cover from remotely sensed imagery. *International journal of remote sensing, 19*, 2721-2738

Zhang, Y., Moran, M.S., Nearing, M.A., Ponce Campos, G.E., Huete, A.R., Buda, A.R., Bosch, D.D., Gunter, S.A., Kitchen, S.G., & Henry McNab, W. (2013). Extreme precipitation patterns and reductions of terrestrial ecosystem production across biomes. *Journal of Geophysical Research: Biogeosciences*

Zhou, L., Tucker, C.J., Kaufmann, R.K., Slayback, D., Shabanov, N.V., & Myneni, R.B. (2001). Variations in northern vegetation activity inferred from satellite data of vegetation index during 1981 to 1999. *Journal of Geophysical Research: Atmospheres, 106*, 20069-20083

Chapter 6: Conclusions and Future Perspective

Amplification of the water cycle, as a consequence of climate change, has been shown to result in increasing frequency and severity of droughts and wet extremes. This is predicted to markedly alter current hydrological regimes later this century, exerting adverse impacts on water resources, natural ecosystems, agriculture and human well-being over the globe. Australia, as the driest inhabited continent in the world, is characterized by extreme climate variability and has been experiencing increasingly common large-scale hydroclimatic extremes since the last four decades. Therefore, studies are urgently needed to investigate the causes and ecohydrological implications of the hydroclimatic extremes, as well as to address the pressing challenges that may arise from these events in the coming decades for better management and protection of water resources and ecosystems across the continent.

In this thesis, we studied the ecohydrological dynamics and their interactions across the Australian continent over a period of more than one decade in the early 21st century (2002 – 2015), in particular, under the impacts of three recent extreme hydroclimatic events including a prolonged millennium drought, a dramatic wet pulse period and another anomalous El Niño dry event. We achieved thesis objectives by using remote sensing and statistical methods, based on a combination of complementary data, i.e. integrating the total water storage anomaly (TWSA) data derived from the Gravity Recovery and Climate Experiment (GRACE) with various other satellite observations derived from MODIS, TRMM, Landsat, AVHRR etc; modelling and field datasets, including rainfall from Bureau of Meteorology (BOM), soil moisture from Global Land Data Assimilation System (GLDAS), ET and runoff from Australian Water Availability Project (AWAP) etc; and other gridded products such as land cover type, soil classification, hydrological maps and so on.

In summary, we first investigated spatial partitioning and temporal evolution of Australia's Total Water Storage (TWS) from 2002 to 2014, encompassing the 'big dry' and 'big wet' events. We then evaluated the relative contributions of three major climate modes to the partitioning and variations of TWS across Australia over the same period and an additional 2015 El Niño year. Meanwhile, we highlighted the value of GRACE-TWSA for effectively linking the extreme climate variability with vegetation productivity dynamics. Furthermore, at regional scale, we examined the dynamics and resilience of an arid wetland ecosystem in Central Australia to multi-decades of drought and flood events, specifically under these early 21st century hydroclimatic extremes. At

last, we conducted a synthesized assessment of the various components in water resources, ecosystems and their interactions during the hydroclimatic events for improved ecohydrological management and conservation in Australia.

6.1 Summary of key methodology and conclusions

The major methods and conclusions of this thesis are:

1. We analysed spatial-temporal impacts of the recent 'big dry' and 'big wet' events on Australia's water storage dynamics using the GRACE-TWSA data. Previous studies have concentrated on the causes of recent dry and wet hydroclimatic events and their impacts on agriculture and ecosystems, treating the 'big dry' and 'big wet' as discrete periods over the entire continent. This isn't very realistic given the diversity of Australia's climate patterns. To better understand the timing of changes in total water storage across the continent, we developed a new automated method to define a per-pixel transition date between dry and wet periods based on GRACE observations. This enabled us to individually derive information on the 'big dry' and 'big wet' change-over for each pixel. We also applied statistical methods of trend analysis, spatio-temporal variability and cross correlation analysis, and calculated the rate of recovery in TWS based on accumulated water loss and gain.

Our results showed 1) large-scale reductions in water storage across Australia during the prolonged 'big dry' period (2002-09) followed by a quick recharge of water resulted from a short-term intensive rainfall-pulse during the 'big wet' (2010-11). In total, Australia gained three times more water during the 'big wet' than was lost in the 'big dry'. This enormous continental water loading in such a short time was enough to lower sea level and eventually altered the global carbon cycle; 2) the timing of the transition date between the 'big dry' and 'big wet' varied considerably across the continent. Overall, there was a 12 month lag in the hydrologic shift from 'big dry' to 'big wet' conditions between eastern and western parts of Australia; 3) highly variable continental patterns were observed in water resources, involving differences in the direction, magnitude, and duration of total water storage responses to drought and wet periods. These responses clustered into three distinct geographic zones that correlated well with the influences from three large-scale climate modes including El Niño Southern Oscillation (ENSO), the Indian Ocean Dipole (IOD) and Southern Annular Mode (SAM); 4) among the three

geographic zones, an overall drying trend over drier areas (western Australia) and an overall wetting trend over wetter areas (northern and north-eastern Australia) were identified, i.e., dry gets drier and wet gets wetter, indicating a potential sign of spatial hydrological cycle intensification; 5) The water deficit during the 'big dry' exerted pronounced impacts on Australia's agriculture production, groundwater storage, and ecosystem functions. For example, the two crop-belts located in south-western and south-eastern areas of Australia experienced the most dramatic TWS declines during the drought, which resulted in great reductions in crop production over irrigated and dryland agriculture. Moreover, the water storage over Murray-Darling Basin, which is the most important basin in Australia for crop production, wetlands, and biodiversity, was found to be highly sensitive to hydroclimatic variations as it exhibited the most dramatic swings in water loss/gain over the drought and wet periods.

2. We characterised and evaluated the spatial-temporal responses, dynamics and trends of Australia's hydrologic and productivity patterns with the three climate systems from 2002 to 2015, encompassing the recent hydroclimatic extremes of the prolonged 'big dry', dramatic 'big wet' pulse and anomalous 2015 El Niño event. Climate index, GRACE-TWSA, TRMM-rainfall and MODIS-EVI data were used to represent the variations in climate modes, hydrological conditions and vegetation productivity across Australia during the study period. As the relationships between the climate modes and TWS are expected to show significant and finite lags, Partial Cross Correlation Analysis and Semi-Partial Cross Correlation Analysis techniques were applied, which enabled us to capture the control from each climate driver on TWS with the effects from the phase lags and other two drivers removed.

Our results showed 1) the dominant influence of the climate modes and their preferred geographic impacts on the continental scale ecohydrological patterns. These varying spatial influences from the climate modes during the 'big dry' and 'big wet' corresponded with the three distinct hydrologic zones in TWS patterns observed in our previous study, which were more pronounced than the continental rainfall patterns; 2) distinct changing patterns in surface greenness within the three zones were further observed, which were largely driven by respective Climate mode-TWS relationships, and less correlated with rainfall patterns; 3) the 2015 El Niño event, which caused severe declines in TWS and vegetation productivity over many parts of Australia, corroborated the three-zone-like influences from the climate modes; 4) GRACE derived

TWSA can be used as a valuable hydrological factor for effectively linking the extreme climate variability with Australia's ecosystems, which have recently been recognized to significantly contribute to the global carbon and water cycles.

3. We investigated the hydrological dynamics and ecosystem functioning of the Coongie Lakes arid wetland in central Australia, one of the world's largest Ramsar-designated wetlands, by integrating multi-sensor satellite observations over a 24-year period (1988-2011). Wetland vegetation growth and flood inundation extent derived from Landsat imagery were used to provide a long-term ecohydrological processes and their interactions over the wetland where there is scarcity of observational data. We also applied GRACE-derived TWS changes, as a surrogate of terminal water storage from the headwaters after transmission losses, to connect the wetland dynamics with water source variations.

First, 1) our results indicated variations in arid wetland vegetation growth were highly correlated with flood extent dynamics driven by ENSO; 2) meanwhile, we showed that GRACE-derived TWS changes can be used as a valuable hydrological indicator for complex dryland river systems; 3) furthermore, we found arid wetlands exhibit strong eco-hydrological resilience to hydroclimatic extremes, and are presumably sensitive to future altered water regimes due to climate change; 4) our study is valuable to develop a better understanding of arid wetland dynamics under large-scale hydrological fluctuations and extreme drought conditions. This also has important implications for how arid wetlands respond to climate change and extremes in the future.

4. We examined spatial patterns and temporal dynamics of water resources and ecosystems across Australia during the recent dry and wet hydroclimatic extremes, by integrating GRACE and other satellite observations with field and modelling data. Multiple methods were used to achieve various objectives, including geostatistics methods, water balance, hydrological use efficiency and marginal response calculation, regression, correlation and time series analysis and so on. We focused on conducting a synthesized assessment of monitoring and analysing changes in various hydrological factors (TWS, rainfall, ET, soil moisture, groundwater and runoff etc) and ecological components (e.g. grass and trees), and their interactions under these extreme hydroclimatic events.

First, 1) results based on geostatistics confirmed the temporary sign of water cycle intensification in Australia during the study period, with water storage increasing in dry areas (western Australia) while decreasing in wet areas (north and northeastern tropical/semi-tropical region); 2) meanwhile, we observed a general close relationhip between rainfall and TWS (rainfall antecedent) but demonstrated that GRACE-TWSA is better than rainfall in detecting drought especially "hidden drought"-groundwater depletion; 3) moreover, monthly ET and groundwater variations derived from water balance equation based on GRACE observations were found to be reasonable; 4) we observed ET significantly increased during the 'big dry', which may partly explain the conflict between the decreasing TWS and increasing rainfall during the dry period; 5) We also found that soil moisture across Australia largely drives the seasonal variations in TWS while groundwater contributes to its long-term trends; 6) our results showed that TWS has overall better, spatially more uniform and temporally more direct correlations with surface greenness than rainfall across Australia, indicating GRACE-TWSA as a valuable indicator for ecological system performance particularly under hydroclimatic events.

6.2 General discussion and future research directions

1. Chapter 2 provided a better understanding of the combined impacts from recent dry and wet hydroclimatic extremes on Australia's water storage dynamics, and demonstrated the value of GRACE data as a valuable indicator of hydrological system performance, and thus can be used for improving the management of water resources. However, GRACE has a major limitation of coarse spatial resolution (~300 km), of which observations are only suitable for quantifying TWS changes over areas larger than GRACE footprint of ~200,000 km^2. With current spatial downscaling limitations of GRACE, it may result in decreased usefulness for smaller scale basin management. With the dynamics and complexity of climate and water cycles, particularly in Australia, more robust mathematical approaches and hydrological models should be developed for better exploiting and processing GRACE data in order to provide higher spatial (less than 300 km) and temporal (sub-monthly) resolution hydrological variations from GRACE and GRACE follow-on missions.

2. Chapter 3 discussed the geographic and temporal varying importance of three major climate systems (ENSO, IOD and SAM) on Australia's water storage and

ecosystems under hydroclimatic extremes. In reality, hydrological conditions across the continent are in control of many climate drivers including both synoptic (higher frequency) processes like cutoff low, blocking high, jet stream as well as large-scale (lower frequency) oceanic and atmospheric phenomena such as ENSO, IOD, SAM and Madden–Julian oscillation (MJO) etc. Therefore, future studies towards a comprehensive framework involving more climate modes are needed to better understand the mechanisms for linking the dynamics of these drivers and changes in water resources. Moreover, although in this chapter we suggested GRACE data can be used as a valuable hydrological factor for effectively linking the climate variability with Australia's ecohydrological dynamics, results are confounded by the short temporal coverage of GRACE observations (14 years). Continuous monitoring from GRACE follow-on missions and applications of modelling are necessary in future to extend the time series of TWS changes to validate our findings. This chapter so far only considered the ecohydrological implications from individual climate modes, so we plan to use more robust statistics methods and models in order to disentangle and quantify both the impacts of each climate mode and their complicated interactions on TWS dynamics over different parts of Australia.

3. Chapter 4 used multiple remote sensing sources (optical to gravitational) to examine the ecohydrological behaviours of an inland wetland (Coongie Lakes) in central Australia under multi-decadal hydroclimatic extremes. As this study is based on satellite observations only, there is limited knowledge of detailed species composition and new species assemblages (e.g. invasive species) over the wetland, which might partly contribute to the increase in wetland vegetation greenness during the 'big wet' period observed by EVI. Future field work thus is essential to collect more ground data to validate our finding on this aspect and to conduct uncertainty analyses for flood extent and wetland vegetation growth mapping. In addition, rainfall that falls in the headwaters at the very upper part of the catchment will not show good correlation to floods in downstream due to a very high transmission losses in the dryland anabranching rivers. As a consequence, our future arid wetland study may also include using hydrological modelling to estimate the effective rainfall (original rainfall minus transmission losses) in the data-sparse, multi-channel and low-gradient dryland river systems.

4. Chapter 5 investigated the impacts of the 'big dry' and 'big wet' events on water resources and ecosystem functioning across Australia, aiming for an improved

ecohydrological management and conservation particularly under hydroclimatic extremes. As we applied many methods in this chapter to achieve multiple objectives, some of the results have not been fully validated. For example, the monthly ET and groundwater variations derived from water balance equation based on GRACE observations were only compared with modelling data, which need further validation. This long chapter needs following work to be detailedly analysed and carefully checked.

Overall, our future research requires a comprehensive analysis of Australia's ecohydrological dynamics and their interactions using combined remote sensing, field and land surface modelling approaches. Moreover, additional studies are also needed to understand the environmental and societal impacts of Australia's hydroclimatic extremes.

6.3 Final conclusion

In this thesis, I investigated ecohydrological interactions and landscape response to recent hydroclimatic events in Australia. Doing so I met all objectives and conducted my analyses within a framework of essential and important criteria. Given the importance of consistent monitoring and successful management of water resources and associated ecosystems across Australia, particularly under increasing frequency and severity of hydroclimatic extremes, I believe this thesis makes a meaningful and significant contribution for this purpose.